EPRI
Electric Power
Research Institute

Topics:
Inconel alloys
Steam generators
Stress corrosion cracking
Cracking

EPRI NP-6626-SD
Project S404-14
Final Report
March 1990

Belgian Approach to Steam Generator Tube Plugging for Primary Water Stress Corrosion Cracking

Prepared by
Belgatom
Brussels, Belgium

REPORT SUMMARY

SUBJECT	Steam generator reliability
TOPICS	Inconel alloys; Steam generators; Stress corrosion cracking; Cracking
AUDIENCE	Design engineers / R&D staff

Belgian Approach to Steam Generator Tube Plugging for Primary Water Stress Corrosion Cracking

Belgian steam generators operate with numerous through-wall cracks in the expansion transition region of the tubesheet without impairing plant reliability or safety. A crack-length-based plugging limit coupled with advanced eddy-current inspection techniques to determine actual crack lengths makes this possible.

BACKGROUND For a number of years, three Belgian nuclear power plants have experienced primary water stress corrosion cracking (PWSCC) in the expansion transition area on a very large number of tubes. One of the plants has part-depth rolled tubes, and others have full-depth expansion. The cracks in these tubes are predominantly through-wall, and though they have posed neither a safety nor a reliability problem, a unique management approach has been needed to avoid the excessive plugging required with a depth-based plugging limit.

OBJECTIVES To document the Belgian experience with PWSCC in the tubesheet expansion zone; to present the safety philosophy and underlying principles of a crack-length plugging limit.

APPROACH The authors, scientific and technical personnel representing the Belgian utilities, gathered historical information about the Belgian plants, including in-service leak rate data. They examined the outage leak measurement methods in use and made a statistical evaluation of the number and length of cracks, determined by rotating pancake eddy-current coil examination. They also analyzed the development of plugging limits and supporting bases. Two reports were prepared: EPRI report NP-6626-SD, a detailed compilation of the results, and NP-6626-M, a brief summary.

RESULTS Leakage experienced with expansion transition PWSCC in three plants—the Doel-2, Doel-3, and Tihange-2—and pulled-tube examinations from Doel-2 and -3 correlate with eddy-current indications associated with these cracks. Calculation procedures used in Belgium, different from NRC Regulatory Guide 1.121 (draft), determine critical crack sizes for axial and circumferential defects. A multifrequency eddy-current method using a rotating pancake coil (RPC) allows 100% inspection of the affected zone without impairing the unit-outage schedule. Derived plugging limits, designed to account for eddy-current inaccuracy and crack growth during the next cycle, allow through-wall axial defects up to 11 to 14 mm long or circumferential defects up to 15 to 18 mm, depending on tube diameter.

EPRI PERSPECTIVE

All steam generator tubes are expanded either partially or over the full thickness of the tubesheet. Many early expansions were performed by mechanical rollers; others have been accomplished by explosive and hydraulic methods. Mechanical roller expansion methods develop high residual stresses that can increase the chance of PWSCC in the roll transition, particularly in certain types of steam generators. Many of the expansion zone cracks are short (6 mm) and axial and have very low leak rates. The current NRC regulatory position allows through-wall cracks if they occur during operation and leak at less than 0.35 gpm (72 l/h). However, NRC requires that defects of greater than 40% of the wall thickness, if detected during an inspection, be repaired or plugged before restarting.

The Belgian approach to PWSCC in the roll transition zone is based on the rationale that short axial through-wall cracks are not a safety or operational problem, especially if they exist deep within the tubesheet. The Belgians have developed a length-based plugging limit, rather than a depth-based limit, to guard against rupture under normal and accidental conditions and have developed an advanced eddy-current inspection method that allows sizing of cracks by length. This report documents this approach, one that may someday find application domestically.

PROJECT

RPS404-14
EPRI Project Manager: Allan R. McIlree
Nuclear Power Division
Contractor: Belgatom

For further information on EPRI research programs, call
EPRI Technical Information Specialists (415) 855-2411.

Belgian Approach to Steam Generator Tube Plugging for Primary Water Stress Corrosion Cracking

NP-6626-SD
Research Project S404-14

Final Report, March 1990

Prepared by

BELGATOM
rue de la Loi, 75
B-1040 Brussels, Belgium

Principal Investigators
G. Frederick
TRACTEBEL

P. Hernalsteen
D. Dobbeni
LABORELEC

Prepared for

Electric Power Research Institute
3412 Hillview Avenue
Palo Alto, California 94304

EPRI Project Manager
A. R. McIlree

Steam Generator Reliability Program
Nuclear Power Division

Price: $10,000.00

Prepared by
Belgatom
Brussels, Belgium

ABSTRACT

For a number of years, three Belgian nuclear power plants have experienced primary water stress corrosion cracking (PWSCC) in the expansion transition area on a very large number of tubes. One of the plants has part depth rolled tubes and the others have full depth expansion. The report presents a review of the leakage experience associated with PWSCC in the Doel 2, Doel 3 and Tihange 2 Nuclear Power Plants and illustrates the type of cracking observed on pulled tubes from Doel 2 and Doel 3.

The Belgian units operate with numerous through wall cracks without impairing the safety and the reliability of the plants. This is achieved by a safety approach based on the extensive use of advanced non-destructive examination (NDE) techniques and the development of new plugging limits. These limits are derived from a realistic interpretation of NRC Regulatory Guide 1.121 and are backed up by a substantial experimental program.

The report details the establishment of plugging limits for both axial and circumferential cracks in the roll transition area of full depth rolled tubes. The LABORELEC eddy current rotating probe (RPC) technology and associated crack sizing methodology are also described.

ACKNOWLEDGMENTS

The authors are grateful to M. J. BERTHE, J. MATHONET and M. GETTEMANS from TRACTEBEL and M. ZAVADSKY from LABORELEC for their contr.bution to the completion of the present report.

CONTENTS

Section 1

SUMMARY

STATEMENT OF THE PROBLEM

In some Belgian plants, cracks at roll transitions caused by primary water stress corrosion cracking (PWSCC) have been detected in large numbers of tubes, ranging up to over 90 % of the tubes in one Doel 2 steam generator. Doel 2 has part depth rolled tubes while Tihange 2 and Doel 3 have full depth rolled tubes. Many of the roll transition cracks are through-wall. However, these plants have been able to continue to operate for the following reasons :

- The leak rate associated with the PWSCC cracks has been very low. This is due to the fact that most of the cracks are short axial cracks.

- For Doel 2 with part-depth rolled tubes, the roll transition region cracks do not present a safety problem since a postulated rupture of the tube deep in the tubesheet would not result in a large leak or allow the tube to whip and cause additional tube failures.

- For plants with full-depth rolled tubes, the presence of through wall PWSCC cracks has been justified to regulatory authorities. Tube plugging or sleeving are not required as long as the cracks do not exceed an established length threshold value.

OBJECTIVE

The objective of this report is to document Belgian plant experience with primary water stress corrosion cracking in the tubesheet expansion zone, and to present the Belgian approach to steam generator tube plugging. The report presents a review of the leakage experience associated with expansion transition PWSCC in the Doel 2, Doel 3, and Tihange 2 units and illustrates the type of cracking observed on pulled tubes from Doel 2 and 3. The report also provides corresponding eddy current indications associated with these cracks. The overall safety philosophy is detailed and the underlying principles of the

Belgian approach are illustrated. Deviations from the NRC Regulatory Guide 1.121 (draft) are identified and the rational presented. Both axial and circumferential cracks are addressed to show the consistency of the crack length approach.
The calculational procedures used to determine critical crack sizes are outlined both for axial and circumferential cracks and illustrated by sample calculations. The corresponding calculation bases are explained and finally the actual plugging limits are derived from the critical sizes. This safety approach requires the length of the cracks in the steam generators to be determined. Therefore, the LABORELEC multifrequency eddy current method, using a rotating pancake coil (RPC) for the PWSCC sizing, is described.
The qualification results for longitudinal SCC are presented and fully discussed in terms of accuracy and reproducibility. Artificial defects (EDM notches) have been used for the study of the reproducibility of the position and the length measurements, while actual SCC cracks obtained from pulled tubes of Doel 2 and Doel 3 and surrogate material (sensitized Alloy 600) have been used to demonstrate the length measurement accuracy. The report further shows how the present LABORELEC technology allows 100 % RPC inspection of the tube roll transitions (or any predefined length within the tubesheet area) without impairing the unit outage schedule. This can only be achieved by using the most recent hardware and software developments such as applied to the Tihange 2 and Doel 3 inspections (100 % tubes inspected in 2½ days per SG).

Finally the compatibility of the RPC inspection method with present NRC requirements and EPRI NDE Guidelines is demonstrated and discussed.
The safe and reliable operation of the Belgian steam generators, despite the existence of thousands of through-wall cracks, is demonstrated through :

- historical background
- in-service leak rate data
- outage leak data (helium test and secondary side pressure test)
- RPC statistical data (distribution of crack lengths, number of cracks per transverse section, ...)

correlation between inspection data.

1

IMAGE EVALUATION TEST TARGET (MT-3)

1

IMAGE EVALUATION TEST TARGET (MT-3)

150mm

6"

1

IMAGE EVALUATION TEST TARGET (MT-3)

150mm

6"

1

IMAGE EVALUATION TEST TARGET (MT-3)

150mm

6"

Section 2

PLANT EXPERIENCE

2.1. INTRODUCTION

For a number of years, three Belgian nuclear power plants have experienced primary water stress corrosion cracking (PWSCC) in the expansion transition area. Some cracks have resulted in leakage during operation. The characteristics of the roll transition area for these plants are given in Figure 2-1. The corresponding plant and tube data are shown in Table 2-1, together with the type of corrective action taken. Eddy current inspection techniques have been developed to detect and characterize the defects. Tubes have been pulled in order to determine the type of cracking. Correlation between observed cracking on pulled tubes from Doel 2 and 3 and eddy current indications is presented.

2.2. LEAKAGE EXPERIENCE

In Belgium, the first occurrence of PWSCC and associated leakage goes back to 1977 at the Doel 2 power plant (1st criticality : December 1975). The defects were located in the upper roll transition of the expansion zone made by two step rolling. Since that time, the corrosion has progressed quickly and to date, it has reached up to 90 percent of the tubes in one steam generator (estimated figure on basis of "bobbin coil" ECT). Several shutdowns for excessive leak rates have occurred since the plant start up but none of them was related to roll transition cracking.

In 1983, PWSCC was discovered in two other units (Doel 3, 1st criticality August 1982 and Tihange 2, 1st criticality October 1982) during their first cycle of operation. In these cases, the cracking was located in the full depth rolled region and in the transition between normal and kiss roll expansion areas. The rapid crack initiation and propagation was attributed to tubes being rolled into over-sized holes and cannot be considered as representative of the entire tube bundle.

Section 7 gives a full history of the roll transition leaks for the three units. It should be noted that in a few cases only, the leak rates reached the limits imposed by the technical specifications (0.35 gpm - 79 l/hr) and forced the plant to shutdown (in February 1985 at Tihange 2 and in May 1987 at Doel 3).

Tables 2-2 and 2-3 give the list of tubes that were pulled from the Doel 2 and 3 SG's. The reasons for extraction are provided for information in the tables but only the data related to the PWSCC cracks are analysed here.

Various types of cracking were observed both by eddy current inspection and by metallographic examination of the pulled tubes, and can be categorized in four families :

a - axial cracks - hot leg

b - circumferential cracks - hot leg

c - axial cracks observed after shot peening - hot leg

d - axial cracks - cold leg.

a. Axial Cracks - Hot Leg (Fig. 2-2)
Axial PWSCC in the roll transition was observed at Doel 2 on the first tubes pulled in 1980 (see case 1 below). As the number of cracked tubes increased, the problem has been monitored by periodic bobbin coil EC inspection. The last tubes were pulled in 1987 for the purpose of examining nickel coatings which were deposited in 1985 and 1986. Metallographic examination performed on these tubes confirmed that primary water stress corrosion cracks were not longer than 14 mm after 10 years of operation. It should be noted that higher values have been observed in the kiss rolled Doel 3 SG's (up to 22 mm - 0.866 in). If this observation is confirmed in the future, the lower value could be attributed to the single step of the roll transition area so that once the crack reaches the straight, undeformed portion of the tube, stresses could be low enough to prevent further propagation.

However, a statistical RPC data base for the Doel 2 steam generators has not been performed as it has for the Doel 3 and Tihange 2 steam generators. Such an inspection is not needed for Doel 2 as the cracks are judged to have no safety significance since they are inside the tubesheet. The conclusion about a maximum length must therefore be used with care.

Axial PWSCC has also been observed at Doel 3 by RPC inspection and pulled tubes. In this case, the following characteristics have been observed : crack length can be much longer (up to 22 mm - 0.866 in) than those observed on tubes with a single step transition; two small axial cracks can be generated separately in the same alignment to form a single long crack; numerous small cracks (up to 20 in one transverse cross section) can be seen; crack initiation and propagation can be influenced by score marks.

b. Circumferential Cracks - Hot Leg (Fig. 2-3)
This type of cracking has only been observed so far on a tube pulled out of Doel 3 (case 3). The cracks were initiated and propagated in a score mark (probably resulting from the rolling tool in fabrication) in the circumferential direction. The longest circumferential crack was however quite short (3.5 mm - 0.138 in).

c. Axial Cracks Observed After Shot Peening - Hot Leg
Fig. 2-4 shows typical cracking observed on the Doel 3 shot peened tubes, from tube R27C52 pulled in 1986. Crack propagation seems to have been stopped on the surface but not underneath. It should be remembered however that this pattern has been observed after a short time period (one year) and that subsequent RPC inspections evidenced crack propagation on a wider scale. The observed "bubble" shape of the crack might have been a temporary condition.

d. Axial Cracks - Cold Leg
RPC inspection has not been performed routinely in the cold leg, and therefore, no trend can be given as far as PWSCC is concerned. However, as part of a sample examination aimed at establishing the cold leg tubes condition, ten tubes were pulled from the cold leg of a Doel 2 steam generator. These tubes were selected from a statistical sampling of 150 tubes inspected with the rotating probe in 1984. Only one tube had a ECT crack indication. Eight of the ten tubes were

examined and only one (with the ECT indication) of them showed some cracking. Most of the crack lengths were short (less than 4 mm - 0.158 in), none were through wall, and some could be associated with roller marks (Fig. 2-2). Cracking was of the same type as in the hot leg, i.e. IG SCC (5).

Three cases are detailed hereafter to illustrate the type of cracking observed on pulled tubes and the corresponding eddy current indications.

Case 1 - Tube R14C72 From Doel 2

The first implementation of LABORELEC prototype rotating pancake coil was performed in December 1979 to identify the geometry of the PWSCC defects in Doel 2. The eddy current results of the bobbin and rotating coils can be observed from one pulled tube R14C72. The sequence of inspection before and after pulling was :

- bobbin coil examination with multifrequency eddy current and one mixing to identify the cracked area (Figure 2-5 (a));

- rotating probe inspection to identify the circumferential or axial direction of the crack (Figure 2-5 (b)).

The metallurgical analysis (1) is shown on Figure 2-5 (c) and resulted in the following observations :

- although the tube was not leaking, three through wall axial intergranular cracks were observed, over a 90° segment. The cracks extended upwards from the top of the roll transition over a distance of about 7 mm (.275 in).

- all the cracks had approximately the same axial extent on both OD and ID surfaces, making it difficult to establish the initiation side of the cracking;

- detailed optical metallography and Scanning Electron Microscopy (SEM) examinations revealed multiple shallow cracking on the ID surface at the elevation of, and adjacent to, the through-wall cracks. OD cracking was absent. No additional cracking was found at elevations adjacent to, and above, the through-wall cracks;

The EC inspection resulted in the following observations :

- the bobbin coil signal of the cracked cross section needed mixing to allow clear identification of the cracking;

- the rotating probe showed each of the three cracks on the cross section; the length, amplitude and azimuthal location could be obtained from a single examination.

Consequently, although the rotating probe used for this examination was a laboratory prototype (slow and wobble sensitive), it showed a definite advantage for PWSCC detection and identification in comparison with the bobbin coil method.

Case 2 - Tube R15C29 From Doel 3 (Figures 2-6; 2-7; 2-8; 2-9)

A leak rate of less than 2 l/h (0.009 gpm) during the unit's first cycle prompted detailed investigation at the first refueling outage :

- A secondary side pressure test with fluorescein to detect the leaking tubes (three tubes in the hot leg).
- An extensive EC inspection : bobbin coil (Figure 2-6), rotating p[illegible]e (Figure 2-7) and profilometry (Figure 2-8).
- Extraction of three tubes (only two were leakers).

Tube R15C29 has been selected as an illustration, since it had cracks both in the expansion transition and at some roll steps in the tubesheet. The profilometry indicates that the rolling was abnormal.

During the extraction process, the tube broke at the level of the 14^{th} roll step, at a load half of the usual value experienced for tube pulling. The metallurgical analysis performed on the portion of the tube containing the expansion transition revealed the following :

- 1 crack was evidenced by X-ray at the end of the mechanical expanded zone. X-ray confirmed the crack length of 2 mm (0.079 in) found previously by EC.
- EC inspection detected cracks at three levels, out of which only two were confirmed by X-rays and micrographic examination.

The EC inspection performed before tube pulling gave the following results :

- Multifrequency eddy current (MFEC) inspection by the bobbin coil with mixing technique showed indications between some roll steps (15^{th}, 11^{th}, 8^{th}, 7^{th}), but the mixing signals needed at least a minimum of 4 to 5 cracks on the cross section before developing a detectable indication.

- MFEC inspection with the rotating probe showed cracking indications at the same levels as those identified with the bobbin coil, but in addition, it showed 1 longitudinal crack, 2 mm long located in the roll transition at the limit of the 21st (last) roll step.

- From the comparison between the mechanical measurements performed on the tube hole in the tubesheet during manufacturing(line a on Figure 2-8) and the EC profilometry (lines b on Figure 2-8), it could be assumed that there was only a partial contact between the tube and the tubesheet. The location of the cracks was clearly related to abnormal profiles.

Case 3 - Tube R23C23 from Doel 3

Shot peening was performed at Doel 3 in 1985 on the hot leg roll transitions (190 mm - 7.48 in). Two tubes were pulled out one year later in order to evaluate the effects of the shot peening.

Two types of examination were performed (reference 8) : radiographic examination on the as-pulled tubes and visual examin tion on the tubes after flattening.

On the tube discussed here, one circumferential and axial cracks were observed by X-rays in an area centered on the transition between the last roll step and the kiss roll (see Fig. 2-10 for defect location). The longest crack was 8 mm (0.315 in) and resulted from the summation of two cracks almost aligned with each other (see Fig. 2-11).

The visual examination performed after tube flattening showed the real cumulated length of these two aligned cracks to be 11 mm (0.433 in) on the ID. The same visual examination indicated 17 axial, one "L" shaped and 3 circumferential cracks. Except for one axial 5 mm (0.197 in) long crack located in the kiss roll step, all the cracks were located in the top hard roll to kiss roll transition. The circumferential cracks (Fig. 2-3) were linked to ID scratches in the upper part of the "hard" roll. The longest single axial crack measured 8 mm (0.315 in) and the longest circumferential crack was 3.5 mm (0.138 in).

Eddy current profilometry performed during pre-service inspection did not show any defect, nor abnormal tube hole dimensions.

Eddy current inspection performed with the RPC detected cracks at the limit of the last roll to kiss roll transition. One signal had an amplitude of 340 mV and several indications were close to the detection threshold of about 80 mV. The length of the largest defect was 9 mm (0.354 in), which was comparable to the X-ray measurements and the shortest indications were in the range of 1 to 2 mm (0.039 to 0.079 in). The circumferential cracks were not detected by E.C., and the maximum number of axial cracks detected were 10 to 12.

The results of the examination of the other tube were very similar. Figure 2-12 illustrates the correlation between RPC indications and visual examination (after flattening) on the two tubes. An average length underestimation of about 1 mm (0.04 in) results from the ECT sizing; this has been corrected to yield a new calibration curve (see Fig. 4-13 and section 5).

REFERENCES

1. Doel 2 Nuclear SG Tubing samples. Metallurgical Investigation Results. August 5, 1980
WESTINGHOUSE Report 80-5D9-Doel-R1/SG-80-09-020
F.W. PEMENT

2. Metallurgical and Chemical Evaluation of tubes R17C85, R28C32 and R26C50 from Doel 2 SG A
EPRI Report NP-5022LD Dec. 1986
H. TAS, J. VAN DE VELDE SCK/CEN MOL BELGIUM

3. Laboratory Examination of Minisleeved Tube Samples from the Doel 2 "A" Steam Generators - August 17, 1984
Research and Development Division S.C. INMAN Babcock & Wilcox Company

4. First results of tubes R18C32, R17C45, R15C46, R10C58 examination SCK/CEN MOL BELGIUM

5. Examination of Cold Leg Tube Segments of the Doel 2 Steam Generator A
H. TAS, L. DRIESEN, J. VAN DE VELDE, L. SANNEN
SCK/CEN MOL BELGIUM

6. Examination of Kiss-Sleeved Tube R18C61 From Doel 2 SG A
J. STUBBE, CH. LAIRE
LABORELEC Report PV/C01-02615/1/JS/Cg

7. Report C-Chl/1d/C01-02615-003 for Kiss-Sleeved Tube R18C51 SG A
LABORELEC/FRAMATOME, december 18, 1987
J. STUBBE, CH. LAIRE, F. ANXIONNAZ

8. "Centrale de Doel 3 : Examen de deux tubes du générateur de vapeur B. Réf. doc. : D.5004/CTT/R.84.37"
April 20, 1984
F. CATTANT, J.M. THOMAS, P. HUBERT
Groupe des Laboratoires EDF.

9. "Centrale de Doel 3 - Examen des tubes R23C23 et R27C52 extraits du générateur de vapeur B - Réf. doc : D.5004/CTT/R.87.11"
March 31, 1987
F. CATTANT, A. CONTRE, P. HUBERT.
Groupe des Laboratoires EDF

Table 2-1 - Belgian units and steam generators affected by PWSCC

	DATE OF COM. OPER.	POWER MWe	No OF SG's	SG W SERIES x	TUBE					GENERIC CORRECTIVE ACTION		
					Φ IN	MATERIAL	MANUFAC.	APPROXIM. PROCESSING DATE	MECHANICAL HARD ROLLING (IN)	DATE	TYPE	EXTENT
DOEL 2	75	400	2	44	7/8	MA INCONEL 600	MANNES-MAN		2.28	-	-	-
DOEL 3	82	900	3	51M	7/8	"	W (Blairs-ville)	MAY - OCT 76	WHOLE TUBESHEET THICKNESS + KISS ROLLING	JUL 85	SHOT-PEENING	HOT LEG (190 MM)
TIHANGE 2	82	900						OCT 76 - APR 77		FEB 86	SHOT-PEENING	HOT LEG (TUBESHEET FULL HEIGHT)
DOEL 4 #	85	1000	3	E *	3/4	"	W (Blairs-ville)	PROBABLY IDENTICAL TO TIH. 3	WHOLE TUBESHEET THICKNESS + KISS ROLLING	DEC 84	ROTO-PEENING 0	HOT LEG (TUBESHEET FULL HEIGHT)
TIHANGE 3 #	85	1000						APR 79 - MAY 79		FEB 85	ROTO-PEENING 0	HOT AND COLD LEG (TUBE-SHEET FULL HEIGHT)

* INCONEL cladding on tubesheet secondary side
x All manufactured by COCKERILL MECHANICAL INDUSTRIES (WESTINGHOUSE licensee)
\# To date, only minimally affected by PWSCC
0 Before start-up

Table 2-2 - Chronological list of pulled tubes from Doel 2 steam generators

Date of extraction	Number of pulled tubes	Location of pulled tubes	Purpose of extraction	Reference of pulled tube report (see notes)
JAN 1980 (54 months operation)	2	SG A Hot Leg R14C72, R16C72	Evaluation of primary side initiated cracking. Special shutdown for tube extraction	1
DEC 1982*	2	SG A Hot Leg R13C16, R27C49	1) Evaluation of IGSCC in the tubesheet crevice	2
MAR 1983* (70 months operation)	3	R17C85, R28C32, R26C50	2) Evaluation of the primary side roll transition cracking and the repair measures applied (tube expansion beyond original roll transition and mini-sleeves)	
SEP-OCT 1983 Normal outage (74 months operation)	9	SG A Hot Leg 5 sent to Babcock & Wilcox R06C33, R15C54 R15C63, R16C45, R17C43 4 sent to SCK/CEN Mol R10C58, R15C46, R17C45, R18C32 for examination	Purpose of the analyses : B & W : Determine origin of cracking CEN : 1) Evaluation of 3 minisleeved tubes subsequently stress relieved 2) Evaluation of one tube presenting a secondary side indication above the roll transition	3 4
AUG-SEP 1984 Normal outage (84 months operation)	10	SG A Cold Leg R10C51, R14C55, R06C34, R11C41, R18C66, R15C59, R13C65, R14C24 + 2 tubes non examined R17C52 and R11C72	Sampling for evaluation of cold leg tubes condition	5

* Same plant outage

Table 2-2 - Chronological list of pulled tubes from Doel 2 steam generators

(continued)

Date of extraction	Number of pulled tubes	Location of pulled tubes	Purpose of extraction	Reference of pulled tube report (see notes)
AUG-SEP 1986 Advanced refueling outage (103,5 months operation)	2	SG A Hot Leg	Evaluation of 2 kiss sleeved tubes	
DEC 1986 (105,5 months operation)	4	SG A Hot Leg R18C61, R18C51 + 2 tubes non examined	Evaluation of Ni electroplated tubes by LABORELEC/FRAMATOME	6 7
JUL 1987 Advanced refueling outage (110 months operation)	3 2	SG A Hot Leg R10C62, R21C59, R21C65 SG B Hot Leg R19C14, R20C75	Evaluation of Ni electroplated tubes by LABORELEC/FRAMATOME	7

Table 2-3 - Chronological list of pulled tubes from Doel 3 steam generators

Date of extraction	Number of pulled tubes	Location of pulled tubes	Purpose of extraction	Reference of pulled tube report
NOV 1983 Normal outage (14 months operation)	3	SG R Hot Leg R10C86 SG B Hot Leg R15C29, R33C36	Phenomenon Evaluation	8
JUN 1986 Normal outage (42 months operation)	2	SG B Hot Leg R23C23, R27C52	Characterization of preexiting cracks one year after the shot-peening treatment	9

ROLL TRANSITION CONFIGURATION

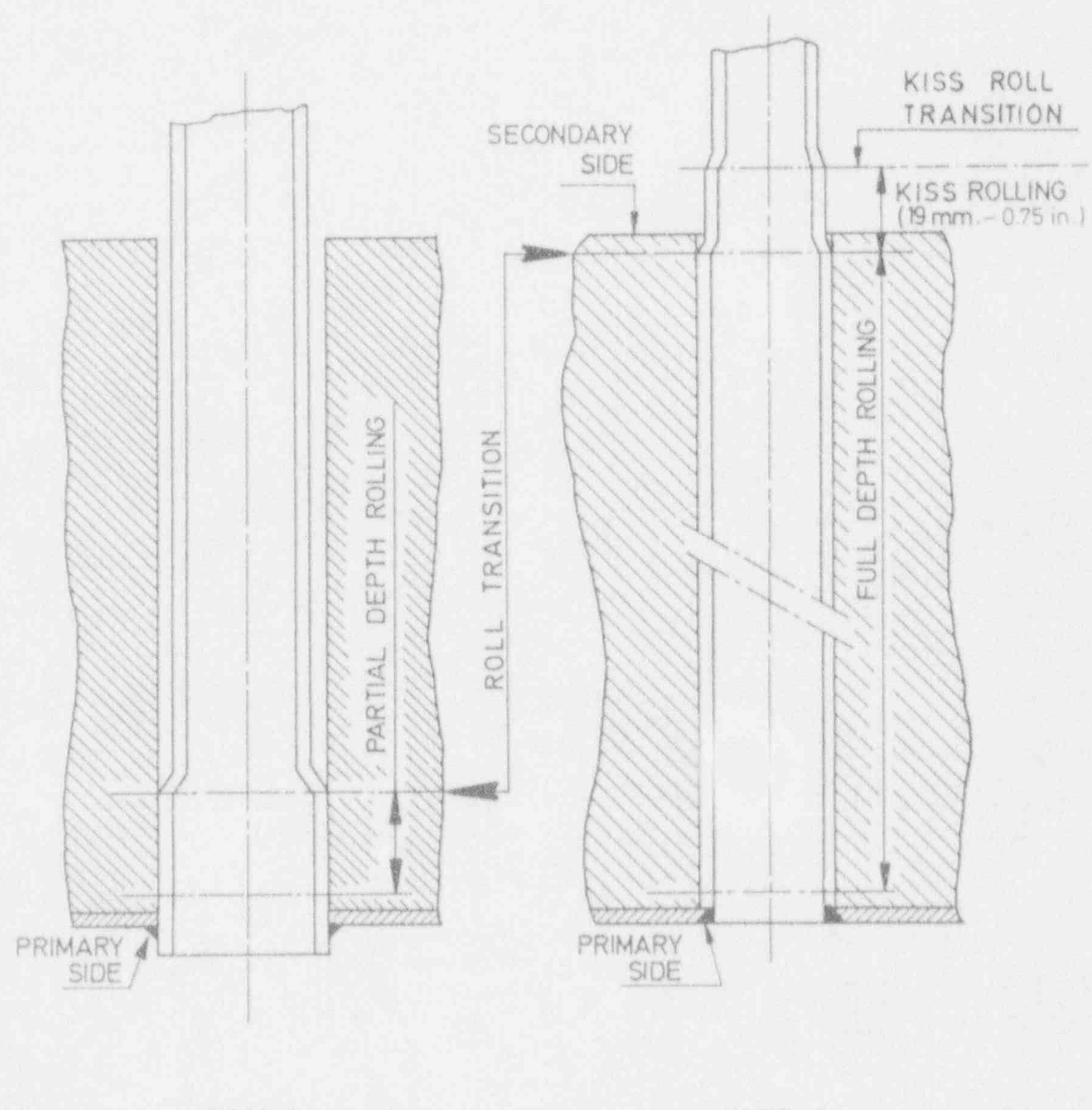

Figure 2 - 1

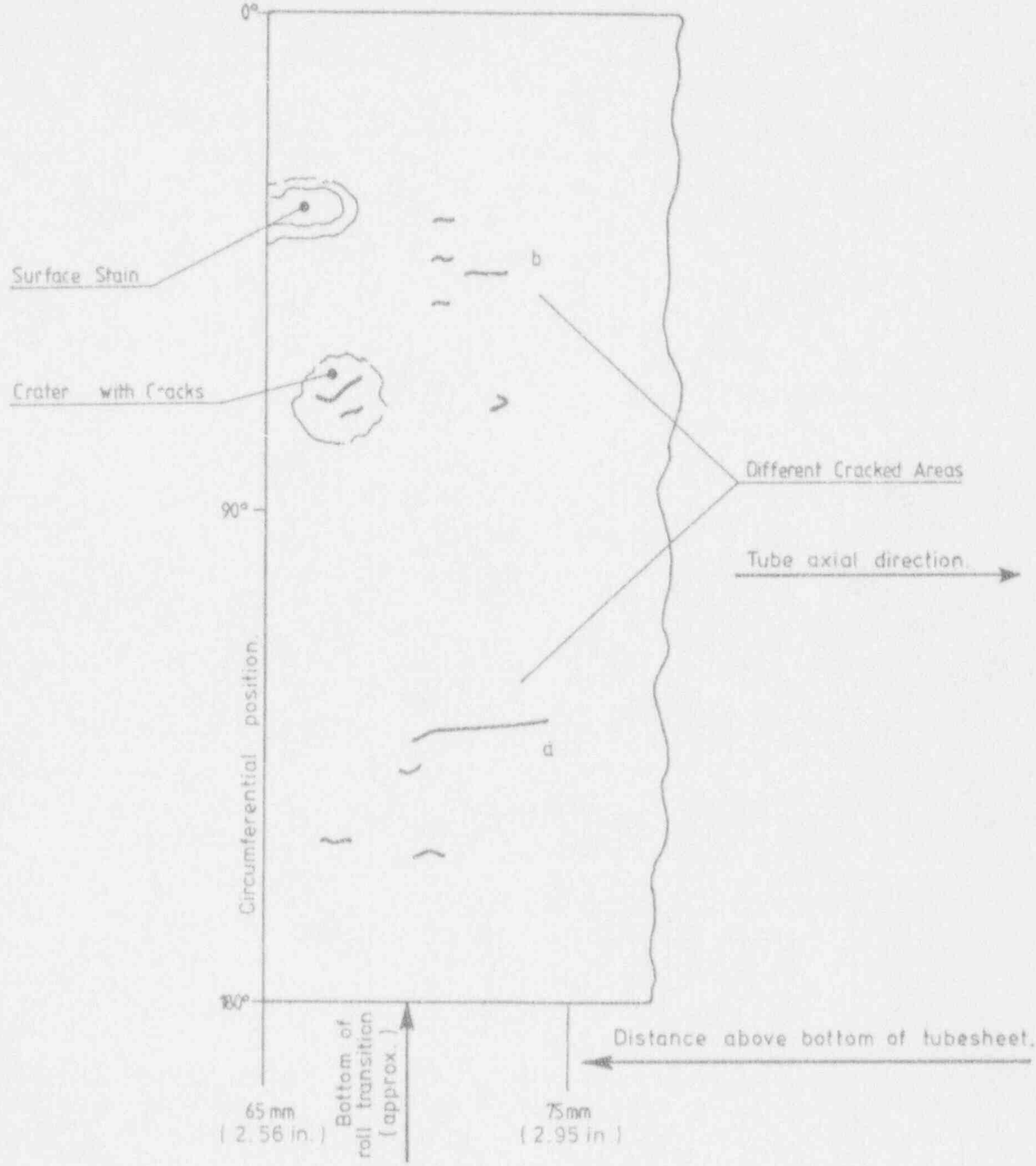

DOEL 2. Tube R 14C 72 pulled from coldside.
Schematic view of inner surface longitudinal cracking.
(Longest crack is 4 mm - 0.158 in.)

Fig. 2-2

DOEL 3 SG-B. - Tube R 23-C 23.

AREA OF DEFECTS 17.

INSIDE SURFACE AFTER FLATTENING AND 120° BENDING.

SECTION 1

Fig. 2 - 3

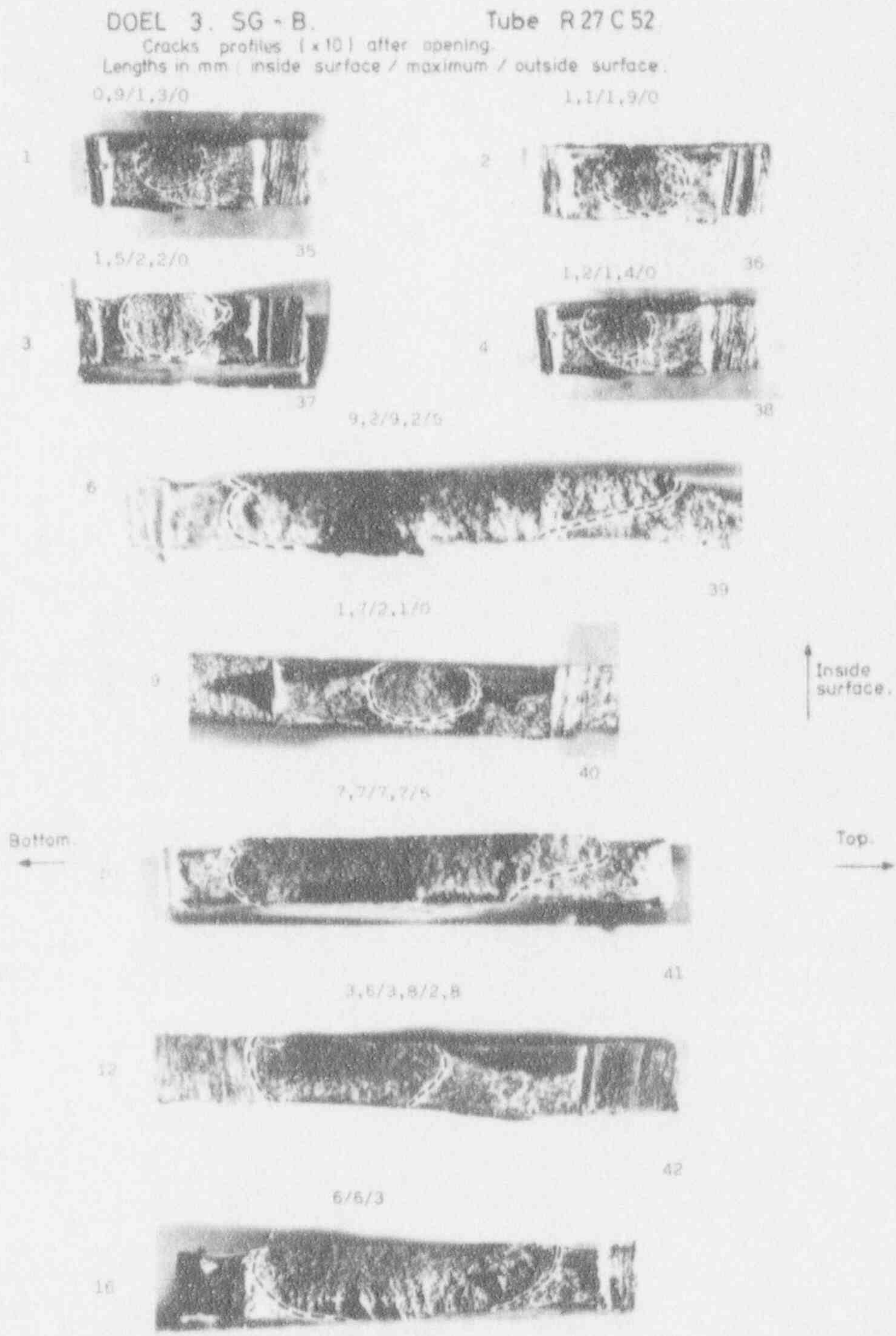

DOEL 3. SG - B.
Tube R 27 C 52
Cracks profiles (x 10) after opening.
Lengths in mm (inside surface / maximum / outside surface.
0,9/1,3/0
1
35
1,1/1,9/0
2
36
1,5/2,2/0
3
37
1,2/1,4/0
4
38
9,2/9,2/5
6
39
1,7/2,1/0
9
40
Inside surface.
Bottom.
Top.
41
3,6/3,8/2,8
12
42
6/6/3
16
43

Fig. 2 - 4

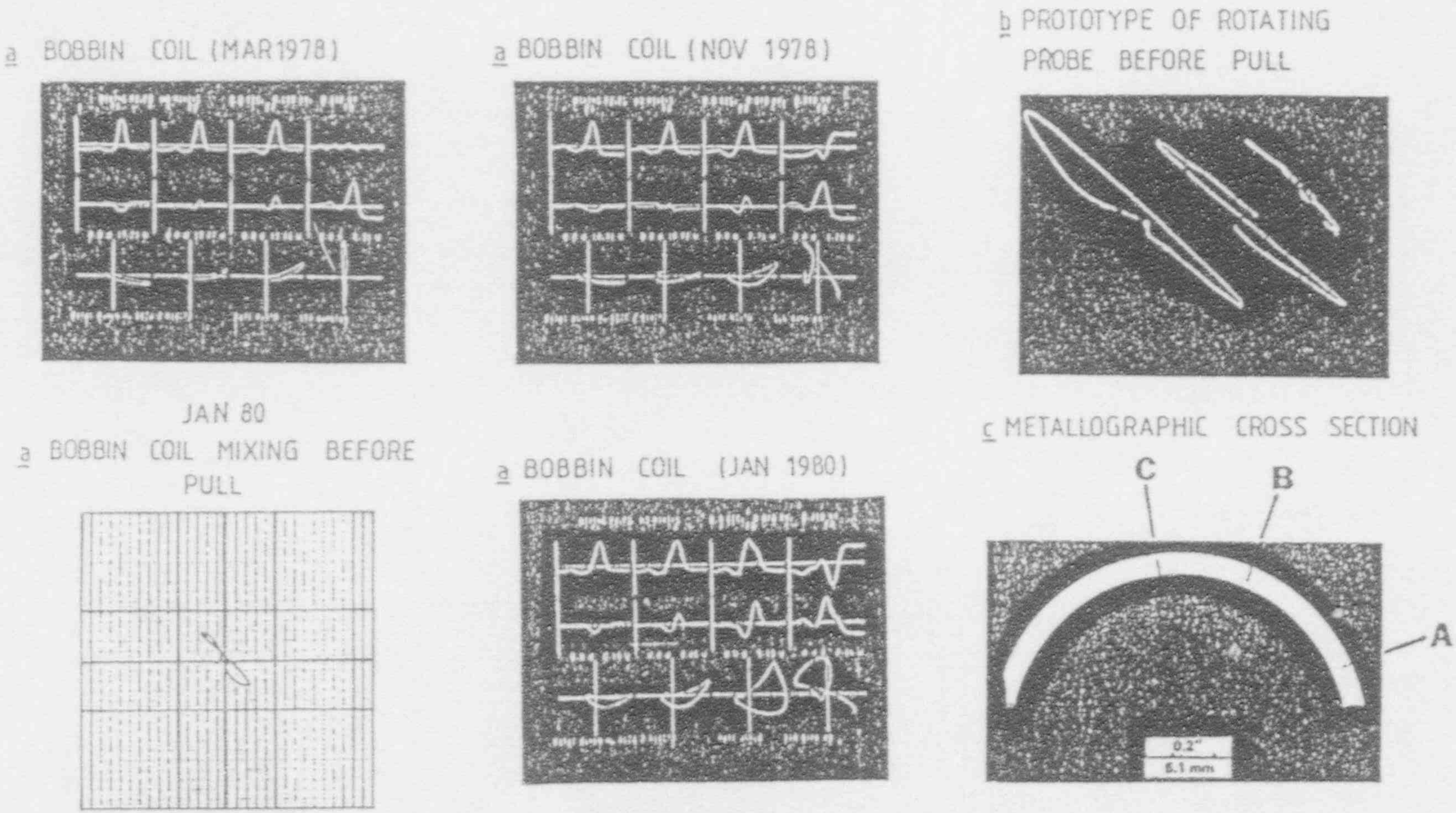

Fig. 2-5 N.D.E. AND METALLOGRAPHIC EXAMINATION OF THE PULLED TUBE R14C72 (DOEL 2 - JAN 80)

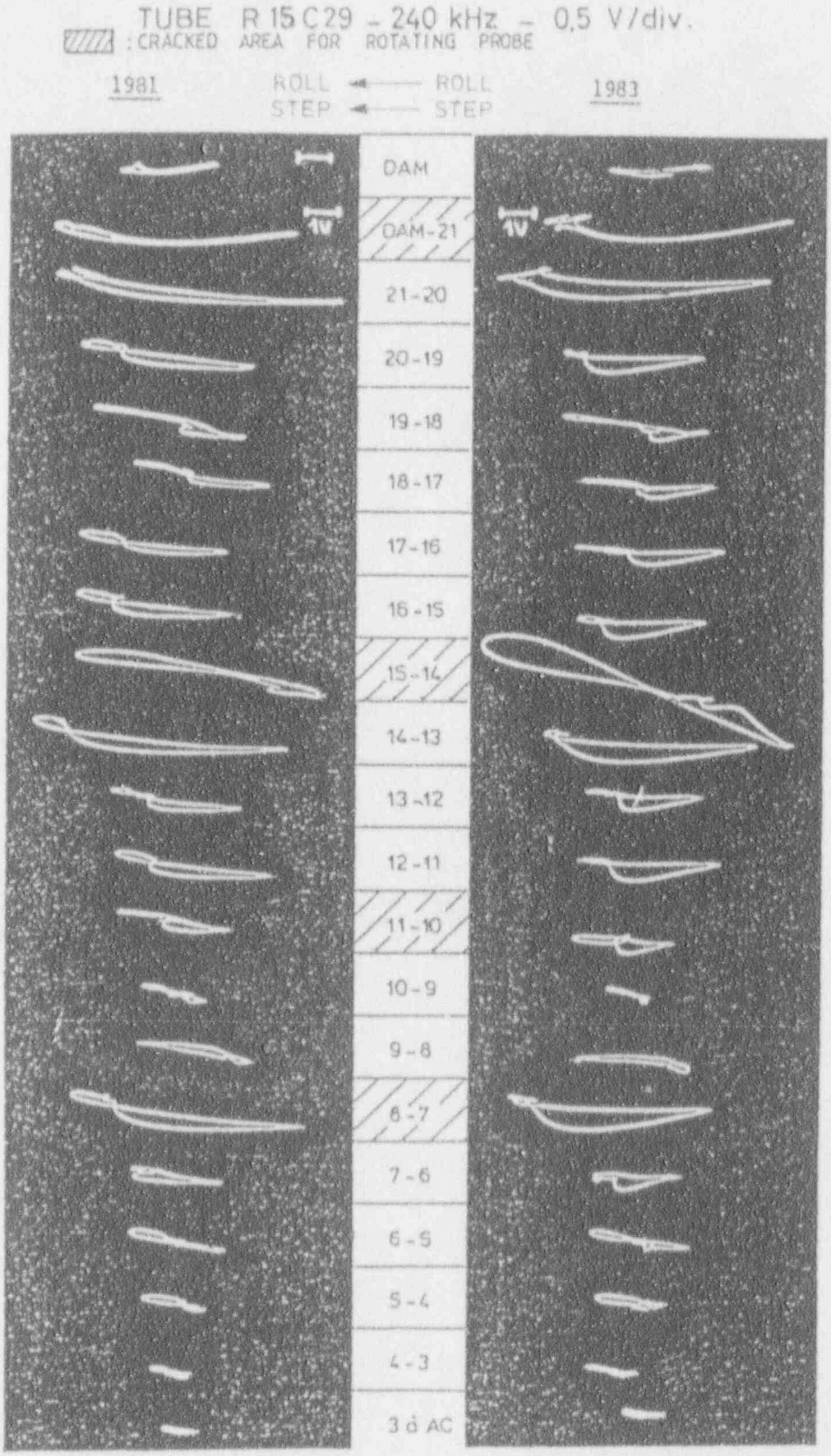

Fig. 2-6 BOBBIN COIL EXAMINATION OF THE EXPANSION AREA OF THE PULLED TUBE R15C29 (DOEL 3 - 1983)

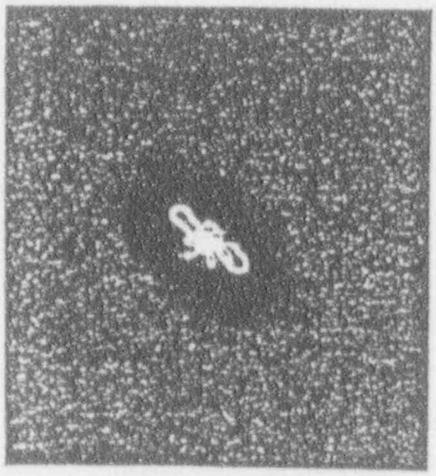

ROLL 21 - DAM
240 KHz
100 mV/div
ONE LONGITUDINAL CRACK
- 2 mm length (0.079 in.)
- 90 %

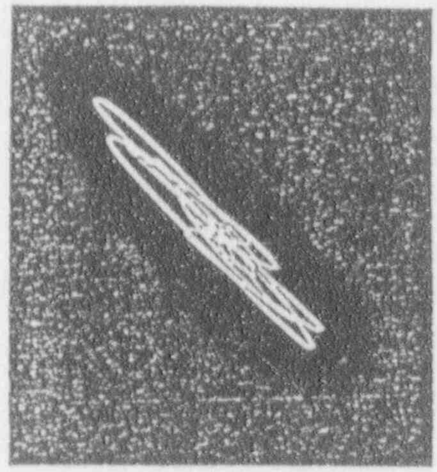

ROLL 14 - 15
240 KHz
200 mV/div
SEVERAL CRACKS
- LONGITUDINAL
- CIRCUMFERENTIAL
- BRANCHED
- 5 mm length - 100 % (0.197 in.)
- AREA BROKEN DURING TUBE PULL

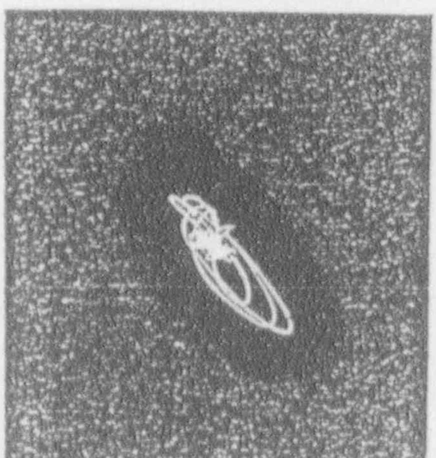

ROLL 10 - 11
240 KHz
200 mV/div
FOUR LONGITUDINAL CRACKS
- 2 mm length (0.079 in.)
- 100 %

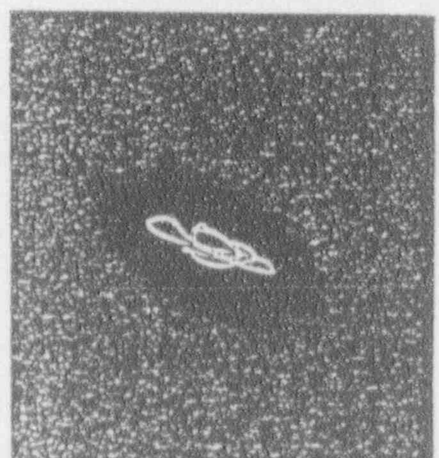

ROLL 7 - 8
240 KHz
200 mV/div
FIVE LONGITUDINAL CRACKS
- 4 mm length (0.158 in.)
- internal ~60 %

Fig. 2-7 ROTATING PROBE EXAMINATION OF THE EXPANSION AREA OF THE PULLED TUBE R15C29 (DOEL 3 - 1983)

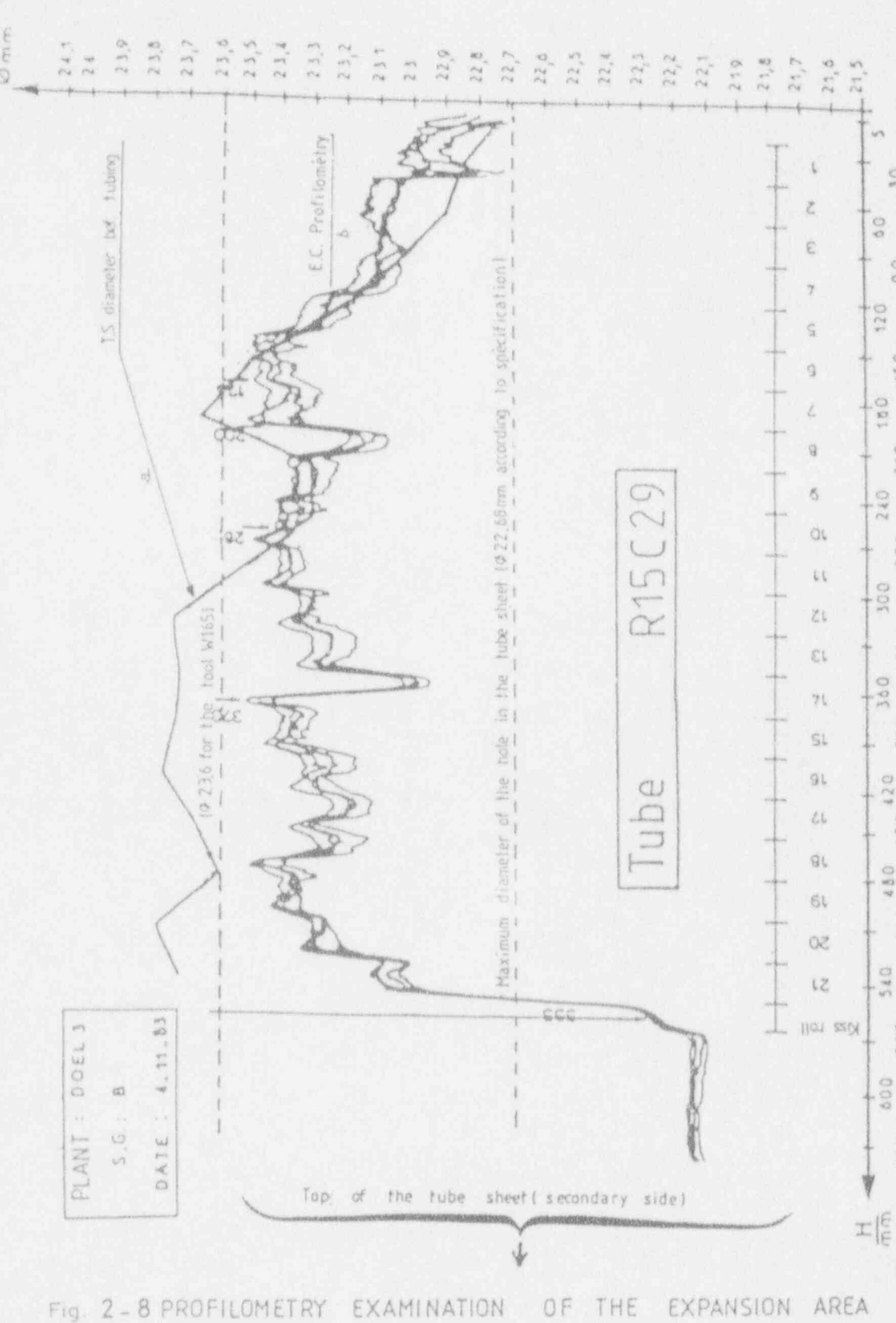

Fig. 2-8 PROFILOMETRY EXAMINATION OF THE EXPANSION AREA OF THE PULLED TUBE R15C29 (DOEL 3 - 1983)

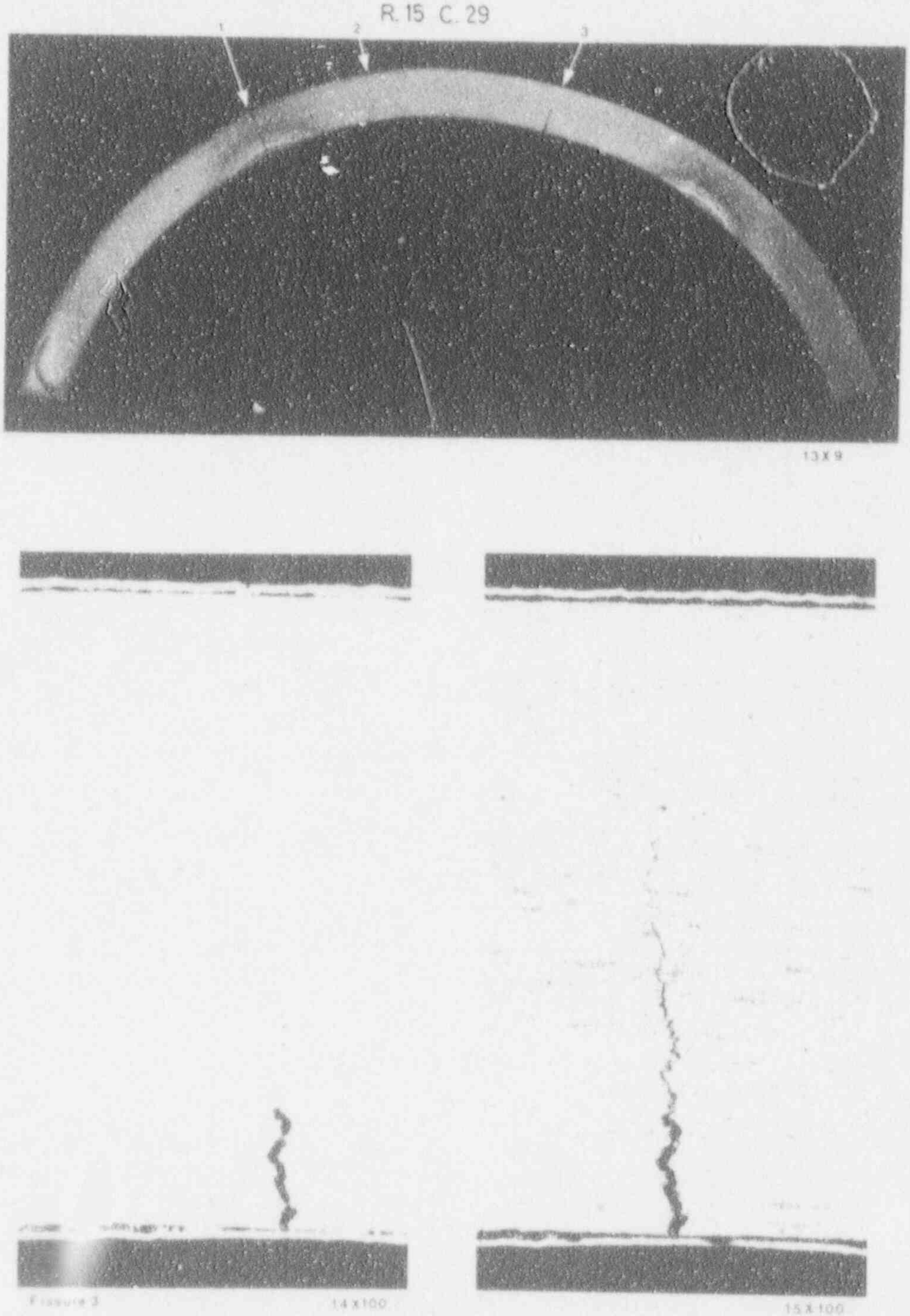

Fig. 2 - 9 METALLOGRAPHY CROSS SECTION OF ONE DEGRADED AREA OF THE TUBE R 15-C 29 PULLED FROM DOEL 3

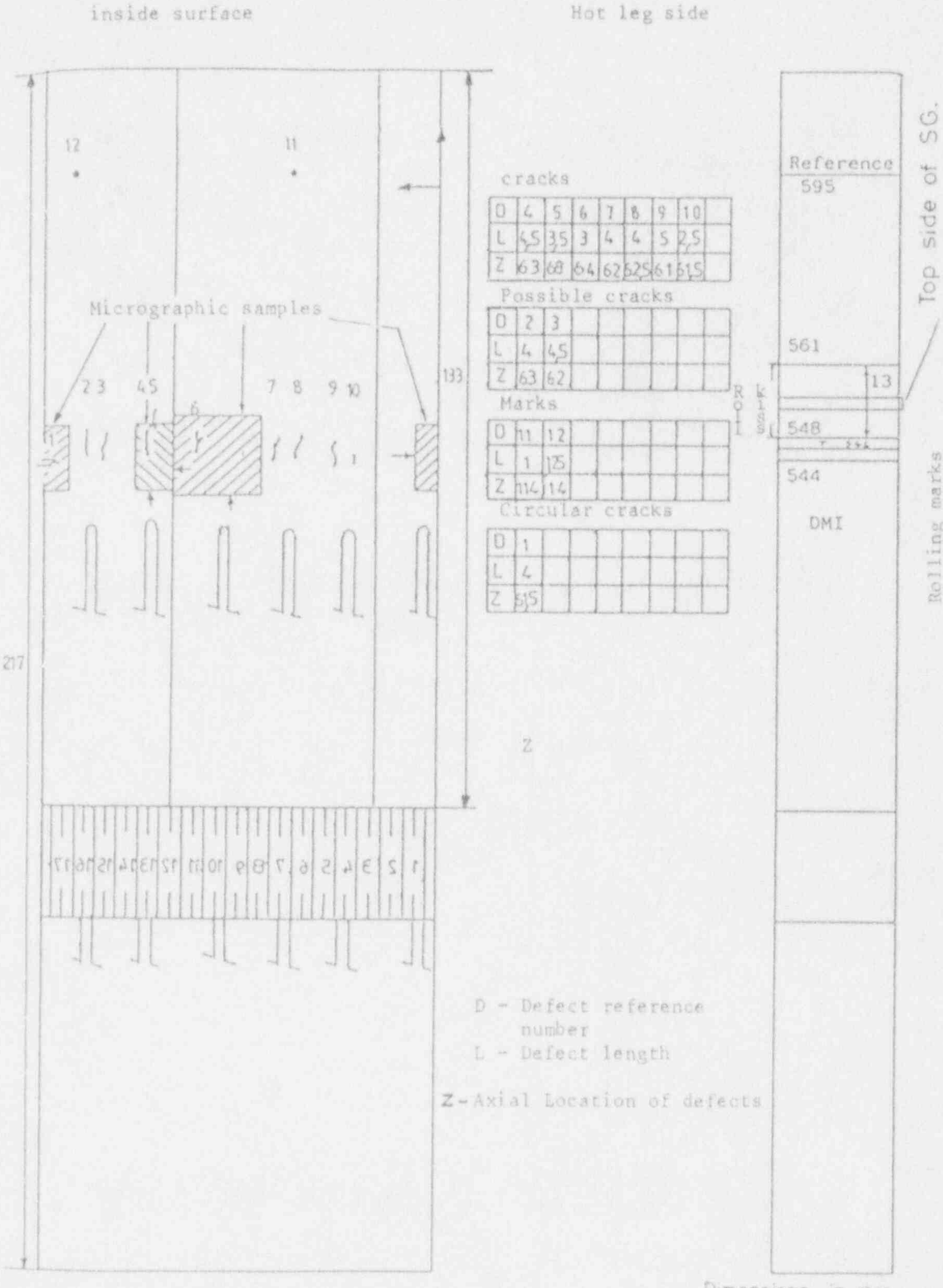

cracks

D	4	5	6	7	8	9	10	
L	4,5	3,5	3	4	4	5	2,5	
Z	63	68	64	62	62,5	61	61,5	

Possible cracks

D	2	3						
L	4	4,5						
Z	63	62						

Marks

D	11	12						
L	1	1,25						
Z	114	14						

Circular cracks

D	1							
L	4							
Z	51,5							

Fig. 2-10 TUBE FROM DOEL 3, S.G.-B. — LOCATION OF DEFECTS.
TUBE P.23 C.23

DOEL 3. SG-B. – Tube R.23-C.23.

INSIDE SURFACE AFTER FLATTENING TEST.

Number above the cracks : reference number for visual exam.
Number under the cracks : length of crack in mm.

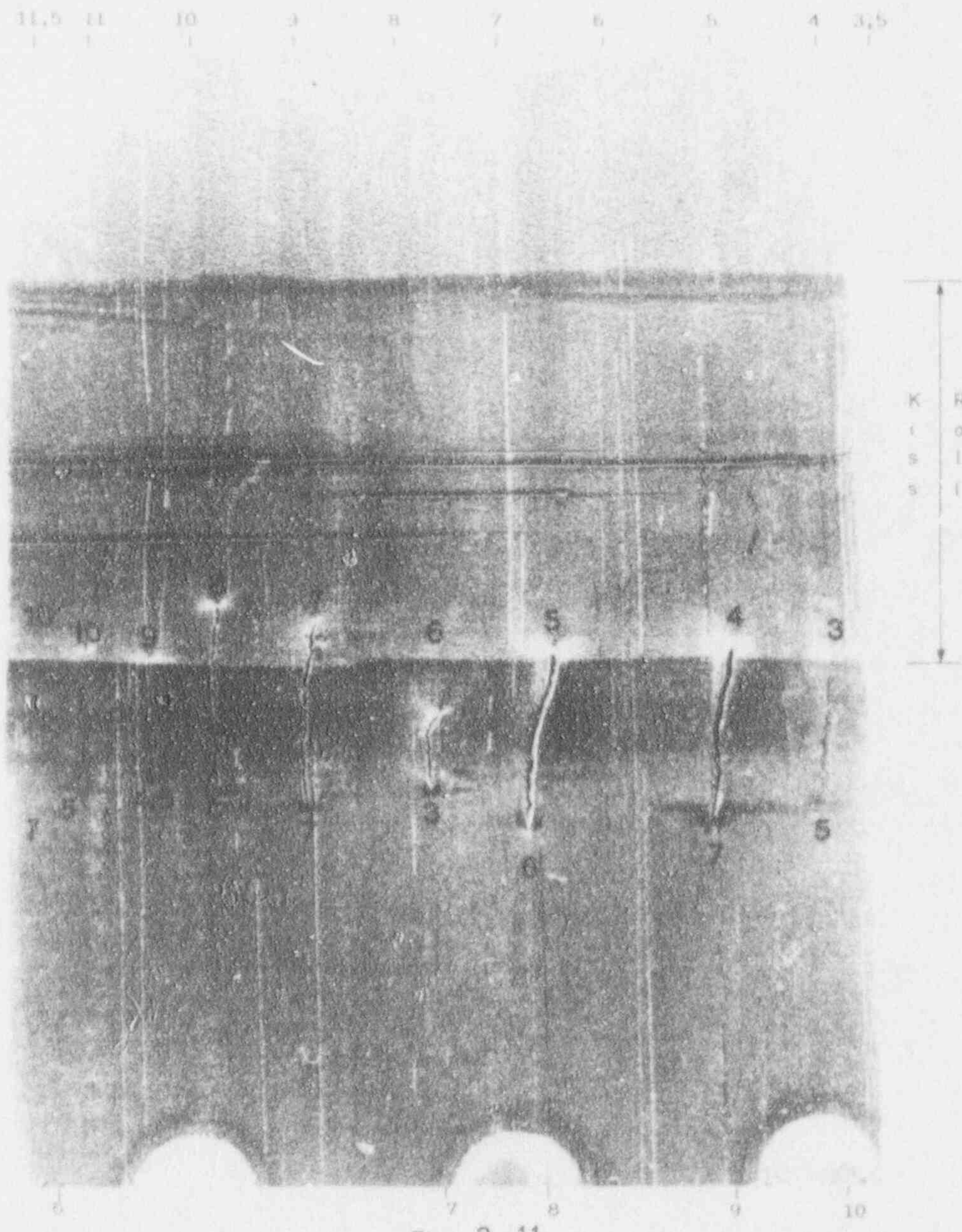

Fig. 2-11

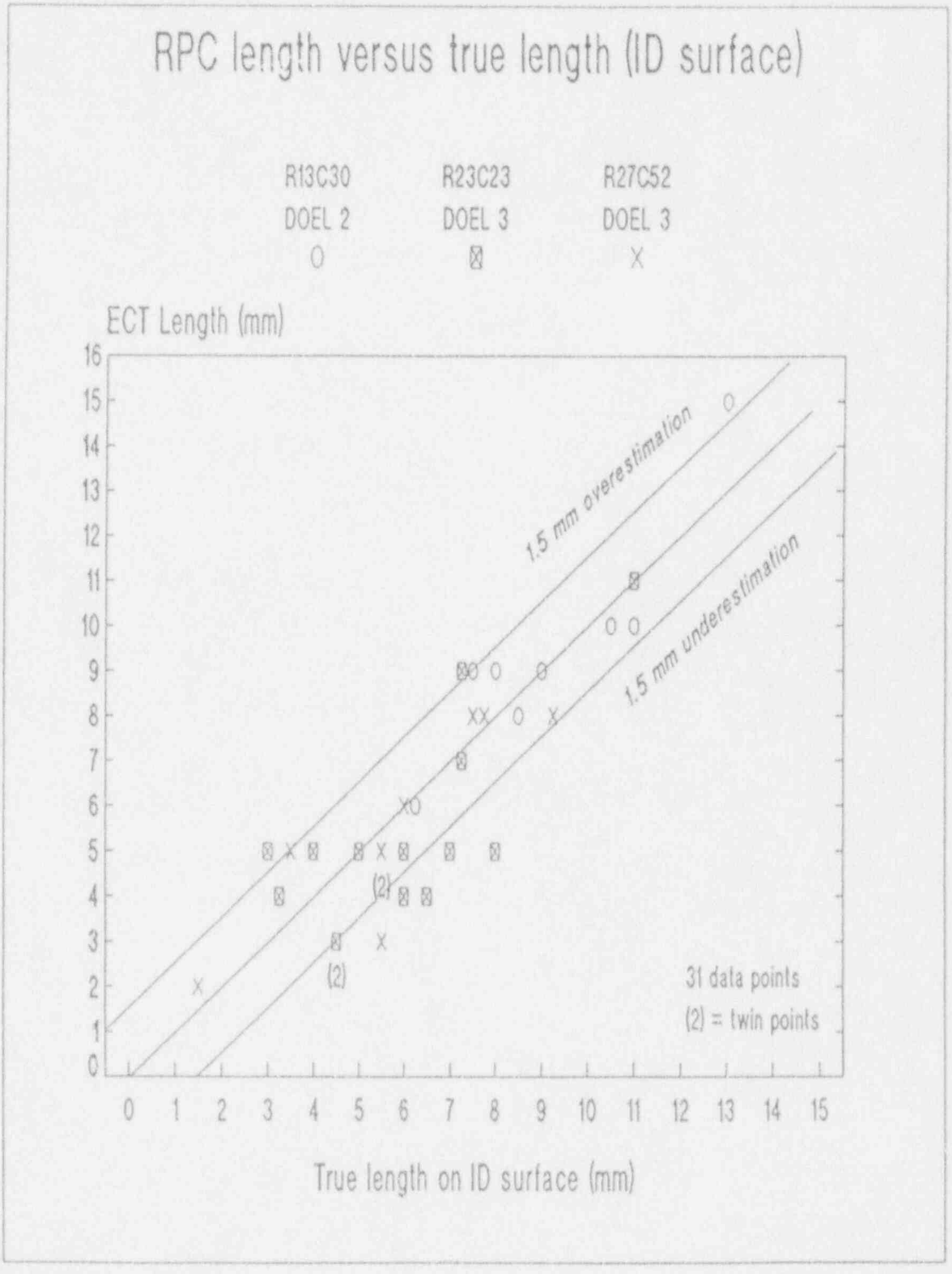
RPC length versus true length (ID surface)
R13C30
DOEL 2
O
R23C23
DOEL 3
R27C52
DOEL 3
X
ECT Length (mm)
0
1
2
3
4
5
6
7
8
9
10
11
12
13
14
15
16
1.5 mm overestimation
1.5 mm underestimation
(2)
(2)
31 data points
(2) = twin points
0
1
2
3
4
5
6
7
8
9
10
11
12
13
14
15
True length on ID surface (mm)

Fig. 2 -12

Section 3

SAFETY PHILOSOPHY

3.1. HISTORICAL BACKGROUND

Basically, Belgian Utilities are committed to follow the U.S. nuclear safety rules; however duly justified deviations (or interpretations) can be obtained on a case by case basis. In the plant Technical Specifications defining the SG inspection requirements, the usual "40 % plugging limit" is implemented but an allowance is made for alternative criteria based on Regulatory Guide 1.121. (1).

It is useful to recall the origin of the 40 % plugging limit. This requirement originates from the first generic problem encountered with SG's which was a uniform loss of thickness through corrosion, i.e. wastage in the sludge pile. Based on a factor of safety not less than 3 to be maintained under normal service conditions, the required minimum tube wall thickness was 40 %. This value was increased to 60 % in order to have an additional allowance to cover uncertainties regarding measurement of the flaw size and its growth between two consecutive inspections. The 60 % minimum wall thickness meant that tubes with thinning of 40 % or greater were required to be plugged.

Generalizing this same criterion to other types of more local flaws (cracks in particular) can be excessively conservative. The ASME code (3) stipulates the 40 % criterion, but only for flaws in the external skin of the tube (art. IWB-3521.1); moreover further evaluation of defects exceeding the allowable indication standards is possible (art. IWB-3630) "by analyses acceptable to the regulatory Authority having jurisdiction at the plant site".

On these bases the 40 % limit was considered by BELGATOM not to be mandatory in Belgium and alternate approaches were investigated.

The Westinghouse P*, F* and L* approaches (4), (5) were reviewed :

. P* is a criteria which allows cracks to be ignored below a certain distance (P*) below the top of tubesheet based on interferences above the tube preventing tube pull out.

. F* is a criteria which allows cracks to be ignored below a certain distance (F*) from the top of tubesheet, or bottom of roll transition, whichever is lower, based on resistance to tube pull out generated by tube expansion in the tubesheet.

. L* is a criteria which allows axial cracks to exist above the P* or F* distance, but below the L* distance from the top of the tubesheet or bottom of the roll transition, whichever is lower, based on the limited effect on primary to secondary leakage of such cracks.

The three approaches were not considered viable as they avoid the use of the 40 % limit within the tubesheet but maintain it unchanged for the roll transitions (and some depth below the secondary side of the tubesheet) where practically all of the PWSCC cracks are actually located . These latter cracks (above the top of the tubesheet) are also the only significant ones for safety and reliability.

The Leak Before Break (LBB) philosophy was also considered (6), (7). According to this approach "a flaw that would be critical (unstable propagation, leading to Steam Generator Tube Rupture (SGTR)) under accidental conditions (such as Steam Line Break or Feed Water Line Break) would be reliably detected under normal service conditions (i.e. under a much lower differential pressure) by a leak exceeding the Technical Specification allowable limit (79 l/hr or 0.35 gpm)".

Belgatom considers LBB to be an instrinsically safe behavior usually, but not always, exhibited by the tube material. Among the known exceptions, the following are worth mentionning :

- occasional Steam Generator Tube Rupture (SGTR) without prior notice by any measurable leak (such a case was experienced in a first row U bend of a Doel 2 SG in 1979),

- in-service low leak rate (below the expected level from laboratory experiments) of relatively long axial cracks (possibly due to clogging by crud or precipitates),

- aligned axial crack components (separated by small axial or offset ligaments), with an overall critical length, without detectable leakage through the components.

One could also imagine long and deep (but not thruwall) cracks in either axial or circumferential directions (possibly initiated by surface scratches).

While some of these exceptions may be dealt with through use of probabilistic assesments, there is an associated trend to lower the allowable in-service leak rate (7). This latter consequence is believed to be unduly constraining to the plant operator (possible increase of unscheduled shutdowns).

Moreover, even relatively large leaks cannot necessarily be located and removed. Such a case has been recently experienced by a Doel 3 SG, where a 20 to 30 l/h (0.09 to 0.13 gpm) leak could not be located by using all possible detection methods including the Helium leak test. Plant operation was eventually resumed and the leak remained practically unchanged during a full operating cycle (1987-88). After plugging/sleeving about 80 tubes (with the largest detected roll transition defects) during the June 88 scheduled outage, the SG still evidenced the same leakage after start up. At the date of writing (January 1989), the plant is still operating under these conditions.

On the other hand, extensive hardware and software developments by LABORELEC allowed generalization of RPC use for ECT inspection (data acquisition and analysis of all roll transitions can be performed in less than 2 days per SG). This capability of reliably sizing the cracks (without any penalty on plant down-time) led to the decision to develop new plugging criteria derived from the R.G.1.121 type philosophy.

3.2. CRACK SIZE MEASUREMENT PRINCIPLES

Conventional "bobbin coil" ECT techniques have a low potential for detection of PWSCC; based on the extensive experience of LABORELEC in using both the "bobbin coil" and the "Rotating Pancake Coil" (RPC) in roll transitions it can be concluded that several cracks (about 5) of significant length (about 4 mm - 0.158 in) and depth (close to 100 %) are required, in the same tube cross section, to achieve reliable detection by the "bobbin coil"; otherwise "distorted signals" may be observed but do not necessarily correlate with actual cracking.

The sizing capability of the "bobbin coil" is even poorer; phase angle measurements are not likely to yield realistic defect depths when there are several cracks in the same section, while length measurements suffer from an inaccurate knowledge of axial probe location (especially in the roll transition), with a resulting uncertainty in the order of 5 mm (0.2 in).

On the contrary, RPC has the potential for sensitive detection and accurate length sizing of individual cracks; details of the specific LABORELEC methodology are given under sections 5 and 6. It should be noted that practically all of the cracks detected by RPC appeared to be close to 100 % through wall. This has been further confirmed by destructive examination of tubes pulled from Doel 3 (section 2).

Thus, without undue conservatism, any detected axial crack is assumed to be actually through-wall and is evaluated as such. Therefore, only the axial length needs to be measured and documented. Most of the cracks to be found in roll transitions are in the axial direction. Little circumferential cracking has been evidenced; this is fortunate as the corresponding detection capability of even the best available RPC method is still rather poor (it is difficult to mix out the similar discontinuities associated with the profile transition and the outlet of the magnetic tubesheet). LABORELEC is developing a substitute ultrasonic method which holds the promise of sensitive detection and reliable sizing. As such a method might be significantly more time consuming than ECT, there is an ongoing parallel development of the RPC method aimed at the reliable detection of circumferential cracks of size close to the plugging limit. However, "false calls" would not be precluded and the detected indications would finally be confirmed and sized by U.T.

Until further experience is gained about the depth sizing capability of ultrasonics, detected circumferential cracks will also be assumed to be through-wall and evaluated as such. This may prove to be over conservative; if this is the case, plugging criteria based on both depth and length of defect will be established when the NDT performance warrants this.

3.3. CRITICAL SIZE CALCULATION PRINCIPLES

Regulatory Guide 1.121 allows the establishment of acceptable flaw sizes based on the following safety factors (with respect to tube bursting) :

- 3 under normal service conditions,
- a value consistent with the limits set by the ASME III Code (3) art. NB-3225, for accidental conditions (a LOCA, steam line break, or feedwater line break concurrent with the SSE).

R.G. 1.121 does not specify whether :

- the mechanical and geometrical characteristics of the tubes must be taken at their nominal or most unfavourable value (minimum for UTS, YS and thickness, maximum for the diameter, etc.). The frequent reference to the design code (ASME III) seems to imply this unfavourable combination (see, for instance, article NB 3641.1);
- an additional margin must be applied to the dimension of the detected flaw (prior to comparison against the acceptable value) in order to account for :

  . the uncertainty relating to the NDE measurement method,

  . the flaw growth over the period of service until the next inspection.

  The requirements of R.G. 1.83 and of ASME XI (together with the historical basis of the 40 % criterion) suggest these should be taken into account.

Also the following interpretations (considered to be fully justified) are used in order to establish a concrete set of criteria :

- Because of the high ductility of Inconel, tube rupture is preceded by considerable plastic deformation (high COD - Crack Opening Displacement - at both ends of a crack, bulging, etc) so that the "secondary" stresses (as defined by ASME) are relieved and can be neglected (whereas they play a major part in the stress corrosion or fatigue processes). The only "primary" type stresses are those resulting from the differential pressure and, possibly, from the inertial effects induced by a steam line break (SLB) or a feed water line break (FWLB) concurrent with the Safe Shutdown Earthquake (SSE). In case of S.L.B. or F.W.L.B., it is clear that the effects of the steam blowing out the SG by the ruptured pipe may be quite important on the tubes located near the discharging nozzle. On the other hand, the portion of tubes of concern in this study, located just above the tubesheet is far from both nozzles. So, the stresses induced are quite low and probably of the same magnitude as SSE stresses. Those inertial induced stresses are also neglected because

. their value is comparatively low (at the tube sheet level)

. the current evolution of the ASME code (seismic design of piping) tends to classify these also in the "secondary" type.

. the dynamic loads induce essentially tube bending and the resulting stresses do not significantly interact with axial flaws.

However for circumferential cracks the stresses induced by differential expansion between the hot and cold legs could not be negligible despite the "secondary" character usually assigned to thermal stresses. Indeed, the axial deformation on the tube at the flaw level remains low compared with the displacement that would be needed to relieve the stresses. Nevertheless, these stresses will be neglected hereafter, because

. they are low when compared against those resulting from pressure,

. they are compressive in the hot leg, i.e. where practically all the stress corrosion cracks occur:

- In compliance with the spirit of ASME III (and in strict conformity with article IWB 3612 of ASME XI) the safety factors are taken as :

  . 3 for normal and upset conditions (service levels A and B of ASME)

  . √2 for emergency and faulted conditions (service levels C and D of ASME)

  These factors are intended to apply to loads (in practice, the differential pressure). However, Tables 4-1 and 4-2 as well as Figure 3-1 show that at pressures 3 times or √2 times the normal pressure, the margins in terms of flaw size (ratios of critical crack length to actual length) are higher than these values (3 and √2) for axial cracks, and considerably lower for circumferential cracks. This does not appear to be reasonable as the actual uncertainty is more related to size than to load.
  Therefore, these safety factors have been applied to the flaw length rather than to the pressure.

- For axial cracks in the roll transition area, the reinforcing effect of the tube sheet is taken into account based on results of the BELGATOM experimental program

- For circumferential cracks located at the same level, a favourable effect results from the proximity of the Flow Distribution Baffle (FDB) or other next support plate even if, due to manufacturing tolerances and in-service thermal gradients, this leads to some bending of the tube, which may tend to open up the circumferential crack.
  Indeed :

  . the bending stress induced by a displacement at FDB level is of the "secondary" type and therefore, may be neglected in the evaluation of the critical size (whilst this stress may be very significant in crack initiation and propagation);

  . as the instability can be reached only by sufficient deformation of the cracked section (and particularly by considerable angular deformation), the presence of the FDB constrains such deformation, thereby raising the value of the pressure required to initiate instability. This effect is illustrated in Figure 3-2.
  The favourable effect of the FDB is also taken into account based on results of the BELGATOM experimental program.

The detailed calculations are covered by section 4.

3.4. PLUGGING CRITERIA PRINCIPLES

The following is a summary of the procedure which is further detailed under section 4.

- Any crack detected is evaluated as if it were a through-thickness crack; for axial cracks partially engaged within the tube sheet, the crack length to be considered is that extending above the last tube contact point with the tubesheet (upper level of rolled area).

- The average critical length is calculated on the basis of

  . the nominal tube geometry (diameter, wall thickness);

  . the average mechanical properties of the material (Yield Stress, Ultimate Tensile Stress)

  for both the normal and accidental service conditions.

- The minimal critical length is calculated on the basis of :

  . the most unfavourable tube geometry (max. diameter and min. thickness);

  . the most unfavourable combination of the material properties (minimum of the sum YS + UTS);

  . the accidental service conditions.

- All mechanical properties are those measured at 343°C (650°F) on the various batches used in the considered SG.

- For cracks located in the roll transition area, credit is taken for the reinforcing effect of the tubesheet (axial cracks) or the constraining effect of the nearby support plate (circumferential cracks).

- The allowable value of the measured crack length is taken equal to the lowest of the two following evaluations :
  FIRST : <u>best estimate, with safety factor</u>
  + the average critical length is divided by the R.G.1. 121 safety factor, for both the normal and accidental conditions.
    The lowest resulting value is retained.
    The allowable length is obtained by deducting the average value of :

    . sizing inaccuracy resulting from the inspection method,

    . the propagation (in length) of the flaw until the next inspection.

  SECOND : <u>most conservative estimate, without safety factor</u>
  + the minimal critical length is considered
  + the allowable length is obtained by deducting the maximum effect of both sizing inaccuracy and crack propagation rate.

- The plugging limit is taken equal to the (lowest) allowable length, rounded off to the next higher mm.
  The whole procedure is summarized in Table 3-1.

3.5. INFLUENCE OF CRACK LOCATION ON PLUGGING REQUIREMENTS

The plugging requirements resulting from the above principles apply to

- axial cracks located (or extending, at least partially) above the top of the tubesheet

- circumferential cracks located either above or below the top of the tubesheet, but at an elevation such that disengagement of the tube from the tubesheet hole cannot be precluded in case of a complete circumferential severance and in the absence of any pull resistance from the expanded tube section.

This is consistent with the so called P* approach proposed by WESTINGHOUSE; the subsequent F* approach has not been adopted because of the uncertainties related to the actual pull strength developed by the upper roll steps.

There is no possibility of tube bursting from an axial defect, of any length, when entirely engaged in the tubesheet; thus no plugging limit is applicable to that case.

There is also no safety problem (and no plugging limit) for circumferential cracks located below the P* level.

3.6. CONSEQUENCES OF PROPOSED APPROACH

3.6.1. Inspection Requirements

The plugging/repair policy, as outlined above, implies large scale inspections by the rotating pancake coil (RPC).

Once a generic problem, like PWSCC in roll transitions, has been detected, and to the extent that crack lengths in excess of plugging criteria may be expected, a 100 % inspection of the degraded area (i.e. the roll transitions) is indeed a requirement; such an inspection has been performed in both the Doel 3 and Tihange 2 plants because of clear prior indication that crack lengths in excess of 15 mm (0.59 in) might be present.

This does not imply a 100 % reinspection after each cycle. Reinspection may be limited to those tubes with a crack length such that the maximum increase rate (mm/cycle) would allow them to reach the plugging limit; tubes previously uncracked need only be reinspected when they could reach this limit, on basis of a maximum initial length and propagation rate.

3.6.2. Generalization of the approach

Large scale inspection of a specific area affected by a particular problem does not imply any increase of the general basic inspection (performed with the "bobbin coil" EC technique and aimed at detecting unsuspected defects).

It is not intended to extend such base inspection above the present mandatory level of 3 % per SG and per year. However should any other degradation mechanism be evidenced, it would be handled in a way similar to the hereabove outlined PWSCC approach, such as :

- extension of the inspection sample to establish the (potential) generic nature

- inspection by a dedicated method (if required) of a tube sample of sufficient size to allow the establishment of a meaningful distribution curve of the relevant defect dimension(s)

- if and when the distribution curve shows dimension(s) in excess of plugging limit, the inspection would be extended to cover 100 % of the tube bundle area and of the tube length affected by the problem

- the plugging limit would be established along the same guidelines as for the PWSCC problem, using NDE uncertainty and defect propagation rates specific to the case under consideration.

REFERENCES

1. Regulatory Guide 1.121 "Bases for plugging degraded PWR Steam Generator Tubes" (draft August 1976)

2. Regulatory Guide 1.83 "In service Inspection of Pressurized Water Reactor Steam Generator tubes" Rev. 1 (July 1975)

3. ASME Boiler and Pressure Vessel Code (edition 1986)
Section III : Nuclear Power Plant Components
Section XI : In service Inspection

4. "Tubesheet region pluggihg criteria for full depth hardroll expanded tubes"
Westinghouse (September 1985) : private paper

5. "Safety evaluation by the office of nuclear reactor regulation related to amendment nº 59 to facility operating licence NPF-9 (and amendment 40 to NPF-17) - Duke Power Company - Mc Guire Nuclear Station, units 1 and 2" US NRC (August 1986)

6. "Analysis of leak-before-break for steam generator tubes"
J.F. LANG, V.K. CHEXAL, T.J. GRIESBACH and R.C. CIPOLLA (EPRI)
3rd Int. meeting on reactor thermal hydraulics, Newport, Rhode Island (October 1985)

7. "Tube performance at EDF 900 Me Units. An update
J. DE SURGY, J.P. MUTIN, R. SERRES - Nuclear Engineering International (January 1988)

8. "Flaw analysis in steam generator tubes (LBB concept as applied to S.G. tubes)"
J.P. HUTIN (EDF) and F. BILLON (FRAMATOME), 8th SMIRT conference postseminar, Varese/ISPRA (1985)

TABLE 3-1
PLUGGING LIMIT FOR SCC IN ROLL TRANSITIONS
BASIC PRINCIPLES

	BEST ESTIMATE WITH safety factor	MOST CONSERVATIVE ESTIMATE WITHOUT safety factor
CRITICAL LENGTH (thru wall crack)	AVERAGE value, on basis of . nominal tube geometry (diameter, wall thickness) . average of actual mechanical properties (YS, UTS) (*) . service conditions	MINIMAL value, on basis of . unfavourable tube geometry (max. diameter, min. thickness) . lowest material properties (min. of YS + UTS) (*) . accidental service conditions
SAFETY FACTOR (on length)	normal 3, accidental √2 → lowest value	1
ADDITIONAL MARGIN . sizing accuracy . propagation until next inspection	 average average	 maximum maximum
PLUGGING LIMIT	lowest value of $\frac{\text{CRITICAL LENGTH}}{\text{SAFETY FACTOR}}$ - ADDITIONAL MARGIN	

For cracks in ROLL TRANSITIONS, the plugging limit is increased to take credit from the constraining effect
- of tubesheet, for axial cracks
- of support plates, for circumferential cracks.

(*) mechanical properties measured at design temperature (650°F = 343°F) for all Inconel heats used in construction.

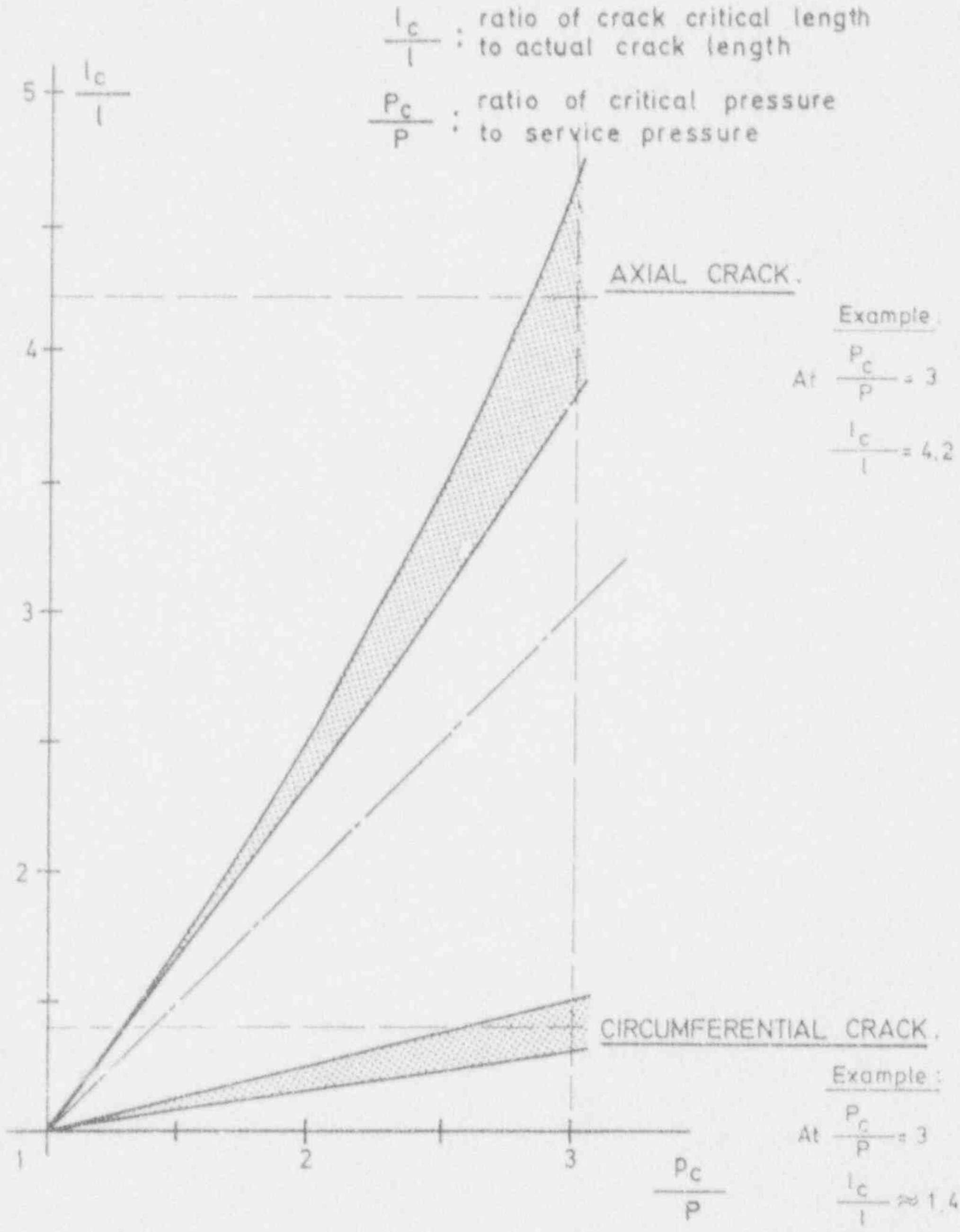

SAFETY MARGIN ON LENGTH

AS A FUNCTION OF

SAFETY MARGIN ON LOAD (pressure).

Figure 3-1

SCHEMATIC ILLUSTRATION OF INFLUENCE OF A F.D.B. OFFSET ON THE BURST OF A TUBE WITH 180° CIRC. CRACK.

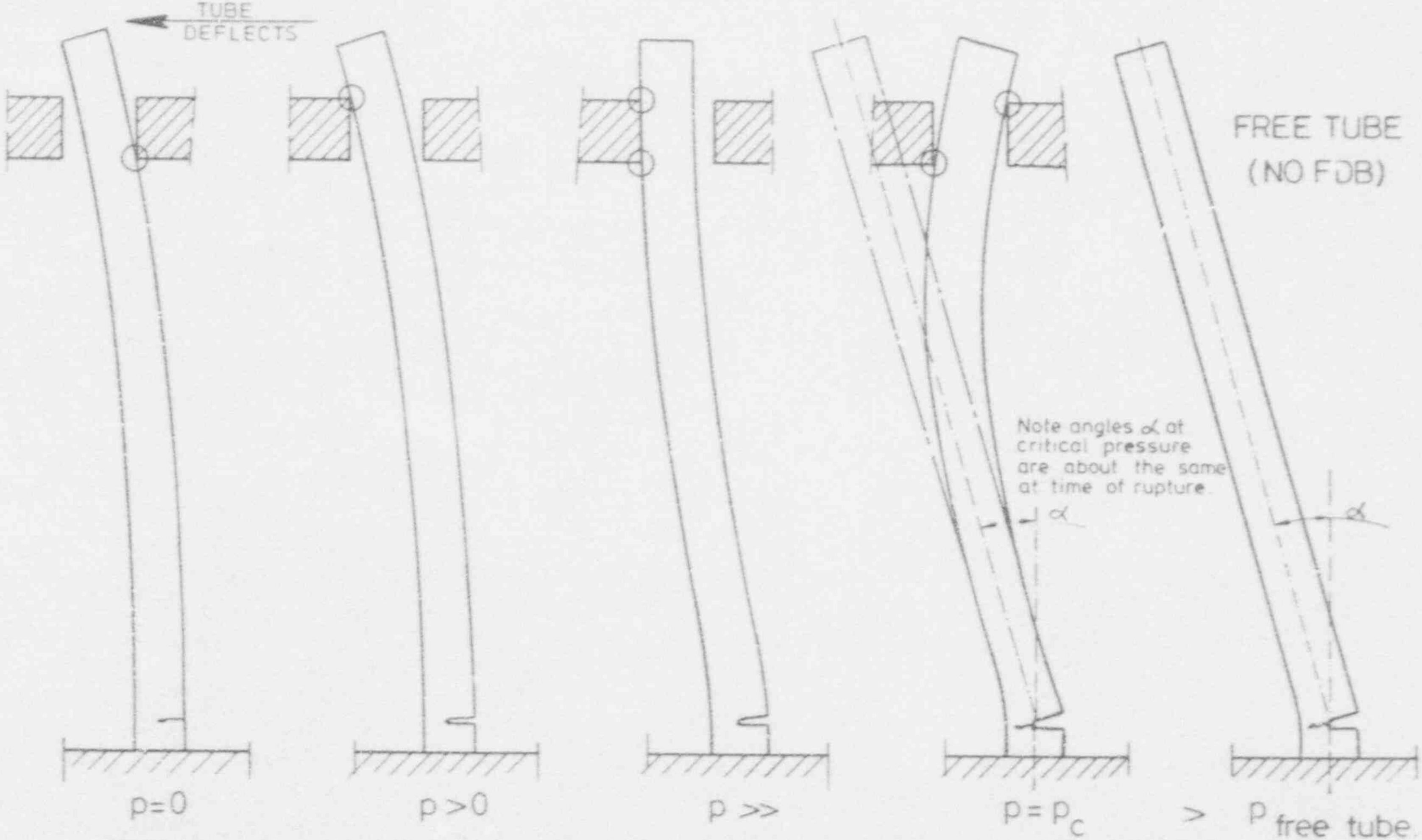

1.) Assumed initial offset condition of F.D.B.

2.) Effect of increased pressure.

3.) Effect of further pressure increase.

4.) Pressure reaches critical value.

5.) Critical pressure for tube with no F.D.B. is much lower.

Figure 3 - 2

Section 4

CRITICAL SIZE CALCULATION

4.1. INTRODUCTION

This section details the methodology for establishing the plugging limits in compliance with the guidelines outlined in section 3.4.

The calculation procedure of critical sizes is outlined in

. section 4.2. for axial cracks

. section 4.3. for circumferential cracks.

The corresponding qualification bases are explained in section 4.4. The procedures are illustrated by sample calculations of critical sizes in section 4.5. Finally the actual plugging limits are derived from the critical sizes in section 4.6.

4.2. CALCULATION OF CRITICAL SIZE OF AXIAL CRACKS

In the elastic field, the membrane circumferential stress at both tips of a through-wall crack can be computed by multiplying the nominal stress (σ) (in an uncracked cross section) by a factor (m), usually called "bulging factor" or "Folias factor" (after respectively, the local bulging shape, and one of the first people to investigate the phenomenon).

Experimental work has demonstrated that the same law remains valid in the plastic field up to the break (unstable axial propagation), i.e. when the local circumferential membrane stress ($m\ \sigma$) reaches a critical value (σ_f) (the flow stress) typical of the material and a function of the conventional values of the yield stress (YS) and the ultimate tensile stress (UTS).

Among the various approximations of m proposed in the literature, that of ERDOGAN (1) appears the most suitable

$$m = 0.614 + 0.386 \exp(-2.25\, c/\sqrt{Rt}) + 0.866\, c/\sqrt{Rt}$$

where c = the half-length of the through-wall crack

R = the mean radius of the tube

t = the tube thickness

This expression differs from that initially proposed by Folias

$$m = \sqrt{(1 + 1.67\, c^2/Rt)}$$

(see Fig. 4.1) and which is still often used today.

A lower bound of the flow stress (σ_f) is given by

$$\sigma_f = 0.513\ (YS + UTS)$$

where YS and UTS are the conventional mechanical properties of the tube material as measured

- in the (usual) longitudinal direction;
- at design temperature (650°F = 343°C) on the actual material used in the SG under consideration (construction records).

The nominal stress (σ) is calculated by

$$\sigma = pR_i/t = p\ (R/t - 0.5)$$

where p is the differential pressure

R_i is the internal radius

R and t are as defined hereabove.

The three parameters (m), (σ_f) and (σ) being related under critical conditions, by

$$\sigma_f = m\,\sigma$$

any of them can be calculated from the knowledge of the two others.

For instance, the critical pressure, for a given defect length (hence m), is given by

$$\sigma_c = \sigma_f/m \text{ and } p_c = \sigma_c/(R/t - 0.5)$$

The critical length, for a given pressure loading (hence σ), is given by

$$m_c = \sigma_f/\sigma \text{ hence } c = f\,(m_c,\ \sqrt{Rt})$$

This procedure is valid for axial cracks in a "free" tube section. If the crack is adjacent to the tubesheet, the corresponding reinforcement increases the critical pressure or the critical length; on basis of the Belgatom experimental test results and for the crack length range of practical interest, the reinforcement effect can be taken into account by a 2 mm (0.079 in) increase of the critical size calculated in a free span, for both 7/8" and 3/4" tubing.

4.3. CALCULATION OF CRITICAL SIZE OF CIRCUMFERENTIAL CRACKS

The critical size of a circumferential through-wall flaw is calculated by the "collapse load" or "net section stress" theory (as documented by various authors, e.g. (2), assuming a perfectly plastic material (as illustrated by Fig. 4.2).

This can be formalized in a way similar to the axial case, by defining a "shape factor" (n).

Tube rupture (unstable circumferential propagation) occurs when the local longitudinal stress ($n\ \sigma$) reaches a critical value (σ_f) (the flow stress) typical of the material.

The shape factor (n) can be easily calculated as

$$n = \frac{\pi}{2} \cdot \left(\arccos \frac{\sin\alpha}{2} - \frac{\alpha}{2}\right) \qquad \text{(see Fig. 4-3)}$$

where (α) = half angle (half arc length) of through-wall crack.

This expression applies to pressure loading of an unsupported tube and would be different for flexure loading through an applied bending moment.

The flow stress (σ_f) is defined by the same expression as for the axial case

$$\sigma_f = 0.513\ (YS + UTS)$$

The nominal stress is calculated by

$$\sigma = p \frac{\pi R_i^2}{2\ \pi R t} = \frac{p}{2} \frac{(R - t/2)^2}{Rt} \approx \frac{P}{2}\left(\frac{R}{t} - 1\right)$$

where (p); (R_i); (R) and (t) are as defined for the axial case.

The three parameters (n), (σ_f) and (σ) being related, under critical conditions, by

$$\sigma_f = n\ \sigma$$

any of them can be calculated from the knowledge of the two others.

In particular :
The critical pressure, for a given defect length (hence n), is given by

$$\sigma_c = \sigma_f / n \text{ and } p_c = 2\ \sigma_c / (R/t - 1)$$

The critical length, for a given pressure loading (hence σ), is given by

$$n_c = \sigma_f / \sigma \text{ hence } \alpha_c = f^{-1}(n_c)$$

It should be noted that the procedure is not valid for small crack lenghts (α < 50 deg.), because failure occurs through the higher circumferential stress (longitudinal burst after extensive bulging).

If a circumferential crack is located close to the tubesheet, the constraining effect of the adjacent flow distribution baffle (FDB) or other support plate increases the critical pressure or the critical length.

The "net section stress" theory can again be used to evaluate this effect by taking into account the additional bending moment induced by the plate support; under failure conditions, this moment can be considered constant at a value corresponding to initiation of plasticity (thus allowing the large angular deflection needed at the crack location). This corresponds to the moment at yield stress

$$M_a = \left(\frac{I}{v}\right) \sigma_y = \pi\ t\ r^2\ \sigma_y \qquad \text{where } \frac{I}{v} \text{ is the bending modulus}$$

and introduces a K factor in the previous critical equation

$$n = \frac{\pi}{2} / \left(\arc\cos \frac{\sin\alpha - K}{2} - \frac{\alpha}{2}\right)$$

with

$$K = \frac{\pi}{2}\ \sigma_y / \sigma_f$$

Because the conventional yield stress corresponds to a relatively high plastic strain (0.2 %), a value closer to the proportional limit (about 2/3 of YS) should be selected for σ_y, so that K = 0.6.
The value of α, in the above formula, cannot exceed the limit value $\alpha = (1 - 1/n)\ \pi$ corresponding to a pure tension failure (no significant bending).

The adequacy of this approach has been verified by the BELGATOM experimental test program (8).

4.4. QUALIFICATION BASES

The "bulging factor" or Folias approach for predicting the ductile failure of axially cracked pipes has been known for a long time. However until the 80's it lacked any experimental background concerning :

- small diameters (ϕ < 3")
- long flaws ($\frac{c}{\sqrt{Rt}} > 4$ i.e. 2 c > 15 mm (0.59 in) for a 7/8" tube)
- the properties of the "Alloy 600" material (σ_f and its dependence on the conventional values for YS and UTS).

For this reason an experimental program was started by BELGATOM in 1980 based on electric discharge machined (EDM) through-wall flaws.

The results of this program were presented at the conferences of SMIRT (Structural Mechanics in Reactor Technology - Paris 1981 and Chicago 1983) as well as at other international symposiums (3) to (6). The main results are given below for axial cracks :

- the bulging factor theory was confirmed as being applicable (Fig. 4.4)
- the flow-stress value could be correlated with the YS and UTS values (Fig. 4.5) allowing extrapolation to mechanical characteristics other than those being tested.
- the break is not preceded by stable crack-growth. However, precritical local deformations are considerable :
  . (Crack Opening Displacement - COD) as illustrated by Fig. 4.6
  . bulging as illustrated by Fig. 4.7
  . fishmouth opening as illustrated by Fig. 4.8
- the experimental program also verified the negligible influence of :
  . secondary stresses (strong initial ovalization);
  . the sharpness of the crack tip (fatigue cracks);
  . the proximity of several parallel flaws.

As to circumferential through wall cracks, tests were also conducted to verify the applicability of the well known "net section stress" theory, with and without bending restraint. The same expression of flow stress σ_f = 0.513 (YS + UTS) was used.
The apparent conservatism of some test results (Fig. 4.9) probably originates from the experimental conditions (a small part of the load being taken by the sealing system used to prevent leakage through the defects).

A complementary program has recently been carried out by BELGATOM in order to evaluate the influence of proximity to tubesheet (the case of flaws in the roll transition area, at the top of the plate). The results are summarized by Fig. 4.10; one can conclude that for cracks adjacent to the tubesheet, having a reduced length $c/\sqrt{Rt}$ (outside the plate) of about 2.5, the bursting pressure is raised to the value corresponding to a 2 mm (0.079 in) shorter crack located in the free area.

Tests were also conducted to evaluate the beneficial effect of the FDB (or other nearby support plate) for tubes with circumferential cracks located close to the top side of the tubesheet. The results are summarized by Figure 4.11; they confirm the adequacy of the net section stress approach and establish the appropriate value of K to be used to take lateral restraint into account.

The results from the BELGATOM program have been compared to those from other similar programs conducted in other countries, to the extent those (generally unpublished) results were made available. Good agreement was found for all available information; in particular all programs conclude that the effect of multiple parallel axial cracks can be evaluated on basis of the single isolated longest crack, at least as long as the number of cracks is lower than about 20.

4.5. SAMPLE CALCULATION OF CRITICAL SIZES

As an illustration of the above procedure, the present section outlines the detailed calculation of critical sizes for axial and circumferential through-wall defects in "free sections" (away from tubesheet or support plate) of 7/8" and 3/4" M.A. Inconel tubing.

Input Data

SG model tube diameter		51 7/8"	E 3/4"
diameter : nominal (mm) (in) max		22.22 (.875) 22.35 (.88)	19.05 (.75) 19.15 (.754)
thickness : nominal (mm) (in) min		1.27 (.05) 1.14 (.045)	1.09 (.043) 0.99 (.039)
H.L. Operating temperature T °C (°F)		323 (613)	330(626)
UTS MPa (ksi)	at T (*)	552 (80)	552(80)
YS MPa (ksi)		243 (35)	243(35)
differential pressure - bar (psi) (**) normal conditions accidental conditions		 100 (1450) 178.5(2590)	 90 (1305) 189.7(2750)

* Minimum specified properties from ASME code case N20-1984; the YS value is interpolated between those given at 600 and 650°F. The code case UTS is kept at the same value from ambient temperature up to 650°F; this is somewhat unconservative as tests on actual SG material currently evidence a drop of about 4 % (see Fig. 4.12).

** Highest differential pressure resulting from a design basis accident (FWLB) in safety analysis report.

Actual Mechanical Properties

For all Belgian SG's, the mechanical properties (YS and UTS) have been measured and documented, for all heat numbers, both at ambient and design (650°F = 343°C) temperatures.

Each SG involves the use of several tens of heats (up to 200); Fig. 4.12 gives a typical distribution of properties for a particular SG.

As each tube (at a particular row/column location) of a SG is traceable to its original heat number, it would be possible to calculate specific critical crack sizes for each tube. This approach has not been considered to be practical but the principle of critical sizes specific to a particular S.G. has been retained. However when comparing the average and minimal values for all 3 SG's of a particular plant, or even for two sister plants (Doel 3 and Tihange 2), the differences appeared to be small (less than 4 %) and did not warrant the administrative burden of managing separate sets of plugging criteria. Thus, it was decided to calculate critical crack sizes applicable to all 6 SG's of Doel 3 and Tihange 2

For the purpose of the following sample calculations, these actual values for 7/8" SG material are also used for the 3/4" case in order to facilitate comparison, although the flow stress is higher by 4 % for the 3/4" tubing (conclusion valid for tubing of Doel 4 and Tihange 3 steam generators).

<u>Calculations</u>

The calculations have been made for a range of

- Geometries
  - . nominal dimensions (diameter and thickness);
  - . conservative combinations (maximum diameter and minimum thickness);
- Mechanical Characteristics
  - . typical;
  - . minimum specified;
  - . actual properties of SG material (on basis of 6 SG's of 2 sister plants);
  - + average value;
  - + absolute minimum (measured on batch);
- Differential Pressures : bar (psi)
  - . normal service pressure : 100 (1450) (7/8") or 90 (1305) (3/4");
  - . same, with safety margin 3 : 300 (4350) (7/8") or 270 (3915) (3/4");

. accidental pressure (SLB/FWLB) : 178.5 (2590) (7/8") or
189.7 (2750) (3/4")

. same with safety margin √2 : 252.5 (3660) (7/8") or
268.3 (3890) (3/4")

The results are given in :

- Tables 4.1 and 4.2 for axial defects (7/8" and 3/4" tubing)
- Tables 4.3 and 4.4 for circumferential defects (7/8" and 3/4" tubing).

Discussion of Results

For Axial Flaws. The most conservative way to apply R.G. 1.121 (minimum specified mechanical characteristics, and safety margins taken on the pressure) lead to a maximum acceptable length of respectively 7.3 mm (0.287 in) for 7/8" diameter and 7.8 mm (0.307 in) for 3/4" diameter.

It should be noted that the normal service conditions are prevailing for 7/8" diameter due to the safety margin of 3; under the same very conservative conditions, the acceptable length derived from the accident conditions (with a √2 safety margin) is 9.75 mm (0.384 in).

If an additional margin had to be taken to allow for NDE sizing uncertainties and crack propagation during the next operational cycle (as discussed in 4.6 hereafter), this would reduce the allowable length to the order of 2 mm (0.079 in), a value which does not even permit reliable detection.

For Circumferential Flaws. The most conservative way to apply the R.G. 1.121 leads to an acceptable length of 139° or 24.5 mm (0.965 in) measured according to the inside of the tube wall for 7/8" diameter and respectively 148° or 22.2 mm (0.874 in) for 3/4" diameter. It should be noted that, again, the service conditions are dominant for 7/8" diameter; the acceptable length derived from the accident conditions is 152° (= 26.6 mm - 1.047 in).

It should be noted that there is a striking difference between axial and circumferential cracks when the safety factor "S" is taken on load (as requested by R.G. 1.121).

The result, when expressed as a safety factor on length,

- is significantly larger than S for axial cracks;
- is much lower than S for circumferential cracks.

This is illustrated by Fig. 3.1, and leads to an unsatisfactory situation as actual uncertainties are more related to defect sizes than to load intensities. This also is the basis for applying the R.G. 1.121 safety factors on crack lengths, rather than on loadings. With respect to original requirements this reduces somewhat the conservatism for the axial crack case but increases considerably this conservatism for the circumferential crack case.

4.6. ESTABLISHMENT OF TUBE PLUGGING CRITERIA

Critical Lengths

Application of the procedures outlined under 4.2; 4.3 and 4.5 allows one to calculate :

- The average critical length, on the basis of :
  . the nominal tube geometry (diameter, wall thickness);
  . the average mechanical properties of the material (Yield Stress, Ultimate Tensile Stress)

  for both the normal and accidental service conditions.
- The minimal critical length, on basis of :
  . the most unfavourable tube geometry (max. diameter and min. thickness);
  . the most unfavourable combination of the material properties (minimum of YS + UTS);
  . the accidental service conditions.

All mechanical properties being those measured at 343°C (650°F) on the various batches (heats) under consideration.

Applicable Margins

The safety factors applicable to the average critical length are :

- 3 for normal service conditions;
- $\sqrt{2}$ for accidental conditions;

the lowest resulting value is to be used (as already explained, the first condition is practically always prevailing).

Two additional margins are to be taken into account :

- allowance for ECT undersizing of the actual defect length;
- length increase of defect during the subsequent operation period of time, up to the next ECT inspection.

Evaluation of these two effects is based on field data obtained from axial cracking (roll transition) of 7/8" tubing.

For the first effect, a good knowledge of the sizing accuracy has been obtained by comparing the RPC ECT length measurements with the actual maximum (ID) length of about 30 PWSCC roll transition cracks from 3 pulled tubes (see Figure 4-13). The calibration has been adjusted so that the average deviation between measured and true values is close to zero. This is conservative as the average length of an actual PWSCC flaw is less than the maximum length measured on the ID; as a confirmation, it has been checked that the RPC method systematically overestimates the length of "square shaped" artificial (EDM) through wall defects.

With respect to the calibration line (Figure 4.13) it can be seen that five cracks show an underestimation in excess of 1.5 mm (0.06 in); they all relate to tubes pulled from Doel 3 (with kiss rolling). From the tubes destructive examination, these cracks are known to be often shaped as illustrated by Figure 4-14. It is clear from this picture, that the apparent length underestimation by RPC results from the particular shape and that a 1.5 mm (0.06 in) accuracy margin more than adequately covers any structural concern.
As a confirmation, for the Doel 2 pulled tube (with standard roll), where the OD length of cracks is close to ID length (1.5 mm - 0.06 in max difference), the ECT underestimation of ID length never exceeds 1 mm (0.04 in).

As a consequence, the ECT (RPC) sizing accuracy margin has been considered to have a maximum value of 1.5 mm (0.06 in).

For the second effect, the margins are derived from the analysis of all data coming from the last two operating cycles of the Doel 3 and Tihange 2 plants (see Table 4-5). As the crack propagation is dependent on the initial crack size, the analysis was restricted to all the cracks with an initial length (at beginning of cycle) of 9 mm (0.354 in) or more (there were 139); on this basis, the average propagation is 1.6 mm (0.063 in)/cycle, with a maximum upper bound of 4 mm (0.158 in)/cycle.

The additional margins are thus summarized in the following table

Value	Cycle propagation	ECT underestimation
average	1.6 mm (0.063 in)	0
maximum	4 mm (0.158 in)	1.5 mm (0.06 in)

For a "best estimate" analysis, the average values of both effects are considered, i.e. 1.6 + 0 = 1.6 mm (0.063 in)

For a "worst combination" analysis, the maximum values of both effects are taken into account : 4 + 1.5 = 5.5 mm (0.217 in).
While these values are strictly applicable to axial cracks measured by ECT in 7/8" tubing, they are kept unchanged (until further information becomes available) :

- for 3/4" tubing;
- for circumferential cracks;
- for UT sizing; (a comparison of ECT and UT sizing was performed in June 88 on 7 tubes of a Doel 3 SG, with close agreement within ± 1 mm).

The mentioned values (1.6 and 5.5 mm) are of course only applicable if an inspection is being performed at each cycle with an RPC inspection technique equivalent to that described in section 6.

Allowable Lengths

The allowable length is taken as the lowest value resulting from the two following analyses.

"Best Estimate" Analysis, With Safety Factors. The average critical lengths are calculated for both normal and accidental conditions. For flaws expected to propagate in the roll transition area, a margin (in length) is added to take into account the reinforcing effect of :

- the tubesheet vicinity for axial cracks;
- the FDB/support plate restraint for circumferential cracks.

Those values are then devided by the recommended safety factors (3 for normal conditions and $\sqrt{2}$ for accident conditions)

The additional margin of 1.6 mm (0.063 in) is subsequently deducted.

The results of the corresponding calculations are summarized in the next table on basis of the following average mechanical properties at 343°C (650°F).

YS = 290 MPa (42 ksi)
UTS = 676 MPa (92 ksi)

The flow stress is taken as

$$\sigma_f = 0.513\ (290 + 676) = 495 \text{ MPa } (72 \text{ ksi})$$

CRACK TYPE	TUBE SIZE	PRESSURE bar (psi)	CRITICAL LENGTH CL	SAFETY FACTOR SF	CL / SF	ALLOWABLE LENGTH
AXIAL	7/8"	100 (1450)	49 mm (1.929in)	3	16.3 mm (0.642in)	16.3 - 1.6 = 14.7mm (0.571 in)
		178.5 (2590)	25 mm (0.984in)	√2	17.7 mm (0.697in)	
	3/4"	90 (1305)	47 mm (1.850in)	3	15.7 mm (0.618in)	
		189.7 (2750)	20 mm (0.787in)	√2	14.1 mm (0.555in)	14.1 - 1.6 = 12.5mm (0.492 in)
CIRCUM-FERE-NTIAL	7/8"	100 (1450)	223 deg. [334]deg	3	74 deg. [111]deg	74 - 9 = 65 deg. = 12.2 mm (0.441 in) [111 - 9 = 102 deg. =17.5 mm (0.689in)]
		178.5 (2590)	194 deg. [313]deg	√2	137 deg. [221]deg	
	3/4"	90 (1305)	227 deg. [336]deg	3	76 deg. [112]deg	76 - 11 = 65 deg. = 9.6 mm (0.378 in) [112 - 11 =101 deg = 14.9 mm(0.587in)]
		189.7 (2750)	190 deg. [310]deg	√2	134 deg. [219]deg	

[...] : Applicable to roll transition because of restraining effect of TSP (circumferential flaws)
The tubesheet reinforcement for axial cracks is negligible because of the large values of critical lengths.

<u>"Worst Combination" Analysis, Without Safety Factors</u>. The minimum critical length is considered. In the roll transition area, credit (i.e. increase of allowable length) is then taken for the reinforcing effect of :

- the tubesheet vicinity, for axial cracks;
- the FDB/support plate restraint, for circumferential cracks.

The additional margin of 5.5 mm (0.217 in) is subsequently deducted.

The results of the corresponding calculations are summarized in the next table on basis of the following minimum mechanical properties at 343°C (650°F) :

YS = 228 MPa (33 ksi)

UTS = 600 MPa (87 ksi)

The flow stress is taken as :

σ_f = 0.513 (600 + 228) = 425 MPa (62 ksi)

CRACK TYPE	TUBE SIZE	CRITICAL LENGTH		ALLOWABLE LENGTH	
		FREE SECTION	ROLL TRANSITION	FREE SECTION	ROLL TRANSITION
AXIAL	7/8"	16.8 mm (0.661 in)	18.8 mm (0.740 in)	11.3 mm (0.445 in)	13.3 mm (0.524 in)
	3/4"	13.6 mm (0.535 in)	15.6 mm (0.614 in)	8.1 mm (0.319 in)	10.1 mm (0.398 in)
CIRCUMFERENTIAL	7/8"	31.2 mm 178 deg.	52 mm. 297 deg.	25.7 mm 147 deg.	46.5 mm 266 deg.
	3/4"	26.3 mm 175 deg.	44.2 mm 295 deg.	20.8 mm 139 deg.	38.7 mm 258 deg.

Plugging Limit

The two preceding tables are now compared and the lowest value is retained as the allowable measured value. The plugging limit is obtained by rounding-off at the higher mm value.
The calculation procedure is outlined :

- in Table 4.6 for axial defects in 7/8" tubes
- in Table 4.7 for circumferential defects in 7/8" tubes (defects located in roll transition area)

CRACK TYPE	TUBE SIZE	ALLOWABLE LENGTH* ON BASIS OF		PLUGGING LIMIT
		best estimate + safety factor	worst combination analysis w/o safety factor	
AXIAL	7/8"	14.7 mm (0.579 in)	13.3 mm (0.524 in)	14 mm (0.551 in)
	3/4"	12.5 mm (0.492 in)	10.1 mm (0.398 in)	11 mm (0.433 in)
CIRCUMFE-RENTIAL	7/8"	102 deg. = 17.5mm (0.689 in)	266 deg. = 46.5 mm (1.83' in)	18 mm (0.709 in)
	3/4"	101 deg. = 14.9mm (0.587 in)	258 deg. = 38.7 mm (1.524 in)	15 mm (0.591 in)

* Allowable length of flaws situated in the roll transition area.

REFERENCES

1. "Ductile fracture theories for pressurized pipes and containers"
F. ERDOGAN
Int. J. Press. Ves. & Piping 4 (1976).

2. "Practical application of extremal elastic-ideally plastic solutions for the assessment of the severity of cracks"
C. RUIZ and R.J.S. CORRAN
Int. J. Pres. Ves & Piping 10 (1982).

3. "Evaluation of critical lengths for through thickness axial cracks in steam generator tubing"
P. HERNALSTEEN (TBL), 6th SMIRT Conference, Paris (1981), paper F 7/6.

4. "Evaluation of critical sizes for defects in small diameter tubing"
P. HERNALSTEEN (TBL), 7th SMIRT Conference, Chicago (1983), paper GF 4/3 (only transparencies copies)

5. "Critical flaw sizes in steam generator tubing"
P. HERNALSTEEN (TBL), NEA/CSNI - UNIPEDE specialist meeting on steam generators, Stockholm (Octobre 1984).

6. "Belgian regulatory climate"
G. FREDERICK and P. HERNALSTEEN (BELGATOM)
EPRI-SGOG workshop on primary side stress corrosion cracking, St-Petersburg - Florida (December 1985), présentation réservée aux "Utilities".

7. EDF's Expert's Report on 2 tubes pulled off a Doel 3 SG in june 1986.

8. "Belgian approach to tube plugging for PWSCC in the tubesheet area - Experimental work"
to be published as an addendum to the present EPRI report.

TABLE 4-1

CRITICAL LENGTH OF AN AXIAL THROUGH-WALL DEFECT IN 7/8" TUBING

for a nominal and unfavourable (within brackets) geometry

MECHANICAL PROPERTIES		YS	UTS	σ_f	CRITICAL LENGTH (mm) for P (bar) =			
REFERENCE	T (°C)	MPa	MPa	MPa	100	178.5	$\sqrt{2}$x178.5=252.5	3 x 100 = 300
TYPICAL	20	350	700	540	53.6 (44.2)	27.7 (22.8)	18.1 (14.6)	14.4 (11.5)
ACTUAL AVERAGE	343	290	676	455	48.6 (40.2)	25 (20.5)	16 (13.2)	12.8 (10.1)
ACTUAL MINIMUM	343	228	600	425	41.2 (33.7)	20.8 (16.75)	13.2 (10.5)	9.6 (7.8)
SPECIFIED MINIMUM	20	276	552	425	41.2 (33.7)	20.8 (16.75)	13.2 (10.5)	9.6 (7.8)
	316	244	552	410	38.3 (32.5)	19.7 (16)	12.4 (9.75)	9.3 (7.3)

TABLE 4-1 (cont'd) (British Units)

CRITICAL LENGTH OF AN AXIAL THROUGH-WALL DEFECT IN 7/8" TUBING

for a nominal and unfavourable (within brackets) geometry

MECHANICAL PROPERTIES		YS	UTS	σ_f	CRITICAL LENGTH (in) for P (psi)			
REFERENCE	T (°F)	ksi	ksi	ksi	1450	2590	$\sqrt{2}$x2590 =3660	3 x 1450 = 4350
TYPICAL	70	50.7	101.5	78	2.110 (1.740)	1.091 (0.898)	0.713 (0.575)	0.567 (0.453)
ACTUAL AVERAGE	650	42	92	72	1.913 (1.583)	0.984 (0.807)	0.630 (0.520)	0.504 (0.398)
ACTUAL MINIMUM	650	33	87	62	1.622 (1.327)	0.819 (0.659)	0.520 (0.413)	0.378 (0.307)
SPECIFIED MINIMUM	70	40	80	62	1.622 (1.327)	0.819 (0.659)	0.520 (0.413)	0.378 (0.307)
	600	35	80	59.5	1.508 (1.280)	0.776 (0.630)	0.488 (0.384)	0.366 (0.287)

TABLE 4-2

CRITICAL LENGTH OF AN AXIAL THROUGH-WALL DEFECT IN 3/4" TUBING

for a nominal and unfavourable (within brackets) geometry

MECHANICAL PROPERTIES		YS	UTS	σ_f	CRITICAL LENGTH (mm) for P (bar) =			
REFERENCE	T (°C)	MPa	MPa	MPa	90	189.7	√2x189.7=268.3	3 x 90 = 270
TYPICAL	20	350	700	540	51.5 (43.7)	22.4 (18.6)	14.4 (12)	14.3 (12)
ACTUAL AVERAGE	343	290	676	495	47 (39.8)	20 (16.5)	12.8 (10.5)	12.8 (10.5)
ACTUAL MINIMUM	343	228	600	425	39.6 (34.7)	16.5 (13.6)	10.3 (8.3)	10.3 (8.3)
SPECIFIED MINIMUM	20	276	552	425	40 (34.7)	16.5 (13.6)	10.3 (8.3)	10.3 (8.3)
	316	244	552	410	38.2 (32.2)	15.9 (13.2)	9.7 (7.8)	9.7 (7.8)

TABLE 4-2 (cont'd) (British Units)

CRITICAL LENGTH OF AN AXIAL THROUGH-WALL DEFECT IN 3/4" TUBING

for a nominal and unfavourable (within brackets) geometry

MECHANICAL PROPERTIES		YS	UTS	σ_f	CRITICAL LENGTH (in) for P (psi)			
REFERENCE	T (°F)	ksi	ksi	ksi	1305	2750	$\sqrt{2}$x2750 =3890	3 x 1305 = 3915
TYPICAL	70	50.7	101.5	78	2.028 (1.721)	0.882 (0.732)	0.567 (0.472)	0.563 (0.472)
ACTUAL AVERAGE	650	42	92	72	1.850 (1.567)	0.787 (0.650)	0.504 (0.413)	0.504 (0.413)
ACTUAL MINIMUM	650	33	87	62	1.559 (1.366)	0.650 (0.535)	0.406 (0.327)	0.406 (0.327)
SPECIFIED MINIMUM	70	40	80	62	1.575 (1.366)	0.650 (0.535)	0.406 (0.327)	0.406 (0.327)
	600	35	80	59.5	1.504 (1.268)	0.626 (0.520)	0.382 (0.307)	0.382 (0.307)

TABLE 4-3

CRITICAL LENGTH OF A CIRCUMFERENTIAL THROUGH-WALL DEFECT IN 7/8" TUBING

for a nominal and unfavourable (within brackets) geometry

MECHANICAL PROPERTIES		YS	UTS	σ_f	CRITICAL ARC LENGTH (2α (deg.)) for P (bar) =			
	T (°C)	MPa	MPa	MPa	100	178.5	$\sqrt{2}$x178.5=252.5	3 x 100 = 300
TYPICAL	20	350	700	540	226 (221)	198 (191)	179 (171)	169 (159)
ACTUAL AVERAGE	343	290	676	495	223 (216)	194 (186)	174 (164)	162 (153)
ACTUAL MINIMUM	343	228	600	425	215 (210)	185 (178)	164 (154)	152 (141)
SPECIFIED MINIMUM	20	276	552	425	215 (210)	185 (178)	164 (154)	152 (141)
	316	244	552	410	214 (207)	183 (176)	162 (152)	149 (139)

N.B. : 10 deg. = 1.72 mm (nominal geometry)] as measured around the inner side
= 1.75 mm (unfavourable geometry)

TABLE 4-3 (cont'd) (British Units)

CRITICAL LENGTH OF A CIRCUMFERENTIAL THROUGH-WALL DEFECT IN 7/8" TUBING

for a nominal and unfavourable (within brackets) geometry

MECHANICAL PROPERTIES		YS	UTS	σ_f	CRITICAL ARC LENGTH (2α (deg.)) for P (psi)			
	T (°F)	ksi	ksi	ksi	1450	2590	$\sqrt{2}$x2590 = 3660	3 x 1450 = 4350
TYPICAL	70	50.7	101.5	78	226 (221)	198 (191)	179 (171)	169 (159)
ACTUAL AVERAGE	650	42	92	72	223 (216)	194 (186)	174 (164)	162 (153)
ACTUAL MINIMUM	650	33	87	62	215 (210)	185 (178)	164 (154)	152 (141)
SPECIFIED MINIMUM	70	40	80	62	215 (210)	185 (178)	164 (154)	152 (141)
	600	35	80	59.5	214 (207)	183 (176)	162 (152)	149 (139)

N.B. : 10 deg. = 0.0677 in (nominal geometry) } as measured around the inner side
= 0.0689 in (unfavourable geometry) }

TABLE 4-4

CRITICAL LENGTH OF A CIRCUMFERENTIAL THROUGH WALL DEFECT IN 3/4" TUBING

for a nominal and unfavourable (within brackets) geometry

MECHANICAL PROPERTIES		YS	UTS	σ_f	CRITICAL ARC LENGTH (2 α (deg.)) FOR P (bar) =			
REFERENCE	T (°C)	MPa	MPa	MPa	90	189.7	$\sqrt{2}$x189.7=268.3	3 x 90 = 270
TYPICAL	20	350	700	540	231 (225)	195 (189)	176 (167)	175 (167)
ACTUAL AVERAGE	343	290	676	495	227 (222)	190 (184)	171 (162)	170 (161)
ACTUAL MINIMUM	343	228	600	425	220 (215)	182 (175)	160 (152)	159 (151)
SPECIFIED MINIMUM	20	276	552	425	220 (215)	182 (175)	160 (152)	159 (151)
	316	244	552	410	219 (213)	180 (173)	157 (149)	156 (148)

N.B. : 10 deg. = 1.47 mm (nominal geometry)] as measured around the inner side
= 1.50 mm (unfavourable geometry]

TABLE 4-4 (cont'd) (British Units)

CRITICAL LENGTH OF A CIRCUMFERENTIAL THROUGH-WALL DEFECT IN 3/4" TUBING

for a nominal and unfavourable (within brackets) geometry

MECHANICAL PROPERTIES		YS	UTS	σ_f	CRITICAL ARC LENGTH (2 α (deg.)) FOR P (psi)			
REFERENCE	T (°F)	ksi	ksi	ksi	1305	2750	√2x2750 = 3890	3 x 1305 = 3915
TYPICAL	70	50.7	101.5	78	231 (225)	195 (189)	176 (167)	175 (167)
ACTUAL AVERAGE	650	42	92	72	227 (222)	190 (184)	171 (162)	170 (161)
ACTUAL MINIMUM	650	33	87	62	220 (215)	182 (175)	160 (152)	159 (151)
SPECIFIED MINIMUM	70	40	80	62	220 (215)	182 (175)	160 (152)	159 (151)
	600	35	80	59.5	219 (213)	180 (173)	157 (149)	156 (148)

N.B. : 10 deg. = 0.0579 in (nominal geometry) } as measured around the inner side
= 0.0591 in (unfavourable geometry }

TABLE 4-5

MAXIMUM PROPAGATION (FOR 1 CYCLE) OF "LONG" CRACKS (≥ 9 mm)

Reference : 2 last cycles of Doel 3 and Tihange 2

UNIT	DOEL 3								TIHANGE 2			
SG nr	B		R		G		B		1		3	
CYCLE	1986 - 1987		1987 - 1988		1987 - 1988		1987 - 1988		1987 - 1988		1987 - 1988	
INITIAL LENGTH	δmax (mm)	x/y	δmax (mm)	x/y	δmax (mm)	x/y	δmax (mm)	x/y	δmax (mm)	x/y	δmax (mm)	x/y
8 mm	2	1/3	-	-	4	1/10	5	5/104	2	1/3	4	1/12
9 mm	3	1/4	-	-	3	3/9	4	3/60	3	1/3	3	1/5
10 mm	0	1/1	0	1/1	4	1/5	4	5/31	0	3/3	1	1/4
11 mm	-	-	-	-	3	1/1	4	1/4	-	-	1	1/1
12 mm	-	-	-	-	-	-	3	1/5	3	1/1	-	-
13 mm	-	-	-	-	-	-	2	1/1	-	-	-	-
CONCLUSIONS : for 139 cracks of ≥ 9 mm, δ max = 4 mm (10 cases i.e. 7 %) for 132 cracks of 8 mm, δ max = 5 mm (5 cases i.e. 4 %)												

x/y = ratio of number of cracks with indicated δmax, to total number of cracks with indicated initial length.

(*) not included :
SG R and G for cycle 86-87 (no inspection in 1986)
all SG of Tihange 2 for cycle 86-87
(no crack ≥ 9 mm)
SG 2 for cycle 87-88

The average propagation rate, for all SG of Doel 3 (cycle 87-88), is 1.6 mm based on 117 cracks with an initial length ≥ 9 mm

<u>TABLE 4-5</u> (cont'd) (British Units)

MAXIMUM PROPAGATION (FOR 1 CYCLE) OF "LONG" CRACKS (≥ 0.354 in)

<u>Reference</u> : 2 last cycles of Doel 3 and Tihange 2

UNIT	DOEL 3								TIHANGE 2			
SG nr	B		R		G		B		1		3	
CYCLE	1986 - 1987		1987 - 1988		1987 - 1988		1987 - 1988		1987 - 1986		1987 - 1988	
INITIAL LENGTH	δmax (in)	x/y	δmax (in)	x/y	δmax (in)	x/y	δmax (in)	x/y	δmax (in)	x/y	δmax (in)	x/y
0.315 in	0.0787	1/3	-	-	0.158	1/10	0.197	5/104	0.0787	1/3	0.158	1/12
0.354 in	0.118	1/4	-	-	0.118	3/9	0.158	3/60	0.118	1/3	0.118	1/5
0.398 in	0.0	1/1	0.0	1/1	0.158	1/5	0.158	5/31	0.0	3/3	0.039	1/4
0.433 in	-	-	-	-	0.118	1/1	0.158	1/4	-	-	0.039	1/1
0.472 in	-	-	-	-	-	-	0.118	1/5	0.118	1/1	-	-
0.512 in	-	-	-	-	-	-	0.0787	1/1	-	-	-	-
CONCLUSIONS :	for 139 cracks of ≥ 0.354 in, δ max = 0.158 in (10 cases i.e. 7 %) for 132 cracks of 0.315 in, δ max = 0.197 in (5 cases i.e. 4 %)											

x/y = ratio of number of cracks with indicated δmax, to total number of cracks with indicated initial length.

(*) not included :
SG R and G for cycle 86-87 (no inspection in 1986)
all SG of Tihange 2 for cycle 86-87 } (no crack ≥ 0.354 in)
SG 2 for cycle 87-88 }

The average propagation rate, for all SG of Doel 3 (cycle 87-88), is 0.063 in based on 117 cracks with an initial length ≥ 0.354 in.

TABLE 4-6

PLUGGING LIMIT FOR SCC IN ROLL TRANSITIONS
SAMPLE CALCULATION
AXIAL CRACKS IN 7/8" TUBE OF A TYPICAL PLANT

	BEST ESTIMATE WITH safety factor		MOST CONSERVATIVE ESTIMATE WITHOUT safety factor
CRITICAL LENGTH (thru wall)	Differential pressure normal (100 bar)	Differential pressure accidental (178.5 bar)	Differential pressure YS = 228 MPa, UTS = 600 MPa at 343°C
	49 mm	25 mm	16.8 mm
TUBESHEET REINFORCEMENT	+ 0	+ 0 mm (*)	+ 2 mm
	49 mm	25 mm	18.8 mm
SAFETY FACTOR (on length)	3	$\sqrt{2}$	1
	16.3 mm	17.7 mm	
	16.3 mm		18.8 mm
ADDITIONAL MARGIN (**)			
. sizing accuracy	- 0 mm		- 1.5 mm
. propagation (1 cycle)	- 1.6 mm		- 4.0 mm
ALLOWABLE LENGTH	14.7 mm		13.3 mm
Lowest of	13.3 mm		
Rounded off to			
PLUGGING LIMIT	14 mm		
	(13 mm acceptable; ≥ 14 mm = plugged)		

TABLE 4-6 (cont'd) (British Units)

PLUGGING LIMIT FOR SCC IN ROLL TRANSITIONS
SAMPLE CALCULATION
AXIAL CRACKS IN 7/8" TUBE OF A TYPICAL PLANT

	BEST ESTIMATE WITH safety factor		MOST CONSERVATIVE ESTIMATE WITHOUT safety factor
CRITICAL LENGTH (thru wall)	Differential pressure		Differential pressure
	normal (1450 psi)	accidental (2590 psi)	YS = 33 ksi; UTS = 87 ksi; at 650°F
	1.929 in	0.984 in	0.661 in
TUBESHEET REINFORCEMENT	+ 0 in	+ 0 in	+ 0.079 in
	1.929 in	0.984 in	0.740 in
SAFETY FACTOR (on length)	3	$\sqrt{2}$	1
	0.642 in	0.697 in	
	0.642 in		0.740 in
ADDITIONAL MARGIN (**)			
. sizing accuracy	- 0 in		- 0.058 in
. propagation (1 cycle)	- 0.063 in		- 0.156 in
ALLOWABLE LENGTH	0.579 in		0.524 in
Lowest of	0.524 in		
Rounded off to			
PLUGGING LIMIT	0.551		
	(0.511 in acceptable; ≥ 0.551 in = plugged)		

TABLE 4-7

PLUGGING LIMIT FOR SCC IN ROLL TRANSITIONS
SAMPLE CALCULATION
CIRCUMFERENTIAL CRACKS IN 7/8" TUBE OF A TYPICAL PLANT

	BEST ESTIMATE WITH safety factor		MOST CONSERVATIVE ESTIMATE WITHOUT safety factor
CRITICAL LENGTH (thru wall)	Differential pressure normal (100 bar)	Differential pressure accidental (equiv.) (178.5 bar)	Differential pressure YS = 228 MPa, UTS = 600 MPa at 343°C
. unsupported	38 mm (223 deg)	34 mm (194 deg)	31.2 mm (178 deg)
. restrained by TSP	57 mm (334 deg)	55 mm (313 deg)	52 mm (297 deg)
SAFETY FACTOR (on length)	3	$\sqrt{2}$	1
	19 mm (111 deg)	38.6mm(221 deg)	
lowest of	19 mm (111 deg)		52 mm (297 deg)
ADDITIONAL MARGIN			
. sizing accuracy	- 0 mm (0 deg)		- 1.5 mm (9 deg)
. propagation (1 cycle)	- 1.6 mm (9 deg)		- 4 mm (22 deg)
ALLOWABLE LENGTH	17.5 mm (102 deg)		46.5mm (266 deg)
Lowest of	17.5 mm (102 deg)		
Rounded off to			
PLUGGING LIMIT	18 mm (104 deg)		
	(17 mm acceptable / 18 mm = to be plugged or repaired		

TABLE 4-7 (cont'd) (British Units)

PLUGGING LIMIT FOR SCC IN ROLL TRANSITIONS
SAMPLE CALCULATION
CIRCUMFERENTIAL CRACKS IN 7/8" TUBE OF A TYPICAL PLANT

	BEST ESTIMATE WITH safety factor		MOST CONSERVATIVE ESTIMATE WITHOUT safety factor
CRITICAL LENGTH (thru wall)	Differential pressure		Differential pressure
	normal (1450 psi)	accidental (equiv.) (2590 in)	YS = 33 ksi, UTS = 87 ksi at 650°F
. unsupported	1.496 in(223 deg)	1.339in (194 deg)	1.228 in (178 deg)
. restrained by TSP	2.244 in(334 deg)	2.165in (313 deg)	2.047 in (297 deg)
SAFETY FACTOR (on length)	3	$\sqrt{2}$	1
	0.748 in(111 deg)	1.520 in(221 deg)	
lowest of	0.748 in (111 deg)		2.047 in (297 deg)
ADDITIONAL MARGIN			
. sizing accuracy	- 0 in (0 deg)		- 0.058 in (9 deg)
. propagation (1 cycle)	- 0.059 in (9 deg)		- 0.158 in (22 deg)
ALLOWABLE LENGTH	0.689 in (102 deg)		1.831 in (266 deg)
Lowest of	0.689 in (102 deg)		
Rounded off to			
PLUGGING LIMIT	0.709 in (104 deg)		
	(0.669 in acceptable /0.709 in to be plugged or repaired		

BULGING FACTOR "m"

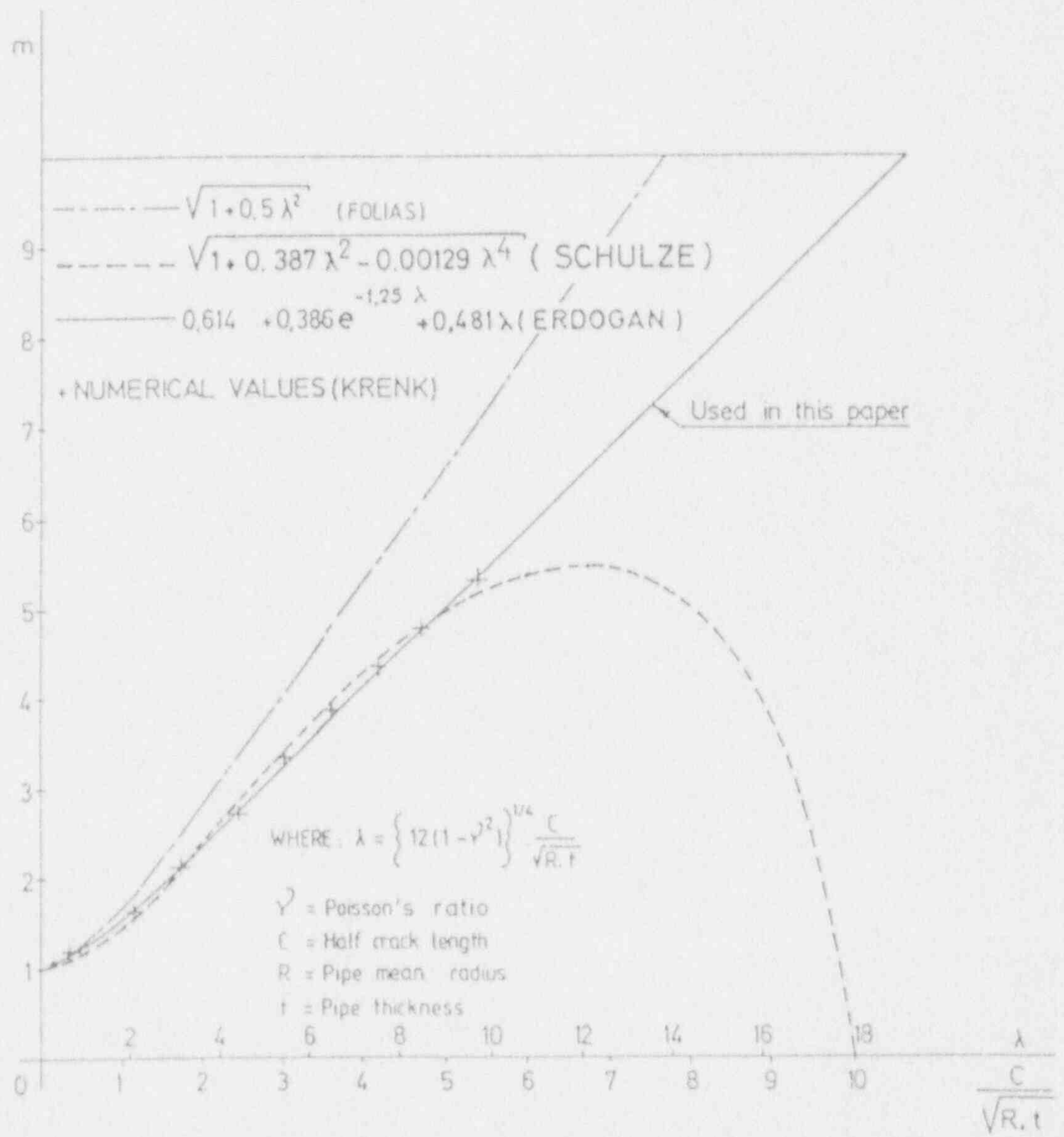

Figure 4-1

BURSTING PRESSURE PREDICTION BY USING

THE "NET SECTION COLLAPSE CRITERION"

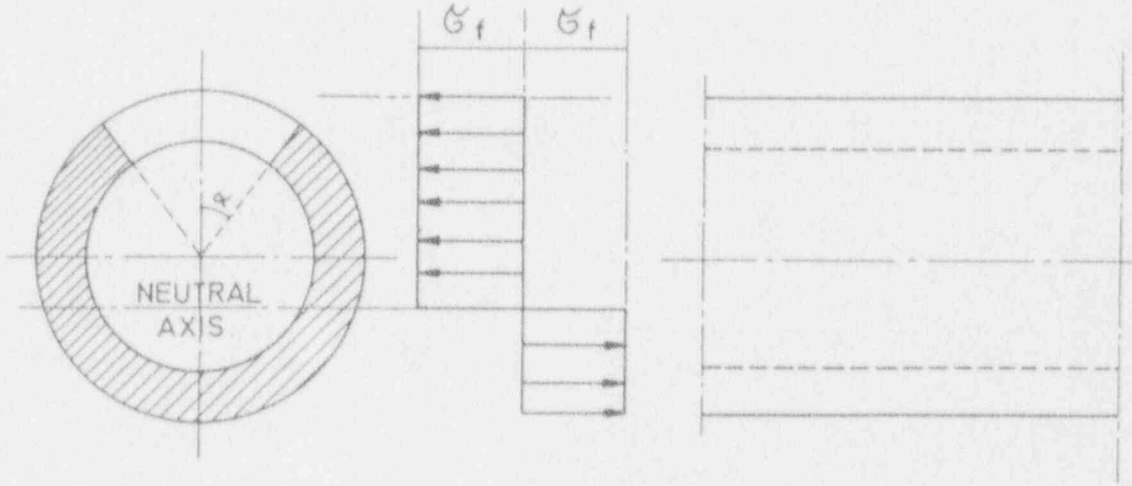

$$\frac{\sigma_{CR}}{\sigma_f} = \frac{2}{\pi}\left[\cos^{-1}\left(\frac{\sin\alpha}{2}\right) - \frac{\alpha}{2}\right]$$

Figure 4-2

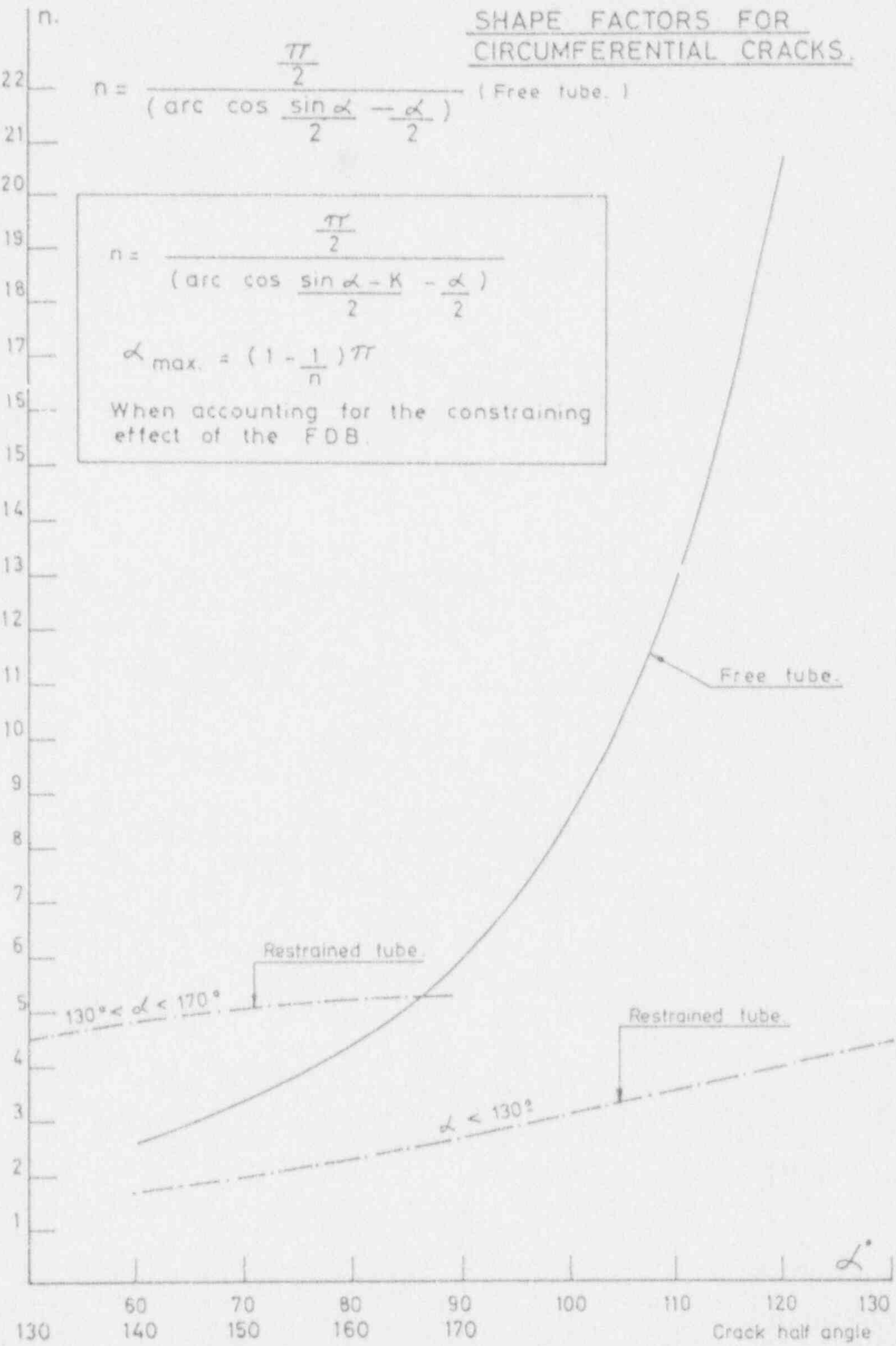

n.
SHAPE FACTORS FOR CIRCUMFERENTIAL CRACKS.
$n = \frac{\frac{\pi}{2}}{(\arc\cos\frac{\sin\alpha}{2} - \frac{\alpha}{2})}$ (Free tube.)
$n = \frac{\frac{\pi}{2}}{(\arc\cos\frac{\sin\alpha - K}{2} - \frac{\alpha}{2})}$
$\alpha_{max.} = (1 - \frac{1}{n})\pi$
When accounting for the constraining effect of the FDB.
Free tube.
Restrained tube.
130° < α < 170°
Restrained tube.
α < 130°
α°
Crack half angle

Figure 4 - 3

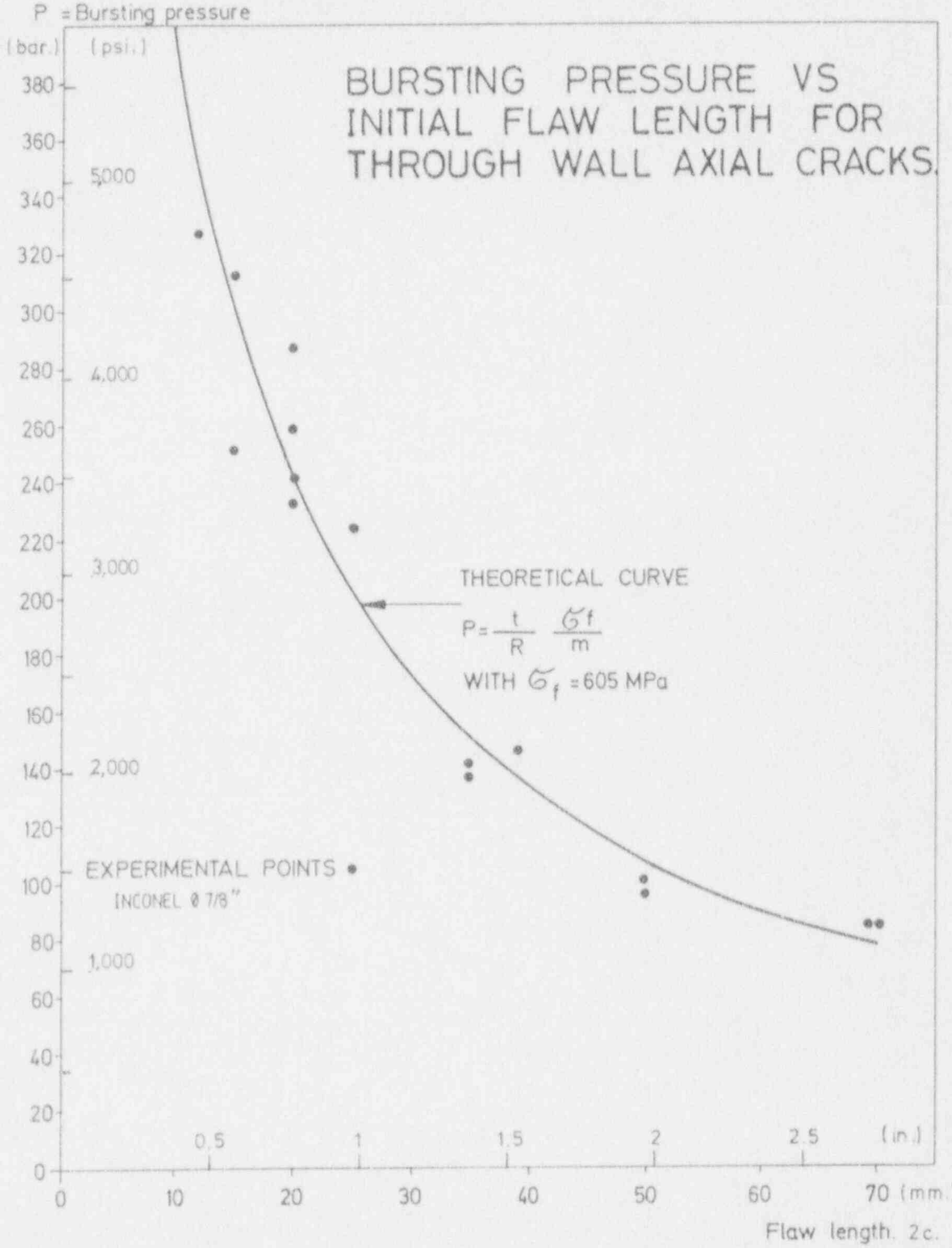
P = Bursting pressure
(bar.) (psi.)
BURSTING PRESSURE VS INITIAL FLAW LENGTH FOR THROUGH WALL AXIAL CRACKS.
380
360
5,000
340
320
300
280
4,000
260
240
220
3,000
200
180
160
140
2,000
120
100
80
1,000
60
40
20
0
THEORETICAL CURVE
P = t/R σf/m
WITH σf = 605 MPa
EXPERIMENTAL POINTS
INCONEL Ø 7/8"
0,5
1
1,5
2
2,5
(in.)
0
10
20
30
40
50
60
70 (mm.)
Flaw length. 2c.

Figure 4-4

CORRELATION BETWEEN "FLOW STRESS" AND THE TRANSVERSE MECHANICAL PROPERTIES YS AND UTS.

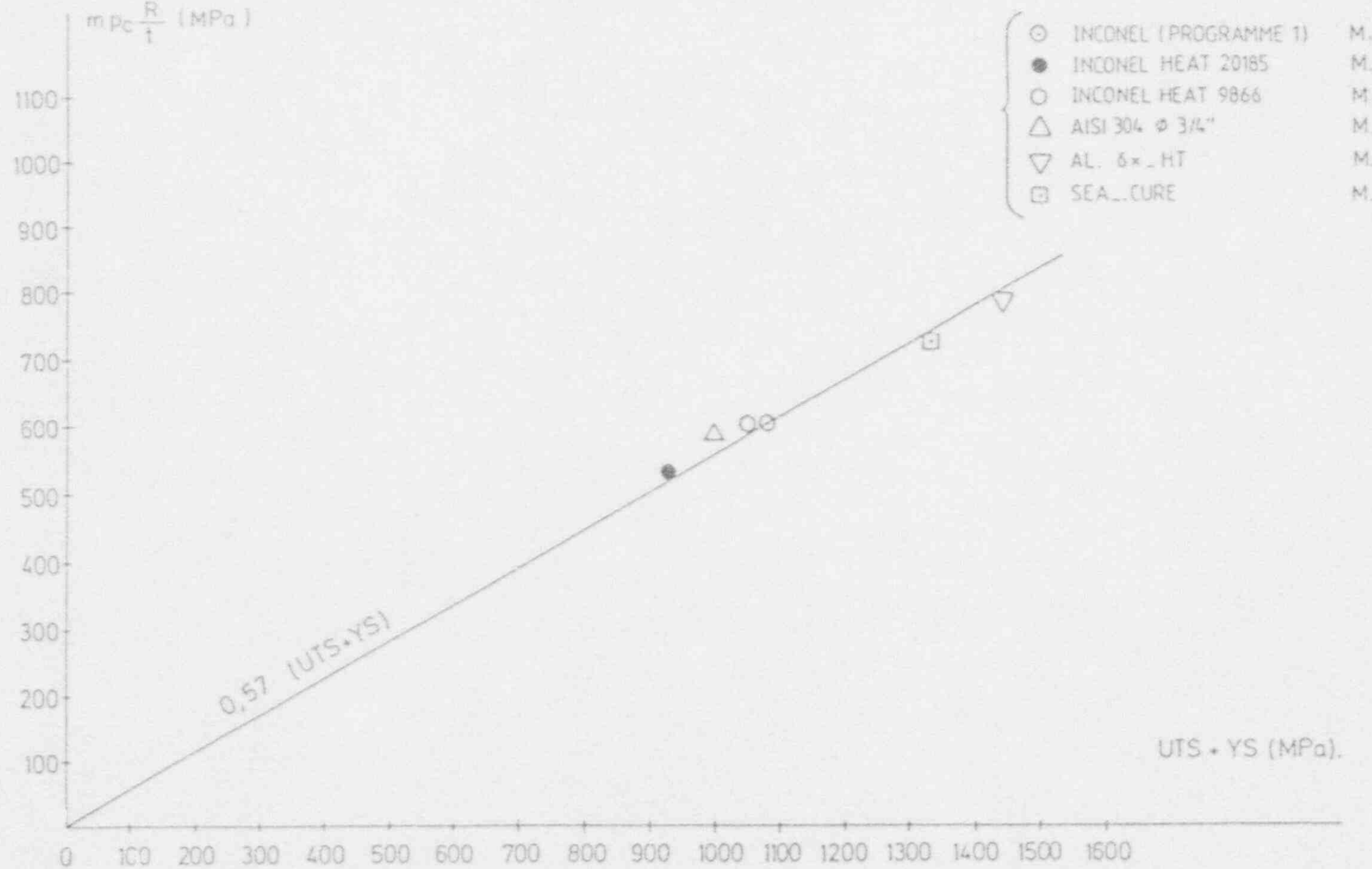

Figure 4 – 5

COD (AXIAL FLAWS) AS A FUNCTION OF PRESSURE

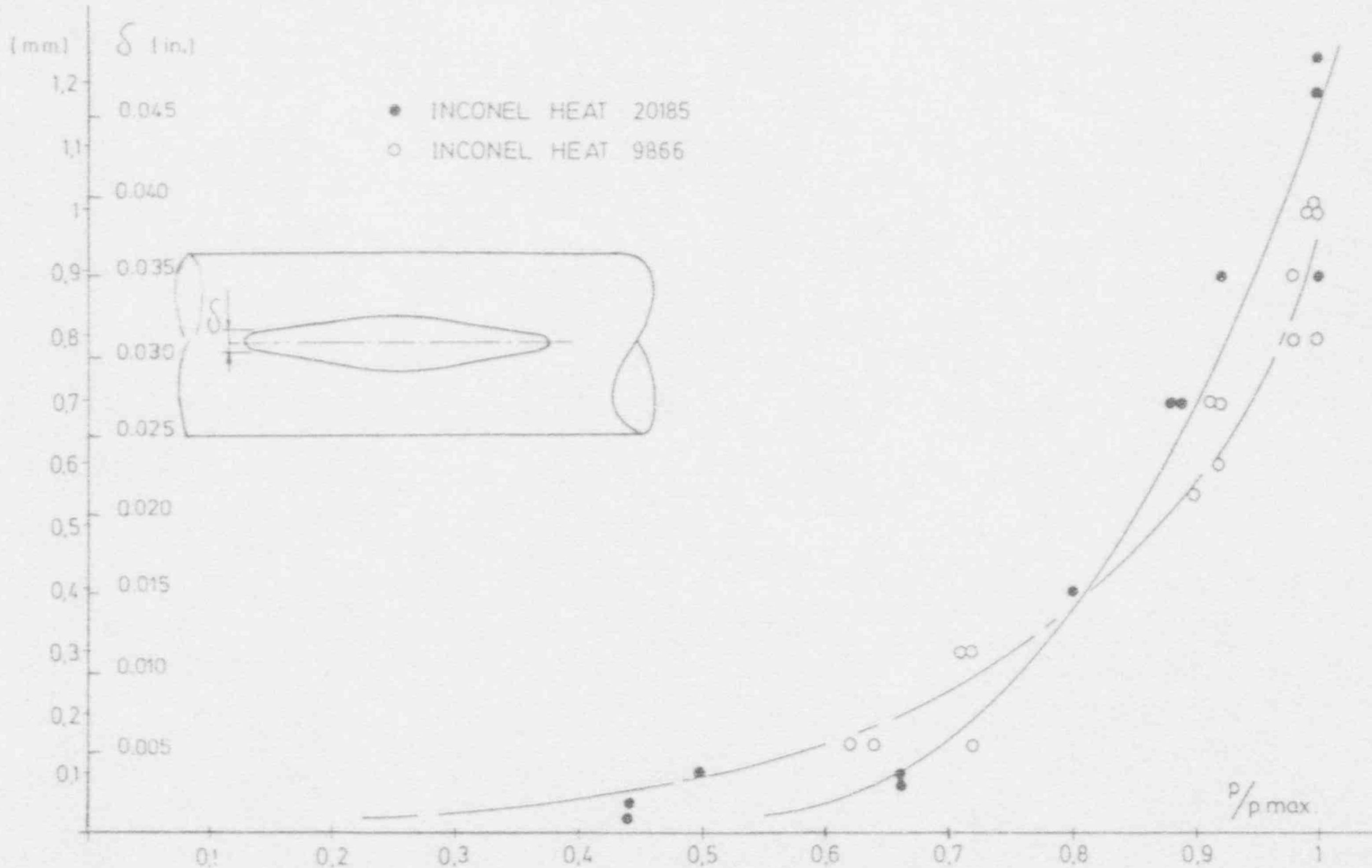

Figure 4-6

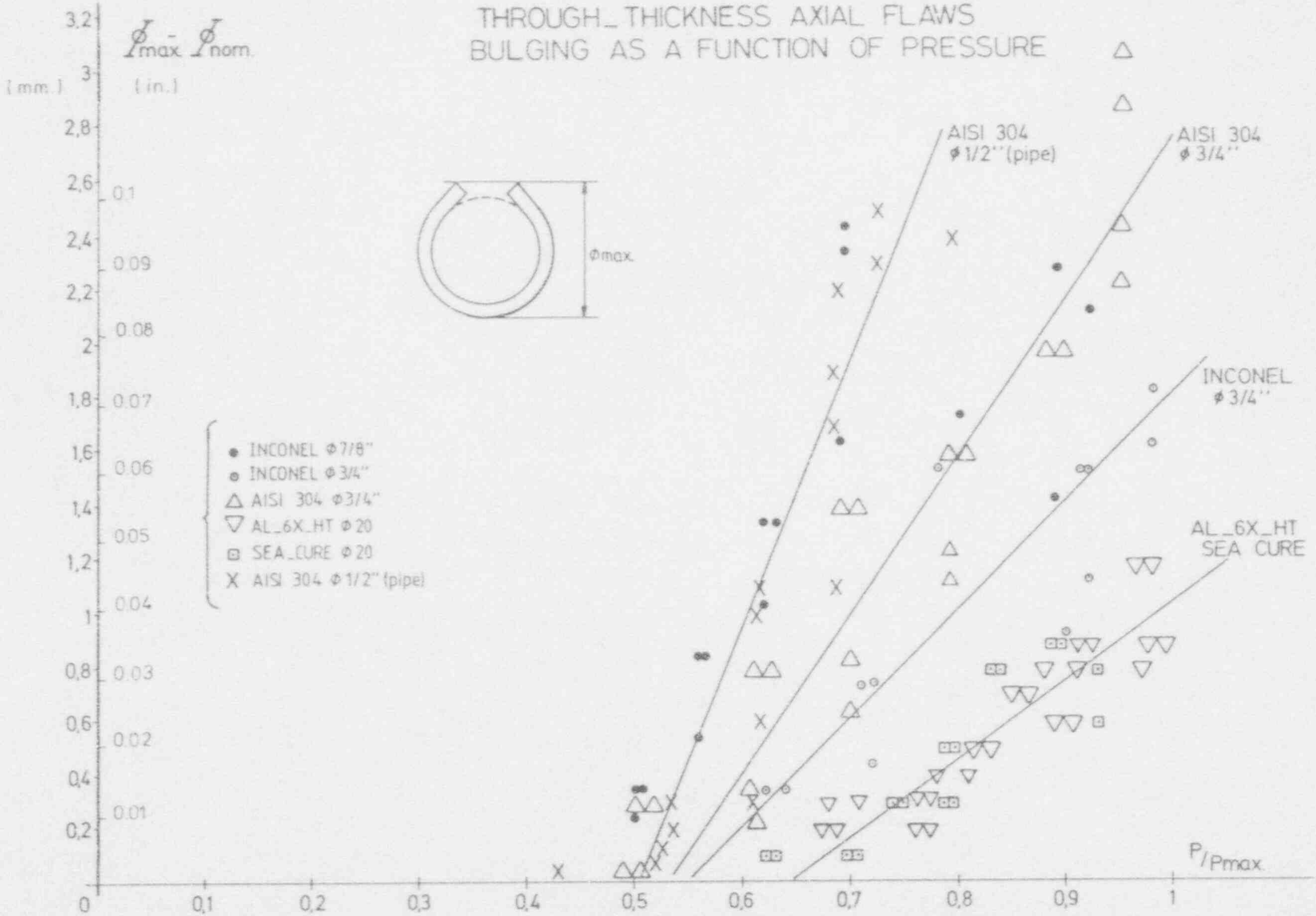
THROUGH_THICKNESS AXIAL FLAWS
BULGING AS A FUNCTION OF PRESSURE
Ømax - Ønom
(mm.)
(in.)
Ømax
INCONEL Φ7/8"
INCONEL Φ3/4"
AISI 304 Φ3/4"
AL_6X_HT Φ20
SEA_CURE Φ20
AISI 304 Φ1/2" (pipe)
AISI 304 Φ1/2" (pipe)
AISI 304 Φ3/4"
INCONEL Φ3/4"
AL_6X_HT SEA CURE
P/Pmax
0
0,1
0,2
0,3
0,4
0,5
0,6
0,7
0,8
0,9
1
0,2
0,4
0,6
0,8
1
1,2
1,4
1,6
1,8
2
2,2
2,4
2,6
2,8
3
3,2
0.01
0.02
0.03
0.04
0.05
0.06
0.07
0.08
0.09
0.1

Figure 4-7

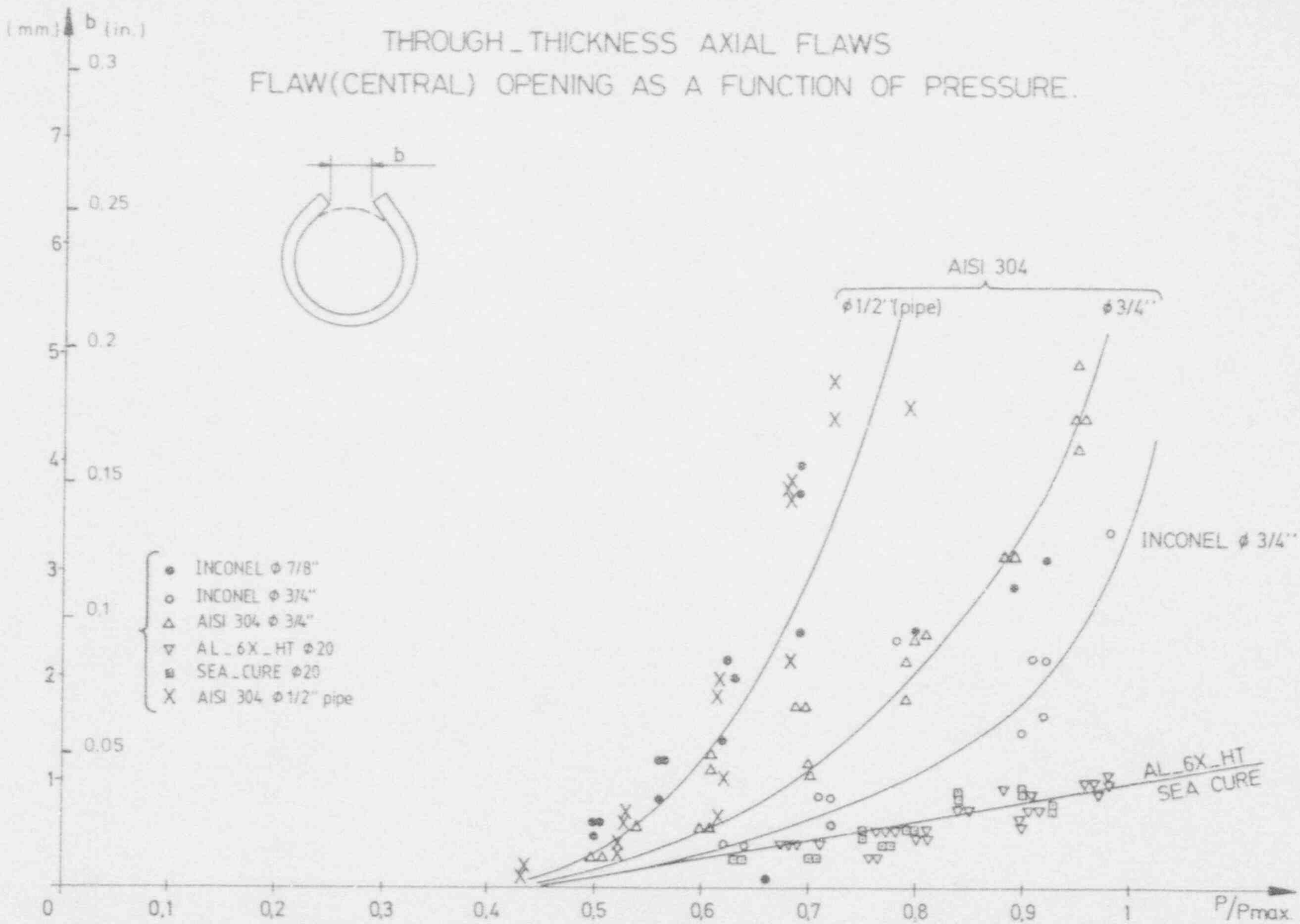
THROUGH_THICKNESS AXIAL FLAWS
FLAW(CENTRAL) OPENING AS A FUNCTION OF PRESSURE.
(mm) b (in.)
0,3
0,25
0,2
0,15
0,1
0,05
b
AISI 304
ϕ 1/2" (pipe)
ϕ 3/4"
INCONEL ϕ 3/4"
AL_6X_HT
SEA CURE
INCONEL ϕ 7/8"
INCONEL ϕ 3/4"
AISI 304 ϕ 3/4"
AL_6X_HT ϕ 20
SEA_CURE ϕ 20
AISI 304 ϕ 1/2" pipe
P/Pmax

Figure 4- 8

CIRCUMFERENTIAL THROUGH_THICKNESS FLAWS
INCONEL ϕ 3/4"

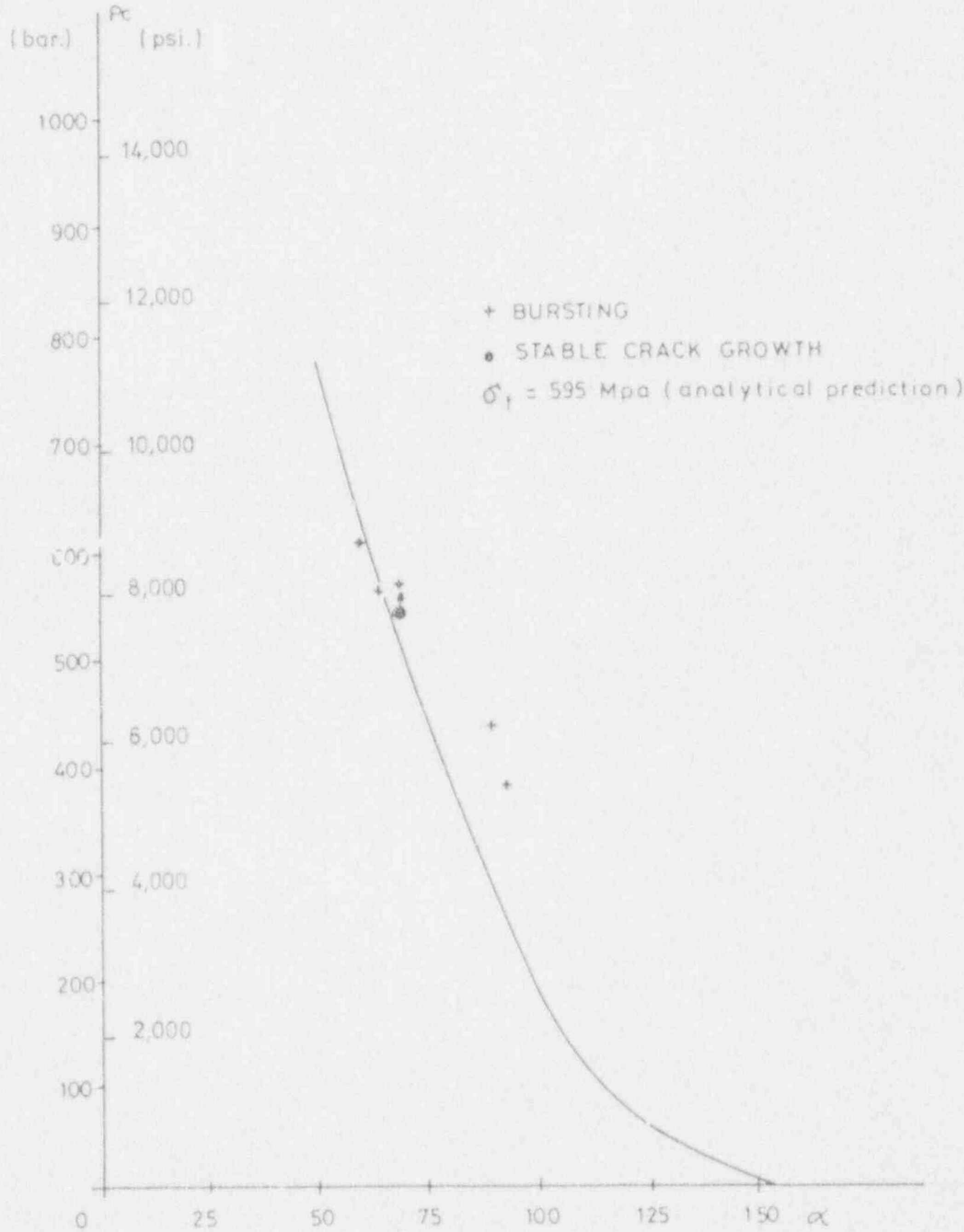

Figure 4 - 9

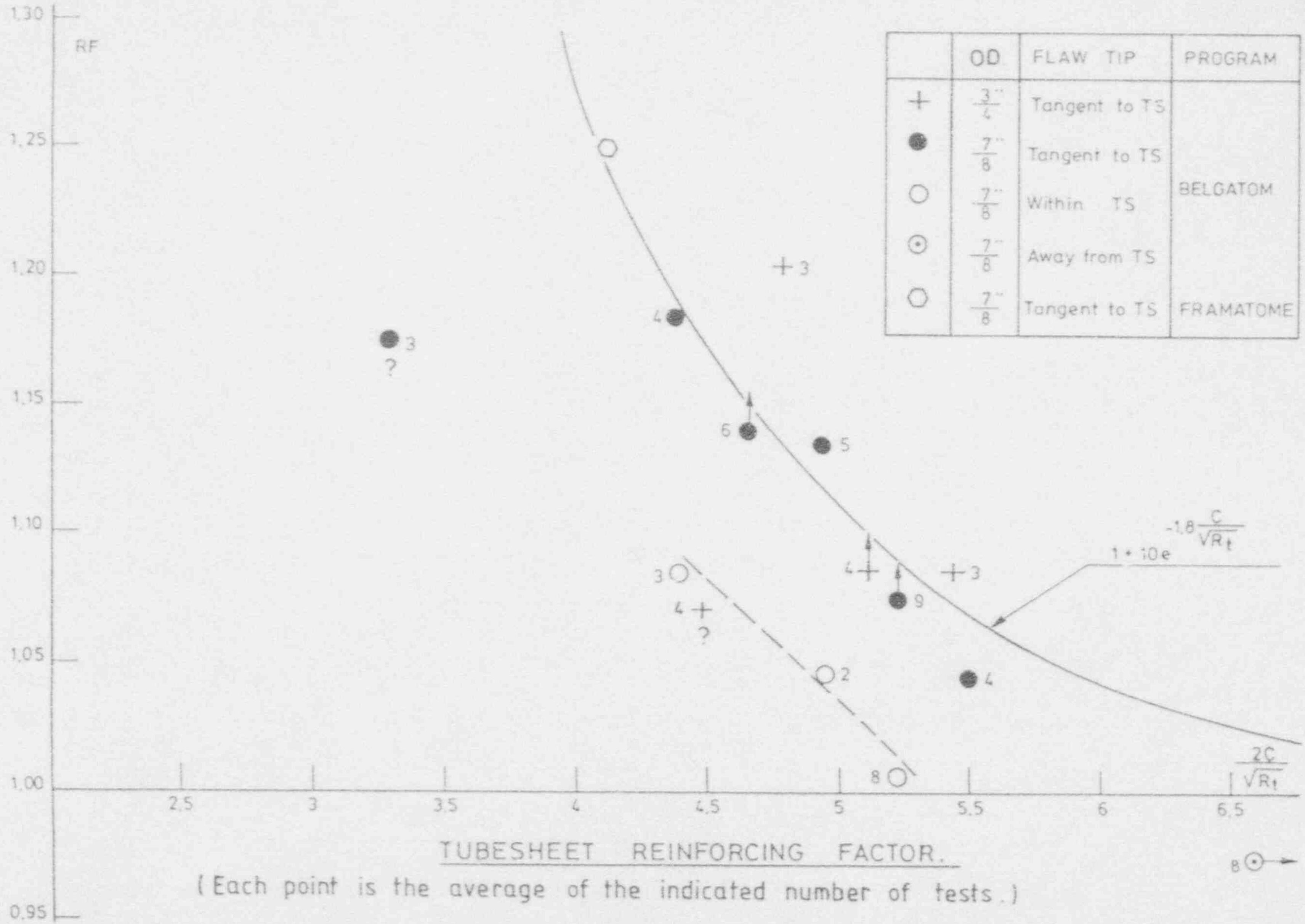

TUBESHEET REINFORCING FACTOR.

(Each point is the average of the indicated number of tests.)

Figure 4 – 10

CIRCUMFERENTIAL THROUGH WALL CRACKS.

with and without lateral restraint

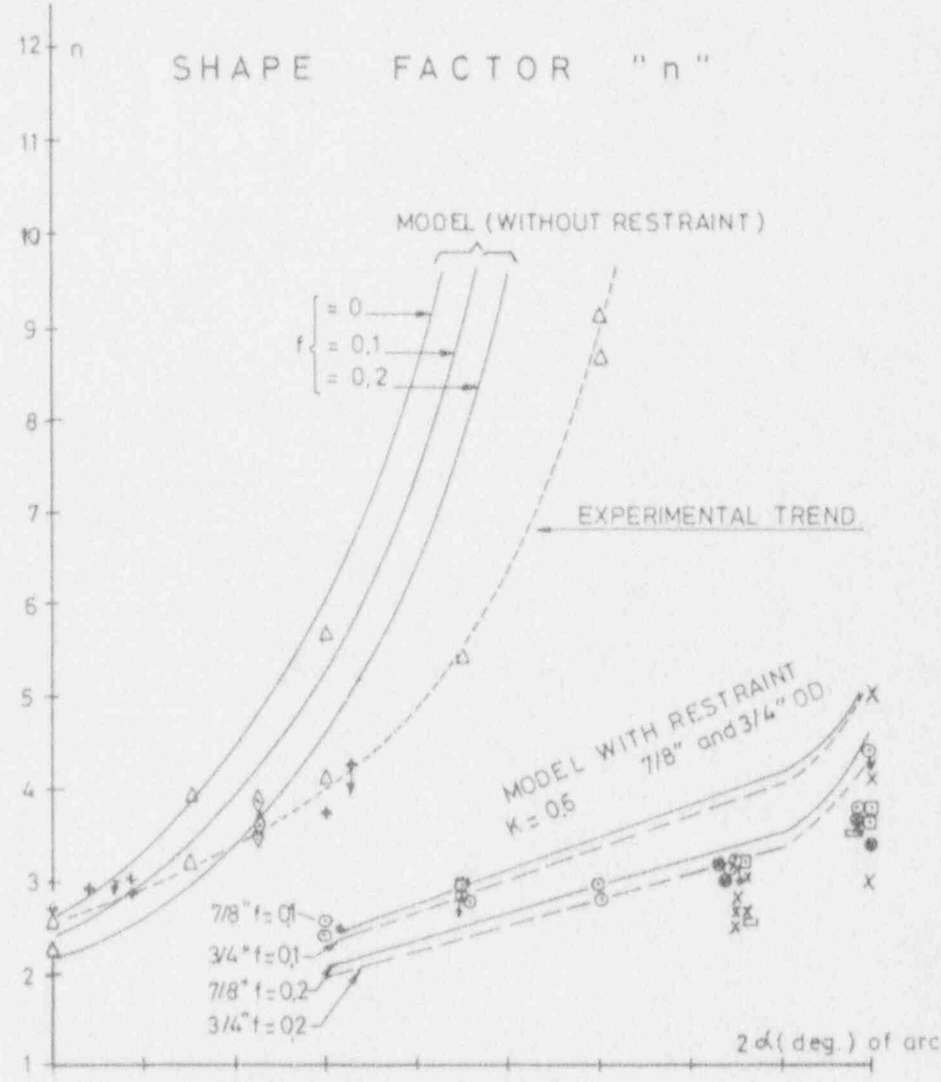

Figure 4 — 11

MECHANICAL PROPERTIES OF DOEL 3.(S.G.B.)

ALLOY 600 MILL ANNEALED TUBING.

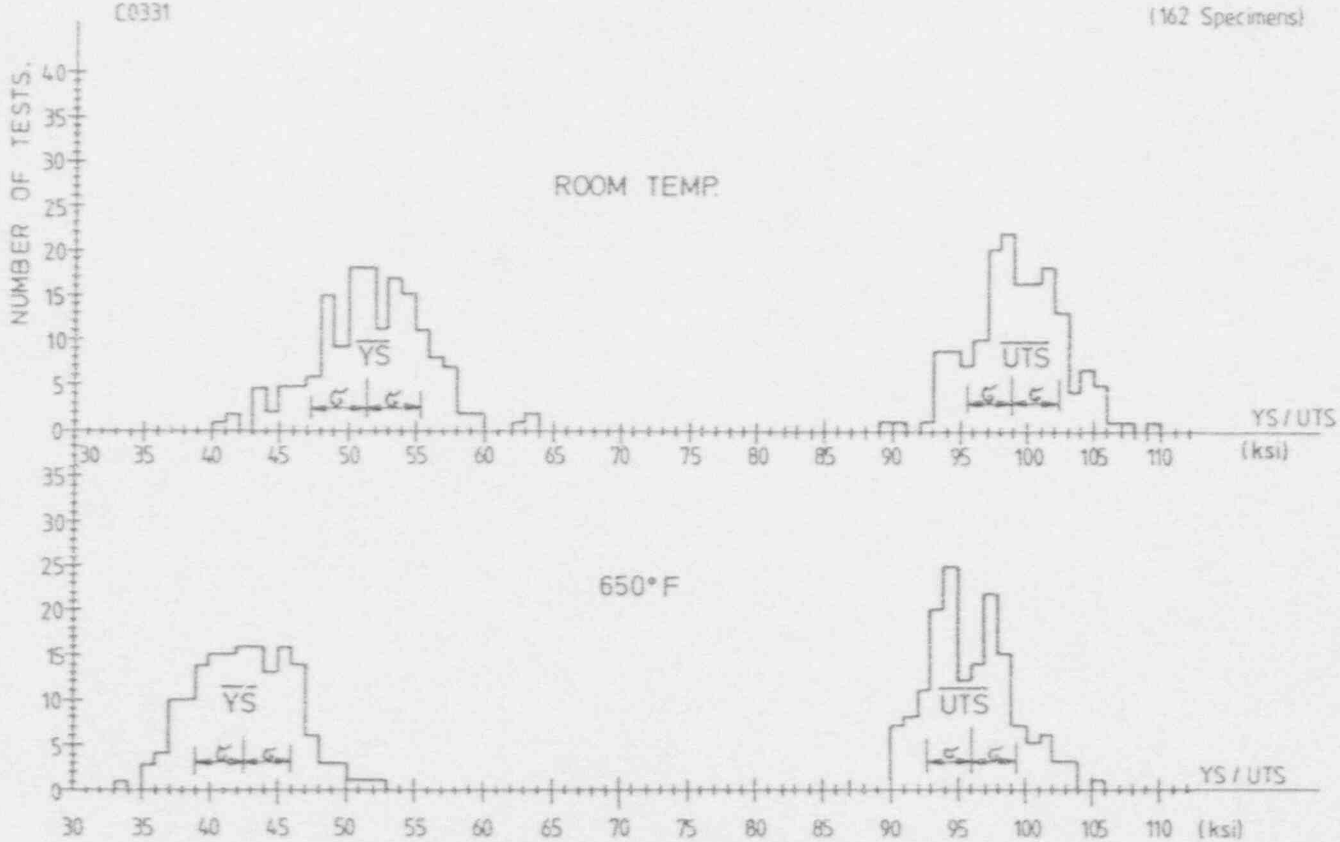

Figure 4-12

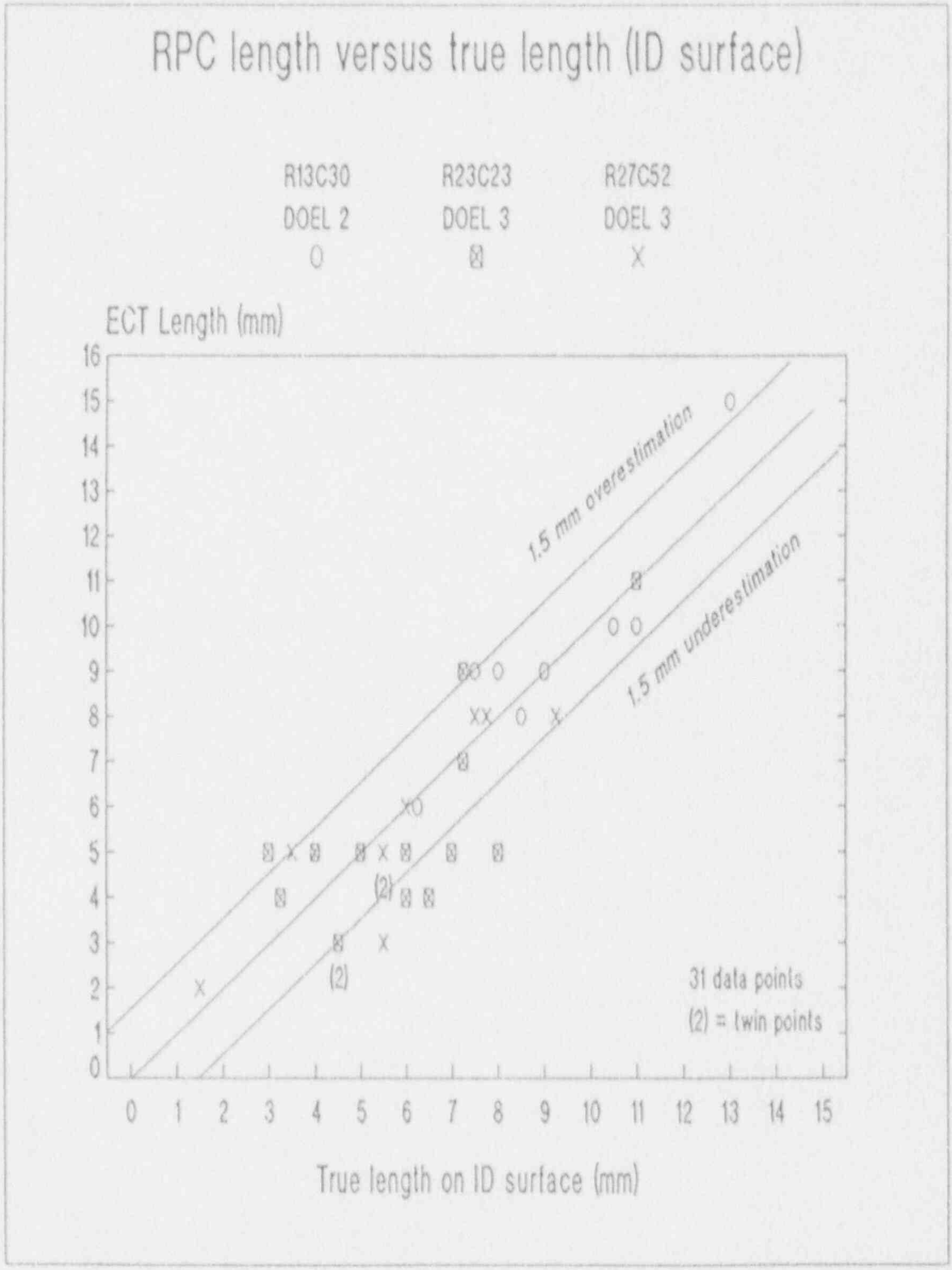

RPC length versus true length (ID surface)
R13C30
DOEL 2
O
R23C23
DOEL 3
⊠
R27C52
DOEL 3
X
ECT Length (mm)
1.5 mm overestimation
1.5 mm underestimation
(2)
(2)
31 data points
(2) = twin points
0 1 2 3 4 5 6 7 8 9 10 11 12 13 14 15 16
0 1 2 3 4 5 6 7 8 9 10 11 12 13 14 15
True length on ID surface (mm)

Figure 4-13

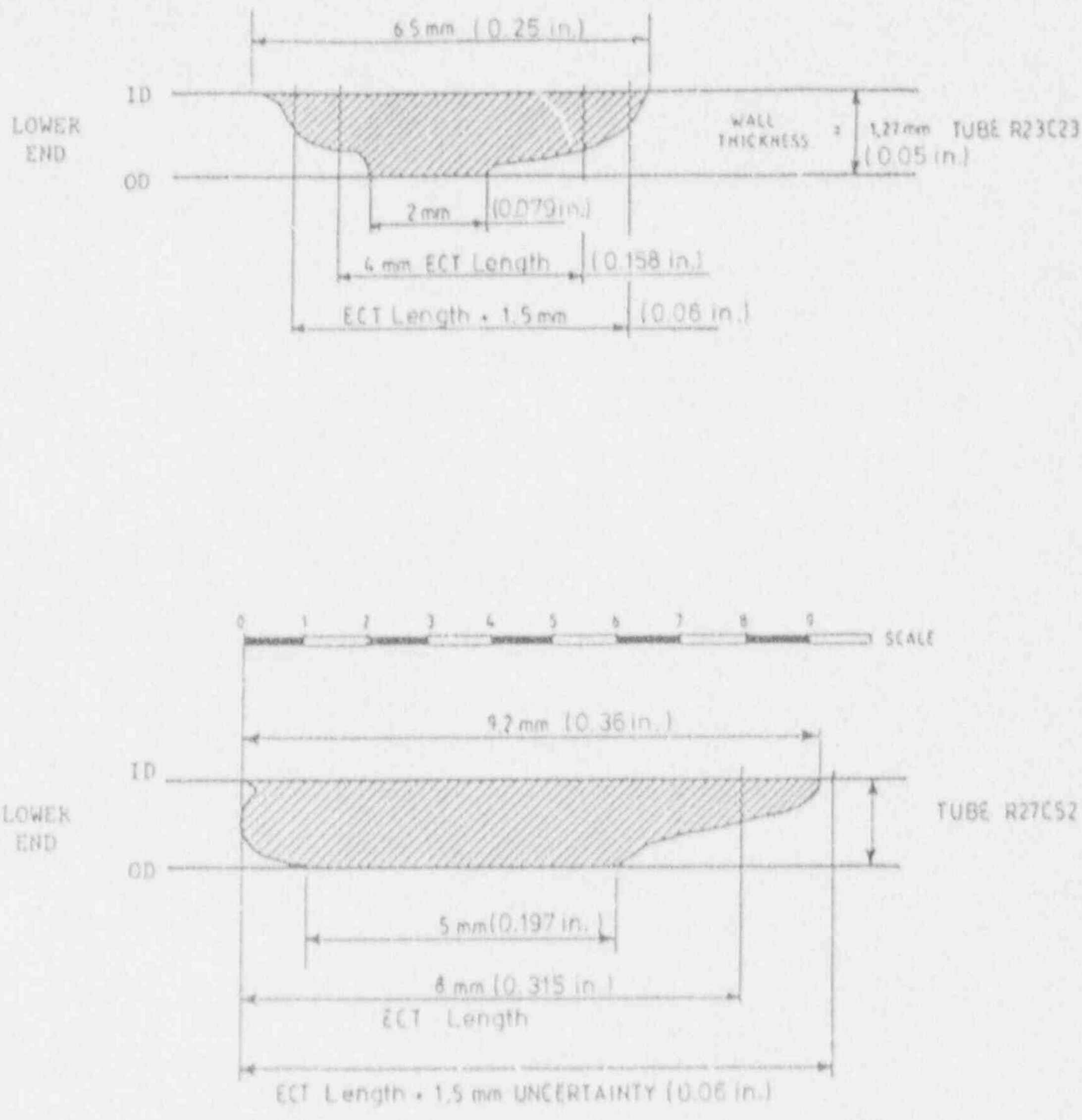

Actual shape of through-wall cracks in the roll transition of 2 tubes pulled from DOEL 3. Comparison with ECT (RPC) length measurement.

Figure 4-14

Section 5

CRACK SIZING METHODOLOGY

5.1. INTRODUCTION

The development of a multifrequency eddy current technique using a rotating pancake coil (RPC) answered the need for improved detectability of the small axial stress corrosion cracks (SCC) observed within the roll transitions. As a side effect, the measurement of the crack length and of the number of indications within the same cross section provided a powerful tool to study the evolution of the primary water stress corrosion cracking (PWSCC) phenomenon. After the shot peening operation at Doel 3 and Tihange 2, these parameters showed that the growth of existing cracks was not stopped by the peening. As plugging limits based on the crack length were established, the use of the RPC shifted from an expertise mode to a production mode. The accuracy of the length measurements became more important as it had a direct influence on the maximum allowable crack length.

The qualification of the RPC method included determining the accuracy of the length measurements. The initial qualification was based on electrical discharge machined (EDM) notches. The calibration curve was established for relatively long EDM defects (ranging from 5 to 15 mm - 0.2 to 0.59 in) with a large signal amplitude. It was applied between 1984 and 1986. During the in-service inspection of Doel 3 in July 1986, two tubes were selected from the RPC data and pulled from the B steam generator. The metallographic examination provided the first comparison between eddy current results and actual defects. Two main conclusions were obtained :

- the RPC was unable to detect some small SCC cracks (< 2 mm - 0.08 in).
- the RPC was undersizing the SCC length (as measured on ID) by an average value of 1 mm (0.04 in).

The rules used to measure the crack length were modified to remove the systematic error observed for the SCC length range of the pulled tubes (33 data points). These rules were applied to the in-service inspections since 1987 and to a retroactive analysis of inspection data (back to June 85). It is important to note that the relationships between the eddy current length and the actual length are different if the reference defects are EDM notches, laboratory defects or actual plant SCC specimens. These differences are the consequence of the complex relationship between the crack morphology and the magnetic field produced by the coil. This relationship can be described as the convolution between the coil response in the presence of an infinitely small defect and the response for a infinitely small eddy current field to a crack. The main variables that influence the RPC response will be :

. the width and penetration depth of the pancake coil detection area.

. the crack profile as a function of the tube wall thickness.

. the difference in lengths on the ID and OD of the tube.

. the width of the crack opening.

Although the width and penetration depth of the magnetic field produced by the coil can be controlled to some extent, the other parameters are unknown. The probe design was optimized to obtain a small magnetic field both axially and tangentially to the coil tip. The calibration was performed on actual defects observed on the two pulled tubes in order to minimize the influence of the unknown crack parameters.

Three parameters were initially studied : the length, the depth and the number of signals within the same cross section. Although an eddy current phase angle to defect depth could be established for EDM notches, laboratory results on artificial SCC cracks indicated that the EDM calibration curve for depth measurements was not representative of the real penetration. Also, on site inspections showed most cracks to be through-wall. For these reasons, the SCC depth was assumed to be 100 % through the tube wall for all axial defects detected in the roll transitions.

The detection and sizing of circumferential cracks was not a concern because only longitudinal SCC was expected in the kiss and hard rolls configurations. However with the increased operating time of these plants, the possibility of circumferential SCC may increase. Several developments are currently under way using both eddy current and ultrasonics in order to detect and to measure the azimuthal length of circumferential flaws. Some preliminary measurements performed in the laboratory and on site with ultrasonics indicates that a [illegible] industrial inspection can be developed.

The following paragraphs detail the qualification results for longitudinal SCC in terms of accuracy and reproducibility. EDM notches were used for the laboratory study of the reproducibility of the position and length measurements (1984). Actual SCC cracks obtained from pulled tubes in July 1986 (Doel 3) and July 1987 (Doel 2) were used to demonstrate the length measurement accuracy. All the measurements were performed with the same equipment and procedure that were used during the 100 % RPC inspection of Tihange 2 (February 1988) and Doel 3 (June 1988), as described in Section 6. Laboratory examinations were performed from the trailer using the polar manipulator installed into a steam generator mockup in order to simulate as close as possible the on site conditions. It was considered necessary to repeat the recording of the EDM notches because of the significant changes in hardware and software since 1984.

5.2. STUDY OF THE ACCURACY AND REPRODUCIBILITY OF EDM NOTCHES

Program

Five parameters were studied : the position and length of the defect, the number of signals within the same cross section, their amplitude and their phase to depth relationship. The signals were also analysed to determine the detectability and the importance of the dynamic range for the eddy current instrument. The measurements were performed on a set of EDM axial and circumferential notches summarized in Table 5-1.

The length ranges from 1 mm to 25 mm (0.04 in to 1 in) and the number of EDM notches from 1 to 6 in the same cross section. The notch depth ranges from 10 % to 100 % through the tube wall thickness.

Detectability And Dynamic Range

The detection of the EDM notches can be studied as a function of their length and penetration depth. It appears that the minimum detectable penetration depth has to be defined as a function of the length, the width and the initiation side of the defect. The minimum detectable depth for external (OD) EDM notches ranges from 80 % for a 1 mm (0.04 in) notch to 40 % for a 25 mm (1 in) notch with a 1 mm (0.04 in) width. These values for internal (ID) defects are 80 % for a 1 mm notch and 20 % for a 25 mm (1 in) notch with a 1 mm (0.04 in) width. Also, all ASME standard defects (which are large volume defects) were easily detected and sized. It should be pointed out that the amplitudes of the signal for EDM flaws of 100 % depth are three to four times larger than the greatest amplitude observed so far in steam generators. The amplitude ratio of the majority of SCC flaws to the RPC calibration defect (longitudinal through wall notch of 25 mm (1 in) length) is approximatively - 30 dB and decreases for the smallest detectable signals to - 45 dB.

It should be noted that the coil has been designed to optimize the accuracy of the crack length measurement. To this end, the coil diameter respective to the ferrite coil diameter was held as small as possible. It produces a smaller EC field which improves the resolving power. As a drawback, this technique reduces the detectability for OD cracks and modifies the phase to depth relationship.

Accuracy And Reproducibility

Position Measurement. Two series of tests have been performed using the setup presented in Figure 5-2. Tube number 69237 was probed sequentially 25 times from top to bottom. The tube position was reversed and probed again another 25 times. The correct position of the defects on the mockup was measured manually before and after each sequence. Figure 5-3 summarizes the results. The reproducibility for locating known defects is +/- 1 mm (0.04 in) for 97.5 % of the measurements. These results indicate that locating defects is precise enough to use an automated analysis technique to measure defect growth.

Length Measurement. These measurements were performed on the full set of EDM longitudinal flaws using the "actual SCC" length analysis rule. The length of the longest notch in each cross section was measured by the analysis software. Shorter flaws were not taken into account. This sequence results from the use of the normal on site software which reports only the length of the longest SCC crack. The length is always measured axially to the tube.

As expected from the "actual SCC" calibration, the length estimations for EDM notches are oversized from 1 to 5 mm (0.04 to 0.2 in) as a function of the defect amplitude and shape. It is important to note that the length analysis rules were defined for the defects observed in two pulled tubes from Doel 3 with amplitudes ranging from 0.050 volts to 0.650 volts. The length measurement is based on a fixed threshold that does not take into account the influence of the defect end (abrupt for EDM and smooth for SCC) or its amplitude. Thus, the over or undersizing effect will be a consequence of the defect morphology. As a result, the analysis rules have to be determined as a function of the signals and defects observed in the steam generator tubes. The reproducibility of the length measurements is shown in Figure 5-4. It can be observed that the error is within ± 1 mm (0.04 in) for 99 % of the measurements.

Number of Signals on the Same Cross Section. These measurements were performed on the full set of EDM flaws. The overestimation of 1 to 3 notches resulted from the large amplitude of the EDM notches that produces small signal overshots after signal processing. These overshots are large enough to trigger the signal counter. The same situation does not occur for real SCC defects.

Amplitude Measurement. The same measurements used for the study of the defect position accuracy (longitudinal and circumferential notches) provided the information for the study of amplitude reproducibility. Although the signal amplitude is not useful for sizing SCC cracks, its reproducibility has an influence on defect detection. The distribution of the largest amplitude in each cross section measured with the analysis software is shown in Figure 5-5. The software reports only the amplitude of the most significant indication. The reproducibility is +/- 4 % of the amplitude for 98 % of the sample. This value is strongly affected by the rotationnal noise produced by the misalignement between the test tubes (200 mm length) and the test bench. The probe centering devices are located

85 mm apart which results in the EDM notches being measured while the probe upper and lower centering wheels are located in different tube parts. The amplitude reproducibility is therefore much better during on site inspections where such misalignment does not occur.

Depth Measurement. The complete set of tubes was analysed in order to determine the eddy current phase to defect depth relationship. Figure 5-6 shows the curve obtained for EDM longitudinal defects. The phase was measured manually because the software used for on site inspections does not provide this function for the RPC analysis. The phase was measured only for the defects that are longer than the magnetic field created by the pancake coil in order to reduce the uncertainty. As it appears from these results, the depth of defects longer than 10 mm (0.4 in) can be estimated from the eddy current phase angle with an accuracy of +/- 20 % at 240 kHz and +/- 10 % at 500 kHz. The reproducibility of the depth estimations for EDM notches relies on the accuracy of the phase measurement and the signal to noise ratio.

5.3. STUDY OF THE ACCURACY AND REPRODUCIBILITY FOR ACTUAL CRACKS

Program

This study is based on three tubes :

. two pulled tubes from the B steam generator of Doel 3 which were analyzed by RPC and metallographic examination

. one pulled tube from the A steam generator of Doel 2 which was analyzed by RPC, visual examination and dye penetrant.

The tubes from Doel 3 are hard rolled for the full length of the tubesheet with a final kiss roll; they show only PWSCC in roll transitions. The tube from Doel 2 had a partial depth hard roll for a length of 70 mm (2.75 in) from the bottom of the tubesheet. It has two types of defects : PWSCC on the roll transition area and one secondary water stress corrosion crack (SWSCC) at 60 mm (2.36 in) above the roll transition.

Four parameters were studied : the length, the number of signals along the same cross section, their amplitude and their phase to depth relat[illegible]). The signals were also analysed to determine crack detectability. A representative sample of Doel 3 and Doel 2 cracks is summarized in Tables 5.2.1 to 5.2.3.

For the Doel 3 tubes, the ID lengths range from 1 mm to 11 mm (0.04 in to 0.43 in), the number of cracks from 20 to 22 along the same transverse cross section. Their depth and the amplitude range respectively from 63 % to 100 % through wall and from 0.050 volts to 0.650 volts. As the Doel 2 tube has not been examined destructively, only the indications observed from the ID and OD dye penetrant tests can be used. The ID lengths range from 3.3 mm to 13 mm (0.13 in to 0.51 in), the number of cracks ranges from 1 (SWSCC defect) to 10 (roll transition area). The depth is 100 % penetration for all the PWSCC defects.

Detectability and Dynamic Range

The detection of actual SCC cracks can be studied as a function of their length and penetration depth. Tables 5.2.1 to 5.2.3 indicate the results obtained for each flaw.

The minimum detectable depth for external cracks cannot be estimated as the actual crack depth of the SWSCC is not known. The PWSCC defects that were not detected by RPC are between << 1 mm and 2.0 mm (0.04 in and 0.08 in) long with penetration depths between 71 % and 100 %. Also, the two circumferential defects of 51 % and 53 % depth and an azimuthal length of 1.5 mm and 3.5 mm (0.06 in and 0.14 in) were not detected. A close examination of the crack locations along the tube circumference (Figures 5-7a to c) shows that several cracks are close enough to produce a single eddy current signal. For tube R23 C23, this is the case for the cracks 8/9, 10/10', 11/12/12' and 16/17/17'. In particular, the two circumferential cracks are included in the signal produced respectively by the longitudinal defects 11/12/12' and 16/17/17'. The same situation occurs for cracks 2/3/3', 7/8, 11/12/13 and 15/16 of tube R27 C52 and 10/1 of tube R13 C30. This phenomenon results from the eddy current detection field being about of 5 mm in diameter. For a non optimized coil design, the diameter of influence can exceed 10 mm further reducing the resolving power of the RPC probe. These results indicate that all defects with 100 % penetration depth and a length greater than 2.0 mm lead to a detectable signal.

Accuracy and Reproducibility

Position Measurement. Position measurements were performed only on the Doel 2 tube. Three inspections of the same tube were analysed in order to determine the accuracy of the position measurement. The accuracy and the reproducibility of positioning are within +/- 1 mm (0.04 in).

Length Measurement. The study of the accuracy of the length measurements was performed in 1986 on the two pulled tubes from Doel 3 (see Fig. 5-8). This led to the interpretation rules used since 1987. The results for the Doel 2 defects were determined using this calibration curve. The length of the longest crack in each cross section was measured by the analysis software. The other cracks were measured manually using the same rules. This procedure was required since the on site software reports only the length of the longest SCC crack.

The results of the comparison between real and measured crack lengths are shown on Figure 5-8. The regression line is given by RPC length = - 0.123 + 0.981 * (ID crack length) with a correlation coefficient of 0.882. The analysis of the effect of the crack profile on the RPC over or underestimation indicates that the error is mainly a function of :

- the difference between the OD and ID crack lengths
- the profile between the OD and ID crack extremities
- the presence of two or more cracks close enough to produce a single RPC signal.

The overestimation was already observed during the measurements of EDM notches with rectangular profiles. As an example, the overestimation can be seen on the PWSCC crack 12 of the tube R27 C52 (Figure 5-9). However, triangular or trapezoidal profiles will produce an underestimation of crack length as can be seen for cracks 7 of tube R23 C23 and 6 of tube R27 C52 (Figure 5-10). As a confirmation, for the Doel 2 tube (R13 C30) where the OD length of the cracks is close to the ID length (difference of 1.5 mm max (0.06 in)), the RPC underestimation of the ID length never exceeds 1 mm. As a consequence of both Doel 2 and Doel 3 tube examinations, the RPC sizing accuracy margin has been considered to have a maximum value of 1.5 mm

(0.06 in). This value is conservative as the average length of an actual PWSCC flaw is less than the maximum length measured on ID. Consequently, it more than adequately covers any structural concern.

Number of Signals in the Same Cross Section. Tables 5.2.1 and 5.2.2 summarize the number of signals detected by the software on the same cross section. It appears that this value underestimates the real number of defects for the Doel 2 and 3 tubes. Two reasons explain this observation : the small volume of SCC cracks and the integrating effect of the eddy current field. Some very small defects of the Doel 3 tubes not detected by eddy current, radiography and visual testing were only detectable after the tube had been flattened. As the eddy current field has a radius of 2.5 mm (0.1 in) at the detection frequency, it will integrate the influence of cracks that are closer than this distance. Consequently, although the study of the number of signals along the same cross section provides useful information about the increase in number of SCC cracks, it has to be considered as an underestimation of the actual progression.

Amplitude Measurement. From the comparison of several hundreds of repeated records in Doel 3 and Tihange 2, the reproducibility of the amplitude measurement is better than 0.05 volts for 90 % of the sample. In most circumstances, the difference results from the influence of the probe lift-off during the rotationnal movement.

Depth Measurement. The PWSCC defects that were detected in the pulled tubes show a 100 % penetration depth. The same observation can be obtained from the analysis of the 100 % inspection of all steam generator tubes of Doel 3 and Tihange 2. Therefore, since the crack length and amplitude influence the phase/depth relationship, it has been considered that this information was not sufficiently accurate to be usefull for the SCC examination. This conclusion about the RPC capabilities to size the depth of defects is only true for small length and small volume defects like PWSCC. Accurate depth measurements can be obtained for wastage or wear.

5.4. CONCLUSIONS

This work had the objective of defining the detection capability, accuracy, and the reproducibility of the multifrequency eddy current method using a rotating pancake coil for primary water stress corrosion cracking in roll transitions. Two types of defects were used : EDM defects and actual cracks from pulled tubes. A first observation is the significant difference between EDM defects and real SCC cracks. The EDM notch results have been restricted to equipment calibration and signal reproducibility. The results of RPC measurements using EDM defects should not be used for the qualification of either the detectability of cracks or the accuracy of the length estimates.

The RPC method is able to measure with a good reproducibility the length (+/- 1 mm - 0.04 in), the amplitude (+/- 0.05 volts) and the position (+/- 1 mm - 0.04 in)) of SCC flaws. Defects longer than 2.0 mm (0.08 in) and with 100 % penetration depth showed a 100 % detectability. For smaller defects, the minimum signal to noise ratio, which depends mostly on the crack shape, defines the detection threshold. Again, if one considers EDM notches which are large volume flaws, detectability limits can be expressed in terms of 20 % (ID) to 40 % (OD) penetration depth. All ASME standard defects, which are large volume defects, were easily detected and sized. The good reproducibility of the amplitude measurements indicates that the detectability will be fairly constant. This conclusion has been confirmed from on site data where the percentage of very small defects that "disappear" between two consecutive inspections is less than 0.5 %.

The measured number of cracks in the same cross section should be considered as an approximate indication of the actual number of cracks. This is because defects up to 2.0 mm (0.08 in) may not be detectable and two or more closely spaced cracks can be integrated into a single signal. Nevertheless, the RPC method constitutes an efficient tool to study the PWSCC progression.

The length estimate constitutes the main objective of the inspection. It has been confirmed that the technique is optimized for the measurement of longitudinal PWSCC cracks between 2 and 15 mm (0.08 and 0.6 in). The reproducibility of the length measurements has been demonstrated within +/- 1 mm (0.04 in). It has been confirmed from on site data where the percentage of defects with an apparent length decrease (not exceeding 1 mm) between successive inspections is less than 5 %. The accuracy of the length estimates can be expected within +/- 1.5 mm (0.06 in) of the ID real crack length. The error in length estimates results from the crack morphology in terms of profile (rectangular, triangular or trapezoidal shapes), respective ID to OD lengths and the opening of the crack. An optimized coil design with a small eddy current field (axially and tangentially to the coil tip) associated with a calibration curve established from actual defects minimizes the influence of the unknown crack parameters on the EC length measurement.

TABLE 5.1

EDM notches (1)

Tube #	Notches						
	type (3)	origin	length (mm)	width (mm)	depth (4) (%)	Nr.	Remarks
57.969	L	OD	25	1	40	1	
	L	ID	25	1	20	1	
58.712	TWH	100 %	Φ 1.25	-	100	4	ASME tube from LABORELEC
	FBH	OD	Φ 4.82	-	19	4	
	FBH	OD	Φ 4.83	-	41	1	
	FBH	OD	Φ 2.85	-	64	1	
	FBH	OD	Φ 2.2	-	82	1	
	TWH	100 %	Φ 1.72	-	100	1	
69.237	C	100 %	10	0.2	100	1	] same cross section
	C	ID	15	0.2	80	1	
	L	100 %	25	0.2	100	1	] same cross section
	L	100 %	15	0.2	100	1	
	L	100 %	10	0.2	100	1	
	L	100 %	5	0.2	100	1	] same cross section
	L	100 %	2	0.2	100	1	
	L	100 %	1	0.2	100	1	
	C	100 %	5	0.2	100	1	] same cross section
	C	100 %	2	0.2	100	1	
69.777	L	ID	25	0.2	40	4	
	L	OD	10	0.2	20	6	
	L	ID	25	0.2	60	2	
69.778	L	ID	25/26	0.2	10	6	(see Fig. 5-1b)
	L	OD	2	0.2	10	1	-
	L	ID	25	0.2	80	1	-
69.780	L	ID	25/31	0.2	80	1	(see Fig. 5-1b)
	L	OD	2	0.2	40	4	-
	L	ID	25/29	0.2	60	2	(see Fig. 5-1b)
69.781	L	OD	10	0.2	40	4	
69.782	L	OD	10	0.2	60	2	
69.785	L	ID	10	0.2	80	1	-
	L	OD	25/28	0.2	20	6	(see Fig. 5-1b)
	L	ID	10	0.2	60	2	-

TABLE 5.1 (continued)

Tube #	Notches						
	type (3)	origin	length (mm)	width (mm)	depth (4) (%)	Nr.	Remarks
69.788	L	OD	25	0.2	60	2	-
	L	OD	25/31	0.2	80	1	(see Fig. 5-1b)
	L	ID	2	0.2	20	6	-
69.789	L	OD	25	0.2	80	1	
	L	ID	2	0.2	20	2	
69.792	L	ID	2	0.2	80	1	
	L	OD	10	0.2	80	1	
76/001	FBH	OD	Φ 4.8	-	20	4	ASME tube from WESTINGHOUSE (2)
	FBH	OD	Φ 4.8	-	40	1	
	FBH	OD	Φ 2.8	-	60	1	
	FBH	OD	Φ 2	-	80	1	
	TWH	100 %	Φ 1.7	-	100	1	
84/004	C	ID	5	0.2	10	1	] same cross section
	C	ID	5	0.2	20	1	
	C	OD	5	0.2	10	1	] same cross section
	C	OD	5	0.2	20	1	
	C	OD	5	0.2	40	1	] same cross section
	C	OD	5	0.2	60	1	
	C	OD	5	0.2	80	1	] same cross section
	C	ID	5	0.2	40	1	
	C	ID	5	0.2	60	1	] same cross section
	C	ID	5	0.2	80	1	
84/006	L	ID	1	0.2	10	1	] same cross section
	L	ID	1	0.2	20	1	
	L	OD	1	0.2	10	1	] same cross section
	L	OD	1	0.2	20	1	
	L	OD	1	0.2	40	1	] same cross section
	L	OD	1	0.2	60	1	
	L	OD	1	0.2	80	1	] same cross section
	L	ID	1	0.2	40	1	
	L	ID	1	0.2	60	1	] same cross section
	L	ID	1	0.2	80	1	

TABLE 5.1 (continued)

Tube #	Notches						
	type (3)	origin	length (mm)	width (mm)	depth (4) (%)	Nr.	Remarks
84/007	L	ID	5	0.2	10	1	] same cross section
	L	ID	5	0.2	20	1	
	L	OD	5	0.2	10	1	] same cross section
	L	OD	5	0.2	20	1	
	L	OD	5	0.2	40	1	] same cross section
	L	OD	5	0.2	60	1	
	L	OD	5	0.2	80	1	] same cross section
	L	ID	5	0.2	40	1	
	L	ID	5	0.2	60	1	] same cross section
	L	ID	5	0.2	80	1	

General Remarks :

(1) Except for tube 76/001, all notches and holes (flat bottom or through wall) are electrical discharge machined.

(2) Holes of tube 76/001 are drilled

(3) The notches are :

- L : longitudinal
- C : circumferential

The holes are :

- TWH : through wall hole
- FBH : flat bottom hole

(4) Except for tube 58712, all the depth values are only theoretical values.

<u>Table 5.2.1</u>

COMPARISON OF EXAMINATION RESULTS

Doel 3 (tube R23 C23)

EdF # (*)	Length (**)			Depth %	LE # (*)	EC length	Remark
	Visual	ID	OD				
1	4.5	4.5	-	79	10	3	-
2	4	-	-	-	9	5	-
3	5	-	-	-	8	5	-
4	6.2	-	-	-	7	5	-
5	6.3	-	-	100	6	5	-
6	3	3.2	-	79	5	4	-
7	7	6.5	2	200	4	4	-
8	7	7.2	1.5	100	3	7	Σ (8 + 9)
9	4.5	4.5	-	79	3		
10	5	4.9	-	82	2		Σ (10 + 10')
10'	7	7.2	-	90	2	8to 10	
11	5 (+T 1.5)	-	-	79/53		11	Σ (11 + 12 + 12')
[12	5	-	-	86	1	11	
12']	7.5	-	-	94.5			
13	4.5	-	-	-	12'	(3?)+1	
14	8	-	-	-	12	5	
15	6	6	-	86	11'	(4?)+1	
16	3	-	-	-	11	5	Σ (16 + 17 + 17')
17	3.5 T	-	-	63/51	11		
17'	-	-	-	-	11		

* identification numbers differ between LABORELEC (LE) and EdF (destructive examination)

** measurement by destructive examination
- . visual : ID surface of sectionned half tube
- . ID] from metalographic examinations
- . OD] (cross sections or opened cracks)

Table 5.2.2

COMPARISON OF EXAMINATION RESULTS
Doel 3 (tube R27 C52)

EdF # (*)	Length (**)			Depth %	LE # (*)	EC length	Remark
	Visual	ID	OD				
1	1	0.2	-	71	ND	-	-
2	1.5	1.1	-	94			-
3	2	1.5	-	94	6	2	Σ (2 + 3 + 3')
3'	1.5	-		?			
4	1.5	1.2	-	71	ND	-	-
5	5.5	-	-	?	4	5	-
6	9	9.2	5	100	3	8	-
7	7.5	-	-	100	2	8	2 cracks
8	2.5	-	-	?			Σ (7 + 8)
9	2	1.7	-	87	ND	-	-
10	8	7.7	5	100	1	8	-
11	2	-	-	?			
12	4	3.6	2.8	100	10	5	Σ (11 + 12 + 13)
13	2	-	-	?			
14	5.5	-	-	?	9	5	2 cracks
15	1.5	-	-	?	8	5-6	Σ (15 + 16
16	6	6	3	100			
17	5.5	-	-	?	7	3	-
18	< 1	-		?	ND	-	-
19	< 1	-	-	?	ND	-	-
20	< 1	-	-	?	ND	-	-
21	< 1	-	-	?	ND	-	-

* identification numbers differ between LABORELEC (LE) and EdF (destructive examination)

** measurement by destructive examination
. visual : ID surface of sectionned half tube
. ID] from metalographic examinations
. OD] (cross sections or opened cracks)

TABLE 5.2.3.

COMPARISON OF EXAMINATION RESULTS

DOEL 2 (tube R13 C30)

DATA #	VISUAL LENGTH mm		EC MEASURED LENGTH mm	REMARK
	ID	OD		
1	13	12	15	
2	8.5	7.9	8	
3	6 (?)	5.7	6	
4	6.3	5	6	
5	11	9.5	10	
6	10.5	8.9	10	
7	8.9	7.1	9	
8	8	6.9	9	
9	7.5 - 8(?)	8.4(?)	9	
10	3.3	2.8	-	associated with # 1

TYPE OF NOTCHES

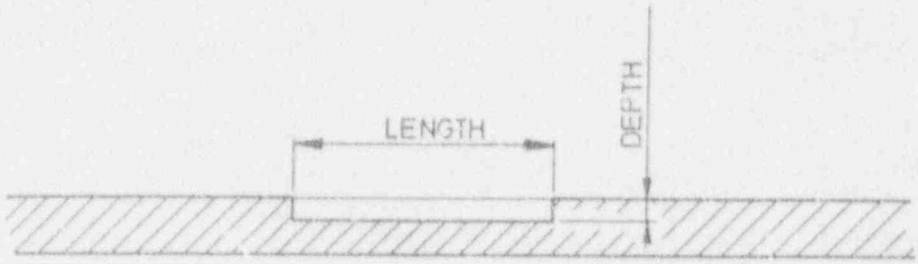

Figure 5-1-a Normal notches.

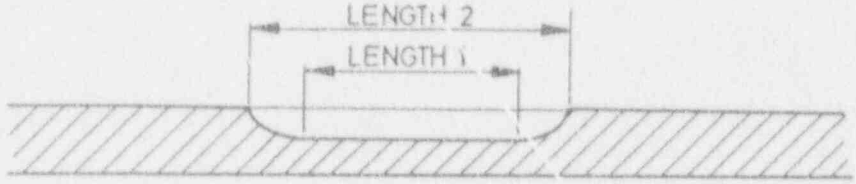

Figure 5-1-b Special notches.

Figure 5-1

TEST SETUP.

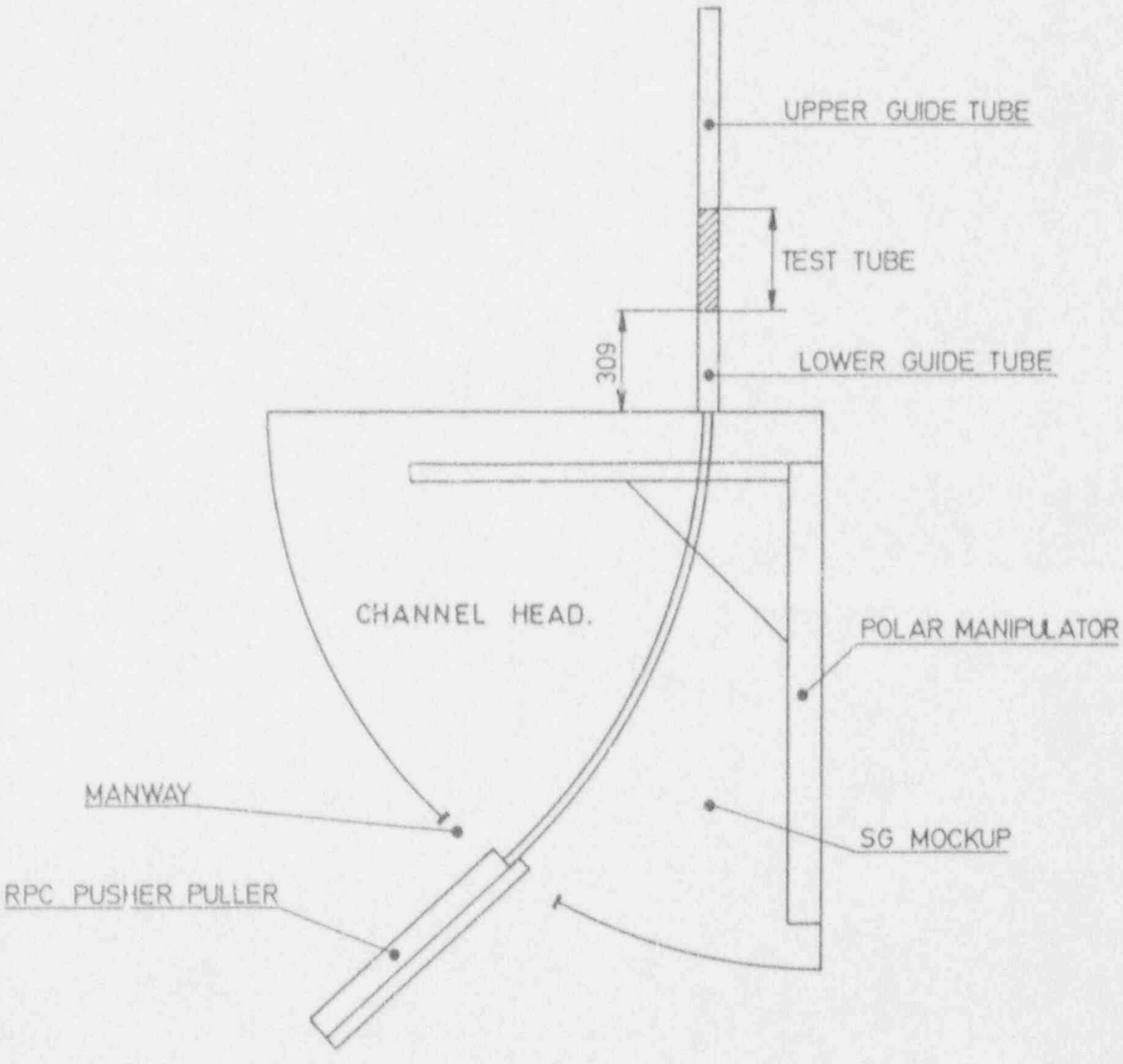

Figure 5-2

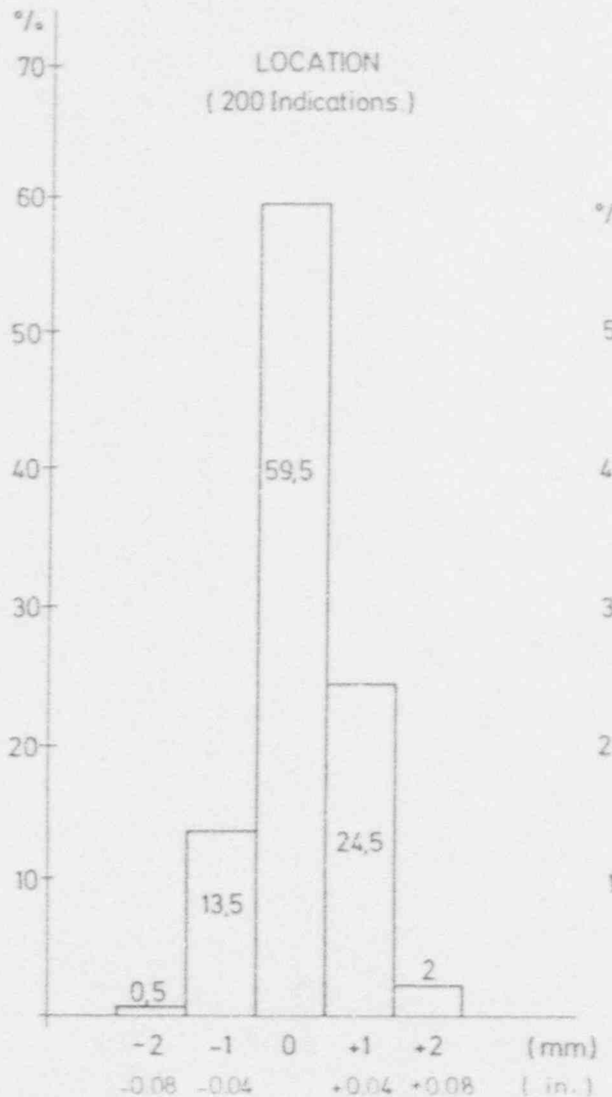

Figure 5-3

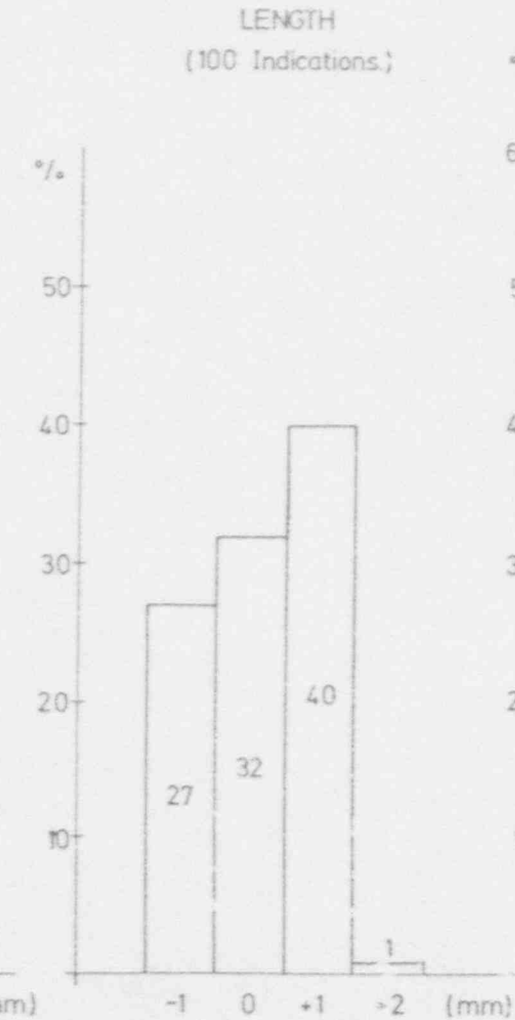

Figure 5-4

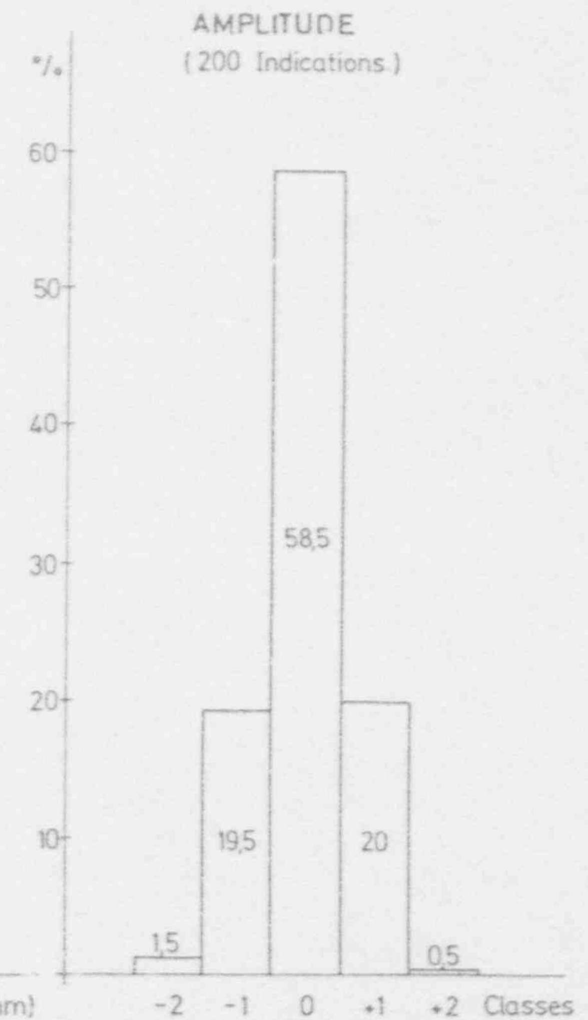

(one class corresponds to Δ ampl. = ±4% or ±50 mV)

Figure 5-5

EDDY CURRENT CALIBRATION CURVE.

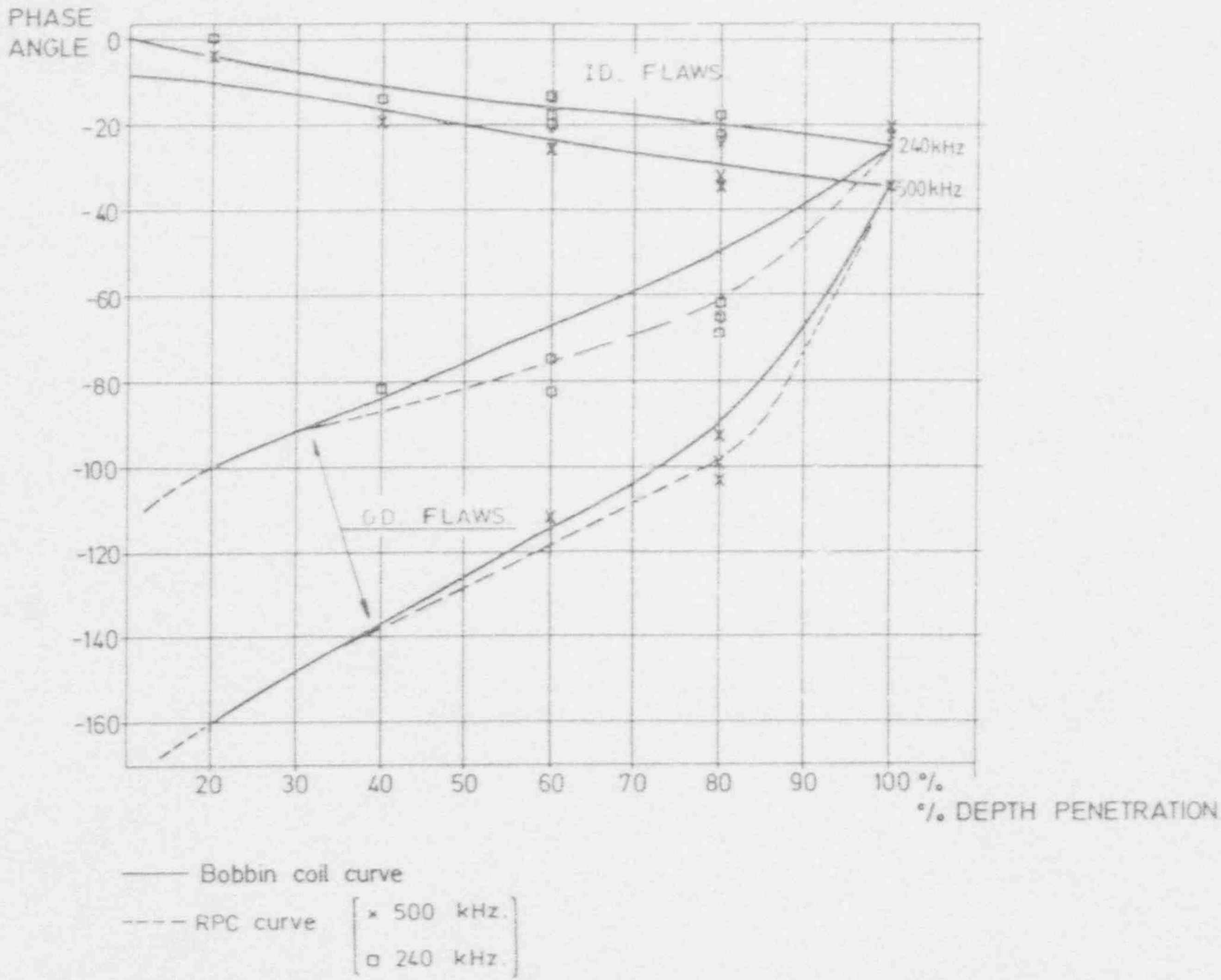

Figure 5-6

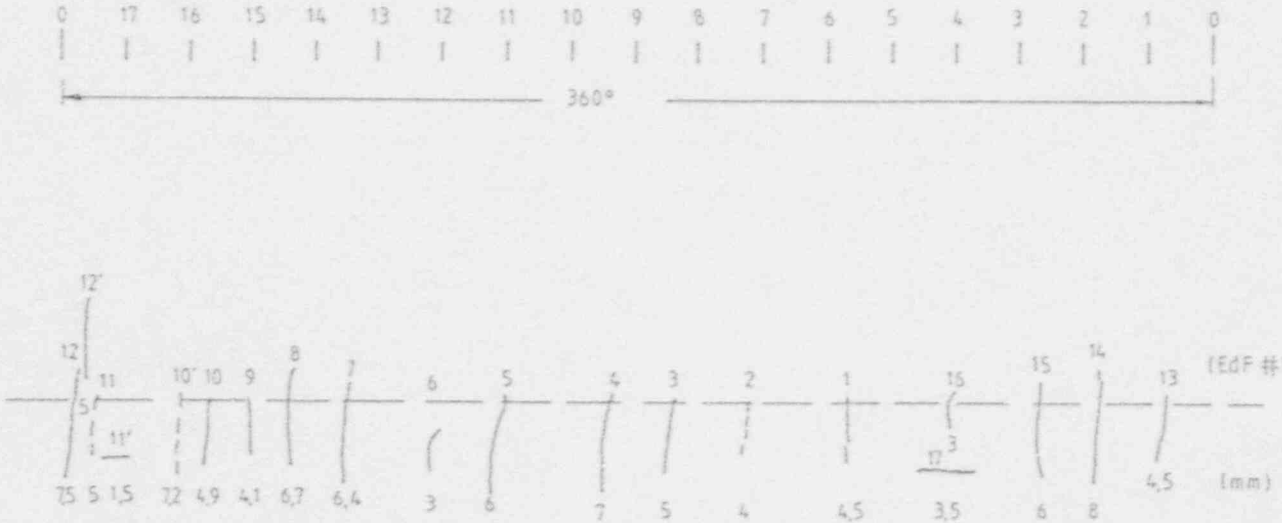

EdF visual and destructive examination

Doel 3 - Tube R23 C23

Figure 5-7 a Cracks location along the tube circonference

EdF visual and destructive examination

Doel 3 - Tube R27 C52

Figure 5-7b Cracks location along the tube circonference

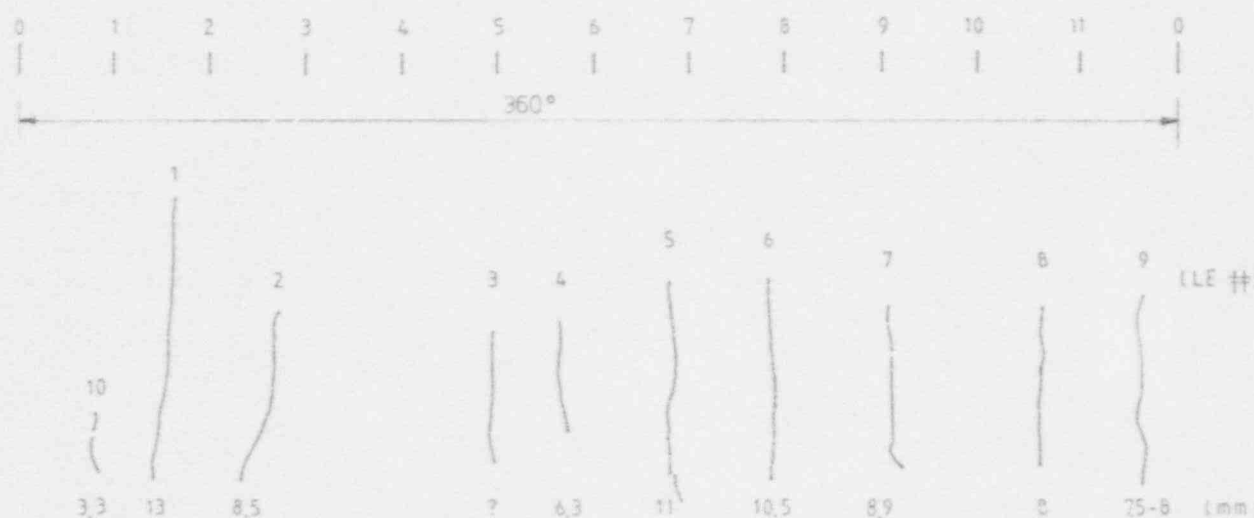

LE visual examination

Doel 2 - Tube R.13 C.30

Figure 5-7c Cracks location along the tube circonference

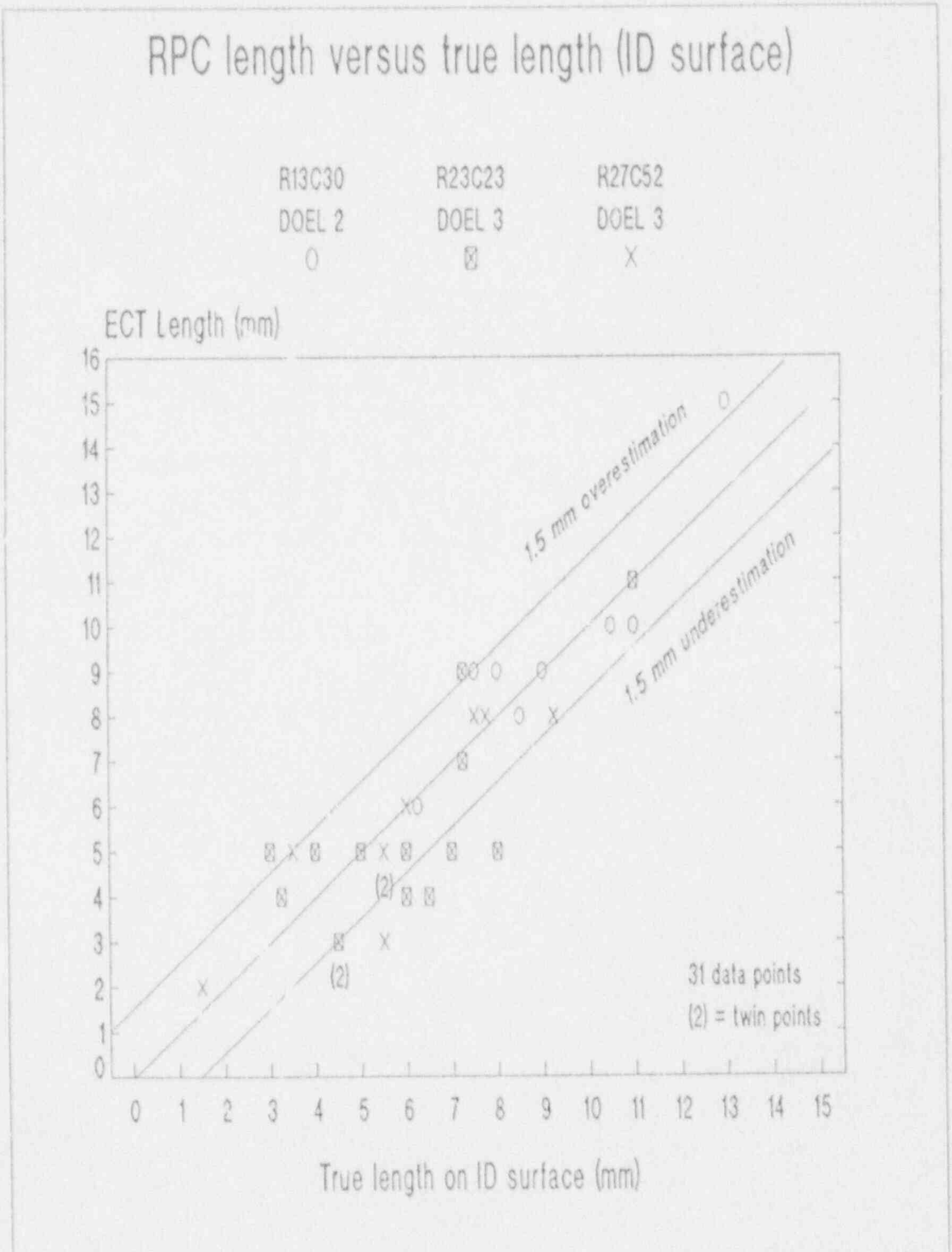
RPC length versus true length (ID surface)
R13C30
DOEL 2
R23C23
DOEL 3
R27C52
DOEL 3
ECT Length (mm)
1.5 mm overestimation
1.5 mm underestimation
(2)
(2)
31 data points
(2) = twin points
0 1 2 3 4 5 6 7 8 9 10 11 12 13 14 15 16
True length on ID surface (mm)

Figure 5-8

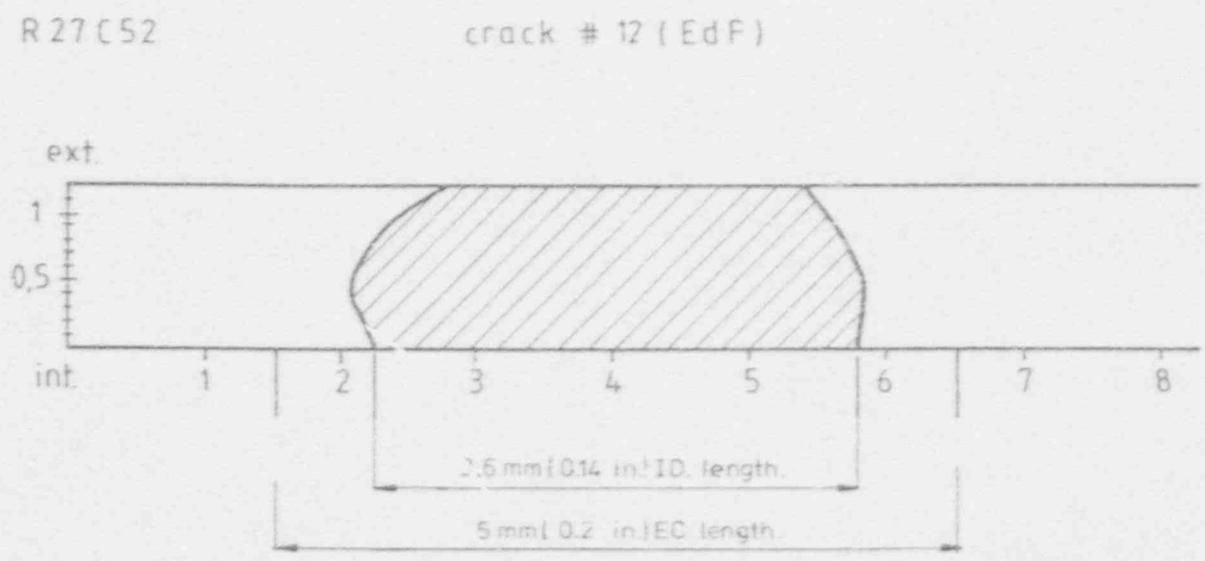

Figure 5-9 EC length - Overestimation

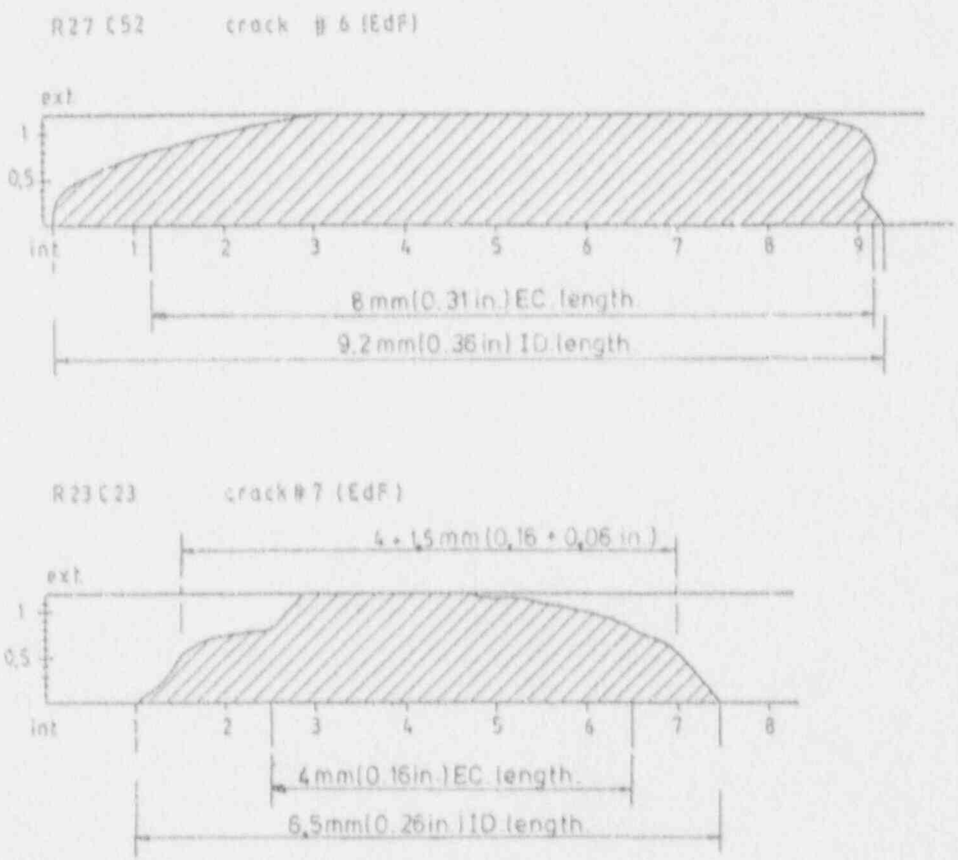

Figure 5-10 EC length - Underestimation

Section 6

ECT INSPECTION TECHNIQUES

6.1. INTRODUCTION

The field application of the rotating pancake-coil (RPC) was focused on the study of the growth of PWSCC between 1984 and 1987. Tube sampling during this period increased from a few tubes to 1500 tubes in some steam generators. The methodology and the equipment were improved so as to reduce the inspection time below two to three days. When it appeared that shot peening had not stopped the length increase of existing cracks, the application of the rotating pancake-coil (RPC) technique increased towards a 100 % inspection of the top of the tubesheet in order to allow the implementation of a plugging limit based on crack length. The acquisition and analysis procedures and the equipment had to be modified to be able to perform the inspection of one steam generator within two to three days.

This optimized RPC system was first applied in February 1988 in Tihange 2. The plans for inspection resulted in the simultaneous examination of two steam generators followed by the inspection of the third one. The inspection team performed the complete operation in 6 days and 10 hours (including equipment installation and removal). Each steam generator was inspected in less than 65 hours. The second inspection was performed at Doel 3 (July 88) following the same sequence. The operation was completed in less than six days. Each steam generator was inspected in less than 60 hours (including equipment installation and removal, as well as performance of the final analysis and preparation of the preliminary report).

6.2. SYSTEM PHILOSOPHY

The NDE equipment is made up of three main parts : data acquisition, data analysis and data management. A mobile trailer contains the equipment to perform the simultaneous inspection of two steam generators (Figure 6-1), (1). Currently, two trailers are operational. When linked, they allow the simultaneous inspection of up to four steam generators. Permanently installed electrical cables connect each steam generator platform to the trailers (Figure 6-2). Several computers control the acquisition and the analysis sequences. There is nearly no human intervention except for maintenance and final signal interpretation. This Computer Controlled Measuring System (CCMS) provides the high inspection efficiency as it integrates each task within a common flow chart (Figure 6-3) :

- the data base is used to select the tube sampling;
- the tube sequence determines the manipulator displacements;
- the quality of the RPC data is checked before each recording;
- each record is immediately analysed;
- the diagnostics are compared with the data base to determine defect evolution.

Each task is performed automatically using either microprocessor control or high performance desktop computers.

6.3. DATA ACQUISITION

The data acquisition system contains the electronic and the mechanical units needed to drive the manipulator and the probe.

Figure 6-4 shows the main components of one data acquisition unit. The rotating pancake coil arrangement is made of two ferrite cores with an impedance match to minimize the differential residue both in temperature and in lift off effect. Probe centering is performed at two different levels with three retractile wheels while the coils are spring loaded against the tube surface (Figure 6-5). The large diameter variations between the unexpanded and expanded (in out of tolerance holes) tube sections (from 19.2 mm (0.76 in) up to 23.0 mm (0.9 in)) required a contacting coil principle.

more accurate. This problem was solved with the addition of a complementary degree of freedom to the probe injection mechanism.

Several other pieces of equipment were optimized in order to reduce as much as possible the need for human intervention during the acquisition sequence (installation, maintenance and measurement).

<u>Installation</u>

Installation of the polar manipulator requires one entry in the channel head for approximatively 2 to 3 minutes. Afterwards 99 % of the tubes can be reached without further S.G. entry. The pusher puller is installed in the manway. The complete installation of the manipulator and the pusher puller takes one hour (including health physics and initial tests). The time needed to link the electrical cables between the remote units and the instruments is especially short because of the permanently installed cables between each steam generator platform and a connection box located outside the reactor building. The total time between the arrival of the trailer at the power plant and the first tube inspection is usually less than 24 hours.

<u>Maintenance</u>

Laboratory simulations and performance analysis have led to a drastic reduction of failures and repair time. Trained jumpers are able to exchange probes within 15 minutes. The probe auxiliary system (cable, rotational encoder and slip rings) has a normal lifetime of 25000 tubes.

Special attention was given to the design of the pusher puller. The unit can be replaced in less than 30 minutes and most of the replacable parts (slip rings, probe, cables) can be exchanged without tooling. The Tihange 2 and Doel 3 inspections were performed with two pusher pullers using only one set of rotational encoder and slip rings for each steam generator.

Measurements

Data acquisition of each steam generator of Doel 3 (about 3330 tubes) was performed at a speed of 120 tubes per hour during 90 % of the inspection.

The sequencing of tasks has taken advantage of the trailer philosophy which includes the permanent installation of as much equipment as possible in a mobile trailer so that as little installation adjustment work is required as practical.

Three operations are performed simultaneously :

. tube inspection;

. quality control of a tube record;

. laser disc recording.

The maximum acquisition efficiency is achieved because there is no waiting period between the end of a tube inspection, manipulator displacement and the laser recording

The measured area is programable in 10 mm (0.4 in) increments to a maximum distance of 700 mm (27.5 in). A typical inspection length of + 30 mm (1.18 in) to - 120 mm (4.70 in) from the top of the tubesheet requires 28 seconds. The probe rotational speed is 12.5 revolutions/second and the pitch is 1 mm (0.04 in)/revolution. This corresponds to a tube surface scanning speed of 750 mm (29.5 in)/second. The analogue to digital conversion rate is 1500 samples/second which ensures a data point every 0.5 mm (0.02 in).

The eddy current equipment is a multifrequency device providing two or three differential frequencies and one or two absolute channels. The absolute channel is used for the location of the roll transitions.

The eddy current signals are encoded with a 15 bits resolution after signal amplification. The dynamic range of the system (from coil to analysis) has been measured higher than 80 dB. Simultaneously with the 15 bits eddy current data, several digital pieces of information are encoded : tube number, probe location in elevation and azimuthal position. This information is transferred to a desktop computer that performs the quality control of the data. It verifies the amplitude and the phase of the reference defect for each tube record.

The probe speed is compared to minimum and maximum thresholds. This on-line quality control goes beyond the ASME and EPRI NDE guidelines. It constitutes a major guaranty of accuracy and reproducibility during the measurements. After this verification, the data are written to an optical disc.

The tube to tube sequence provided by the data base is the single piece of information needed to start the data acquisition. The sequence is shown in Figure 6-6. There is no operator intervention with the exception of the manipulator initialization and the replacements required in case of a system or probe failure.

6.4. DATA ANALYSIS

The data analysis unit contains the electronic interfaces and the computer which takes care of the calibration, the detection and the measurement of the eddy current signals (Figure 6-7).

The analysis sequencing takes advantage of laser disc recording and the trailer philosophy. Three operations occur simultaneously :

- laser disc reading;
- detection and analysis;
- printing of eddy current signals and computer diagnostics.

The analysis sequence is performed with a computer system that calibrates, detects and measures each suspected indication.
The approach is identical for the bobbin coil and the rotating pancake coil analysis. The software has been designed to detect any indication above the detection threshold. It leaves the final decision to human analyst. It is preferred to obtain some false calls rather than missing a potentially dangerous indication.

The optical disc is shared between the acquisition and the analysis units. When a tube has been written on disc, it is sensed by the analysis computer and loaded in memory.

The software locates the reference defect (longitudinal EDM notch) and calibrates each frequency channel as a function of the analysis procedure. This operation rotates and amplifies the eddy current signals in order to guarantee +/- 2 deg. and +/- 1 dB for each record. Extensive checking is built into the software to ensure an optimum dynamic range.

For example, the software is not allowed to amplify the eddy current signal more than 3 dB. If this situation occurs, it is detected during the acquisition sequence and is followed by a calibration of the eddy current instrument prior to recording on the optical disc. This algorithm ensures the optimum dynamic range as expected by the ASME code.

The record is searched to recognize the start and the end of the tubesheet. Each 360 deg. section is scanned for a possible abnormal indication which is flagged. The suspected areas are displayed on the computer bit mapped display and printed by a high speed electrostatic plotter.

The number of signals in the defective cross section, the amplitude and the length of the longest crack are measured by the computer and printed by the plotter. The information is written on the magnetic disc of the analysis computer. The complete analysis sequence is shown on Figure 6-8. However, the final decision depends on the analyst. His interpretation controls when low signal to noise ratio or complex patterns induce erroneous computer diagnostics.

The average analysis speed is 120 tubes per hour. A summary of the suspected areas is printed and in case of a bad record, the reason for the rejection is documented and the tube is flagged for re-inspection.

6.5. EVALUATION OF DEFECT OCCURRENCE AND GROWTH, AND ANALYSIS VERIFICATION

During the inspection, different software programs provide an immediate comparison between the previous data base records and each diagnosis. The longest cracks are inspected twice to ensure the best length evaluation. The plant operator receives twice a day a statistical evaluation of the steam generator situation (number of defects ranked by length, number of cracks, tubes to plug, ...).

Tubesheet maps with the tubes to plug are provided in order to allow preparations to be made for the plugging operation.
At the end of the inspection, the tubes to be plugged are marked with paint using a small dedicated device mounted on the polar manipulator. These operations minimize the intervention time after the RPC inspection.

6.6. FIELD EXPERIENCE

This RPC system was first implemented in March 1988 at Tihange 2. The first steam generator was available on March 9, at 9 a.m.
Two steam generators were inspected simultaneously. The third steam generator was available for inspection 24 hours after the end of the inspection of the first steam generator. The total operation needed 6 days and 10 hours. This time includes equipment installation and removal from each steam generator channel head and platform. The final analysis and the preliminary defect statistics were available two days after the last tube inspection.

The total personnel irradiation exposure was 4.7 R for the Laborelec team and 4.2 R for the jumpers. The general average channel head of each steam generator was measured at 8 R/h. These values include the ASME Section XI bobbin coil inspection and the tube marking operation.

The second inspection occured in June 1988 at Doel 3. The same planning was proposed by the plant. Because of some equipment and software optimization, the inspection time was further reduced. The total operation needed less than 6 days and the final report with crack progression statistics was available 4 hours after the last inspected tube. The total irradiation exposure was reduced by 30 % although the channel head measured value was the same at the both Doel 3 and Tihange 2.

The acquisition team worked 24 hours a day, in three shifts of 8 hours. The team consisted of :

- two site supervisors;
- three shift leaders;

- nine operators;
- three electronic technicians;
- twelve jumpers.

The analyst team worked 24 hours a day in three shifts of 8 hours. The team was made of :

- one site supervisor;
- three shift leaders;
- six analysts;
- six operators.

It should be pointed out that the operators were also responsible for several administrative tasks which resulted, for example, in the filing of more than 15000 signal prints during each inspection.

6.7. COMPLIANCE WITH EPRI GUIDELINES

The RPC inspection technique satisfies each recommendation of the EPRI NDE guidelines. The reproducibility of the measurements is ensured with a high dynamic range and sampling rate. The equipment reaches twice the minimum values for both dynamic range and sampling rate specified in the guidelines. The quality control computer achieves the highest possible quality for each tube record. Such exhaustive and error free check cannot be achieved by human operators during the full work time of their shift.

The analysis procedures fulfill the guidelines both in terms of team organization and computer implementation. The interpretation task can be considered as a three step sequence :

- the signal detection;
- the signal identification;
- the defect characterization.

For the detection task, the computer is by far superior to the human analyst. Indeed, this operation is nothing more than a visual threshold translated into a logical threshold on the x and y

projections of the eddy current patterns. The superior detectability and reproducibility of the software algorithms were confirmed by comparing human and computer detections during a full year qualification period (1985).
Signal identification is usually a context sensitive task.
It implies the codification of analysis rules that are "expert dependent". For the RPC PWSCC inspection, the identification rules are simple because the defect location and the eddy current signal patterns are known.
Defect characterization is also simplified because the values to measure are the number of signals in the same cross section, the longest crack length and the largest signal amplitude. These values can be measured accurately with specific algorithms.

Although the detection task is performed only by the computer, the automated identification and characterization are submitted to a human analyst team. Differences between computer and human analysis are settled by a third analyst team.

6.8. CONCLUSION

The described RPC technology satisfies the safety goal and the utility requirements both in terms of reliability, accuracy and efficiency (inspection time). An optimum has been reached by

- advanced equipment design
- integration of the data acquisition and analysis procedures
- efficient computer data screening
- independent data analysis by computer and human teams

while maintaining compliance with the latest applicable recommandations of the EPRI NDE guidelines.

Field experience demonstrates that 100 % RPC inspection in less than 60 hours per SG can be achieved.

REFERENCES

1. Tubesheet RPC inspection of three steam generators or 6.5 days for 10000 tubes
EPRI Steam Generator Workshop - June 1988 - DOBBENI D.

2. Field experience with an eddy current and graphics display imaging system for primary side cracking
EPRI Steam Generator Workshop - August 1986 - DOBBENI D.

3. Improving NDE in nuclear power plants with computer controlled acquisition and analysis
Belgian Nuclear Society - May 1987 - DOBBENI D.

4. Steam Generator Inspection Engineering
4th European Conference on NDT - London September 1987 - DOBBENI D.

5. PWR Steam Generator Examination Guidelines Rev. 2, December 1988
EPRI NP 6201.

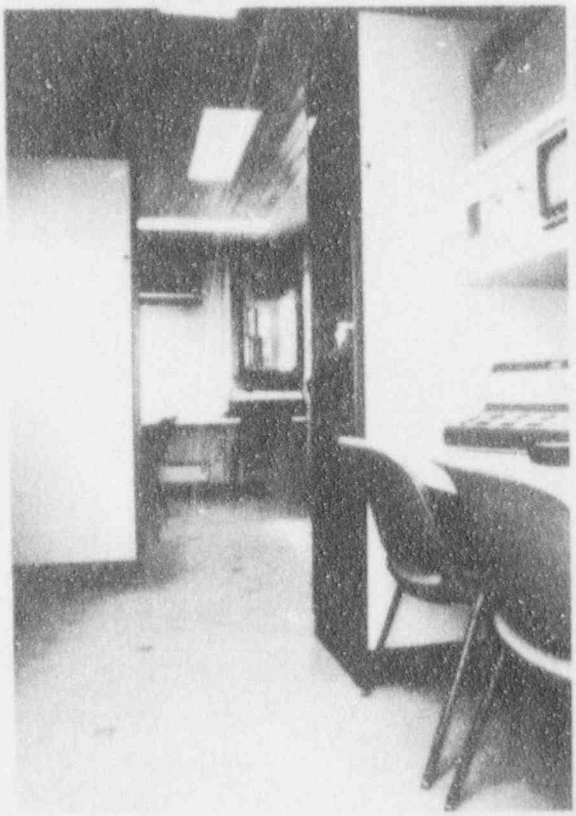

TRAILER.

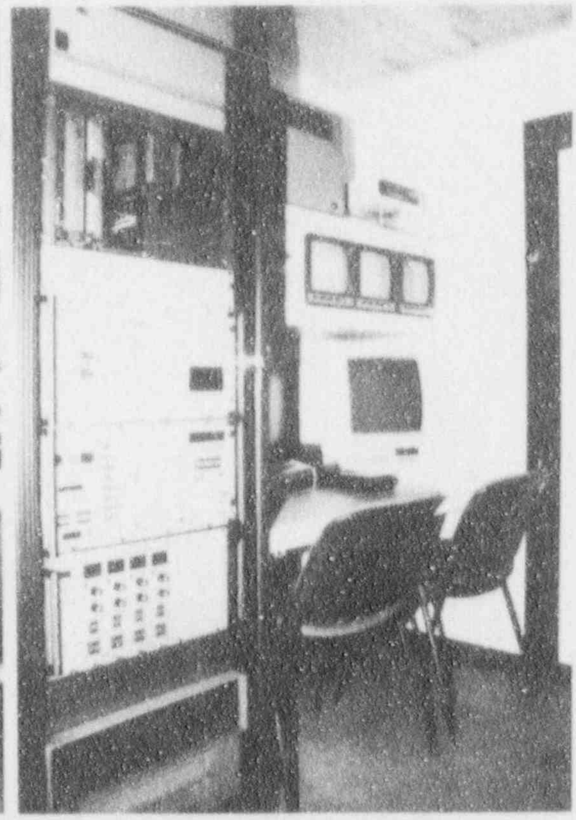

CCMS DATA ACQUISITION.

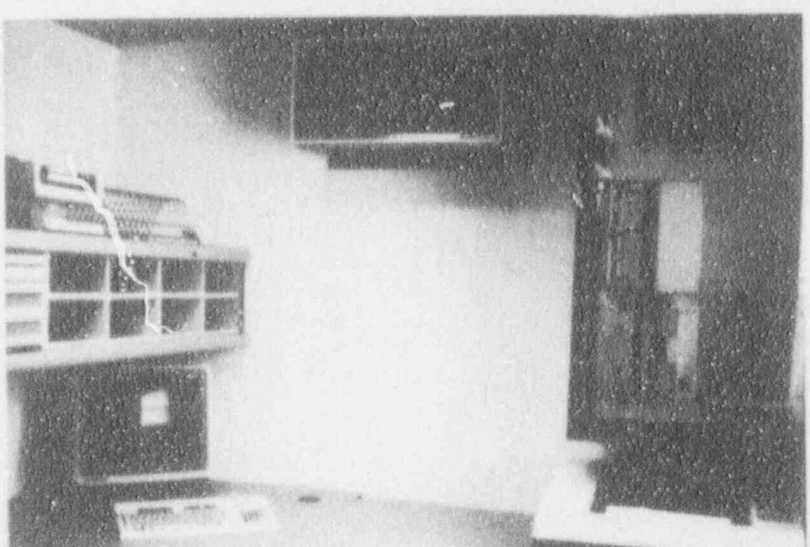

CCMS DATA ANALYSIS

Figure 6-1

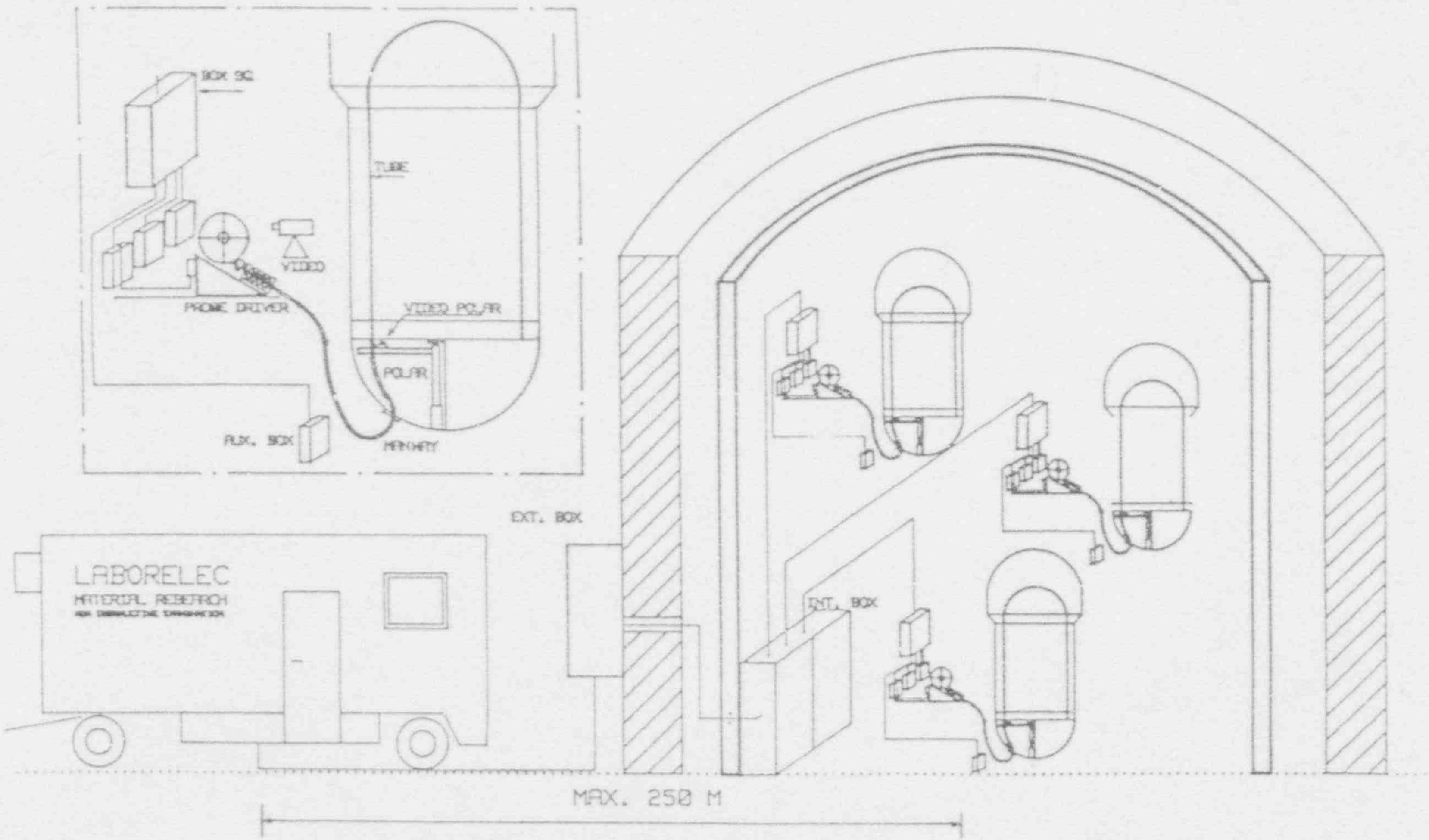

Figure 6-2 Layout of trailer / SG link.

Permanent cable links between SG boxes and containment penetration(internal and external boxes.)

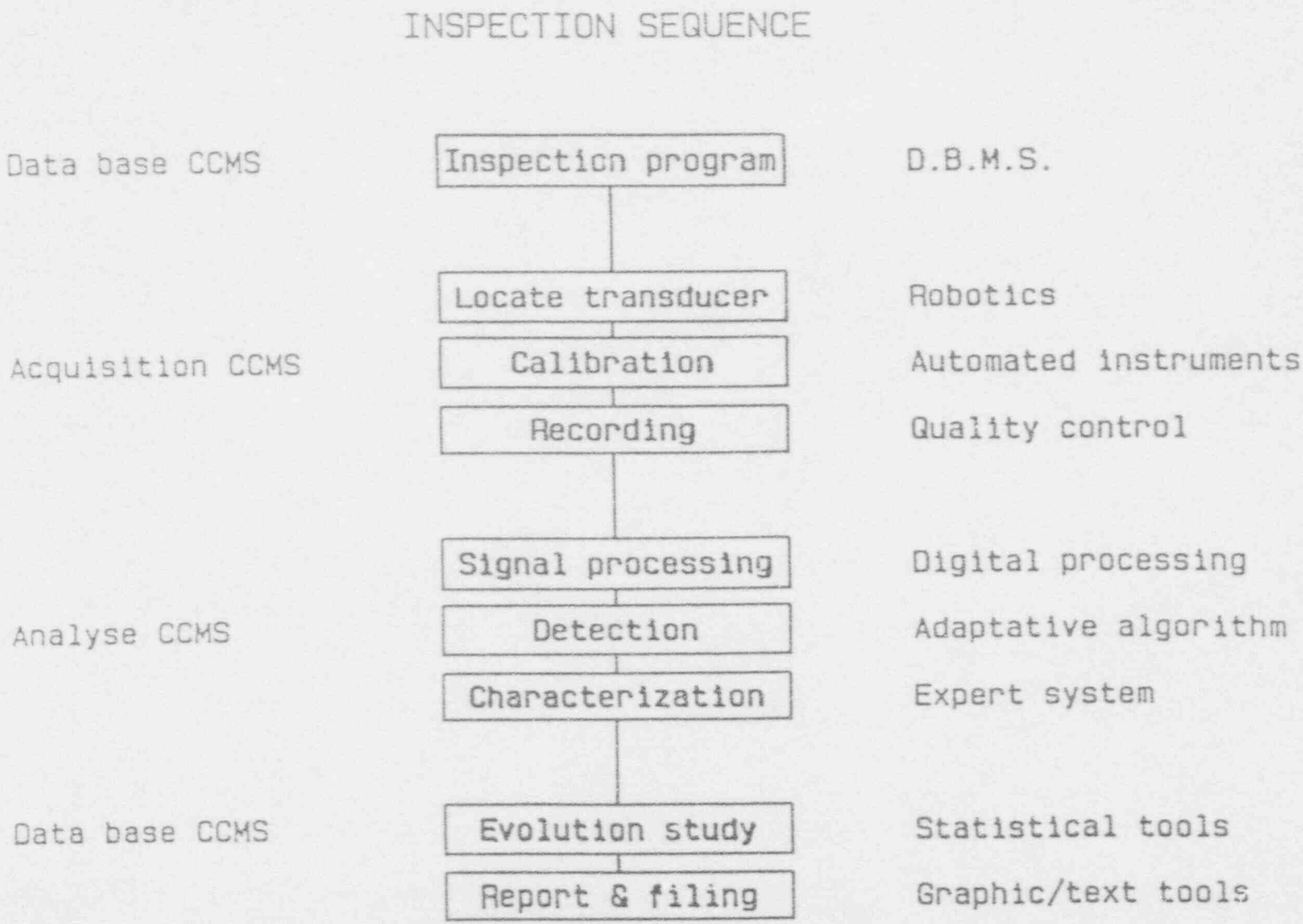

Figure 6-3 NDT tasks submitted to a CCMS equipment

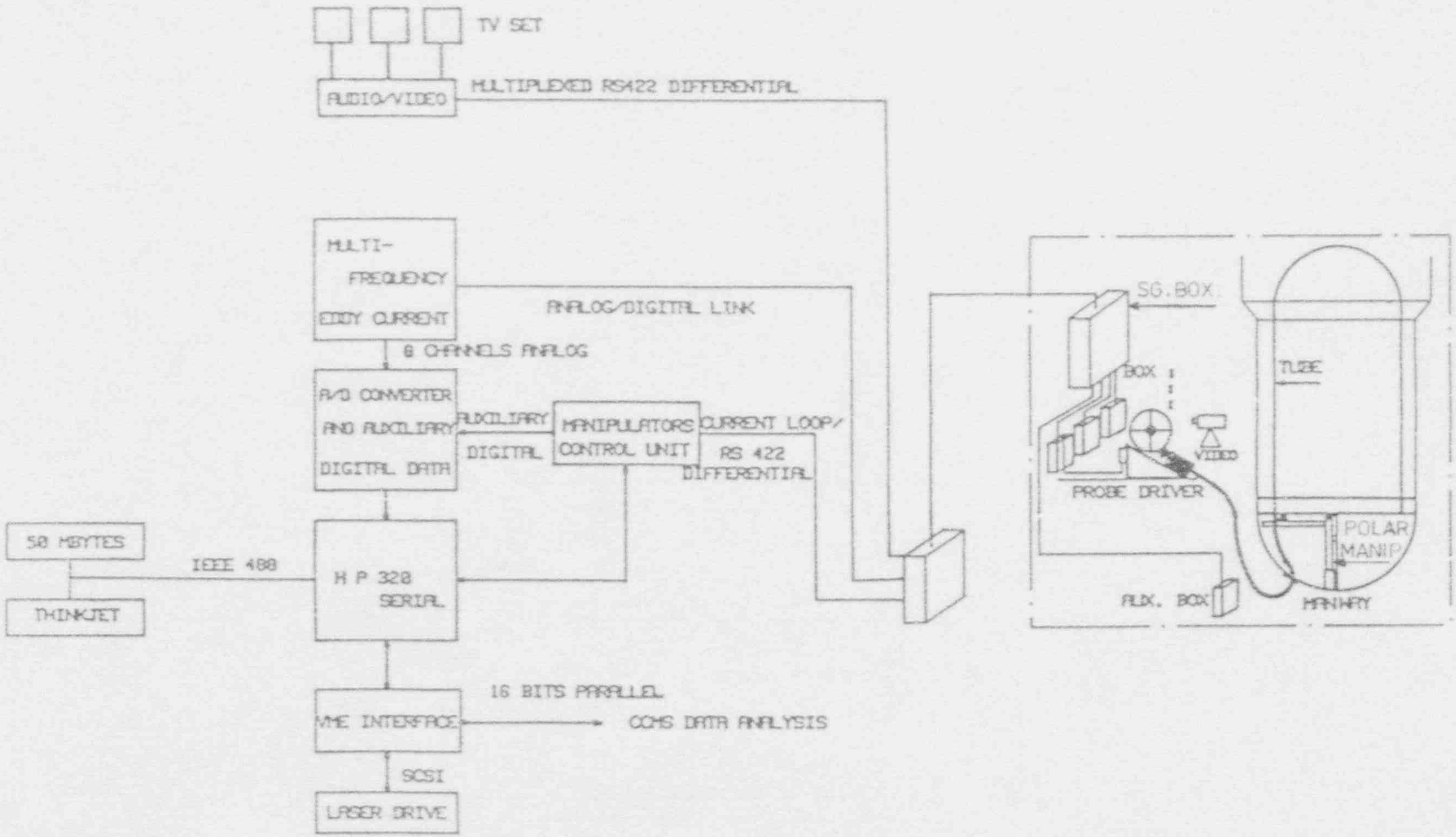

Figure 6-4 Data acquisition hardware.

PRINCIPLE OF THE L/E HELICAL SCAN ROTATING PROBE.

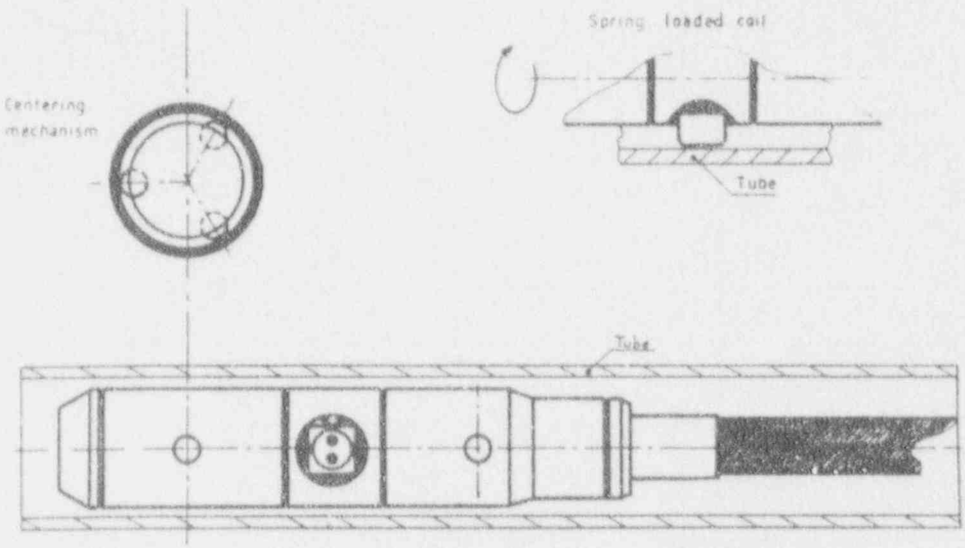

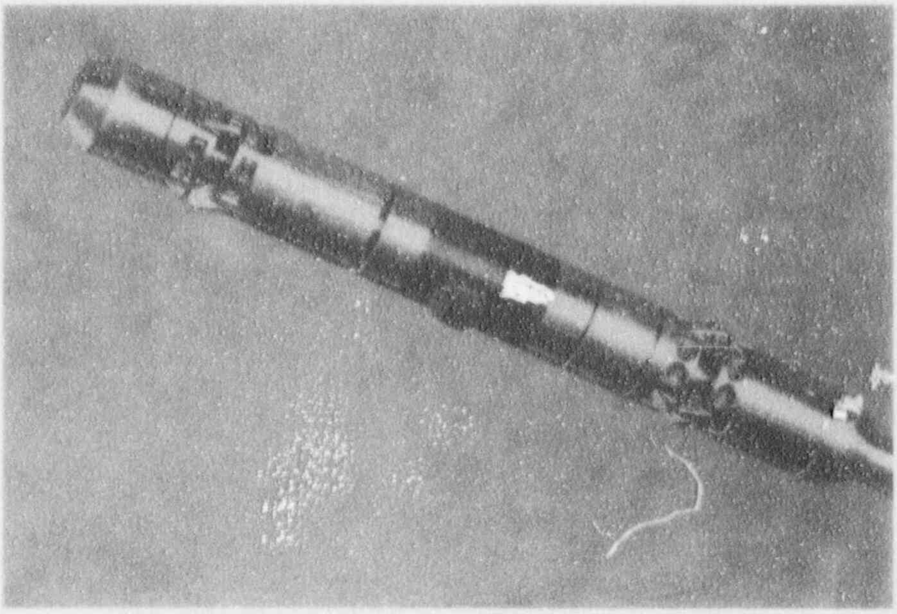

Figure 6 - 5

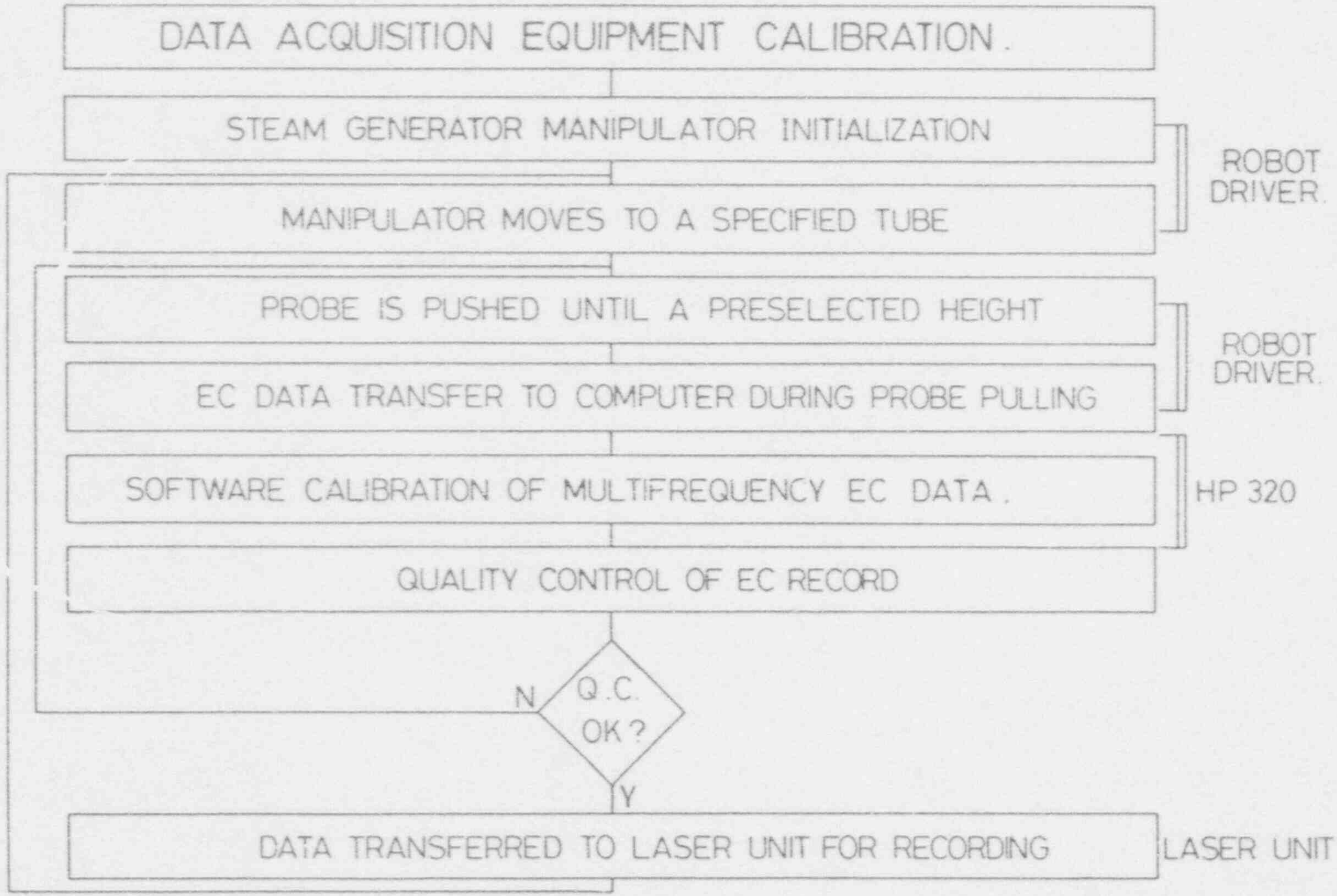

Figure 6-6 Data acquisition sequence.

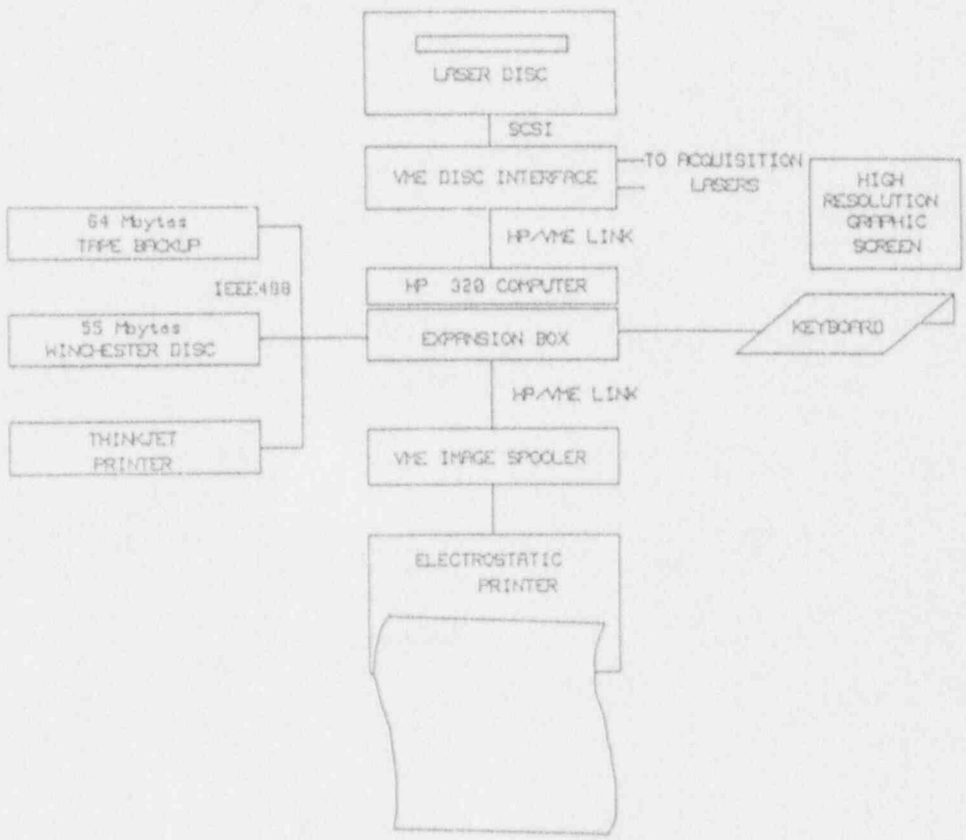

Figure 6-7 Data analysis hardware.

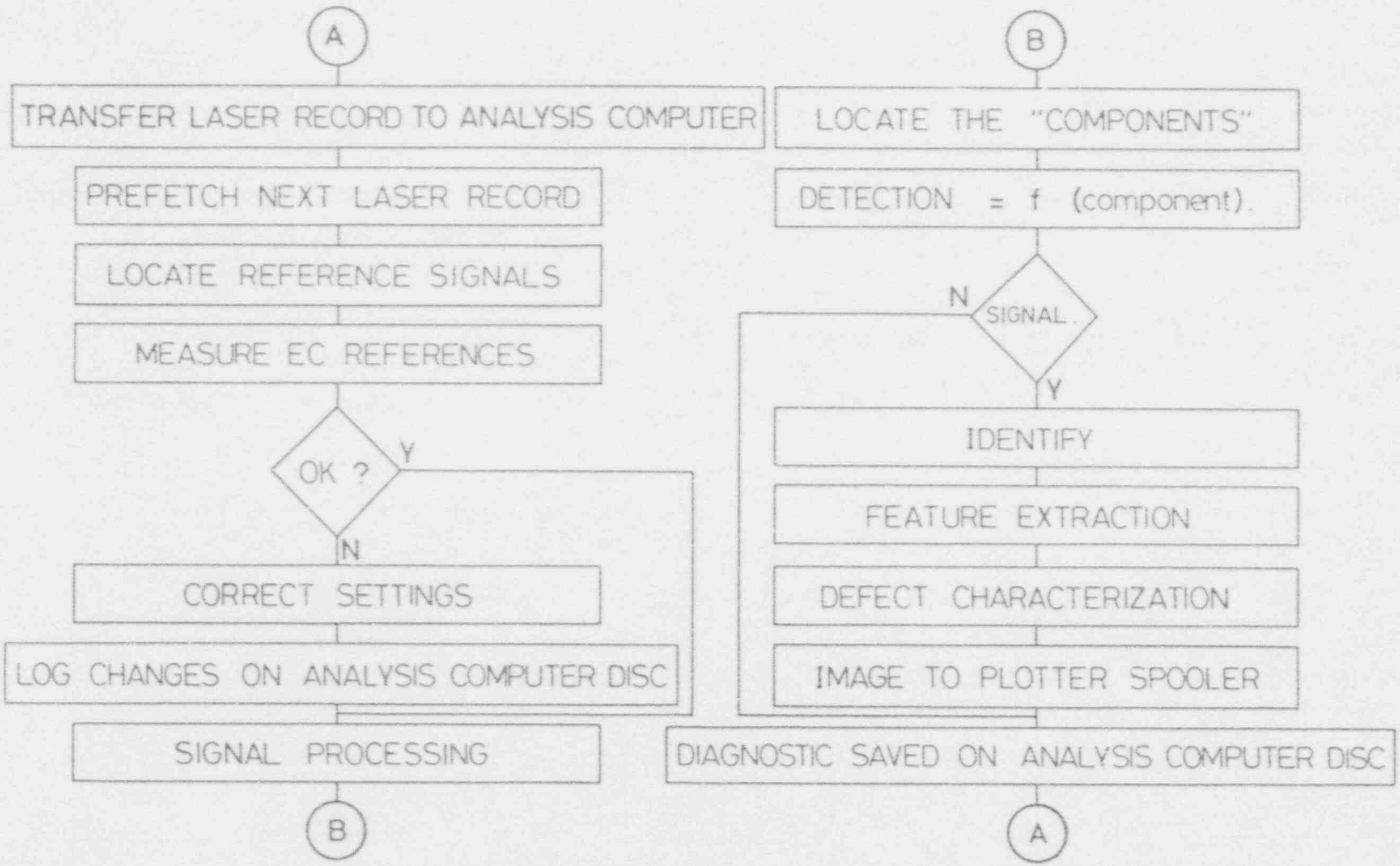

Figure 6-8 Data analysis sequence.

Section 7

SG INSPECTION FIELD DATA

7.1. PURPOSE

The purpose of this section is to demonstrate the safe and reliable operation of the Belgian steam generators despite the fact that some of them are affected by through-wall cracks in several thousand of tubes.

The review of steam generator (SG) inspection field data includes :

- historical background
- in-service leak rate data and channel head radiation level
- outage leak data (helium test, fluoresceine and/or secondary side pressure test, primary side pressure test)
- eddy current Rotating Probe Control (RPC) statistical data (distributions of crack length, number of cracks per section, ...)
- correlation between eddy current "bobbin coil", RPC and helium test data.

7.2. LEAK RATE EVALUATION METHODS

The steam generator primary to secondary leak rate evaluation methods used by the Belgian plant operators are :

- radio-isotope activity balance of fission products in the secondary loop (H-3, N-16, F-18, Na-24, Ar-41, I-131)
- boron balance of the primary and secondary loop
- primary water balance.

The radio-isotope leak rate evaluation method is based on isotope activity measurements by gamma-spectrometry in various parts of the secondary loop (steam generators, main steam, feedwater, blow down, ...). A representative mathematical model of the secondary loop and precise knowledge of the isotope activities at the SG secondary inlets and outlets allow, by a balance, the calculation of the isotope activity leak rate. Finally, the computed primary to secondary SG

activity leak rate (in Ci/h) is translated to a water leak rate (in kg/h*) (Lbm/hr) by dividing it by the isotope specific activity (in Ci/kg) (Ci/Lbm) in the primary water.
The boron balance is based on the same principle : after measurement of the boron content in the primary loop and in the SG secondary inlets and outlets, one can compute the SG leak rate. The primary water balance is a direct method based on the primary leak rate evaluation.

Discussion :
The radio-isotope methods are the most reliable for determining a realistic leak rate. Leak determination by activity measurements of fission products or activation in the primary and secondary loops is only valid if the steady state conditions are established for a sufficient time (approximately one half life of the isotope). When these conditions are not met, activity fluctuations, which follow a power transient, induce a large spread in the evaluated primary to secondary leak levels.

F-18 analysis is performed by each plant at least once a week on a routine basis and when an abnormal global gamma radioactivity (continuously measured) is detected in the secondary loop. Leak rate evaluation by the F-18 method is reliable. Nevertheless, F-18 activity is difficult to measure by gamma-spectrometry and requires long times for computation (especially for small leaks, when the low activities of the secondary samples require a long gamma counting time). Generally, a total time of two and one-half hours is needed when using the F-18 method from the start of water sampling operations to the determination of a leak rate number.

N-16 activity has been used in several cases and will soon be monitored on a continuous basis. Spectrometry allows a very good evaluation of the N-16 content. Isotope N-16's short half-life (7 sec) requires the measurements to be performed in the vicinity of the

* Secondary sample analyses are performed at room temperature and atmospheric pressure. Therefore, leak rates in kg/h and in l/h can be considered as equivalent.

source. Na-24 is also an excellent leak marker. Boron analysis in the primary and secondary loops is a precise (± 10 %) and rapid method for leak rate evaluation as long as the boron concentration in the secondary water is greater than 20 ppb. This method is independent of the power transient history.

The primary water balance method gives absolute leak rates (total primary leak) but depends on many parameters and is not sensitive for small leaks. Great differences between total primary leak rates and individual steam generator leak rates can be observed in the tables of subsection 7.4.

The main lessons learned from the Belgian plant leak experience are :

- the different radio-isotope methods for leak evaluation lead to similar rates. This means that these methods and their corresponding mathematical models are reliable
- a precise leak rate evaluation by chemical analysis requires having about the same blow-down flow rate in each steam generator
- a boron content in steam generators greater than 2 ppm (or lower than 20 ppb) does not allow a reliable leak determination with the boron balance
- spectroscopy determination of Ar-41 allows a quick evaluation of the leak rate
- Tritium (H-3) analysis over a long period of time gives a good total primary leak estimation
- continuous N-16 measurements appear to be the quickest leak evaluation method. However, the N-16 leak determination is partially based on computed values and is strongly dependent on the location of the leak. Therefore, the absolute leak rates have to be confirmed by comparison with other chemical analysis results

7.3. LEAK RATE EVALUATION/PLANT HISTORY

Doel 2

Since the beginning of Doel 2 plant operation, the main method of SG leak rate evaluation has been radiochemical analysis of F-18 (by gamma-spectrometry measurements in the secondary loop) and primary water and boron balances. Both steam generators are now equipped with a permanent gamma-meter. The Doel 2 F-18 model is very reliable and has been improved during the 14 year life of the plant. The knowledge of the isotope activity behavior in the secondary loop at 100 % nominal power has led to the use of a simplified model requiring only the measurement of the specific activity in the primary loop and in the steam generators. The use of this simplified model results in a substantial time savings.

Installation of a continuous N-16 monitoring system is now planned at Doel 2. A temporary system is already in operation. Tritium (H-3) balance leak determination on the basis of repetitive measurements is also planned for the near future.

Doel 3
H-3, F-18, Na-24, Ar-41, I-131, boron and primary water balances and, since August 1987, the N-16 leak rate evaluation method are used at Doel 3. Installation of a permanent gamma-meter for each steam generator is planned.

Tihange 2
Since the first start up, leak measurement methods are global gamma-spectrometry, boron and Na-24 analysis in the secondary water (and occasionally I-131). Each steam generator is equipped with a permanent gamma-meter giving precise radioactivity levels. Na-24 is measured at least once a week. Leak detection by N-16 monitoring is now planned. A temporary system is already in operation.

7.4. IN-SERVICE LEAK RATE DATA

Doel 2 Leak Rate Data

The technical specifications applicable to Doel 2 identify :

- a maximum allowable primary to secondary leak of 28 l/h (0.123 gpm)
- a maximum I-131 activity in the secondary system of 2.10^{-2} Ci/h.

These limits are presently being revised to comply with the other Belgian units (79 l/h) (0.35 gpm). The in-service leak rates are listed in Table 7-1 with the date of the leak evaluation, the possible subsequent outage caused by the SG leak and its origin. Since the first criticality of Doel 2 on August 5, 1975, no significant in-service SG primary to secondary leak occurred until June 1979. From 1986, the leak rates are plotted on a time history diagram (see Fig. 7-1 to 7-3).

A total of eight outages were caused at Doel 2 by leaking SG tubes. Three of them were dealt with during an early refueling. For the first outage, the affected zone of the tube was the U-bend area. Five other forced outages were caused by leaking SG tube plugs, one by secondary water SCC in the crevice area and the last one by a tube damaged by a loose part. None of the forced outages concerned the roll transition area. Leaks due to PWSCC were identified twice in 1978; an earlier, very small leak (October 1977) was probably due to the same cause.

Doel 3 Leak Rate Data

The technical specifications limit the primary to secondary leak to the following rates

- 700 kg/day (1,544 Lbm/day) (29 kg/hr) (64 Lbm/hr) total leak if (I) > 10^{-4} Ci/kg (4.5 10^{-5} Ci/Lbm) or (Xe) > 4.10^{-2} Ci/kg (1.8 . 10^{-2} Ci/Lbm)

- 1,900 kg/day (4,190 Lbm/day) (79 kg/hr) (174 Lbm/hr) per SG if (I) < 10^{-4} Ci/kg (4,5 10^{-5} Ci/Lbm) and (Xe) < 4.10^{-2} Ci/kg (1.8 . 10^{-2} Ci/Lbm).

Since the first criticality of Doel 3 on June 14, 1982, no significant in-service SG leak occurred until August 1985. The in-service leak rates are listed in Table 7-2 with the date of the leak evaluation and the possible subsequent outage caused by the leak. A total of 3 outages were the result of leaks. The first one was related to roll transition cracking. The other two were related to a "mysterious" leak. Up to now, it has been impossible to locate it from all the leak tests performed during several outages (see subsection 7.5.). It has been observed that quick power changes induce peaks in the leaks. These peaks can reach a rate twice as large as the steady state value. Leak rate stabilization occurs normally within about a week.

Tihange 2 Leak Rate Data

The technical specifications limit the primary to secondary leak to the following rates :

if the leak is located in one steam generator :

- at 100 % nominal power, the I-131 leak activity rate from the primary to the secondary side of the steam generator must be limited to $2.8 \, 10^{-2}$ Ci/h.

- the absolute leak rate per steam generator is limited to 1900 l/day (502 gpd) (79 l/h = 0.35 gpm).

- the I-131 mass activity in the secondary side of the SG affected by the primary to secondary leak is limited to 7×10^{-4} Ci/ton (10^{-3} Ci/ton equivalent I-131 dose).

if leaks are located in several steam generators :

- at 100 % nominal power, the I-131 leak activity rate from the primary to the secondary side of two of the three steam generators must be limited to 1.4×10^{-2} Ci/h.

- the absolute leak rate per SG is limited to 79 l/h (0.35 gpm).

- the I-131 mass activity is limited to 3.6×10^{-4} Ci/ton in the total blow down of the 3 steam generators (5.2×10^{-4} Ci/ton equivalent I-131 dose).

The technical specifications for Tihange 2 are now under revision : the former allowable I-131 activities will be divided by 2 : respectively 14×10^{-3} Ci/h and 7×10^{-3} Ci/h. The absolute allowable leak rate per SG will remain 79 l/h (0.35 gpm).

Since the first criticality of Tihange 2 on October 5, 1982, no significant in-service SG primary to secondary leak occurred until February 5, 1985. At that time a leak, rapidly increasing at a rate of 5 to 6 l/h per hour (0.022 to 0.026 gpm) in SG 3 (see Table 7-4) resulted in an earlier than planned outage for refueling (scheduled for 12 days later). The leak rate was about 60 l/h (0.26 gpm) just before shutdown. Three tubes reported to have been rolled in severely out of tolerance holes were affected with cracks in several roll steps (from 2 to 6 steps) ranging from 2 mm (0.08 in) to 9 mm (0.35 in) long (five sections had a crack length ≥ 7 mm (0.27 in); in several sections, as much as ten cracks were detected). The high leak rate is believed to have resulted from the lack of contact between tube and tubesheet hole.

In June-July 1986 another in-service SG leak (steady and limited to 2-3 l/h) (0.009 - 0.013 gpm) did not require an emergency shutdown.

On May 25, 1987, a tube in the first row of SG 3 leaked at the U-bend transition (cold leg side), and caused an emergency cold shut down (173 hours long). The leak rate was about 1 l/h (0.0044 gpm) on May 18, 1987 and increased rapidly (within one hour) on May 25, 1987 from 32 l/h (0.141 gpm) to 91 l/h (0.4 gpm) just before shutdown. The crack length was measured to be between 30 and 45 mm (1.2 and 1.77 in) (bobbin coil inspection did not allow a more accurate evaluation).

Since then no additional significant in-service leaks occurred until 1988. However, a leak was observed during the March 1988 refueling outage in a row 1 U-bend and is discussed in the next section.

7.5. OUTAGE LEAK DATA AND CHANNEL HEAD RADIATION LEVEL

Standard Leak Tests Description

This section provides the results of the standard leak tests performed during normal or forced outages of Doel 2, Doel 3 and Tihange 2 (secondary side pressure test, with or without fluorescein, and primary side pressure tests).

The secondary side pressure test consists of filling up the steam generators with water or with water mixed with fluorescein (about 50 ppm). The secondary side is then pressurized at 40 to 45 bar (570 to 640 psi) and the leaking tubes are visually detected in the channel head (presence of water drops in case of a simple water secondary test, yellow-green colored tube mouths revealed by an ultraviolet (UV) lamp when using the fluorescein dye).

For primary side pressure tests, the primary water (at room temperature) is usually pressurized at about 30 bar (435 psi). Radiochemical analysis performed in the secondary side allows an evaluation of the primary to secondary leak (this test characterizes the size of the leak but does not allow one to locate the leaking tube). To determine the influence of various parameters on the leak, the primary water pressure test is sometimes carried out at other temperature and pressure conditions : e.g., at 50°C or during hot stand-by conditions (260°C, 155 bar) : (500°F, 2200 psi).

A 5 bar (71 psi) helium leak test has been performed once at Doel 3 in an attempt to locate the leaking tubes (results and correlation with RPC ECT data are presented in subsection 7-9). A sniffer measures the helium leak rate at the mouth of each tube on the primary side of the tubesheet. All outage leak tests presented in this subsection are qualitative and do not give the actual in-service leak rate.

Doel 2, Doel 3 and Tihange 2 Outage Test Results

The Doel 2, Doel 3 and Tihange 2 outage leak data are presented in Table 7-5, 7-6 and 7-7 respectively. All the test methods were applied for the detection of the Doel 3 "mysterious" leak and the results of this investigations are described subsequently.

This "mysterious" leak continuously increased following the start up after a normal refueling on July 25, 1987. It resulted in an outage on August 7, 1987. A secondary pressure test with fluorescein performed on SG B revealed only 19 tubes with very small fluorescein indications on the primary side. Secondary pressure tests without fluorescein performed on SG R and G did not reveal any leaking tubes. Eleven tubes were plugged on the basis of ECT with the rotating probe (37 tubes inspected). Start up occurred on August 18, 1987 but a new outage was required on August 20, 1987 because of a remaining leak in SG B. A new fluorescein test revealed 17 leaking tubes. A helium leak test was also performed during this outage (see subsection 7-9) but did not succeed in identifying the leak location. A primary side pressure test (30 bar (435 psi), room temperature) carried out on August 26, 1987 showed only a leak of 0.25 l/h (0.0011 gpm) in SG B. The temperature of the primary water was then increased to 50°C by means of the primary pumps in order to study the temperature effect on the leak rate. After a peak of 15 l/h (0.066 gpm), a non significant leak, less than 2 l/h (0.0089 gpm) was observed in each steam generator (Fig. 7-6 to 7-8). Another primary test (155 bar at 260°C) (2200 psi at 500°F) did not reveal any detectable leak.

The leak which has caused these 2 outages has been called the "mysterious" or "ghost" leak because it disappears when the reactor power is under 30 % of rated power.

The plant was started again on September 9, 1987 and the power increased by steps (50 % on September 11, 75 % on September 14 and full power on September 17). Once at full power, the leak in SG B remained steady (24 l/h) (0.106 gpm) as well as the total leak rate (about 25 l/h) (0.110 gpm). During the June 1988 regular refueling outage, about 70 tubes (with the known larger defects in roll transitions) were either plugged or sleeved. However, the leak rate remained essentially unchanged after resuming power and has slowly decreased down to 15 l/h (0.066 gpm) up to the present time of reporting (March 1989).

Channel Head Radiation Level

Doel 2 and 3

For all Doel power plant units (1 to 4), channel head radiation levels usually range between 80 and 120 mSv/h maximum (8 to 12 Rem/h) after opening of the manholes and decrease to about 40 mSv/h (4 Rem/h) after cleaning at the end of the refueling period.

Tihange 2

The channel head radiation levels are similar to the Doel units and details can be found in table 7-8.

7.6. STATISTICS OF NUMBER OF CRACKED TUBES (Doel 3 and Tihange 2)

The RPC methodology outlined in section 5 has been used on a statistical basis since May 84 (Tihange 2 inspection, after the first operational cycle). The equipment and data acquisition system have remained unchanged since this early date (*); improvements in data analysis (such as automatic computer screening and diagnostics) have been retroactively applied to previous data, so that all sets of inspection data can be reliably compared.

RPC inspection was initially performed in addition to the regulatory inspection using the standard "bobbin coil" method (improved by the multifrequency mixing technique and sophisticated data analysis). During each outage, from 1 to 3 SG's were inspected by RPC over the full height of the tubesheet and the sample size varied from a low of 50 to a high of 2 000 tubes/SG; as the sample selected often included the tubes previously found to be cracked, not all inspected tubes can be used to establish a representative cracking status of the entire tube bundle; the statistical information is based on the best available random samples (the size of which is indicated, within brackets in the graphic presentations); in most cases, a significantly larger number of tubes was actually inspected.

Since February 1988 (Tihange 2 inspection, after the fifth operational cycle) 100 % RPC examination has been performed on all three SG's at each outage but the inspected length limited to the upper part of the tubesheet (about 150 mm (5.9 in), including the 4 upper roll steps, the normal roll transition and the kiss roll). This is the only area of concern where crack plugging limits need to be considered (see Section 3).

The first crack indications were detected by RPC after the first cycle in at least one of the SG's for both plants (Doel 3 and Tihange 2). Two families of tubes should be clearly differentiated.

(*) The only exception is the Doel 3 inspection in October 1983 (after the first operational cycle) where a few tubes (about 10) were examined with a laboratory version of RPC (development stage).

Tubes Rolled in out of Tolerance Tubesheet Holes

This case relates to a very limited percentage of the tube bundle (less than 100 tubes distributed over the 6 SG's of the two plants) but leads to an accelerated initiation and propagation of the PWSCC cracks (as the result of a significant increase of the residual stress level).

In the few extreme cases were the tube was not even rolled against the tubesheet, the cracking was extensive (both in axial and 45 degree oblique directions), to the extent of yielding detectable in service leaks ring the first operational cycle and reducing by half the tube axia' gth (as evidenced during the tube pull performed on Doel , SG-B in August 1983). All tubes in this category have been plugged.

In the other cases (hole diameter tolerance exceeded but rolling expected to be correct), no such behaviour was observed but the rate of increase of cracked tubes with time has clearly shown a steeper slc see Fig. 7-9). Owing to the limited size of the concerned popu ion, this was not considered to be a significant problem as it could easily be solved by plugging.

Normal Tubes

Due to the availability of ECT profilometry measurements for all tubes (along 4 diameters, for the full height of the tubesheet), it was attempted to correlate tube cracking with various known profile irregularities or abnormalies (other than out of tolerance holes). This proved unsuccessfull so that no further "families" need be differentiated.

It should be noted, however, that there is

- no "overrolling", as the rolling specification (roll transition to be located within - 2, - 4 mm (- 0.08, - 0.16 in) from the top of the tubesheet) was strictly adhered to by the SG manufacturer;
- practically no "skip rolls", as all such abnormalies (except when located close to the lower seal weld) were field rep^ired by rerolling before commissioning the plants.

Within this large family of (quasi) normal tubes (close to 100 % of tube bundle), the following behaviour was systematically observed regarding crack locations within the rolled region.

The first crack indications are randomly distributed over the height of the tubesheet (this statement applies statistically to the inspected sample as, in this early stage, each individual cracked tube usually shows no more than 1 cracked section, with a single crack of very short length - typically 1 to 2 mm). With time (1 or 2 years later), the detected cracks tend to concentrate in the roll transition; simultaneously there is an increase in the number of cracks per cracked section but rarely a large number of cracked sections per tube.

In a later stage (after 2 to 3 years), the majority of detectable cracks are located in the roll transition. For instance at the time shot peening was performed (i.e. after 3 operational cycles), the following distribution was observed.

Plant	S.G.	% cracks in roll transition
Doel 3	R	4 %
	G	19 %
	B	55 %
Tihange 2	1	NA
	2	47 %
	3	51 to 64 % (2 samples)

As to the distribution of cracked tubes over the surface of the tubesheet, it may vary, for unknown reasons, from relatively homogeneous (Fig. 7-10) to severely heteroganeous, with concentrations lying either on the nozzle side (Fig. 7-11) or on the manway side (Fig. 7-12).

Rate of Increase of the Number of Cracked Tubes

The percentage of cracked tubes in the tube bundle as a function of time (expressed in months after commissioning) is given in Fig. 7-9).

The diagram is of historical value, because it summarizes the best available information and was produced by successive inspections. However, it is difficult to read because of the significant discontinuities caused by :

- the variation in sample size.
  The sample, especially when of small size (as was initially the case for SG 3 of Tihange 2) may be non representative of the entire tube bundle (especially for a non homogenous distribution of the cracked tubes over the tubesheet surface).

- the variation in inspected length.
  Since the last inspection of both plants was performed on a reduced length (150 mm versus 600 mm) (5.9 in versus 23.6 in), a number of tubes cracked only within the lower part of the tubesheet were "lost", leading to an apparent reduced annual increase rate, or even an apparent reduction, of the number of cracked tubes.

The overall combined effect is

minimal, for SG-B of Doel 3 because of a significant sample size (500 tubes), which proved to be fully representative, and a high concentration of cracks in roll transition; thus resulting only in a 4 % discontinuity (June 87)

maximal, for SG-3 of Tihange 2 because

- of a small initial sample size (50 tubes) switching to a larger sample size (1 030 tubes), with a resulting curve discontinuity of about 10 % (Feb. 86 —> Feb. 87)

- of a lower concentration of cracks in roll transition, with a resulting curve discontinuity of about 15 % (Feb. 87 —> March 88).

Also, since all SG's were not inspected at each outage (and, for the particular inspection of SG-R and G in June 87, the sample was severely biased by a prior "bobbin coil" selection - see Section 7.8.), the curve cannot always be reliably drawn between the available data points; in such cases "best estimate" trends are illustrated by dotted lines.

In order to get a clearer picture of the overall process, all data have been reanalysed to select only those tubes with cracks in the roll transition, while the sample discontinuity has been removed by a proportional adjustment. This leads to Fig. 7-13, which is the "best estimate" of cracking evolution in the roll transition for the most documented cases (SG-B of Doel 3 and SG-3 of Tihange 2); it should be understood that the total percentage of cracked tubes may be significantly larger, especially for the case of the Tihange plant, if cracks in the tubesheet region were also included.

Overall cracking status

From the above statistics, additional information given in the following paragraph (7.7) and the knowledge about the morphology of short non detectable cracks (section 5), it can be inferred that the total number of actual cracks in the roll transitions of the Doel 3 and Tihange 2 units ranges from 6000 to 20 000 cracks per steam generator, with crack lengths between 1 and 14 mm but all very deep (through-wall or thin remaining ligament).
While this amounts, for both units, to about 50 000 cracks with (potential) open leak paths to the secondary side, it does not prevent the safe and reliable plant operation, with only small in-service leakage (Section 7.3).
While the cracking status of the Doel 2 plant is less well defined (limited RPC ECT inspection), the same conclusion holds true since over 2/3 of the tube bundle is known to be affected for at least one of the two steam generators.

7.7. STATISTICS OF CRACK PARAMETERS

For each cracked section (yielding a single "bobbin coil" defect signal, if detectable), the RPC inspection methodology measures and documents the 3 following parameters

- number of axial cracks in the section
- length of the longest crack
- amplitude (mV) of the largest individual signal.

Statistics presently available are based on these parameters. Maximum crack depth is not included because it is systematically found to be (close to) through wall. More information (such as crack topology, length of other cracks than the longest, ...) is stored as raw data or can be produced on graphic displays (see Fig. 7-14); however no detailed computer analysis is systematically performed and the retrieval of this complementary information, if required, is somewhat more time consuming.

When a particular crack section is repeatedly reinspected at each outage, all three characteristic parameters show a continuous increase; the annual rate of increase may vary from 0 up to some upper bound described later.

After peening was performed the (apparent) rate of increase of the number of cracks/section was slowed down, but not reduced to zero. The incre rate was essentially unaffected for the two other parameters.

Furtł discussion of this subject will be limited to the number and length .f cracks, as the signal amplitude is of little practical use.

Statistics will be presented as "distribution curves", with an ordinate (y) axis labeled in percentage and an abscissa (x) axis labeled as either

- the number of cracks per section
- the (maximum) crack length
- the number increase (annual rate)
- the length increase (annual rate).

By definition, the area under any of those histograms is equal to 100 %. The data scatter may result in negative increase values; the corresponding actual (physical) values are of course either zero or slightly positive.

The information presented includes inspections

- for all 3 SG's of Tihange 2, for the last 100 % inspection of March 88;

- for all successive inspections of SG-B of Doel 3 (from the early sample inspection in August 84 up to the last 100 % inspection of June 88).

Tihange 2 March 88 Inspection

Information obtained from the 100 % RPC inspection of SG's # 1, 2 and 3 is summarized in Figures 7-15 through 7-19.

Fig. 7-15 : Length distribution of cracks in the roll transition (from fully expanded to kiss roll area)
This figure gives the absolute number of tubes showing, in the roll transition, (through wall) axial cracks. The maximum crack length ranges from 1 to 16 mm (0.04 to 0.63 in) (only 2 cases). The overall cracking status is comparable for the 3 steam generators and is summarized in the following table :

SG	1	2	3
Number of tubes with cracks	950	850	1 050
Average crack length			
(mm)	4.7	4.6	4.8
(in)	0.185	0.181	0.189
Max. crack length			
(mm)	16	14	16
(in)	0.630	0.551	0.630

Fig. 7-16 : Distribution of number of cracks in roll transitions
This figure gives the absolute number of tubes showing, in the roll transition, the indicated number of cracks (in the same cross-section)
This number of cracks per section ranges from 1 to 13, with an average value from 3.3 (SG-1) to 4.1 (SG-3).

Fig. 7-17 : <u>Distribution of crack length increase</u>

This figure gives the percentage of tubes showing the indicated length increase (yearly rate) since the last RPC inspection.

The length increase ranges from - 1 to + 6 mm/year (- 0.04 to + 0.236 in/year).

The negative values are of course not physically meaningfull but result from data scatter. However, the fact that the amount of data with 1 mm (0.04 in) "decrease" is rather small, and that no "decrease" has been observed in excess of this value, illustrates the high degree of reproductibility and reliability achieved by the RPC methodology.

The following table further summarizes this data :

SG	1	2	3
Last inspection	1987	1986	1987
Number of tubes	63	79	339
Average annual crack length increase (mm/year) (in/year)	1.75 0.069	1.25 0.049	1.18 0.046

Fig. 7-18 : <u>Distribution of the increase in number of cracks in roll transition</u>

This figure gives the percentage of tubes showing the indicated increase in number of cracks/section (yearly rate).

The increase ranges from - 1 to 5 cracks/year. The same sample size has been used to monitor length and crack number increase. The average values range from 0.22/year (SG-3) to 0.54/year (SG-1).

Fig. 7-19 : Dependency of the crack length increase on the initial crack length

This figure illustrates the distribution of crack length increase (from 0 to + 6 mm) (0 to + 0.236 in) as a function of the initial crack length (in 1987) for the 339 cracked tubes sample used to monitor the increase in PWSCC of SG-3.

It is quite clear that "long" cracks tend to propagate significantly less than shorter ones.

Doel 3 - SG-B Evolution From 1984 To 1988

The data obtained from SG-B of Doel 3 during successive RPC inspections from August 84 to June 88 are illustrated by Figures 7-20 to 7-26, which are of the same type as for Tihange 2 (but not including the increase distributions).

A summary of all key data is also provided by Table 7-9.

The overall crack progression obtained from these inspections leads to the following conclusions :

In the early stage of detectable PWSCC, after 2 years of service operation (Fig. 7-20), the cracks are short (usually 1 mm (0.04 in) long) and there is rarely more than a single crack in the roll transition.

At the time shot peening was performed, after 3 years of service operation (Fig. 7-20), both the "crack length" and "number of cracks" distribution curves are extending towards larger values while showing an overall decreasing exponential shape (i.e. a large number of small or isolated defects).

One year after shot peening (Fig. 7-21), the length distribution and, to a lesser extent the number distribution, curves have clearly shifted to the right, with an overall evolution towards a Gaussian bell shape (i.e. there is a decreasing number of small or isolated defects, while there is a marked peak of the curve for an average value of either length or number).

This trend is confirmed by the 1987 inspection results, 2 years after shot peening. Two sets of inspection data are available (Fig. 7-22)

- June 87, based on the same random sample as for the previous inspections
- July 87, based on a larger sample resulting from (and thus biased by) a prior 100 % "bobbin coil" inspection.

The bias introduced by the July tube selection is apparent from a shift of the peak location. The "bobbin coil" pre-selection (screening) resulted in a relatively larger proportion of longer cracks. The magnitude of the effect remains, however, rather small. The increase in crack length is quite clear, with an average value of 1.1 mm (0.043 in). Results from the last June 88 inspection (Fig. 7-23), 6 years after commissionning and 3 years after shot peening, confirm all of the previous observations, except for one unexpected feature : a general acceleration of the degradation process.

This is apparent from the marked shift of both distribution curves and affects all aspects of the degradation process

- proportion of cracked tubes, increasing from 40 % to 57 %
- average crack length increase of 2.5 mm (0.098 in)
- average number of cracks (per section) increase of 1.6

All of these annual rates are larger than for the previous cycle, by a factor of 2 or more. The reason for this unexpected behaviour is still under investigation. However there are strong reasons to suspect features particular to the last operating cycle; these might be related to the several successive cold shutdowns taking place at the time of the regular 1987 outage (from May 28 to September 9 - see Table 7-6).

On the other hand, all other characteristics of the inspection data remained essentially unchanged including the distribution shape and dependance of crack length increase on initial crack length (Fig. 7-24). This also explains why the analytical prediction model developed by BELGATOM on the basis of the previous inspection results still yielded excellent agreement with the field data when a time span of 2 cycles was considered instead of one.

7.8. CORRELATION OF RPC WITH BOBBIN COIL ECT DATA

Because of the May 1987 forced outage of Doel 3, due to a large leak in SG-B, and the subsequent evidence of two leaking tubes from cracks in the roll transition with lengths of 18 and 22 mm (0.709 and 0.866 in), it was considered necessary to perform as soon as possible a 100 % RPC inspection of all SG roll transitions. However the available RPC equipment did not allow such an intensive inspection without intermediate maintenance. It was therefore decided to proceed to a large RPC sample inspection based on a selection from a prior 100 % bobbin coil inspection.

For this purpose a correlation between RPC and bobbin coil was first established in June 87, during the forced outage, on the basis of a sample population of 200 cracked tubes of SG-B. Fig. 7-25 illustrates the correlation obtained between the RPC (max) length and the "bobbin coil" signal amplitude (after mixing out the effect of the roll transition geometrical discontinuity).

The correlation is rather poor but was still helpful since only the longest cracks are of actual interest. Based on a 13 mm (0.512 in) limit, an amplitude threshold of 6.5 V was selected.

It should be noted that a significantly better correlation (see Fig. 7-26) could be obtained between the bobbin coil signal amplitude and the product of (longest) crack length by number of cracks in the same section, as measured by RPC. Such a correlation was indeed to be expected on basis of physical grounds, as the selected index (length x number) is a "measure" of the total amount of material loss in the cracked section, known to be the prime influence factor for signal amplitude for the bobbin coil. The fact that there is also a (less expectable) correlation with crack length only is the result of another empirical correlation between number of cracks and maximum crack length (see Fig. 7-27); this feature has indeed been systematically observed in the continuous degradation process of the SG's.

The July 1987 inspection (scheduled outage) was thus performed on the following basis :

- 100 % bobbin coil inspection of roll transitions for all 3 SG's
- RPC reinspection of roll transitions with signal amplitude in excess of the selected threshold.

The bobbin coil signal amplitude distributions are illustrated by Fig. 7-28 to 7-30 for SG-R, G and B. Integration of these curves (Fig. 7-31 to 7-33) allows one to define the percentage of tubes in excess of any predefined threshold.

To be conservative the threshold was lowered to 4.5 V for the first SG to be inspected (SG-B) while it was kept at 6.5 V for SG-R and G.

The number of RPC inspected tubes, the percentage of "false calls" and the list of "long" cracks detected are summarized in the following table.

SG	THRESHOLD	NUMBER OF TUBES								
		INSPECTED*	FALSE CALLS**	WITH CRACK LENGTH (mm) (in)						
				10 .394	11 .433	12 .472	13 .512	14 .551	15 .591	16 .630
B	4.5 V	775 (24 %)***	166 (21.5 %)	27	2	5	2	1	1	-
G	6.5 V	843 (26 %)	497 (59 %)	5	1	-	1	-	-	1
R	6.5 V	443 (11 %)	113 (48 %)	1	-	-	-	1	-	-

* % of total number of SG tube

** % of inspected tubes

*** the number corresponding to a 4.5 V threshold is 31 % but some tubes were already inspected during the June 87 forced outage.

In order to further check the initial correlation (June 87) between bobbin coil and RPC, all data for the longest cracks (> 10 mm) (0.394 in) have been plotted on a similar diagram (see Fig. 7-34).

It can be seen that the agreement is rather satisfactory, but that it is still possible to occasionally miss a long crack when such a crack is isolated (exceptional case). This is illustrated by a SG-G 16 mm (0.630 in) long crack with a signal amplitude barely in excess of the selected 6.5 V threshold.

7.9. CORRELATION OF RPC ECT DATA WITH HELIUM LEAK TEST RESULTS

As one of the numerous attempts to locate the "mysterious" leak in SG-B of Doel 3, a helium leak test was performed during the forced outage of September 1987 with the best available technique.

Fig. 7-35 and 7-36 show the correlations between the helium leak test results and the previous (June + July 87) RPC length measurements on the detected leakers.

The following conclusions can be drawn

- 335 tubes had detectable helium leaks while 858 had RPC indications of close to 100 % through wall depth.
- There were 27 tubes with a helium leak rate over the "significant" threshold value of 5 cc/hr. while there were 49 tubes with crack lengths over 10 mm (0.394 in) by RPC. Only one of the 27 defects with a helium leak rate over 5 cc/hr. had a length over 10 mm (0.394 in), i.e., the other 48 long defects were not detected by the helium test.
- There was no correlation between helium flow rate and bobbin coil amplitude.
- There was no correlation between helium flow rate and RPC indicated crack length. In fact, the peak flow rate occurred for RPC crack lengths of 7 mm (0.276 in), and was lower for longer cracks.

These conclusions must be considered preliminary as this was the only occurrence of a such testing in a Belgian plant; while the test conditions were considered normal by the experienced service company in charge of the test, it cannot be ruled out that some specific feature might have reduced the method sensitivity below its normal expected level.

Table 7-1 - Overview of the Doel 2 SG primary to secondary in-service leaks since the first start up

Date of leak evaluation and of normal refueling *	SG A ** leak rates (l/h) (gpm)	SG B ** leak rates (l/h) (gpm)	Forced outage induced by SG leak	Leak origin
before October 1977	-	-	NO	-
October 1977	= 0.1 (0.0004	-	NO	Suspected PWSCC
Nov. 1977 : NR	-	-	-	-
March 1978	<< 1 (0.004)	-	NO (1)	PWSCC
July 1978	<< 1 (0.004)	-	NO (1)	PWSCC
November 1978	< 1 (0.004)	-	NO	-
Nov.-Dec. 1978: NR	-	-	-	-
December 1978	-	0 - 0.2 (0 - 0.0009)	NO	-
June 1979	= 2 (0.009)	54 000 ** (238)	YES (2)	SGTR in first row
October 1979	2 (0.009)	-	NO	-
Oct.-Nov. 1979: NR	-	-	-	-
December 1979	≤ 0.5 (0.002)	-	NO	-
April-June 1980	1 - 2.3 (0.004 - 0.01)	3 - 7 (0.013 - 0.031)	NO	-
July-September 1980	≤ 2 (0.009)	18 (0.079)	NO	-
Sep.-Oct. 1980: NR	-	-	-	-

See notes on page 7-28

Table 7-1 - Overview of the Doel 2 SG primary to secondary in-service leaks since the first start up (continued)

Date of leak evaluation and of normal refueling *	SG A ** leak rates (l/h) (gpm)	SG B ** leak rates (l/h) (gpm)	Forced outage induced by SG leak	Leak origin
November-December 1980	< 1 (0.004)	= 2.4 (0.01)	NO	-
January-March 1981	= 2 (0.009)	< 0.5 (0.002)	NO	-
April-May 1981	= 4.5 (0.02)	< 0.5 (0.002)	NO	-
June-July 1981	= 2 (0.009)	< 0.5 (0.002)	NO	-
August 1981	= 1 (0.004)	< 0.5 (0.002)	NO	-
Sep.-Oct. 1981: NR	-	-	-	-
November-December 1981	≤ 0.5 (0.002)	< 0.5 (0.002)	NO	-
January-March 1982	0.2 - 0.5 (0.0009 - 0.002)	< 0.5 (0.002)	NO	-
April 1982	1.5 (0.0066)	≤ 0.5 (0.002)	NO	-
May-July 1982	-	0.2 - 0.4	NO	-
26 August 1982 ER : until 5 October	> 28 (0.123)	-	YES (3)	Leaking plugs ****
8 Oct. 1982	> 28 (0.123)	-	YES (4)	SW SCC (crevice)
Oct.-Nov. 1982	= 5 (0.022)	***	NO	-

See notes on page 7-28

Table 7-1 - Overview of the Doel 2 SG primary to secondary in-service leaks since the first start up (continued)

Date of leak evaluation and of normal refueling *	SG A ** leak rates (l/h) (gpm)	SG B ** leak rates (l/h) (gpm)	Forced outage induced by SG leak	Leak origin
21 Nov. 1982 -	> 28 (0.123)	-	YES (5)	Leaking mini-sleeves
May 1983	4 —> 1 (0.0176 0.004)	1.5 —> ≤ 0.5 (0.0066 0.002)	NO	-
June 1983	1.4 - 2 (0.006 0.009)	0 - 0.3 (0.0013)	NO	-
July 1983	1 (0.004)	≤ 0.2 (0.0009)	NO	-
Aug. 1983 - May 1986	≤ 0.5 (0.002)	≤ 0.5 (0.002)	NO	-
Sep.-Oct. 1983 : NR	-	-	-	-
Aug.-Sep. 1984 : NR	-	-	-	-
Aug.-Sep. 1985 : NR	-	-	-	-
4 June 1986	27.5 (0.121)	-	YES (6)	Leaking plugs ****
after 12 June 1986 (new start-up)	2.5 (0.011)	-	NO (6)	-
27 July 1986	> 28 (0.123)	-	YES (7)	Leaking plugs ****
Aug.-Sep. 1986 : ER	-	-	-	-
Oct.-Nov. 1986	See fig. 7-1	See fig. 7-1	NO	-

See notes on page 7-28

Table 7-1 - Overview of the Doel 2 SG primary to secondary in-service leaks since the first start up (continued)

Date of leak evaluation and of normal refueling *	SG A ** leak rates (l/h) (gpm)	SG B ** leak rates (l/h) (gpm)	Forced outage induced by SG leak	Leak origin
November 1986 - June 1987	See fig. 7-2	See fig. 7-2	NO	-
June 1987	> 28 (0.123)	-	YES (8)	Leaking plugs ****
June-July 1987: ER	-	-	-	-
July 1987 - June 1988	See fig. 7-3	See fig. 7-3	YES (9)	Loose partrt
June 1988 : NR	-	-	-	-

* NR : Normal refueling

ER : Early refueling

** : All leak rates evaluated by F-18 analysis except for the June 1979 leak rate (15 l/s or 54 000 l/h) evaluated with the RELAP 5 model.

*** : leak rate evaluation unreliable due to a much higher leak in SG A (leak ranged from < 0.5 to 1 l/h).

**** : "Leakings plugs" usually resulted from PWSCC of explosively expanded Inconel 600 plugs (W design).

(1) During 2 outages in March and July 1978, leaking tubes due to PWSCC in the tubesheet roll transition area were detected in SG A (by F-18 radioactivity measurements in the secondary loop) and subsequently plugged. The July 1978 leak appeared during the shut down operations.

(2) On June 25, 1979, during the heating of the primary loop (154 bar, 255°C) (2,232 psi, 490°F), a tube break occurred in a first row U-bend of SG-B and was followed by Safety Injection. Other detected leaking tubes and tubes presenting a too large ovality (> 10 %) in the U-bends were subsequently plugged.

(3) Due to a leak in SG A, the normal refueling date was advanced a few days.

(4) On October 8, 1982, a large leak in SG A caused a 7-days outage. During this outage and the former one (3), 9 tubes were plugged in SG A.

(5) On November 21, 1982, a cold shut down due to a high I-131 radioactivity in the secondary side of steam generators (two minisleeved tubes R13C16 and R27C49 were leaking in SG A) was prolonged until April 26, 1983 to perform an extended cleaning campaign on the fuel elements and the primary loop. During this outage, the two leaking minisleeved tubes were pulled in December 1982 and three other tubes probably cracked (R17C85, R28C32 and R26C50), were also pulled in March 1983 (see Section 2).

(6) An emergency outage for leaking steam generator tubes occurred on June 4, 1986 and lasted 8 days. The leak in SG A reached 27.5 l/h (7.265 gpm). After plugging of 17 tubes and start up, the leak remained limited to 2.5 l/h (0.661 gpm).

(7) An early refueling due to a high leak in steam generators started on July 27, 1986. During the outage, 8 tubes were plugged in SG A.

(8) An early refueling due to a high leak in SG A started on June 12, 1987. During the start up operations (July 24, 1987), a large leak in SG B occurred and extended the outage for 9 days. Nine tubes were plugged in SG A and two in SG B.

(9) A cold shutdown due to leaking tubes in SG A lasted from January 28 to February 3, 1988, two tubes were plugged.

Table 7-2 - Overview of the Doel 3 primary to secondary in-service leaks since the first start up

Date of leak evaluation	SG-R leak rate (l/h) (gpm)	SG-G leak rate (l/h) (gpm)	SG-B leak rate (l/h) (gpm)	Total primary leak rate (l/h) (gpm)	Forced outage induced by SG leak	Comments and leak rate evaluation method
24 SEP 1983 21 OCT 1983	-	-	-	< 2 (0.0009)	-	(1)
NOV 1983- JUL. 1985	-	-	-	-	-	(no significant leaks)
AUG-SEP 1985	-	-	5 - 7 (0.022 - 0.031)	-	-	(2)
1986 - MAY 1987	-	≈ 3 0.013	≈ 9 (C.039)	-	-	leak rates evaluated by F-18 activity measurements
27 MAY 1987	-	-	77 (0.34)	-	-	F-18
28 MAY 1987 11 H 00	- -	- -	75 (0.33) 40 (0.18)	- -	- -	F-18 Na-24
21 H 35	-	-	70 - 90 (0.31 - 0.40)	-	Emergency shut-down : leak in SG-B	F-18 (3)
13 JUN 1987 after start up	-	-	≈ 2 (0.009)	-	-	(4)
25 JUN 1987 NR	-	-	<<5(0.022 (very small)	-	-	(5)
27 JUL 1987	-	-	19(0.084)	-	-	(6) (10)
29 JUL 1987	-	-	12(0.053)	-	-	F-18 (6) (10)
02 AUG 1987	-	-	13(0.057)	-	-	F-18 (6) (10)

Table 7-2 - Overview of the Doel 3 primary to secondary in-service leaks since the first start up (continued)

Date of leak evaluation	SG-R leak rate (l/h) (gpm)	SG-G leak rate (l/h) (gpm)	SG-B leak rate (l/h) (gpm)	Total primary leak rate (l/h) (gpm)	Forced outage induced by SG leak	Comments and leak rate evaluation method
03 AUG 1987	-	-	23 (0.1)	-	-	F-18 (6) (10)
04 AUG 1987	-	-	99 (0.44)	-	-	F-18 (6) (10)
05 AUG 1987	- - 	- -	49 (0.22) 78 (0.34)	- -	- -	F-18 (6) (10) B
06 AUG 1987	- -	- -	32 (0.14) 41 (0.18)	- -	- -	F-18 (6) (10) B
07 AUG 1987 01 H 00	-	-	33 (0.14)	-	-	B (6) (10)
10 H 20	- -	- -	48 (0.21) 29 (0.13)	120 (0.53)	Emergency shut-down : too large leak in SG-B	(6) (10) F-18 B
19 AUG 1987 10 H 50 11 H 00 11 H 15	- - -	- - -	155 (0.68) 136 (0.6) 100 -> 51 (0.44) (0.22)	100 (0.44)	- - -	(7) (10) F-18 F-18 N-16
20 AUG 1987 06 H 00 15 H 30 15 H 30 17 H 32	- - -	- - -	153 (0.67) 63 (0.28) 90 (0.4)	- - -	- - Emergency shut-down : leak in SG-B	F-18 F-18 B (7) (10)

Table 7-2 - Review of the Doel 3 primary to secondary in-service leaks since the first start up (continued)

Date of leak evaluation	SG-R leak rate (l/h) (gpm)	SG-G leak rate (l/h) (gpm)	SG-B leak rate (l/h) (gpm)	Total primary leak rate (l/h) (gpm)	Forced outage induced by SG leak	Comments and leak rate evaluation method
09 SEPT 1987 (start up)	-	-	25 (0.11)	30 (0.13)	-	30 % Pn (8) (10)
23 NOV 1987	1.5 0.006	3.8 0.017	21.6 (0.095)	27 (0.119)	-	(9) (10) N-16
	-	2 0.009	16 (0.07)	18 (0.079)	-	F-18
	-	4 0.017	19 (0.084)	23 (0.101)	-	Na-24
	-	-	-	21 (0.093)	-	H-3
	-	-	-	19 (0.084)	-	Ar-41
DEC 87 TO THE JUNE 88 NR	-	-	≈ 20 (0.088)	≈ 20 (0.088)	-	(10)
JUL-OCT 1988	-	-	-	20 ->15	-	(10)

NR = Normal Refueling

(1) The leak appeared on September 24, 1983 after a SCRAM due to a turbine by-pass incident and remained steady until October 21, 1983, date of the normal refueling outage. During this outage, 2 tubes were pulled from SG B (R15C19, R33C36) and one from SG R (R10C86). These 3 leaking tubes were detected by a secondary pressure test with fluorescein (see next subsection "outage leak data"). The examination and analysis performed on the pulled tubes (see Section 2) allowed identification of the origin of the cracking phenomenon as PWSCC. High local stresses were induced by a lack of contact in the roll area between the expanded tube OD wall and the tubesheet due to severely out of tolerance hole diameters in the upper part of the tubesheet (larger than the maximum expansion allowed by the rolling tool).

(2) In August and September 1985, SG-B was affected by a steady leak rate which did not require a plant outage. This leak was found by radioactivity measurements of the secondary water. To avoid imposing stresses on the steam generator tubes which could have increased the leak rate above the allowable threshold requiring an emergency outage, the plant operator was instructed to avoid any power modulation until the end of the fuel cycle in June 1986 (about 9 months later). These instructions had a successful result : only four electrical power modulations occurred until the next normal refueling and the leak did not increase during that time.

(3) Detailed radiochemical leak analyses (F18, N24, I133) during the period from the 23th to the 28th of May 1987 and associated leaks are listed in Table 7-3.
On May 28, 1987, a rapidly rising leak in SG-B (in the tube expansion transition area) resulted in an emergency shutdown which lasted until June 13, 1987.

(4) After plugging of 4 tubes in SG-B (2 selected on the basis of both eddy current signals and a fluorescein test and 2 on the basis of the fluorescein test alone) and start-up, the leak was limited to about 2 l/h (0.009 gpm).

(5) Between the new start up (June 13, 1987) and the next normal refueling (July 25, 1987) the leak rates were difficult to evaluate since the radiochemical activities were near their limit of detection.

(6) Leak rates were observed to be about twice the steady state value during power increases. The peak values then decreased to the steady state value within about one week. This leak rate variation can lead to wrong conclusions about its stabilized value.

(7) Following the 7th of August shutdown, a new start up occurred on August 18, 1987. The plant was soon shutdown on August 20, 1987 (51 hours later) for a large leak still located in SG-B.
This leak was observed with a peak value of 153 l/h (0.674 gpm). It decreased to 63 l/h (0.277 gpm) on the 20th of August. During this period, the first N-16 measurements were performed. N-16

measurements indicated a leak of about 100 l/h (0.44 gpm) (51 l/h (0.225 gpm) after revision of the N-16 model).

(8) Leak data evaluated during the period from the 9th of September until the 19th of November 1987 and plotted on Fig. 7-4 and 7-5 show that :

- under 30 % nominal power (270 MW) no measurable leaks were detected (detection threshold)

- the different methods (N-16, F-18, N_a-24) lead to very similar results which means that the models used for leak evaluation are reliable.

(9) Boron, F-18, A_r-41 and H-3 parameters were systematically measured at 100 % electrical power. The leak rates obtained by the different methods of evaluation are very similar.

(10) From July 27, 1987 to October 1988 the leak is mysterious and probably from a unique origin. It appears at 30 % power and increases with the power level (see Fig. 7-4).

Table 7-3 - Doel 3 leak chemical data from the 23th to the 28th of May 1987

Date hour		El. Power		Primary Loop *			SG-B *			SG-R*	SG-G*	FP *	MS *	Leak rate kg/hr SG-B
		MWe	%	RC F18	Na-24	I-133	F-18	Na-24	I-133	F-18	F-18	F-18	F-18	
23/05	05.30	860	96		18.8	5.7		0.013	0.009					
24/05	08.00	860	96		19.7	7.2	0.621	0.018	0.011	0.28				
25/05	08.10	850	94		18.9	6.9	0.648	0.021	0.017		0.30	0.089	0.094	
26/05	08.00	850	94		19.6	8.2	0.794	0.025	0.013	0.44				
27/05	08.00	850	94		19.1	4.0	1.10	0.035	0.012	0.56	0.31	0.152	0.162	77 (F-18)
27/05	08.00	750	83	3165	18.2	4.0	2.14	0.151	0.067	1.45	1.36	0.39	0.35	
	11.00	750	83	3180	17.9	4.1	2.01	0.163	0.069	1.35	1.30	0.38	0.33	75 (F-18) 40 Na-24
	14.00	750	83	2760			2.7	0.190	0.098	1.50	1.37	0.42	0.36	
	21.00	750	83	3090			1.74			1.06	1.06	0.26	0.24	70 (F-18)

* : activities in MBq/m^3
RC : Reactor Coolant
FP : Feedwater Pump
MS : Main Steam

Table 7-4 - Tihange 2 - Example of in-service rapid SG leak rate growth (estimated by Na-24 radiochemical analysis)

Date and hour of measurement	SG 3 leak rate (1/h) (gpm)	SG 2 leak rate (1/h) (gpm)
End January 1985	1.5 - 2.5 (0.007 - 0.011)	-
4 February 1985		
14 H 30	4.5 (0.02)	-
18 H 40	4.7 (0.021)	-
5 February 1985		
01 H 30	35.7 (0.157)	0.6 (0.003)
03 H 30	46 (0.203)	
05 H 15	53 (0.233)	
07 H 15	61 (0.267)	
08 H 35	(60) (0.264) Emergency outage	

Table 7-5 - Doel 2 outage leak data

Date of outage	Date of start up	SG	Secondary pressure test (with fluorescein)	Primary pressure test	Number of leaking tubes detected
05 MAR 78 Planned outage	21 MAR 78	A	YES	-	4
15 JUL 78 Planned outage	24 JUL 78	A	YES	-	5
16 SEP 83 Normal refueling	15 OCT 83	A	YES	-	20
11 AUG 84 Normal refueling	24 SEP 84	A	YES	-	5
		B	YES	-	3
14 AUG 85 Normal refueling	05 OCT 85	A	YES	-	68
		B			37 (1 cracked in the U-bend as revealed by ECT bobbin coil)
28 JAN 88	03 FEB 88	A	YES	-	2

Table 7-6 - Doel 3 outage leak data

Purpose of outage	Date of shut down	Date of start up	S G	Leak (l/h) before shut down (gpm)	Fluores-cein	p sec test (bar) (psi)	p primary test (bar) (psi)	Number of leaking tubes detected	Comments
Normal refueling	21 OCT 83	23 NOV 83	R B	< 2 (0.009) (total primary leak)	YES	45 (650)	-	3 (1 in SG-R) (2 in SG-B)	
Normal refueling	17 AUG 84	15 SEP 84	B		YES	≈ 40 (580)	-	1	
Normal refueling	14 JUN 85	05 AUG 85	B		YES	≈ 40 (580)	-	1	
Leak in SG-B	28 MAY 87	13 JUN 87	B	70 - 90 (0.31 - 0.40)	YES	≈ 40 (580)	-	23	4 tubes plugged
Normal refueling			B	?					
Leak in SG-B	07 AUG 87	18 AUG 87	B	48 (0.21) (F-18) 29(0.13)(B) 120 (0.53) (Total primary)	YES	42 (610)	-	very little fluorescein indications 19 tubes	11 tubes plugged
			R G		NO	(610)	-	No leak detected	
Leak in SG-B	20 AUG 87	09 SEP 87	B	150 (0.66) (F-16)	YES	42 (610)	-	17	4 tubes plugged after helium leak test

Table 7-6 - Doel 3 outage leak data (continued)

Purpose of outage	Date of shut down	Date of start up	SG	Leak (l/h) before shut down (gpm)	Fluorescein	p sec test (bar) (psi)	p primary test (bar) (psi)	Number of leaking tubes detected	Comments
Leak in SG-B continued		Date of test : 25 AUG 87 26 AUG 87 24 AUG 87	 R G B	(See above)	NO	(800 l in secondary side = water to the SG inspection holes level)	30 (435)	Not detectable by this method	Test leak rates by boron analyses of secondary water samples SG-R: 0 l/h SG-G: 0 l/h SG-B: 0.5 l/h Fig. 7-6 to 7-8
		27 AUG 87	R G B			-	* (50°C) (120°F)	"	Fig. 7-6 to 7-8
			R G B		NO	- -	155 (2250) (260°C) (500°F)	"	No detectable leak

* Primary water temperature increased to 50°C (120°F) (primary pumps) to evaluate the temperature effect on the leaks : after a peak of about 15 l/h (0.066 gpm), the leak decreased to a steady rate lower than 2 l/h (0.009 gpm) in each SG.

Table 7-7 - Tihange 2 outage leak data

Purpose of shut down	Date & hour of shut down	Date & hour of start up	Leak rate (l/h) before shut down (gpm)	S G	Secondary pressure Test	Number of leaking tubes detected
Planned outage	10 OCT 84	19 OCT 84	weak *	3	35 bar hydrotest with fluorescein	5 in SG 3
12 days accelerated refueling outage (leak in SG 3)	05 FEB 85	12 MAR 85	61 (0.269) 0.6(0.0026)	3 2	25 bar hydrotest with fluorescein for 24 hours (360 psi)	R40C44; R05C33 and R03C76 all rolled in severely out of tolerance holes and suspected not to provide leaktight contact
Leak in SG 3	25 MAY 87	01 JUN 87	-	3	hydrotest with fluorescein	1 (U-bend R01C15)
Normal refueling	06 MAR 88	04 APR 88	-	3 2 1	hydrotest with fluorescein **	1 in SG 3 (U-bend R01C77)

* Leak appeared during planned shutdown

** Hydrotests performed after U-bend heat treatment

Table 7-8 - TIHANGE 2 - Channel Head Radiation Level
(in mSv/h or .1 Rem/h)

Refueling	Time	SG 1 HL	SG 1 CL	SG 2 HL	SG 2 CL	SG 3 HL	SG 3 CL
May 1984	Before cleaning (lancing with demineralized water)	80	85	-	-	70	70
	After cleaning	12	-	-	-	-	-
February 1985	Before cleaning	130	50	80	82	64	6[illegible]
	After cleaning	8[illegible] (1st clean.) 100 (2d clean.) 65 (3d clean.)	70 (1st clean.) 70 (2d clean.) 65 (3d clean.)	58.2	50	60	61
February 1986	Before cleaning	-	-	-	-	-	-
	After cleaning D = Days after opening of manholes	D + 2 : 110 D + 4 : 105 D + 5 : 74 D + 6 : 95 D + 8 : 91 D +11 : 89	D + 2 : 85 D + 4 : 115 D + 5 : - D + 6 : - D + 8 : - D + 11 : -	D + 2 : 100 (after 3d cleaning) tubesheet: 130 D + 3,4 : 100 D + 5 : 82 D + 6 : 90	D + 2 : 105 (after 3d cleaning) tubesheet : 140 D +3,4: 100 D + 5 : 92 -	D + 2 : 70 D + 4 : 65 D + 5 : 68	D + 2 : - D + 4 : 79 D + 5 : 75
February 1988	Before cleaning	-	-	-	-	100	85
	After cleaning	80	88	62	70	67	80

Table 7-9 - DOEL 3 - SG B - RPC INSPECTION DATA

INSPECTION	August 1984	June 1985	June 1986	June 1987	July 1987	June 1988
Number of tubes inspected	221	526	505	516	775	3234
Proportion of tubes with (thru-wall) cracks	2.2 %	24.2 %	37.5 %	40.7 %	77 % **	57.1 %
Samples size for crack growth (*)	NA	NA	134	190	NA	210
crack length						
- distribution	Fig. 7-20	Fig. 7-20	Fig. 7-21	Fig. 7-22	Fig. 7-22	Fig. 7-23
- maximum		9 (.35)	10 (0.394)	12 (0.472)	15 (0.59)	15 (0.59)
- average		2.15 (0.085)	4.25 (0.167)	5.4 (0.213)	6.9(0.27)**	7.15 (0.28)
- increase . max.	NA	NA	+6 (0.236)***	+6 (0.236)	NA	+8 (0.32)
. av.		NA	+2 (0.079)	+1.1 (0.043)	NA	+2.5 (0.1)
# cracks / section						
- distribution	Fig. 7-20	Fig. 7-20	Fig. 7-21	Fig. 7-22	Fig. 7-22	Fig. 7-23
- maximum		9	10	10	12	12
- average	NA	3.4	4.3	4.7	5.5 **	5.7
- increase . max.		NA	+6	+ 3.3	NA	+6
. av.		NA	+1.65	+ 0.5	NA	+1.6

(*) number of tubes already cracked, reinspected after one cycle
(**) This figure is biased because all tubes inspected were selected on basis of a prior 100 % "bobbin coil" inspection
(***) This figure might be biased because the 1985 data were obtained before shot peening

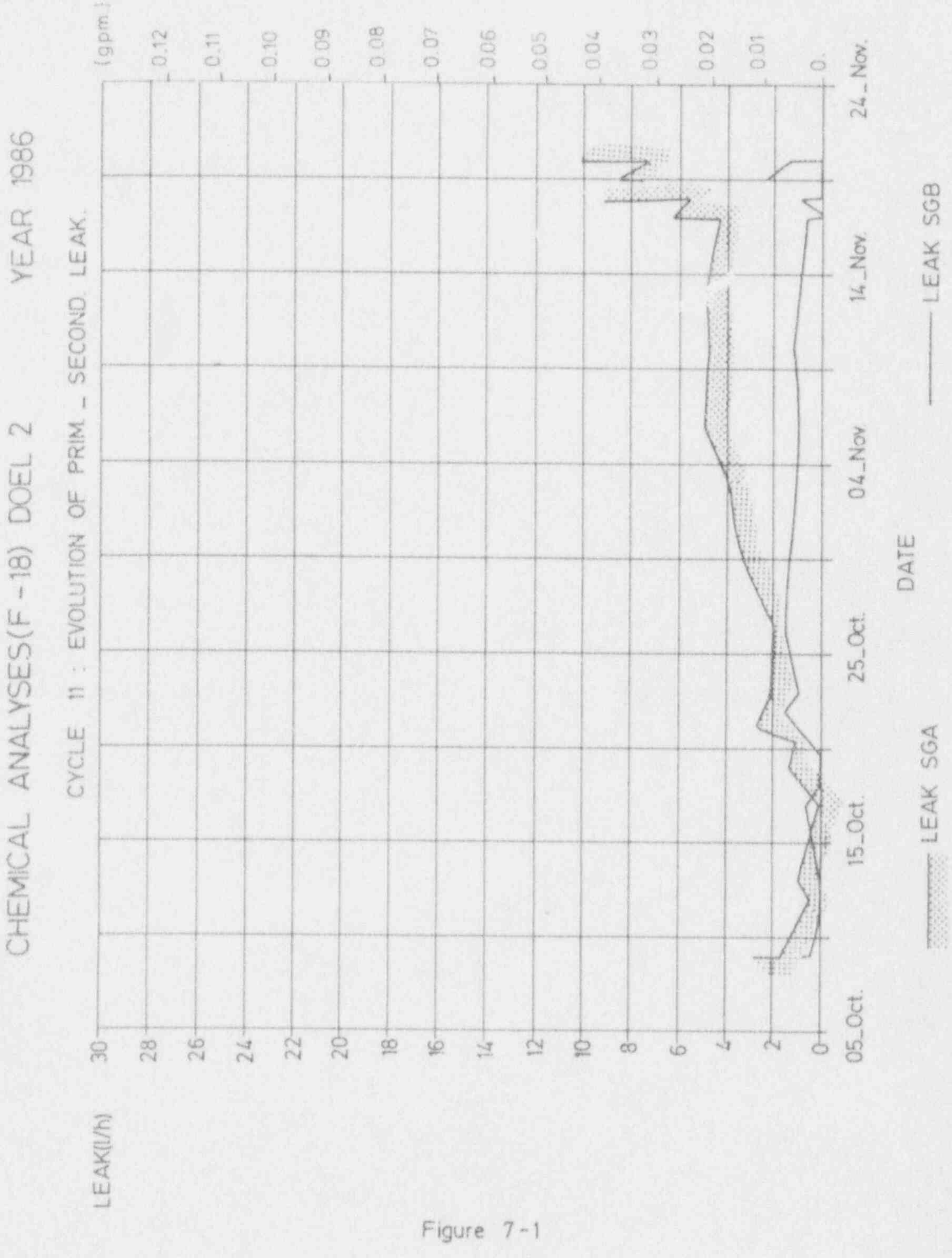

CHEMICAL ANALYSES(F-18) DOEL 2 YEAR 1986
CYCLE 11 : EVOLUTION OF PRIM. - SECOND. LEAK.
LEAK(l/h)
30
28
26
24
22
20
18
16
14
12
10
8
6
4
2
0
(gpm)
0.12
0.11
0.10
0.09
0.08
0.07
0.06
0.05
0.04
0.03
0.02
0.01
0.
05_Oct.
15_Oct.
25_Oct.
04_Nov.
14_Nov.
24_Nov.
DATE
LEAK SGA
LEAK SGB

Figure 7-1

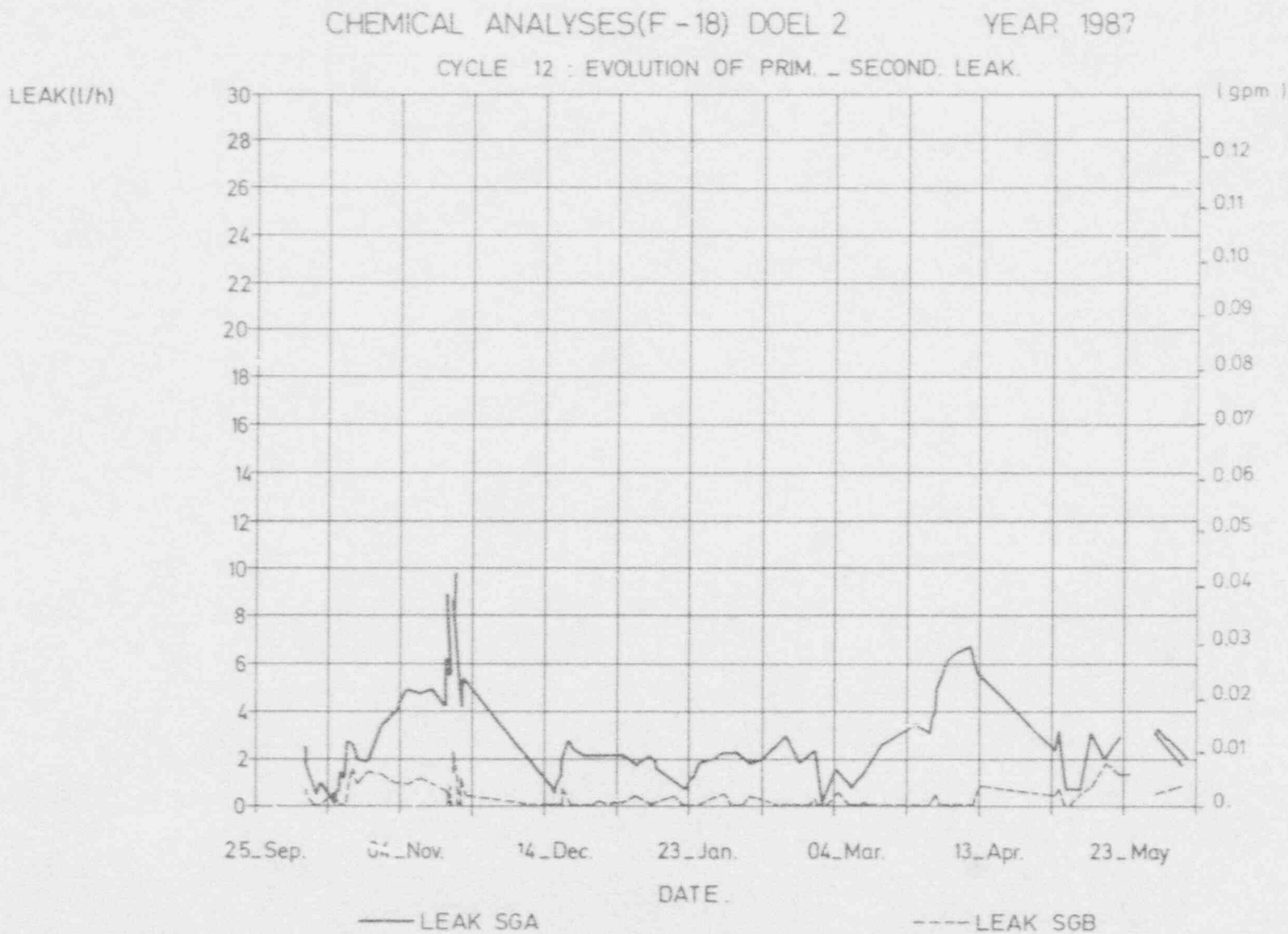
CHEMICAL ANALYSES(F - 18) DOEL 2 YEAR 1987
CYCLE 12 : EVOLUTION OF PRIM. _ SECOND. LEAK.
LEAK(l/h)
(gpm)
30
28
26
24
22
20
18
16
14
12
10
8
6
4
2
0
0.12
0.11
0.10
0.09
0.08
0.07
0.06
0.05
0.04
0.03
0.02
0.01
0.
25_Sep.
04_Nov.
14_Dec.
23_Jan.
04_Mar.
13_Apr.
23_May
DATE.
LEAK SGA
LEAK SGB

Figure 7-2

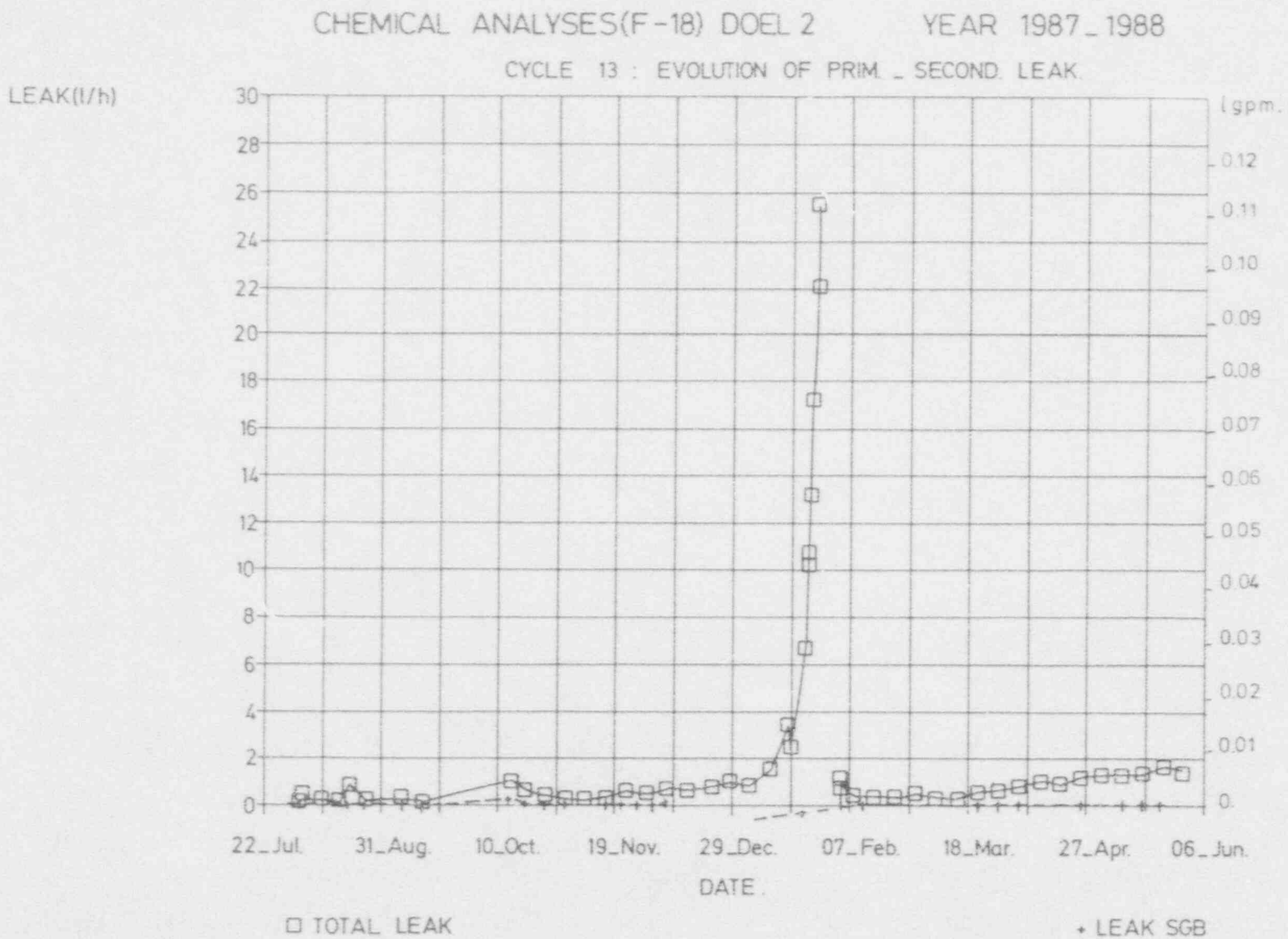
CHEMICAL ANALYSES(F-18) DOEL 2 YEAR 1987_1988
CYCLE 13 : EVOLUTION OF PRIM. _ SECOND. LEAK.
LEAK(l/h)
(gpm.)
0 2 4 6 8 10 12 14 16 18 20 22 24 26 28 30
0. 0.01 0.02 0.03 0.04 0.05 0.06 0.07 0.08 0.09 0.10 0.11 0.12
22_Jul. 31_Aug. 10_Oct. 19_Nov. 29_Dec. 07_Feb. 18_Mar. 27_Apr. 06_Jun.
DATE
□ TOTAL LEAK
+ LEAK SGB

Figure 7-3

DOEL 3 SGB LEAK DATA : INFLUENCE OF ELECTRICAL POWER INCREASE ON LEAK RATES EVALUATED BY DIFFERENT RADIOCHEMICAL ANALYSES (F-18, Na-24, N-16)

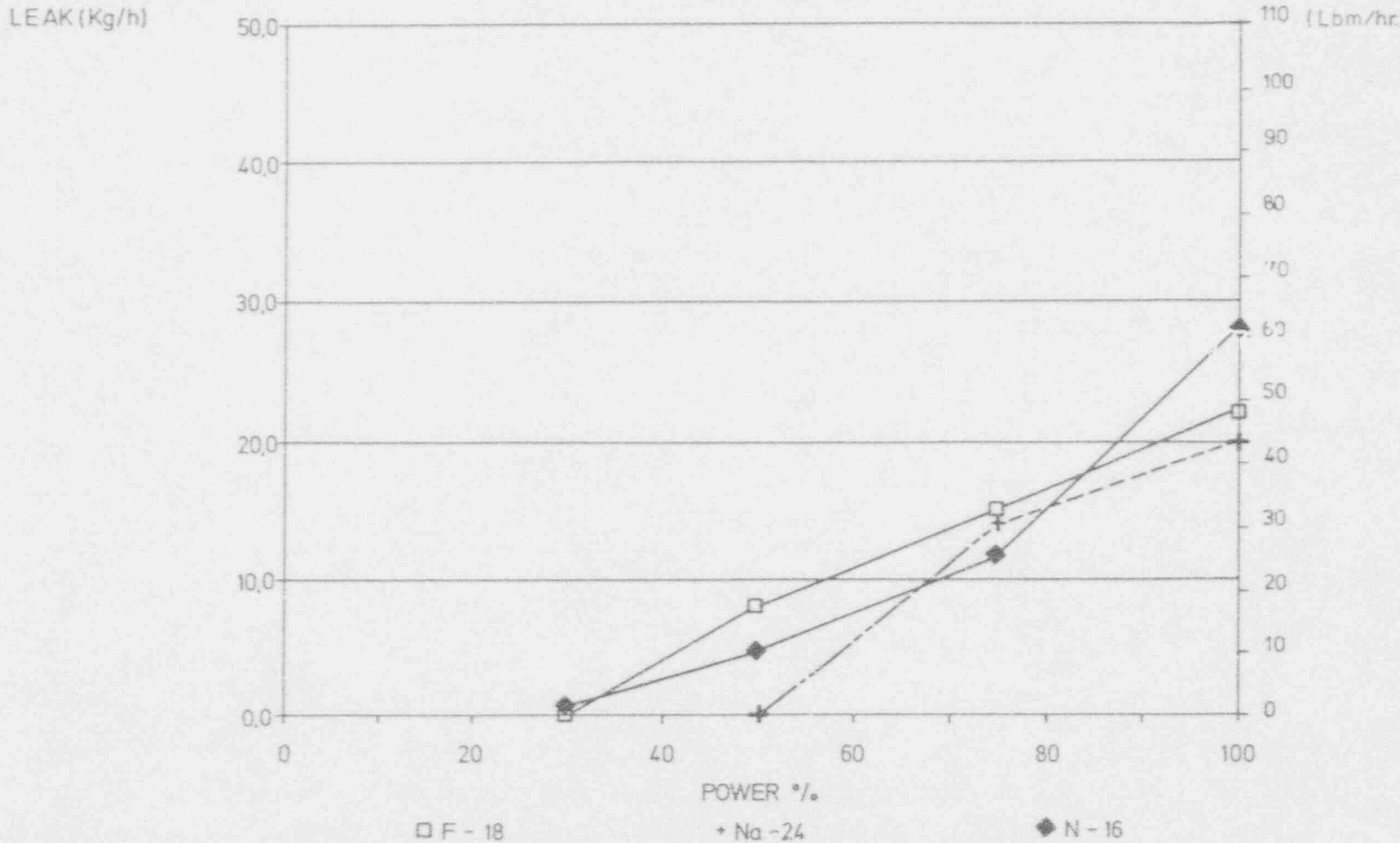

Figure 7-4

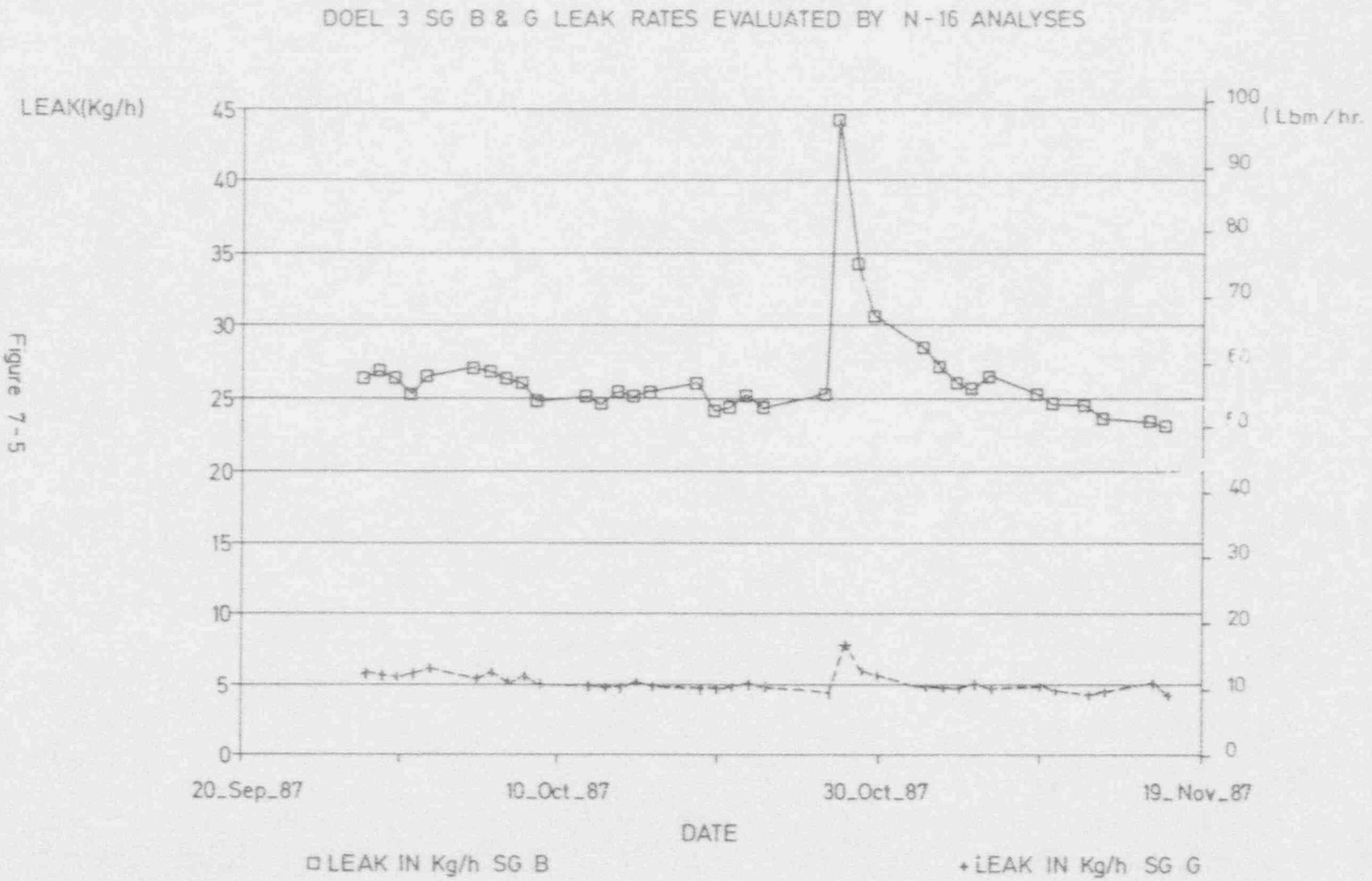
DOEL 3 SG B & G LEAK RATES EVALUATED BY N-16 ANALYSES
LEAK(Kg/h)
(Lbm/hr.)
45
40
35
30
25
20
15
10
5
0
100
90
80
70
60
50
40
30
20
10
0
20_Sep_87
10_Oct_87
30_Oct_87
19_Nov_87
DATE
□ LEAK IN Kg/h SG B
+ LEAK IN Kg/h SG G

Figure 7-5

DOEL 3 OUTAGE LEAK RATE EVALUATION IN SG R WITH THE PRIMARY WATER AT 50°C

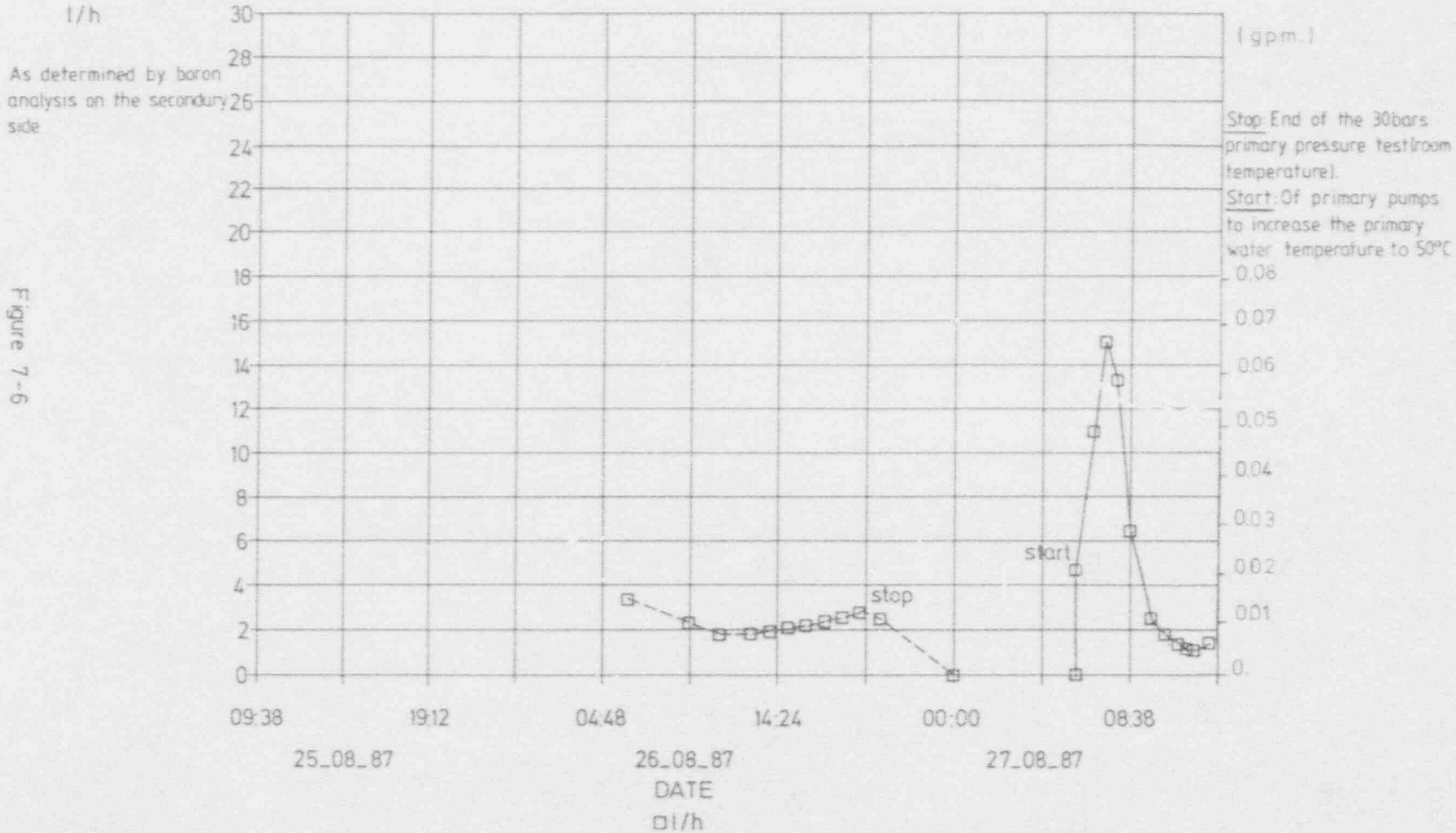

Figure 7-6

DOEL 3 OUTAGE LEAK RATE EVALUATION IN SG G WITH THE PRIMARY WATER AT 50°C

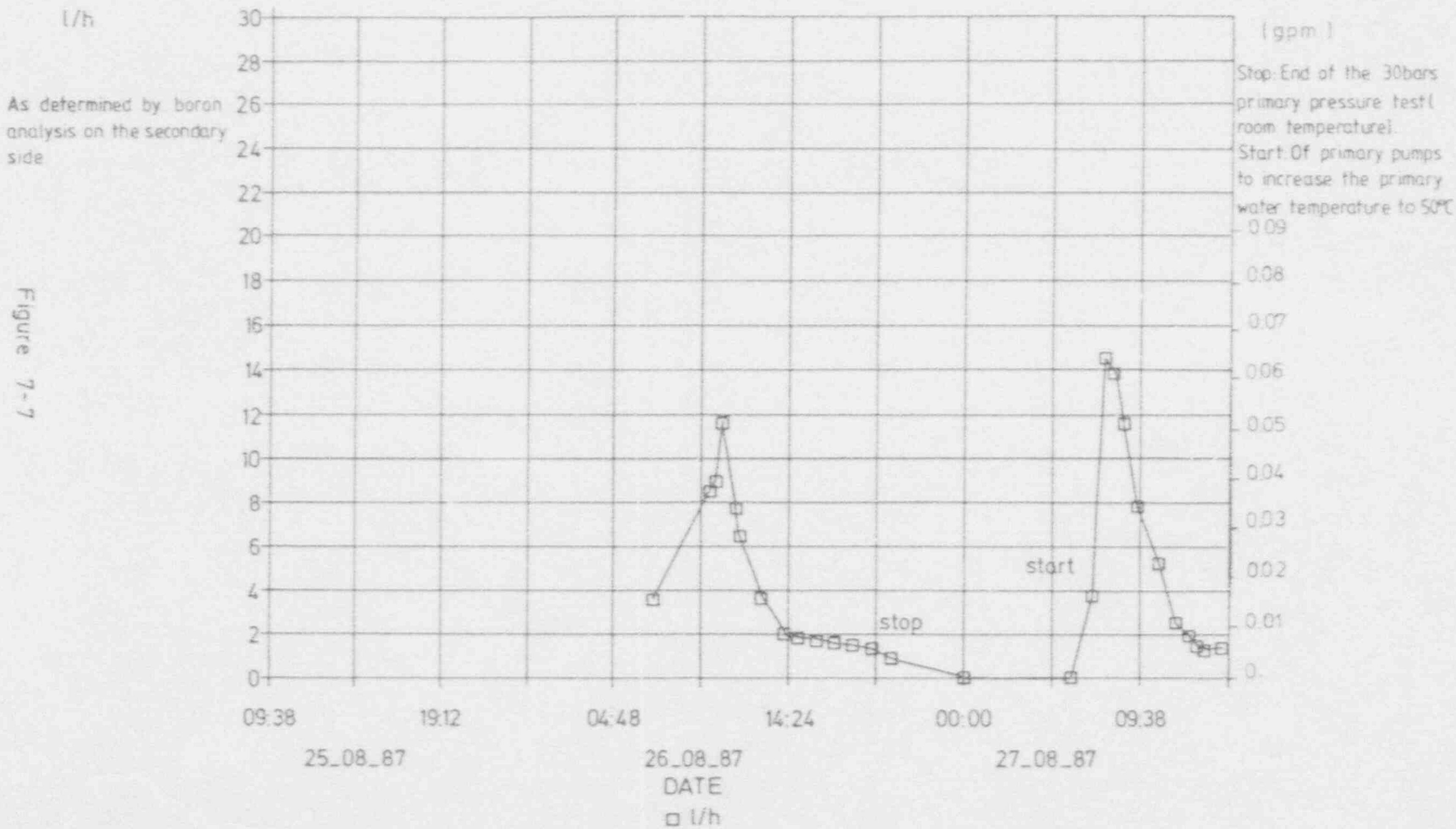

Figure 7-7

DOEL 3 OUTAGE LEAK RATE EVALUATION IN SG B WITH THE PRIMARY WATER AT 50°C

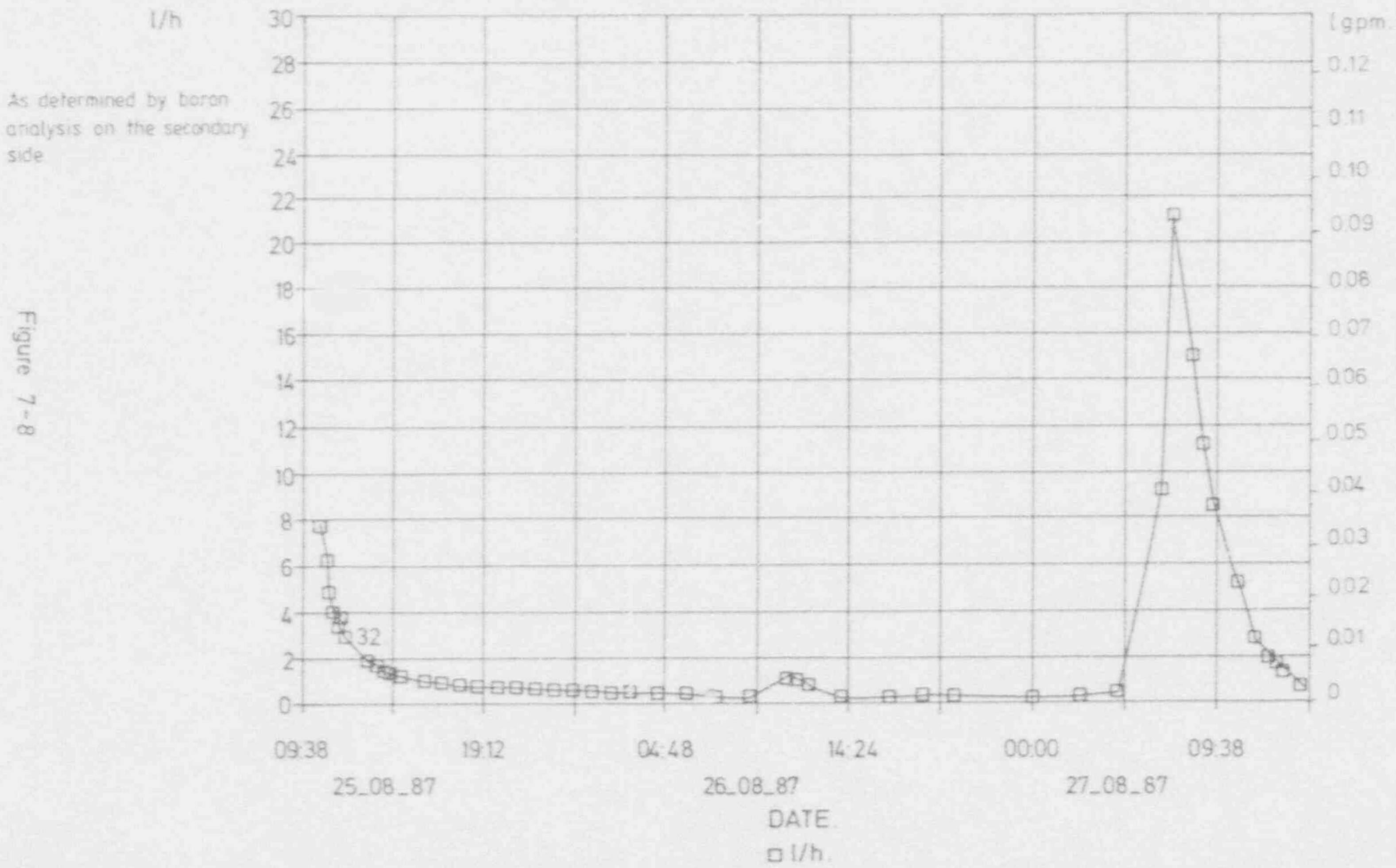

Figure 7-8

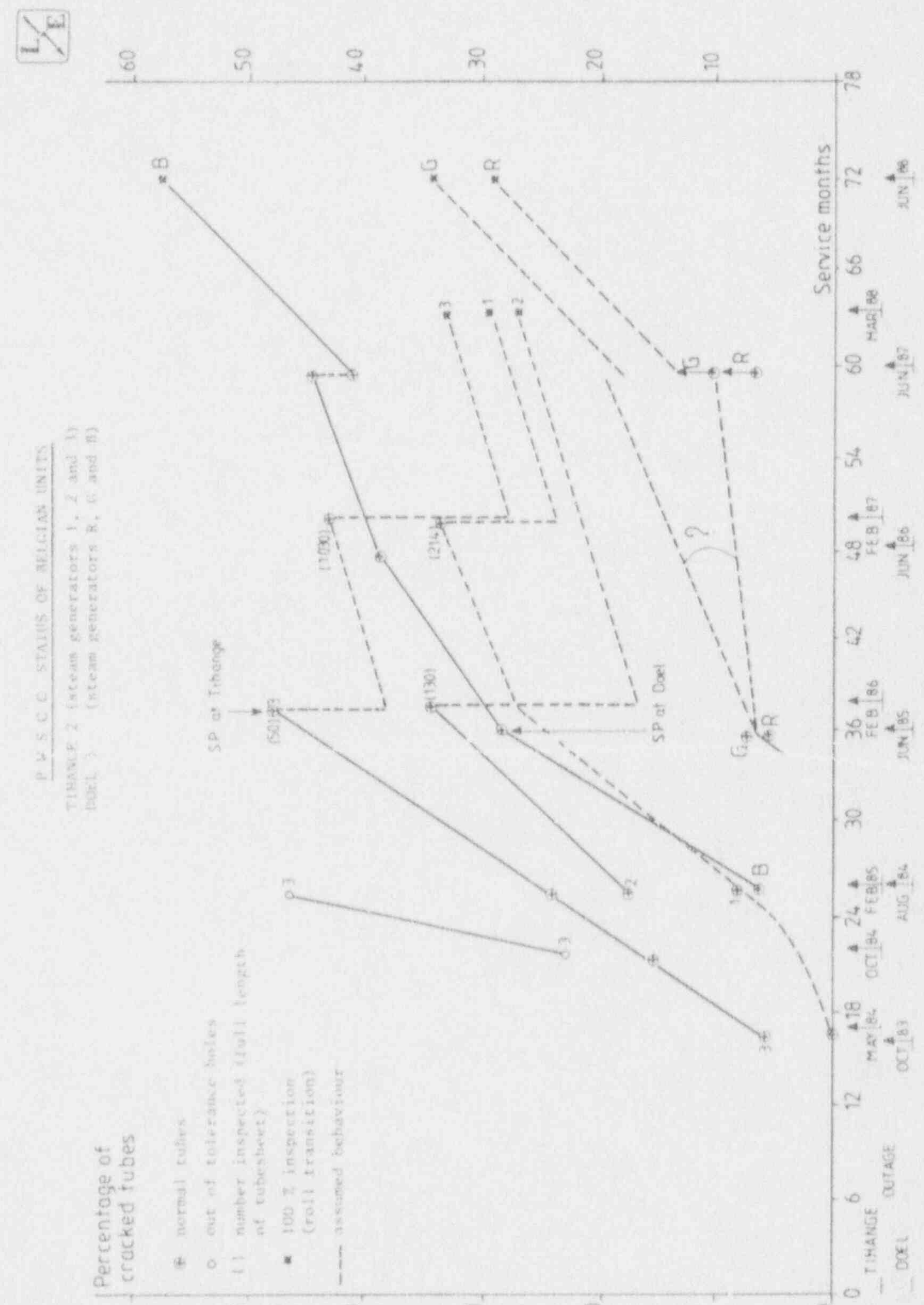
P W S C C STATUS OF BELGIAN UNITS
TIHANGE 2 (steam generators 1, 2 and 3)
DOEL 3 (steam generators R, G and B)
Percentage of cracked tubes
normal tubes
out of tolerance holes
( ) number inspected (full length of tubesheet)
100 % inspection (roll transition)
assumed behaviour
SP at Tihange
SP at Doel
(50)
(130)
(1030)
(214)
Service months
TIHANGE
OUTAGE
DOEL
MAY 84
OCT 84
FEB 85
FEB 86
FEB 87
MAR 88
OCT 83
AUG 84
JUN 85
JUN 86
JUN 87
JUN 88

Figure 7 - 9

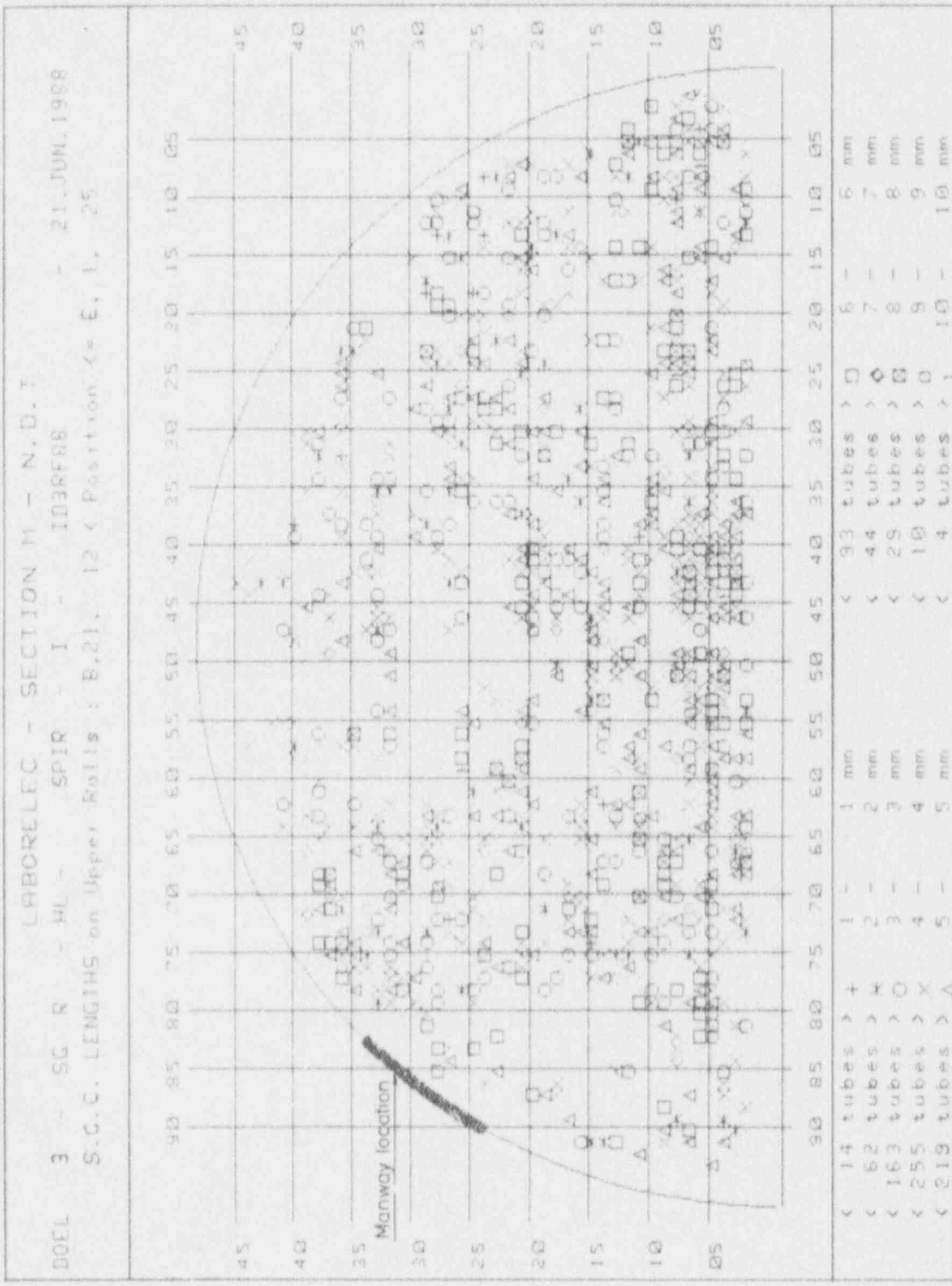

LABORELEC - SECTION M - N.D.T
DOEL 3 - SG R - HL - SPIR - I - ID3RF88 - 21.JUN.1988
S.C.C. LENGTHS on Upper Rolls : B,21. 12 < Position <= E, 1. 25
Manway location
< 14 tubes > + 1 - 1 mm
< 62 tubes > 2 - 2 mm
< 163 tubes > 3 - 3 mm
< 255 tubes > X 4 - 4 mm
< 219 tubes > 5 - 5 mm
< 93 tubes > 6 - 6 mm
< 44 tubes > 7 - 7 mm
< 29 tubes > 8 - 8 mm
< 10 tubes > 9 - 9 mm
< 4 tubes > 10 - 10 mm

Figure 7-10

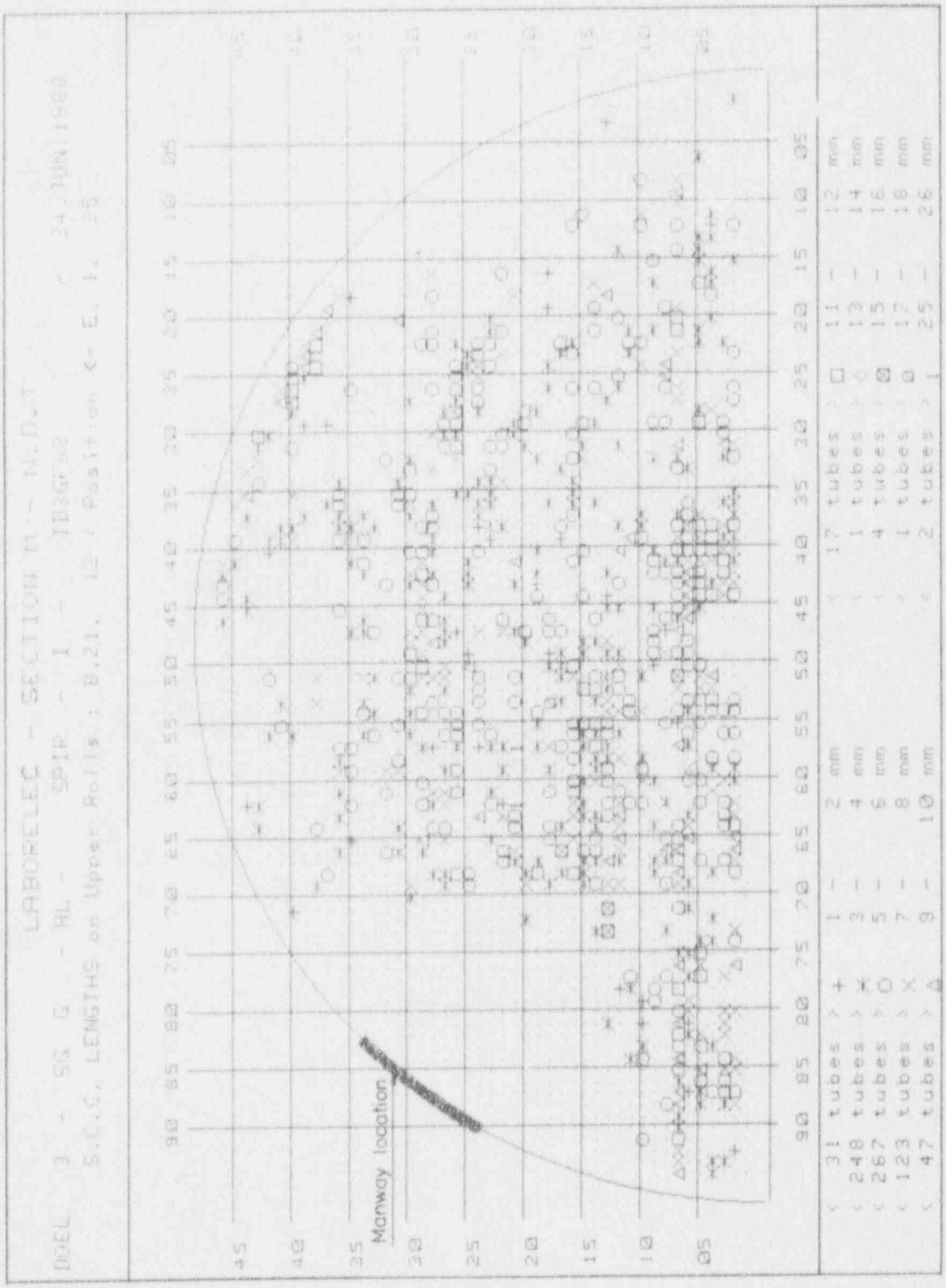
LABORELEC - SECTION M. - N.D.T
S.C.C. LENGTHS on Upper Rolls
Manway location

Figure 7-11

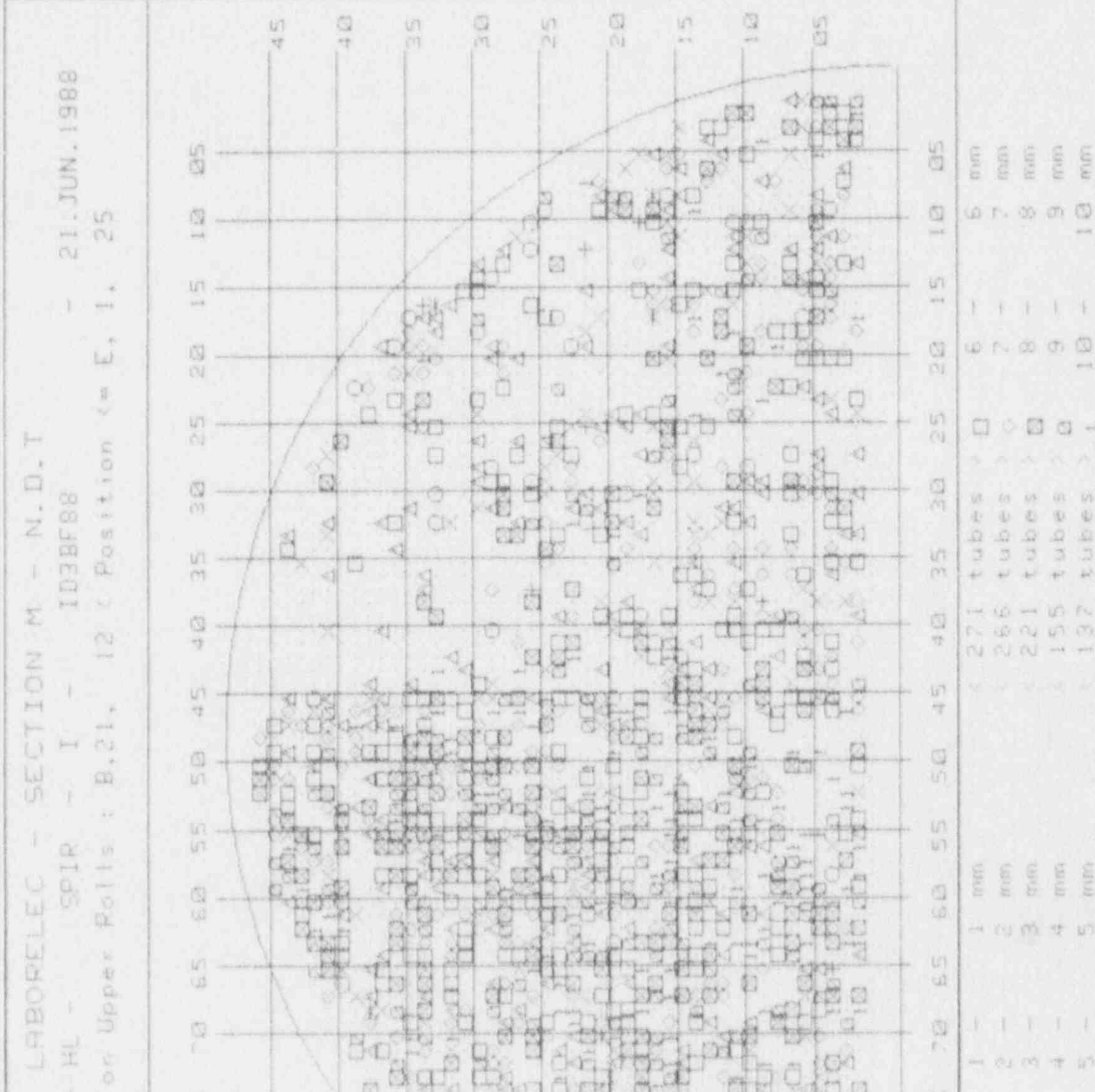
LABORELEC - SECTION M. - N.D.T
DOEL - 3 - SG B - HL - SPIR - I - ID3BF88 - 21.JUN.1988
S.C.C. LENGTHS on Upper Rolls : B.21, 12 (Position <= E, 1, 25
Manway location

Figure 7-12

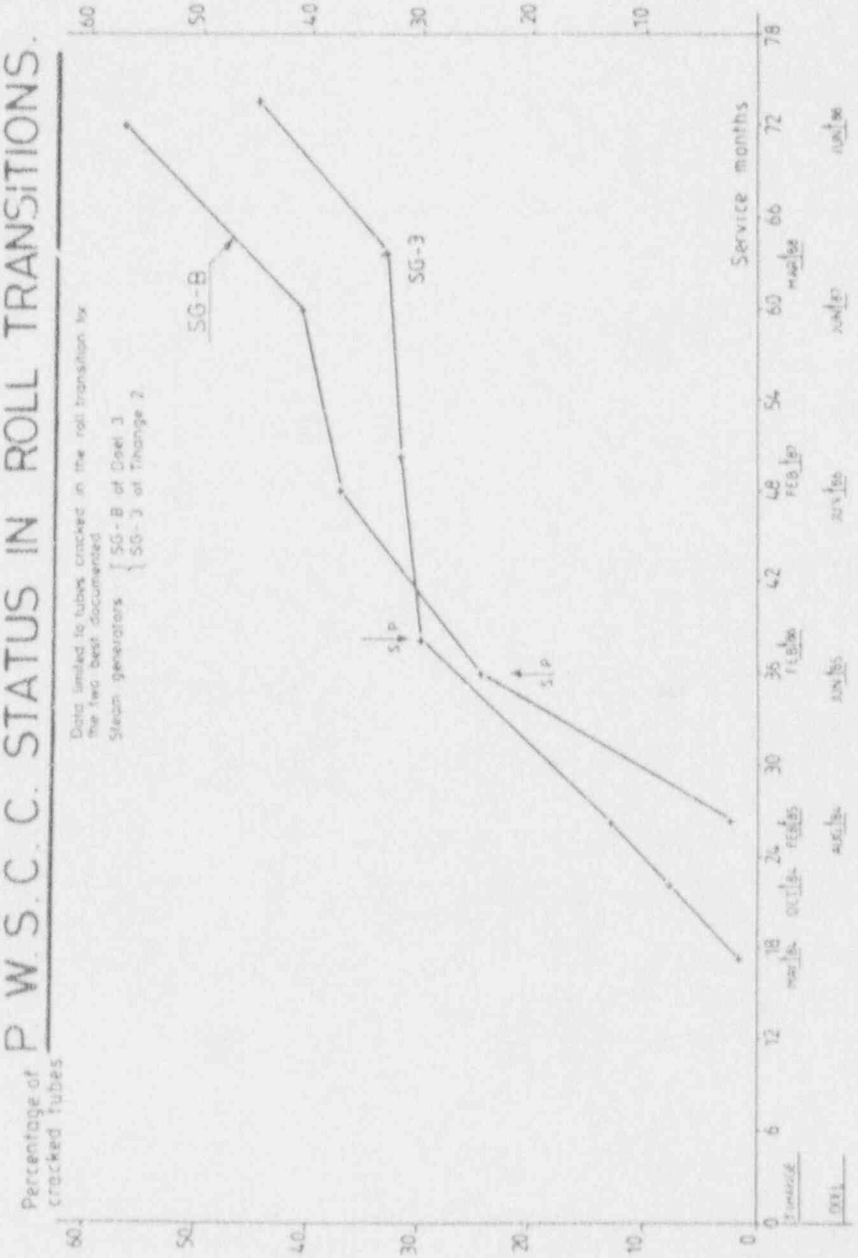
P.W.S.C.C. STATUS IN ROLL TRANSITIONS.
Percentage of cracked tubes
Data limited to tubes cracked in the roll transition for the two best documented
Steam generators
SG-B of Doel 3
SG-3 of Tihange 2
SG-B
SG-3
Service months
0
6
12
18
24
30
36
42
48
54
60
66
72
78
10
20
30
40
50
60

Figure 7-13

TYPICAL GRAPHIC DISPLAY OF RPC - ECT DATA PRODUCED BY THE COMPUTER ANALYSIS FOR EACH CRACKED SECTION

(Roll transition of a Tihange 2 tube is illustrated)

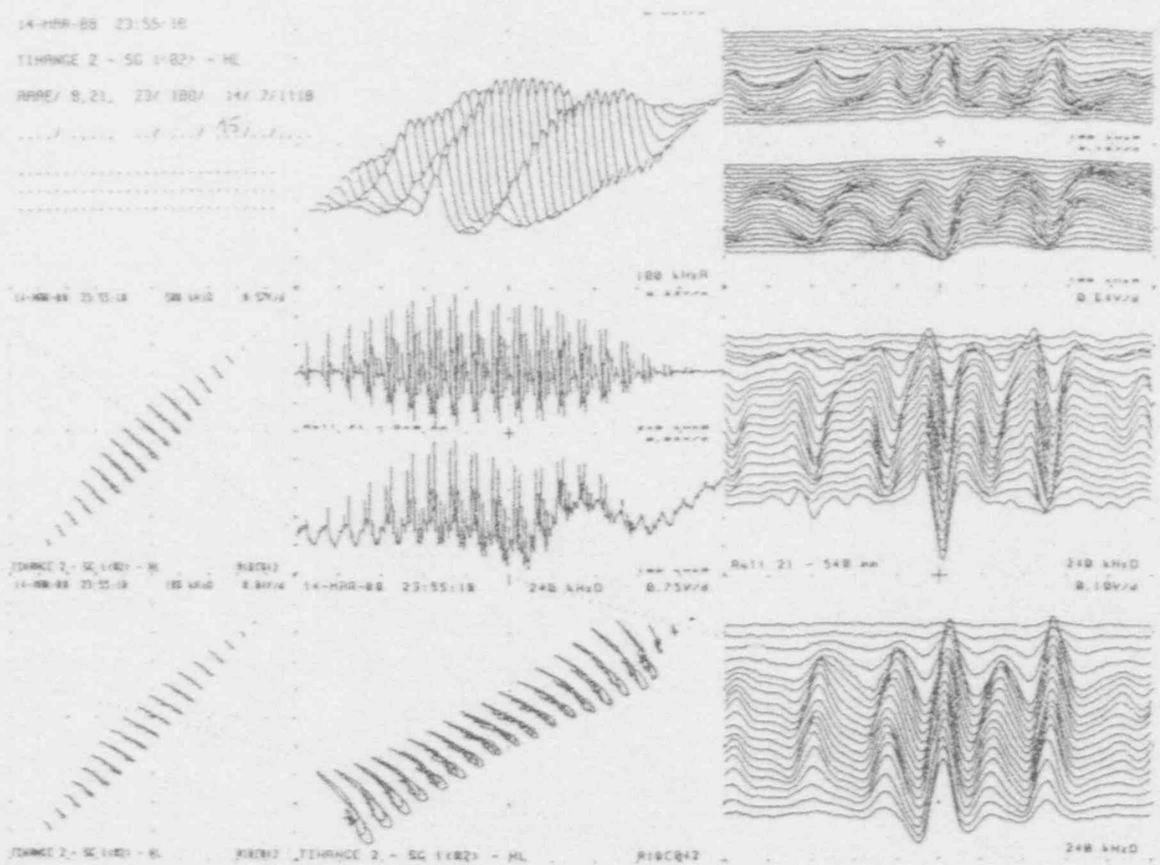

Figure 7-14

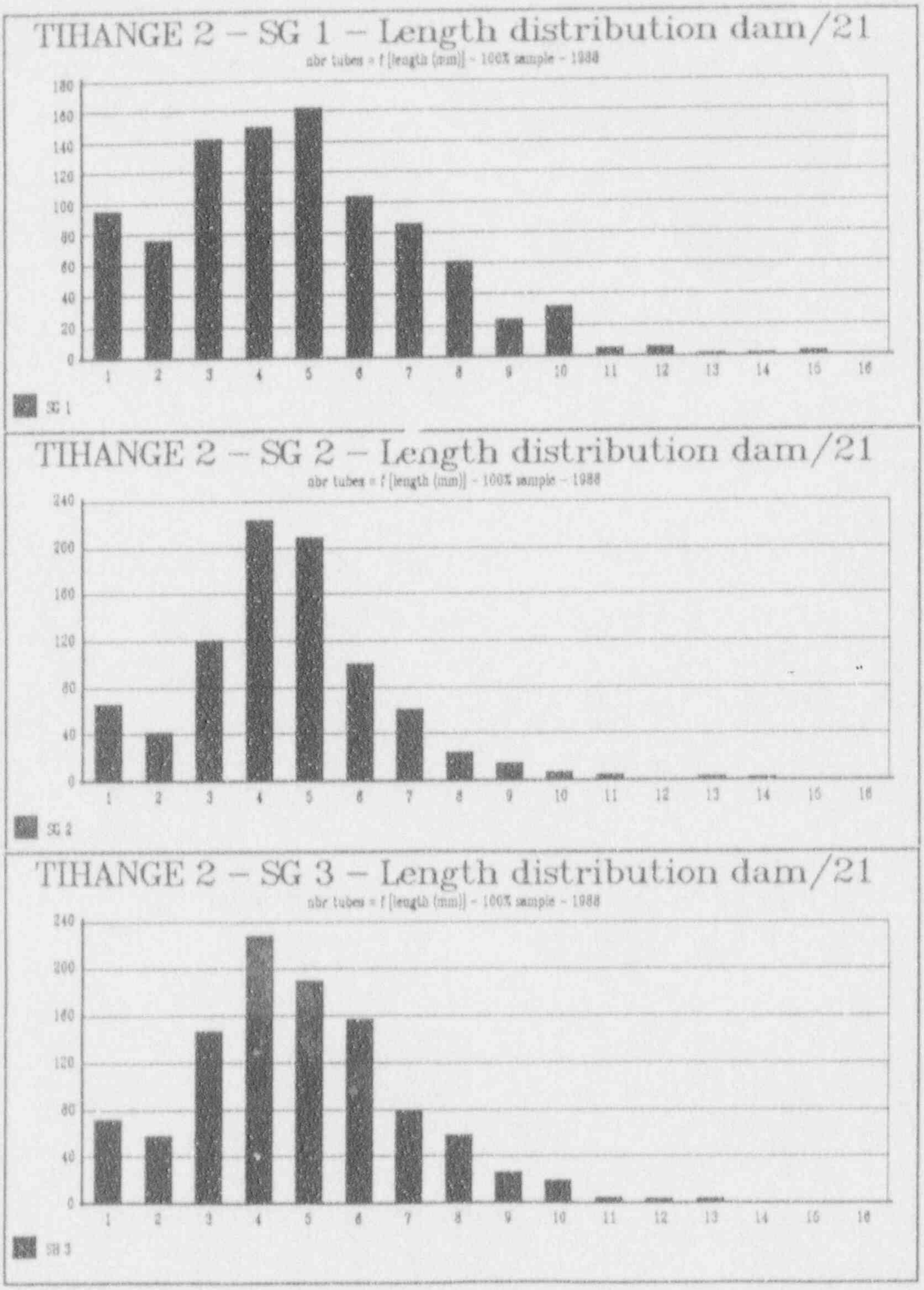

DAM/21 refers to the transition between last hard and kiss roll.

Figure 7-15

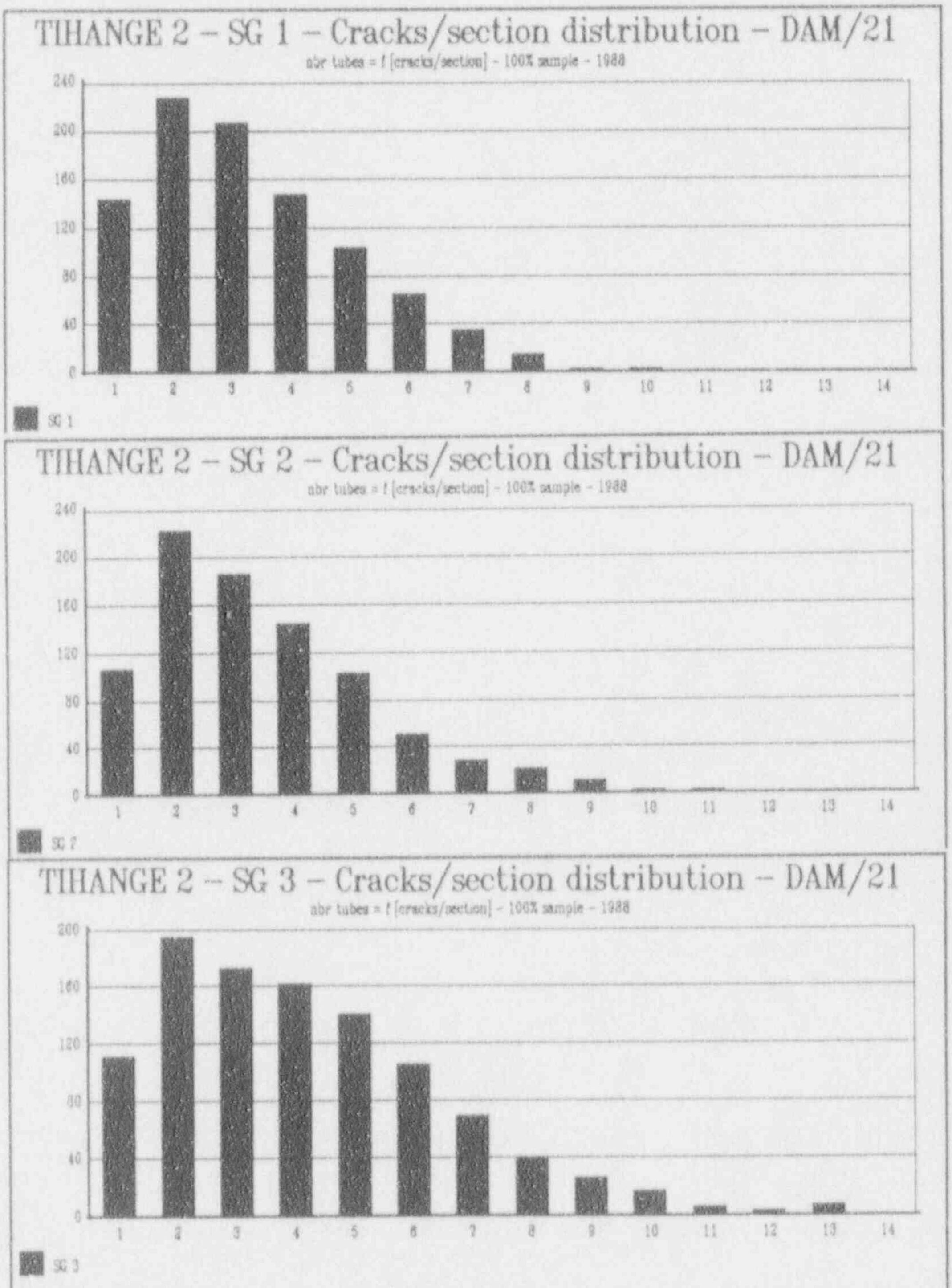

DAM/21 refers to the transition between last hard and kiss roll.

Figure 7-16

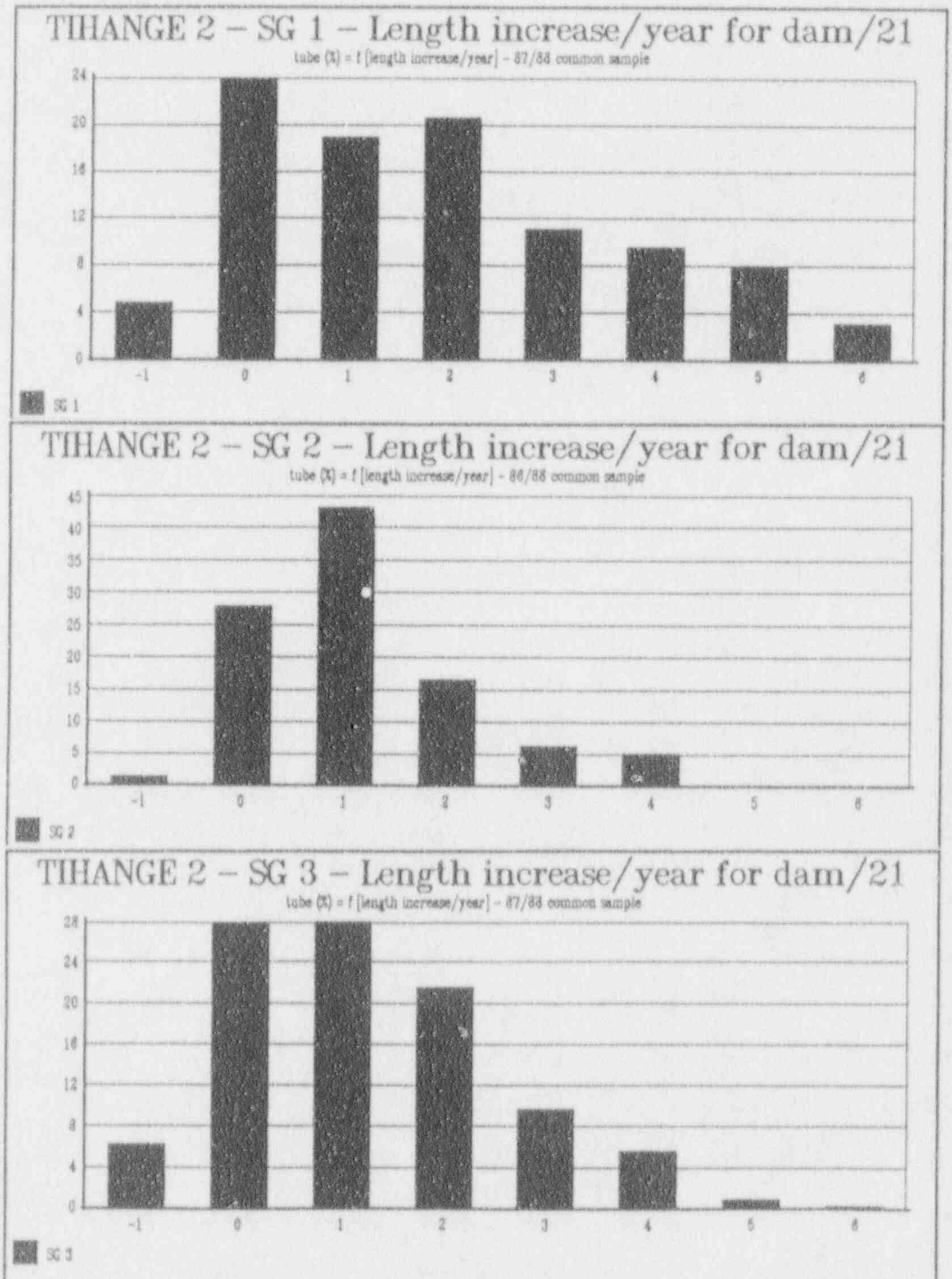

DAM/21 refers to the transition between last hard and kiss roll.

Figure 7-17

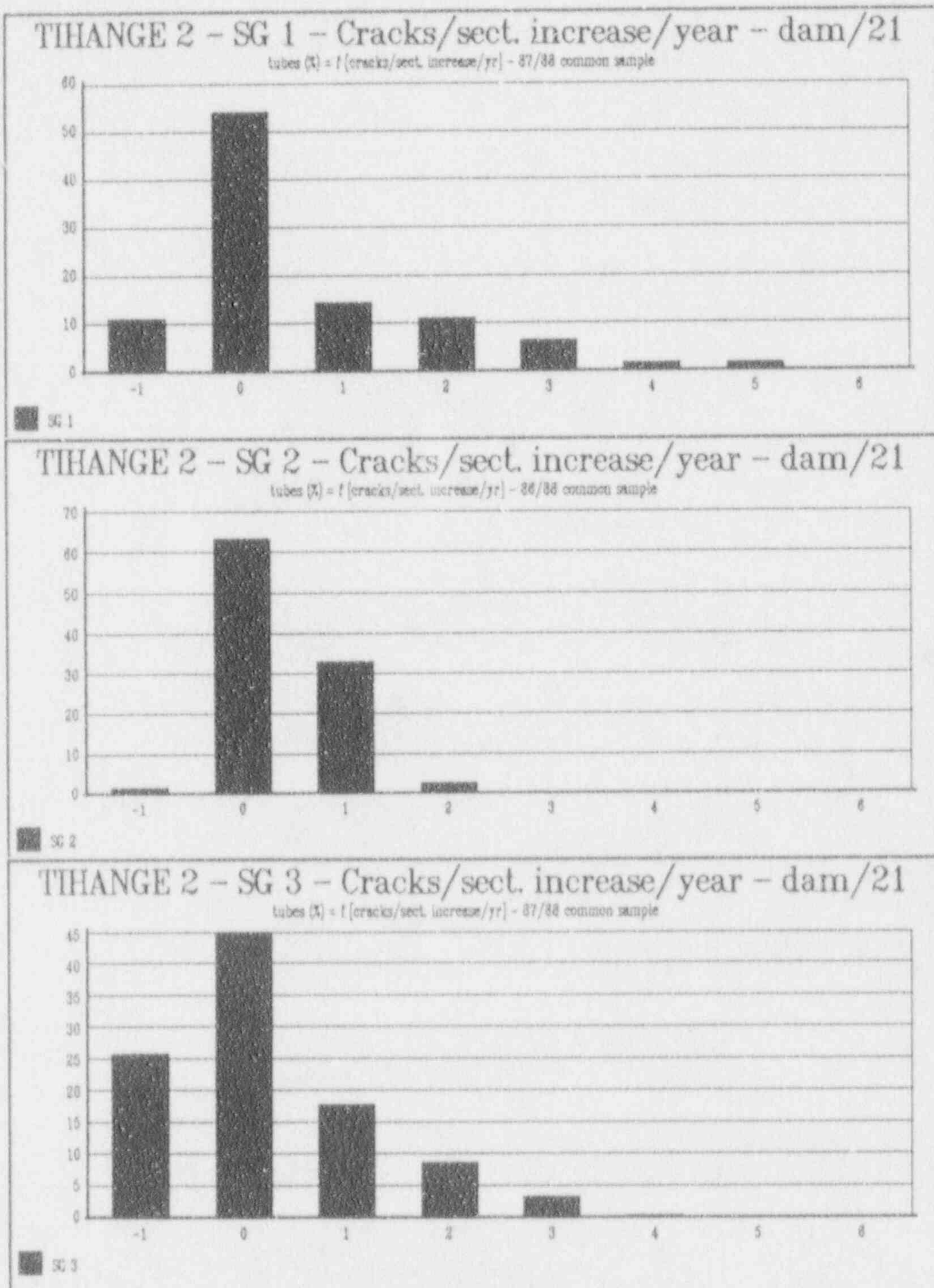

DAM/21 refers to the transition between last hard and kiss roll.

Figure 7-18

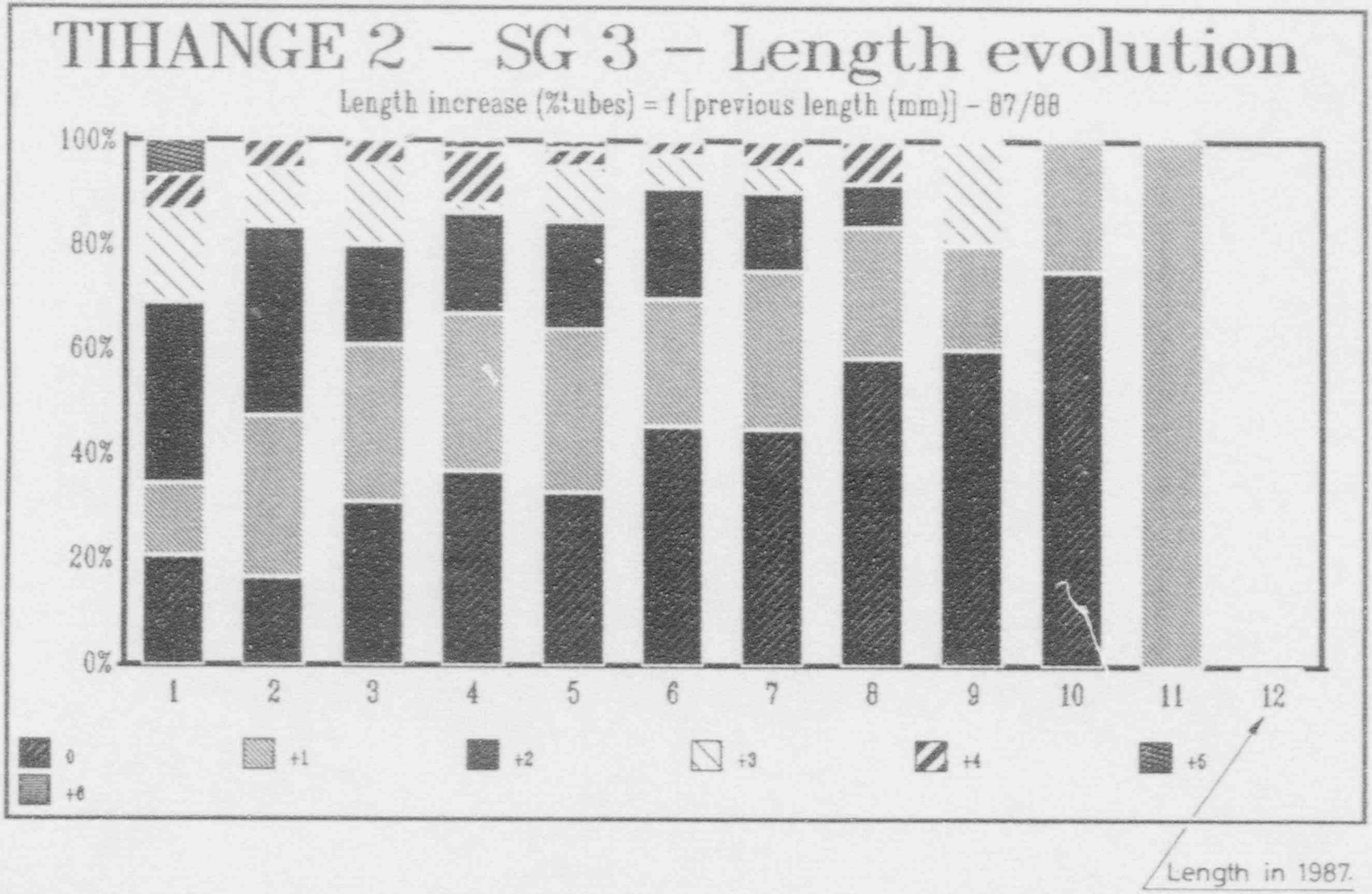

TIHANGE 2 – SG 3 – Length evolution
Length increase (%tubes) = f [previous length (mm)] - 87/88
100%
80%
60%
40%
20%
0%
1
2
3
4
5
6
7
8
9
10
11
12
0
+1
+2
+3
+4
+5
+6
Length in 1987.

Figure 7-19

DISTRIBUTION OF LENGTH AND NUMBER OF CRACKS IN ROLL TRANSITION (DOEL 3.)

OF CRACKS ON SECTION 21-DAM
DOEL 3 SG B

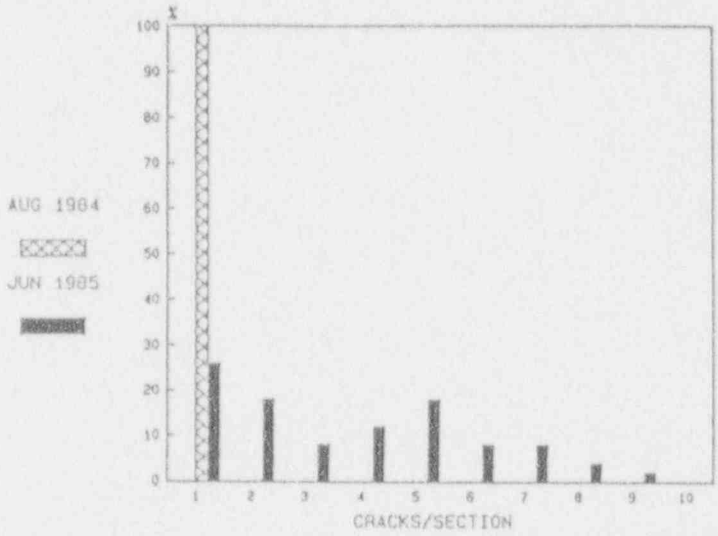

CRACK LENGTH 21-DAM
DOEL 3 SG B

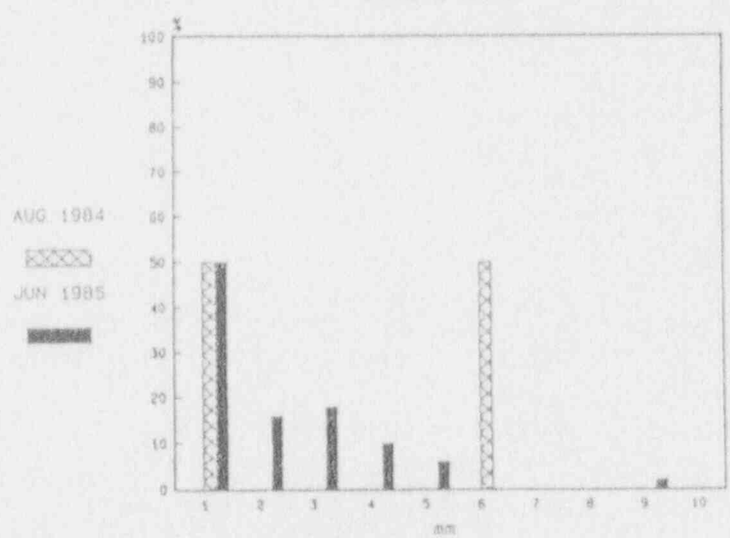

NOTE: 1984 RESULTS NOT STATISTICALLY MEANINGFUL (ONLY 2 CRACKED TUBES.)

Figure 7-20

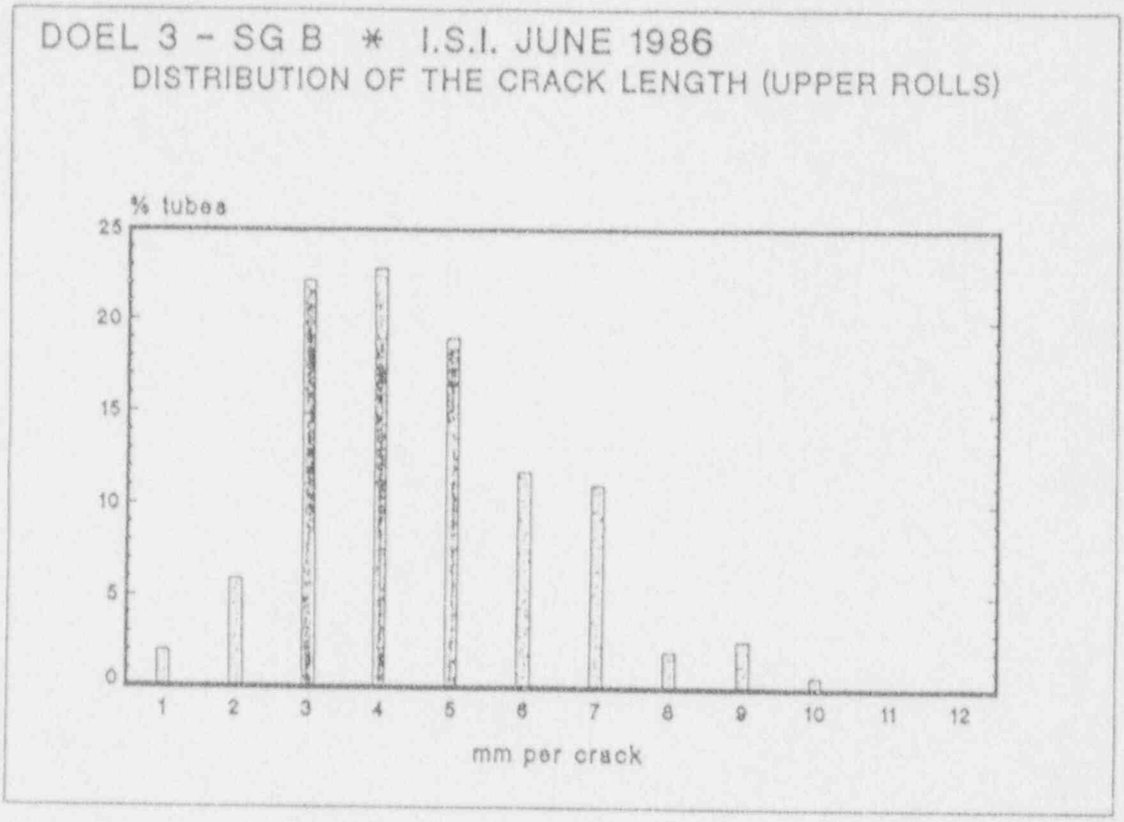

Figure 7-21(a)

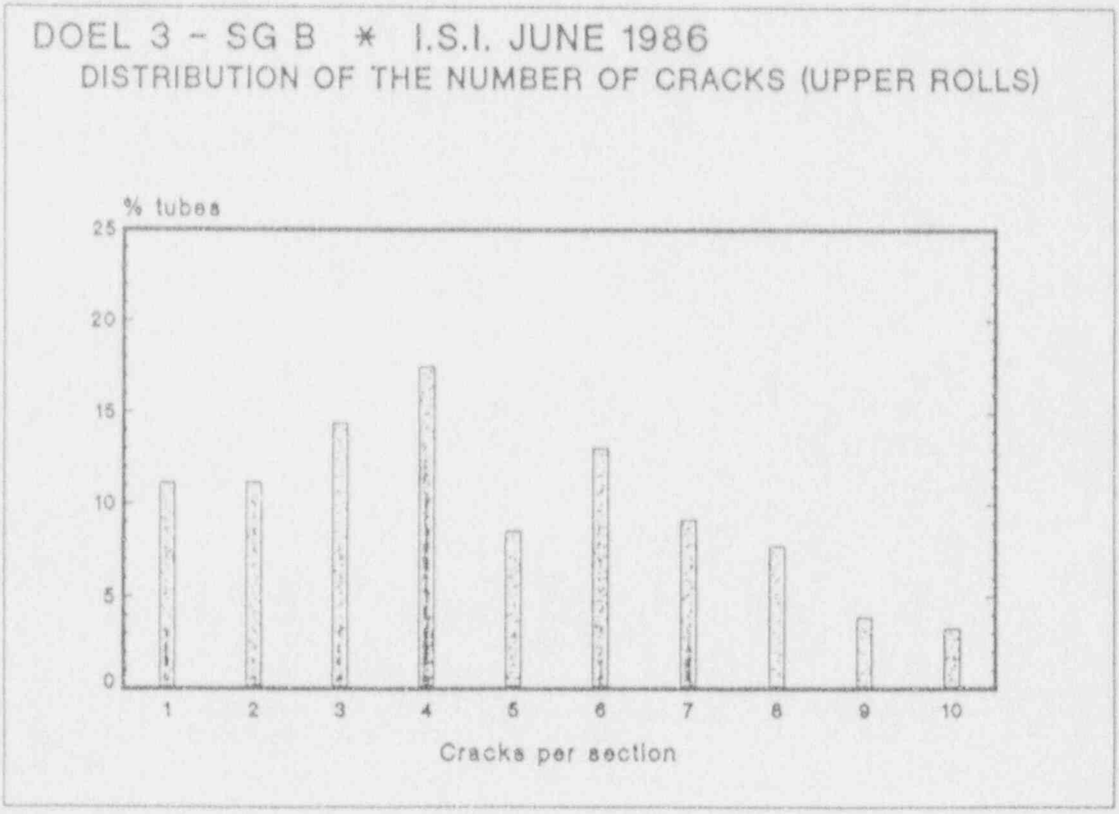

Figure 7-21(b)

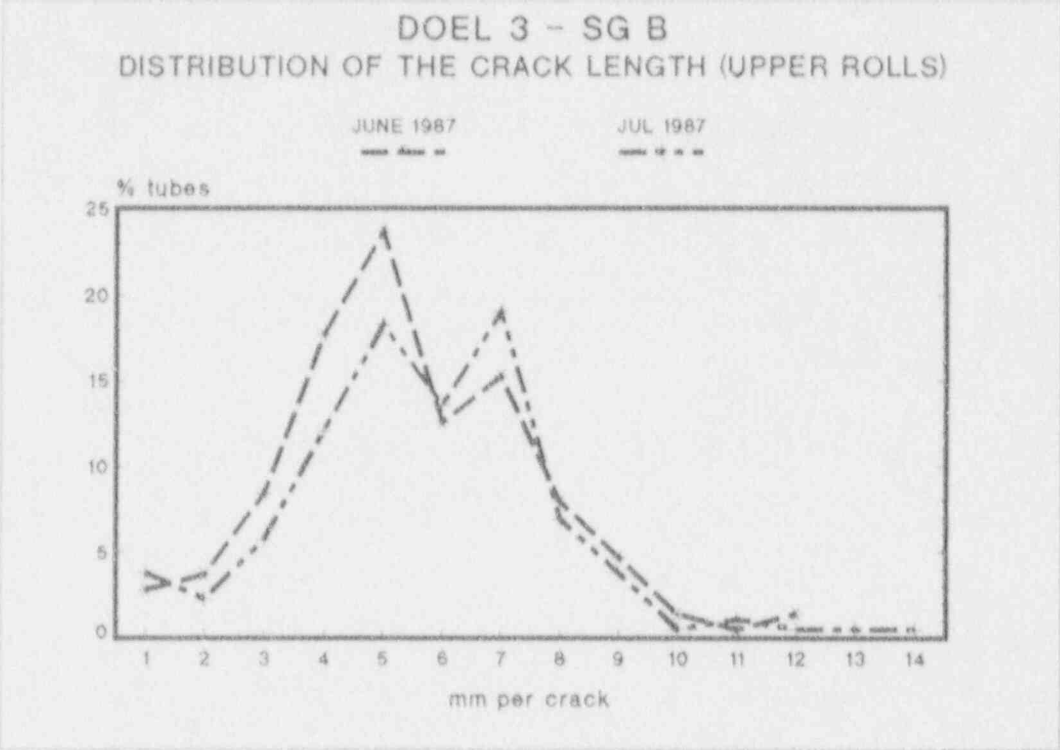
DOEL 3 - SG B
DISTRIBUTION OF THE CRACK LENGTH (UPPER ROLLS)
JUNE 1987
JUL 1987
% tubes
25
20
15
10
5
0
1 2 3 4 5 6 7 8 9 10 11 12 13 14
mm per crack

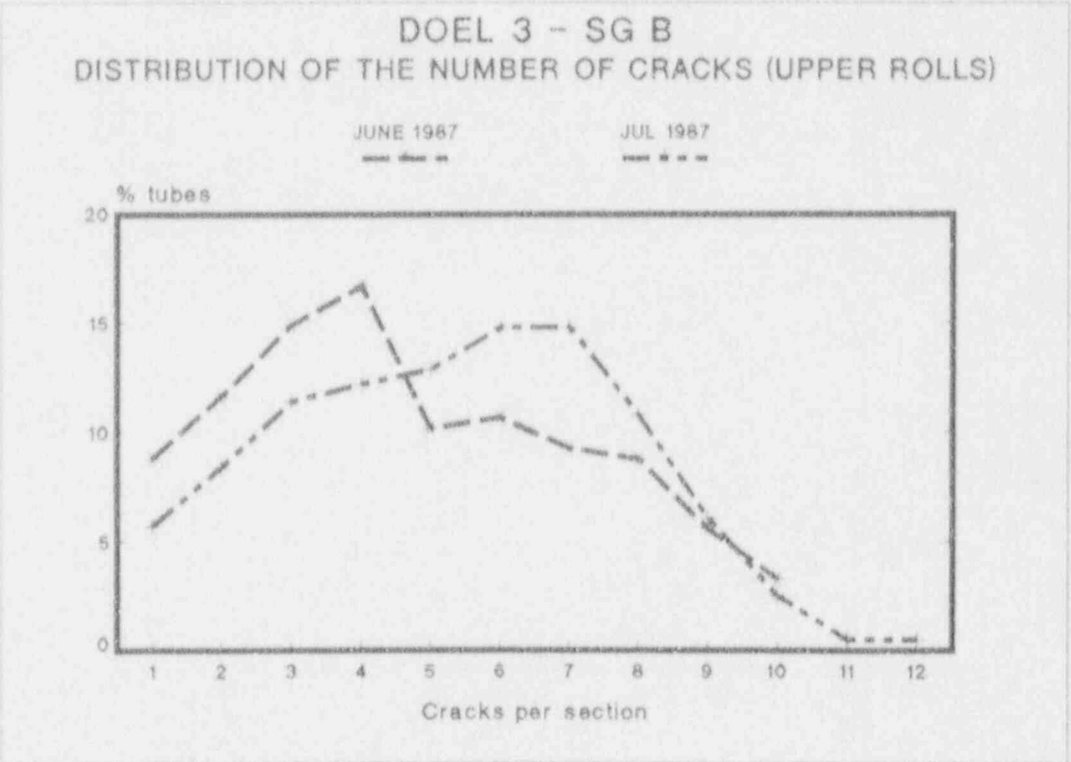
DOEL 3 - SG B
DISTRIBUTION OF THE NUMBER OF CRACKS (UPPER ROLLS)
JUNE 1987
JUL 1987
% tubes
20
15
10
5
0
1 2 3 4 5 6 7 8 9 10 11 12
Cracks per section

Figure 7 - 22

DISTRIBUTION OF LENGTH AND NUMBER OF CRACKS IN ROLL TRANSITION. (JUNE 1988 INSPECTION.) (DOEL 3.)

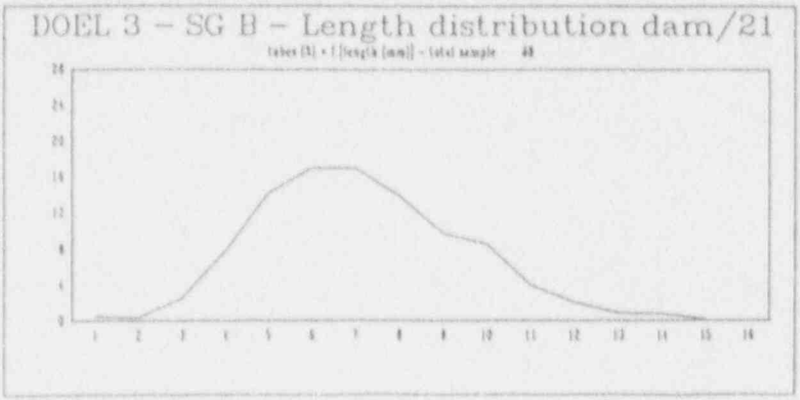

(a.)

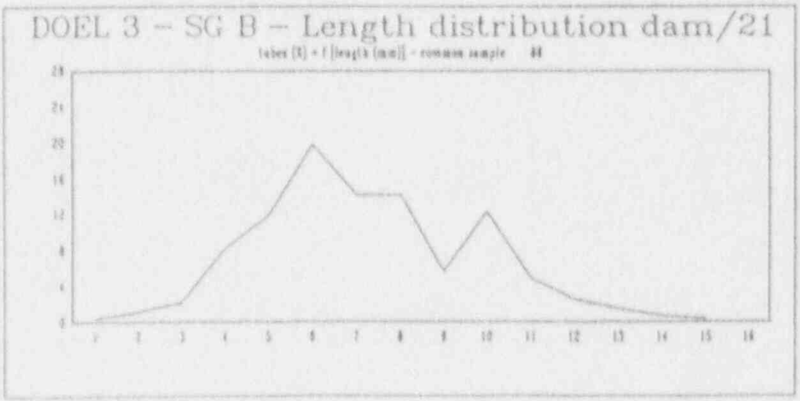

(b.)

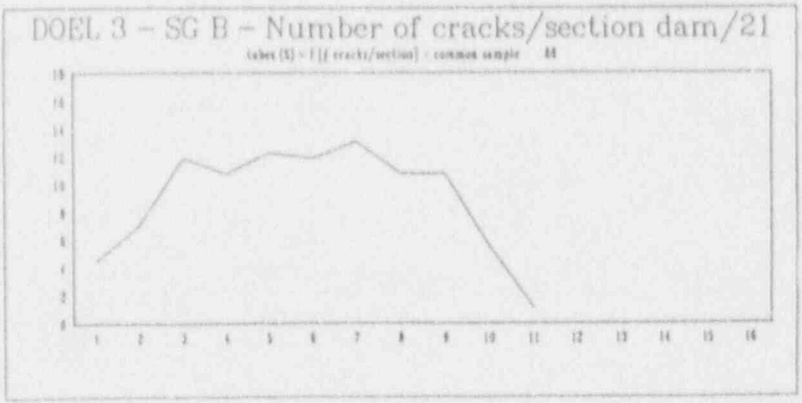

(c.)

Figure 7-23

DEPENDENCY OF THE CRACK LENGTH INCREASE ON THE INITIAL CRACK LENGTH.
(BETWEEN JUNE 1987 AND JUNE 1988 INSPECTIONS)

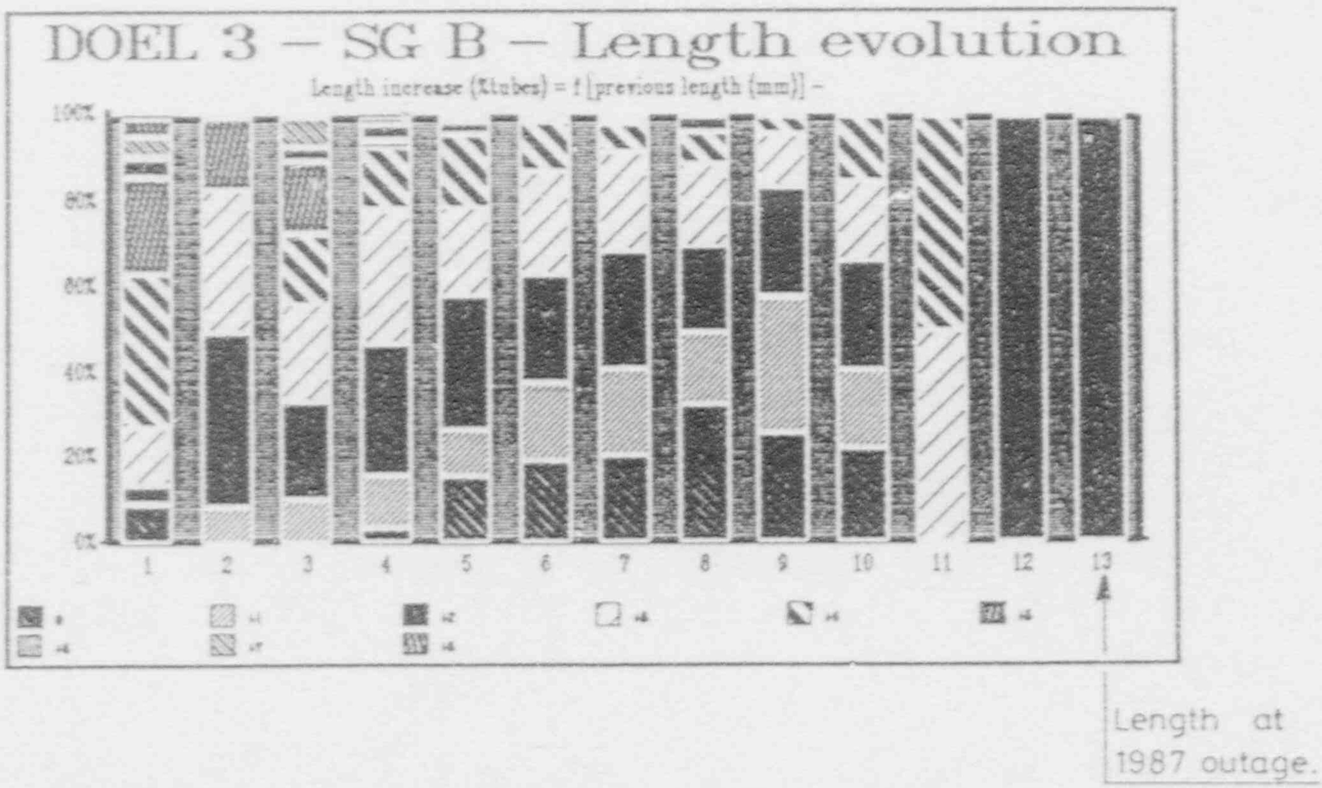

Figure 7-24

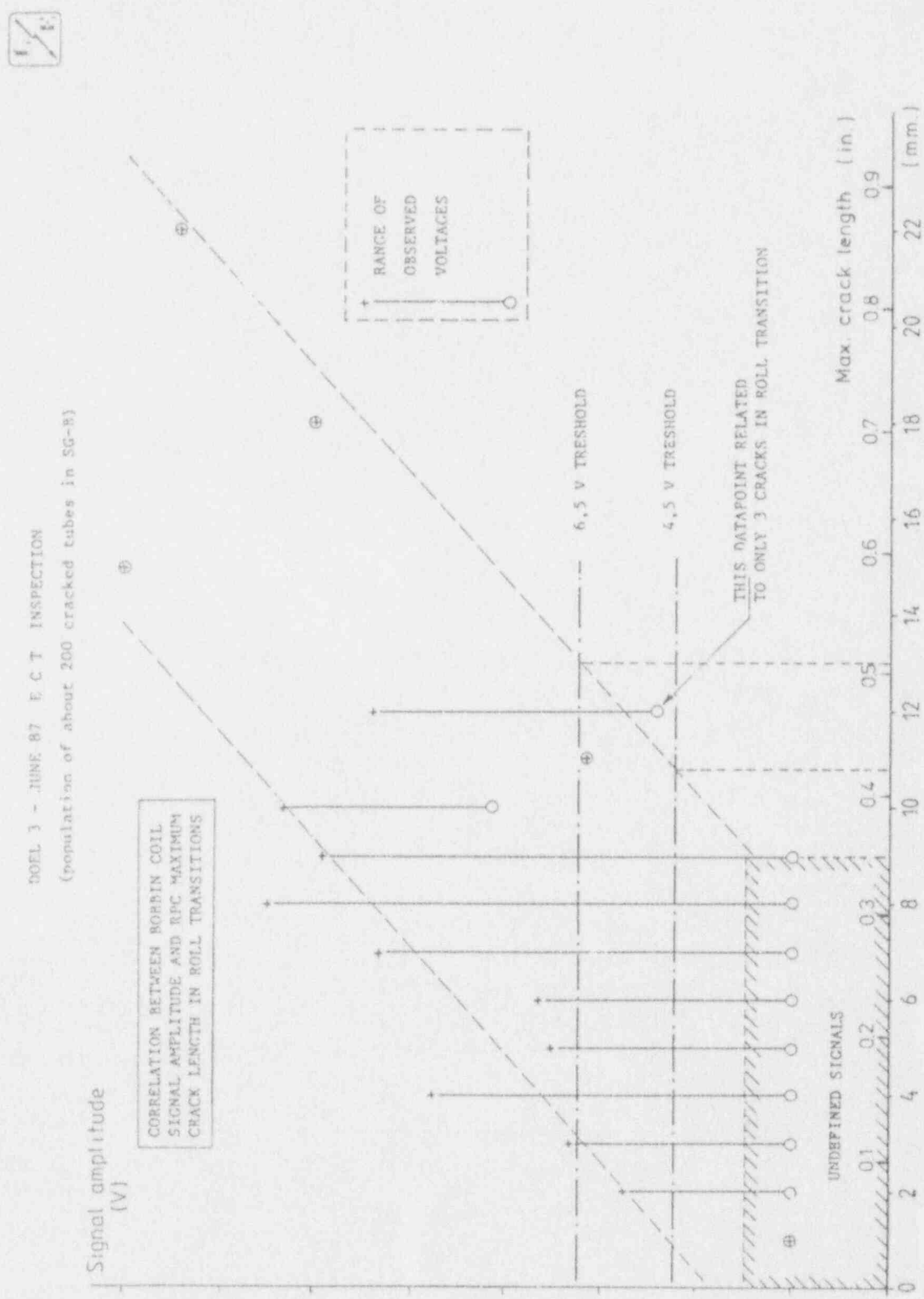
DOEL 3 - JUNE 87 E C T INSPECTION
(population of about 200 cracked tubes in SG-B)
CORRELATION BETWEEN BOBBIN COIL
SIGNAL AMPLITUDE AND RPC MAXIMUM
CRACK LENGTH IN ROLL TRANSITIONS
Signal amplitude
(V)
6,5 V TRESHOLD
4,5 V TRESHOLD
THIS DATAPOINT RELATED
TO ONLY 3 CRACKS IN ROLL TRANSITION
RANGE OF
OBSERVED
VOLTAGES
UNDEFINED SIGNALS
Max. crack length (in.)
(mm)

Figure 7-25

DOEL 3 BOBBIN COIL AND R P C E C T INSPECTION
(june 87 / population of about 200 cracked tubes in SG-B)

CORRELATION OF BOBBIN COIL SIGNAL AMPLITUDE WITH NUMBER OF CRACKS AND MAXIMUM CRACK LENGTH (as measured by R P C)

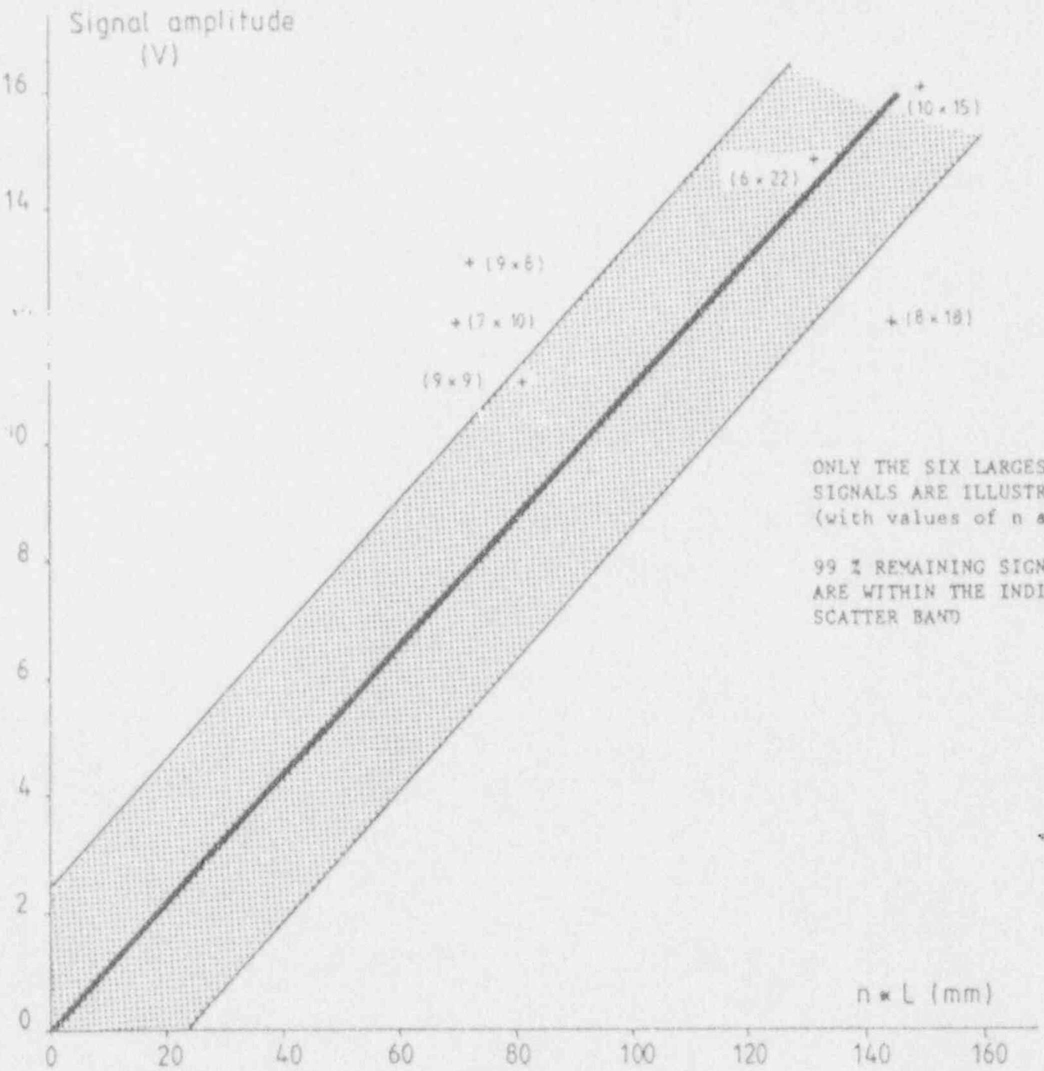

n = number of cracks in roll transition
L = length of longest crack

Figure 7-26

DOEL 3 BOBBIN COIL AND R P C E C T INSPECTION

(june 87 / population of about 200 cracked tubes in SG-B)

CORRELATION BETWEEN NUMBER OF CRACKS AND MAXIMUM CRACK LENGTH
(bobbin coil signal amplitude used as parameter)

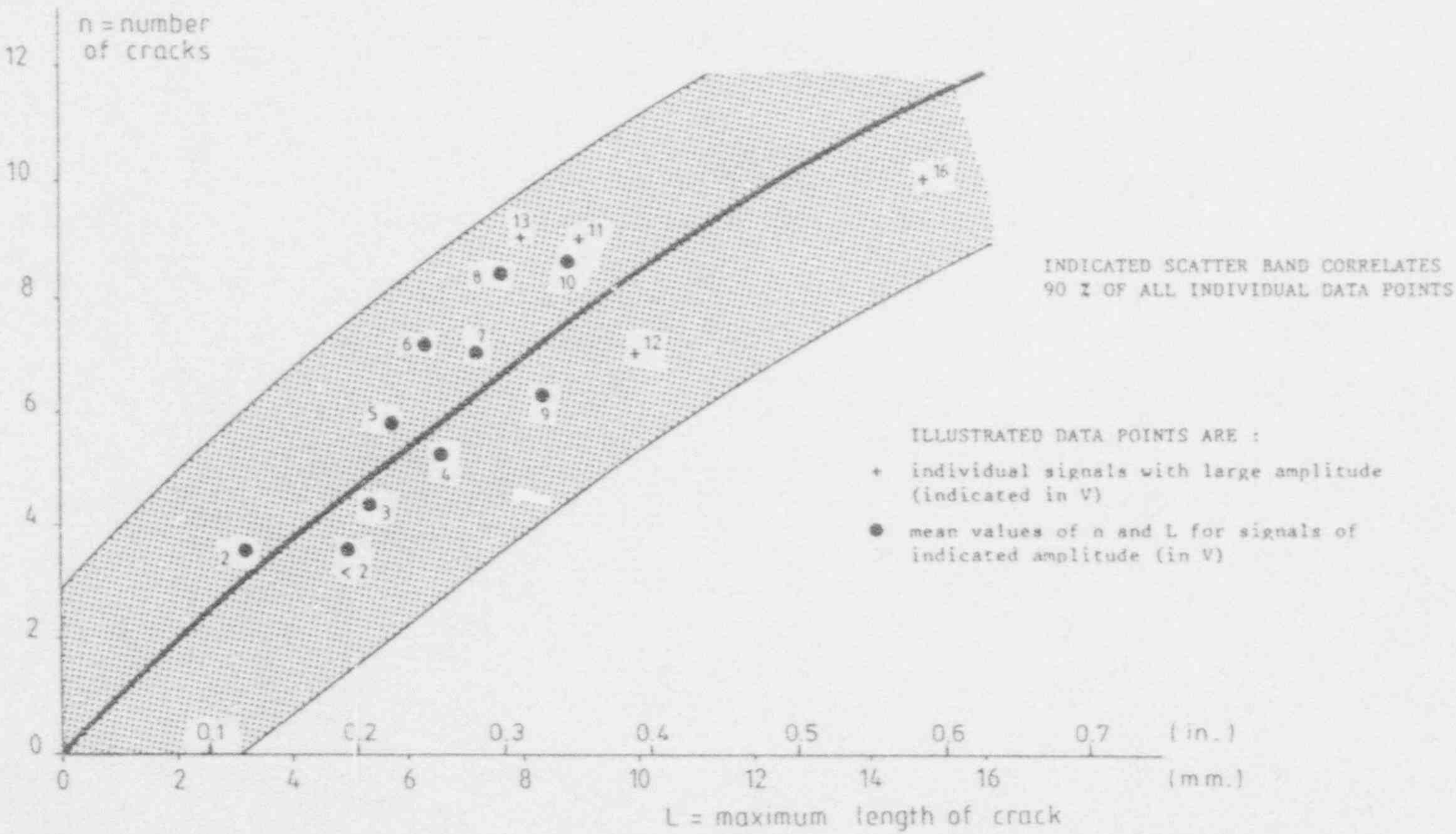

Figure 7-27

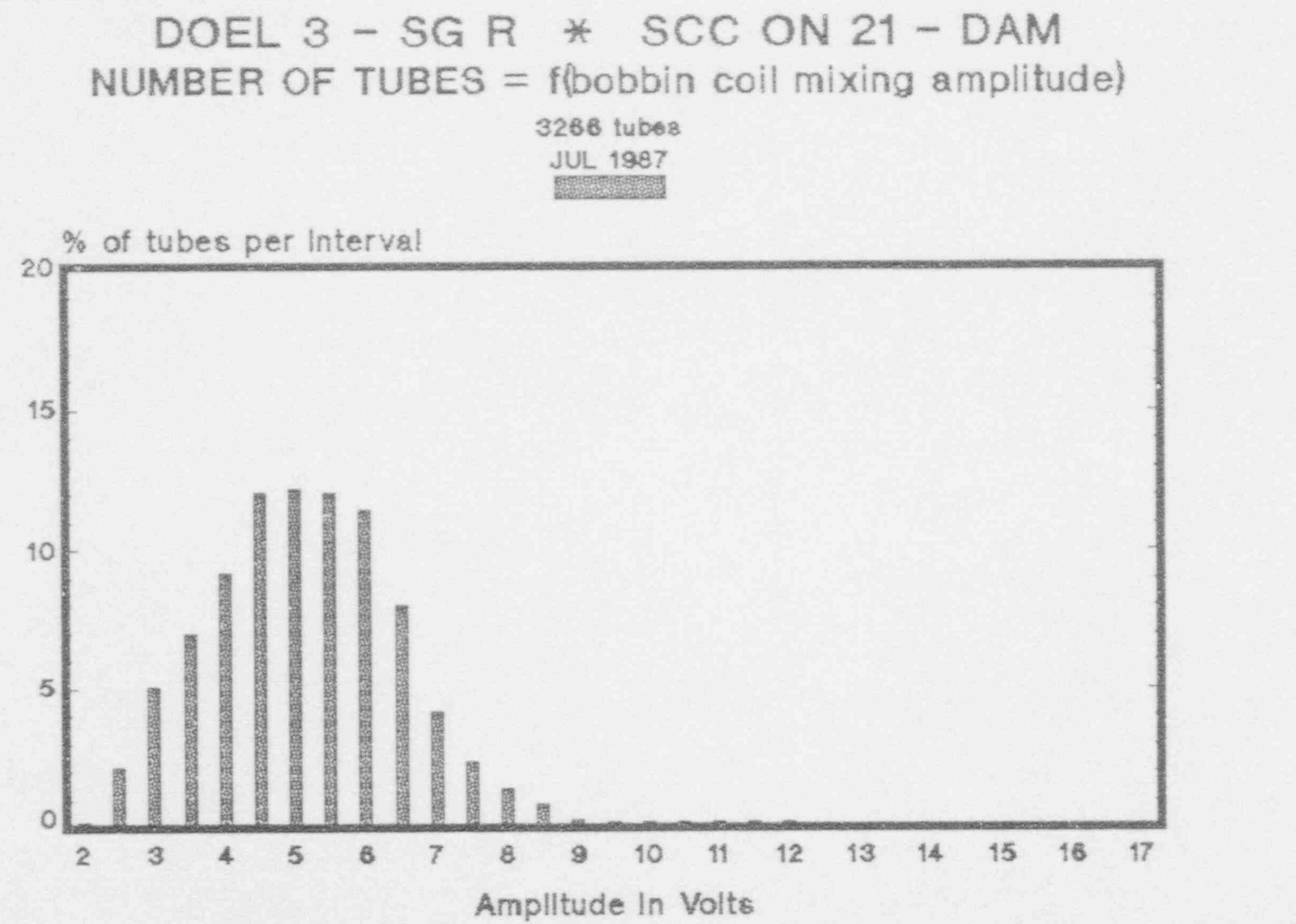
DOEL 3 - SG R * SCC ON 21 - DAM
NUMBER OF TUBES = f(bobbin coil mixing amplitude)
3266 tubes
JUL 1987
% of tubes per interval
20
15
10
5
0
2
3
4
5
6
7
8
9
10
11
12
13
14
15
16
17
Amplitude in Volts

Figure 7-28

DOEL 3 - SG G * SCC ON 21 - DAM

NUMBER OF TUBES = f(bobbin coil mixing amplitude)

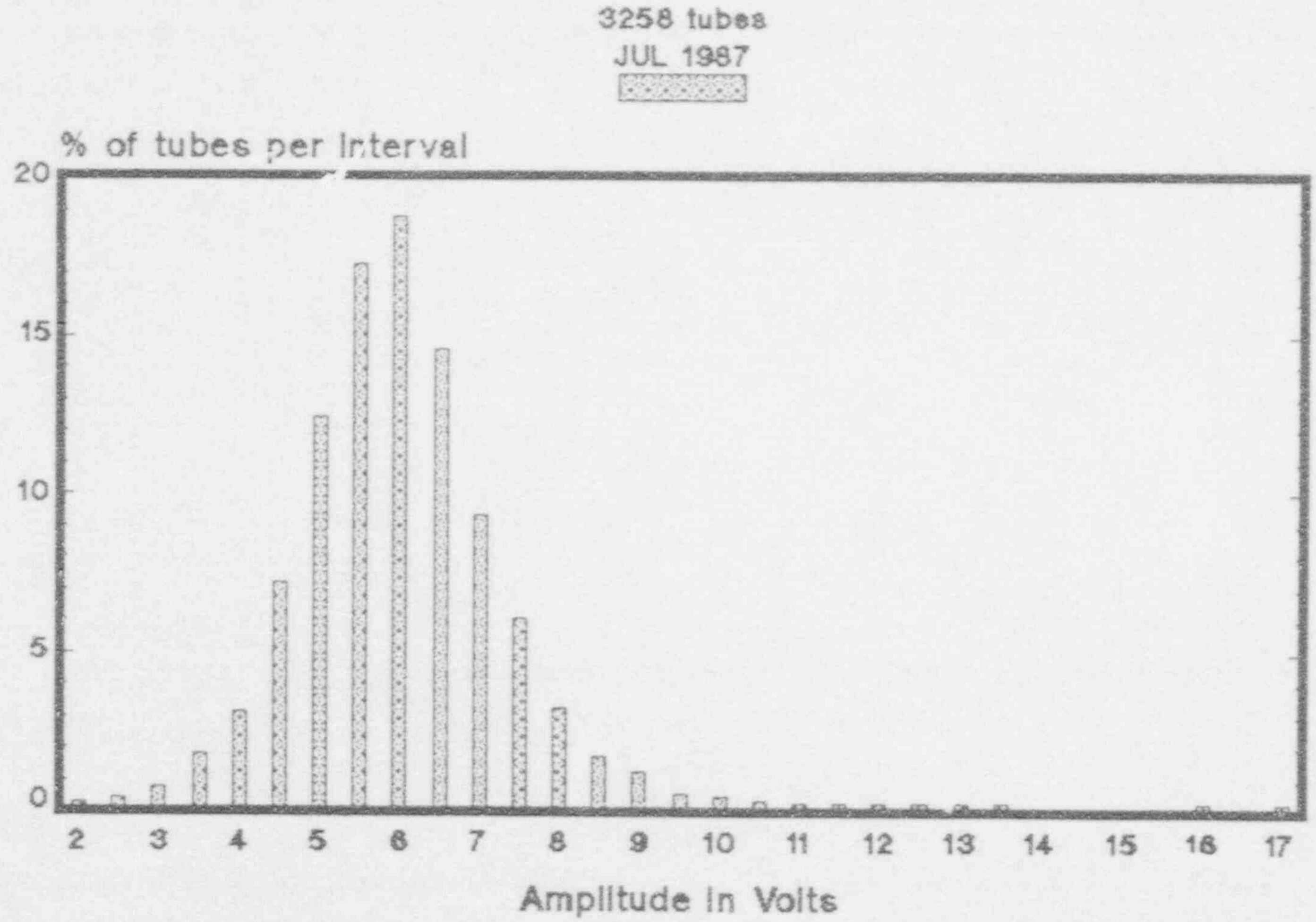

Figure 7-29

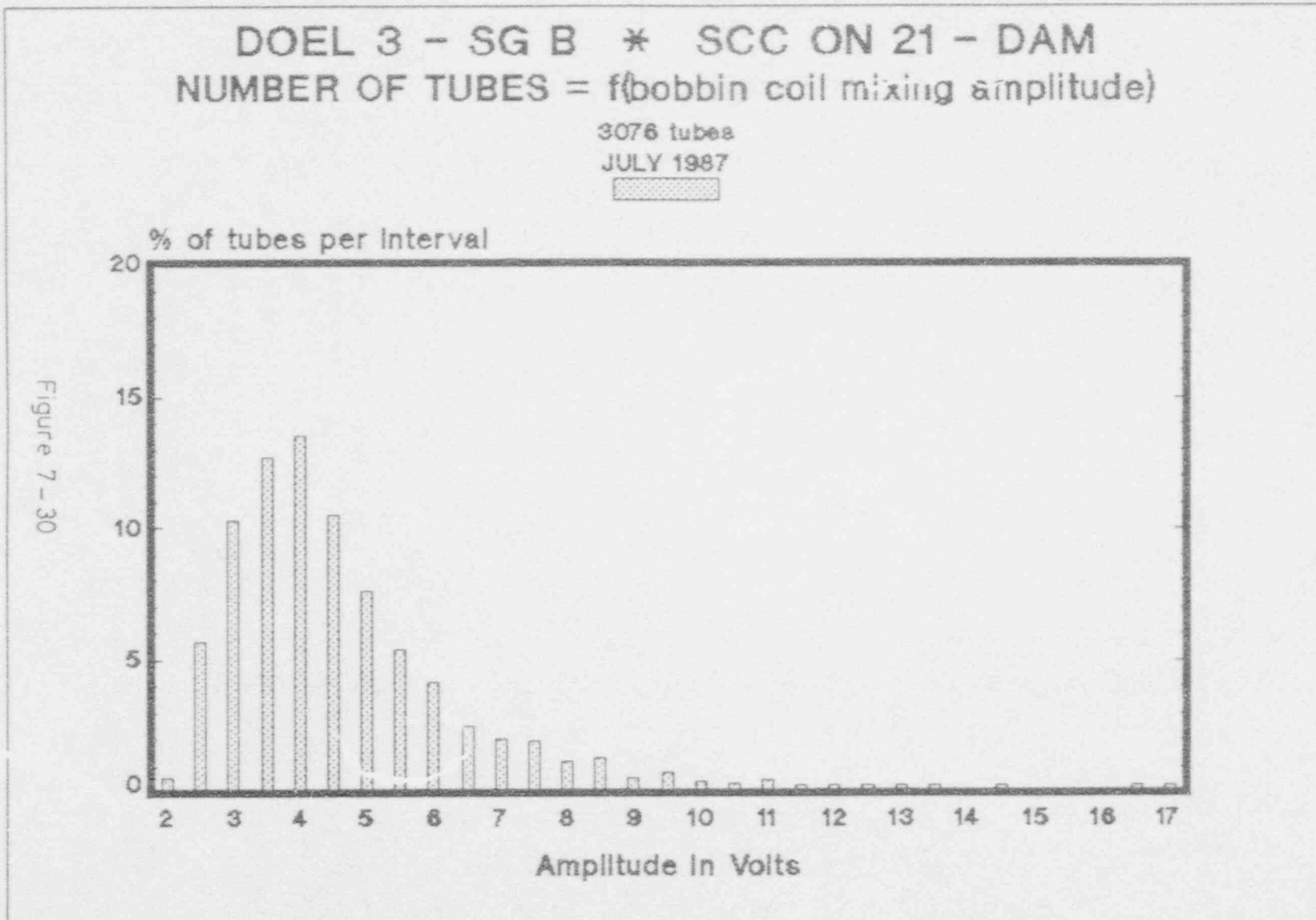
DOEL 3 - SG B * SCC ON 21 - DAM
NUMBER OF TUBES = f(bobbin coil mixing amplitude)
3076 tubes
JULY 1987
% of tubes per interval
20
15
10
5
0
2
3
4
5
6
7
8
9
10
11
12
13
14
15
16
17
Amplitude in Volts

Figure 7-30

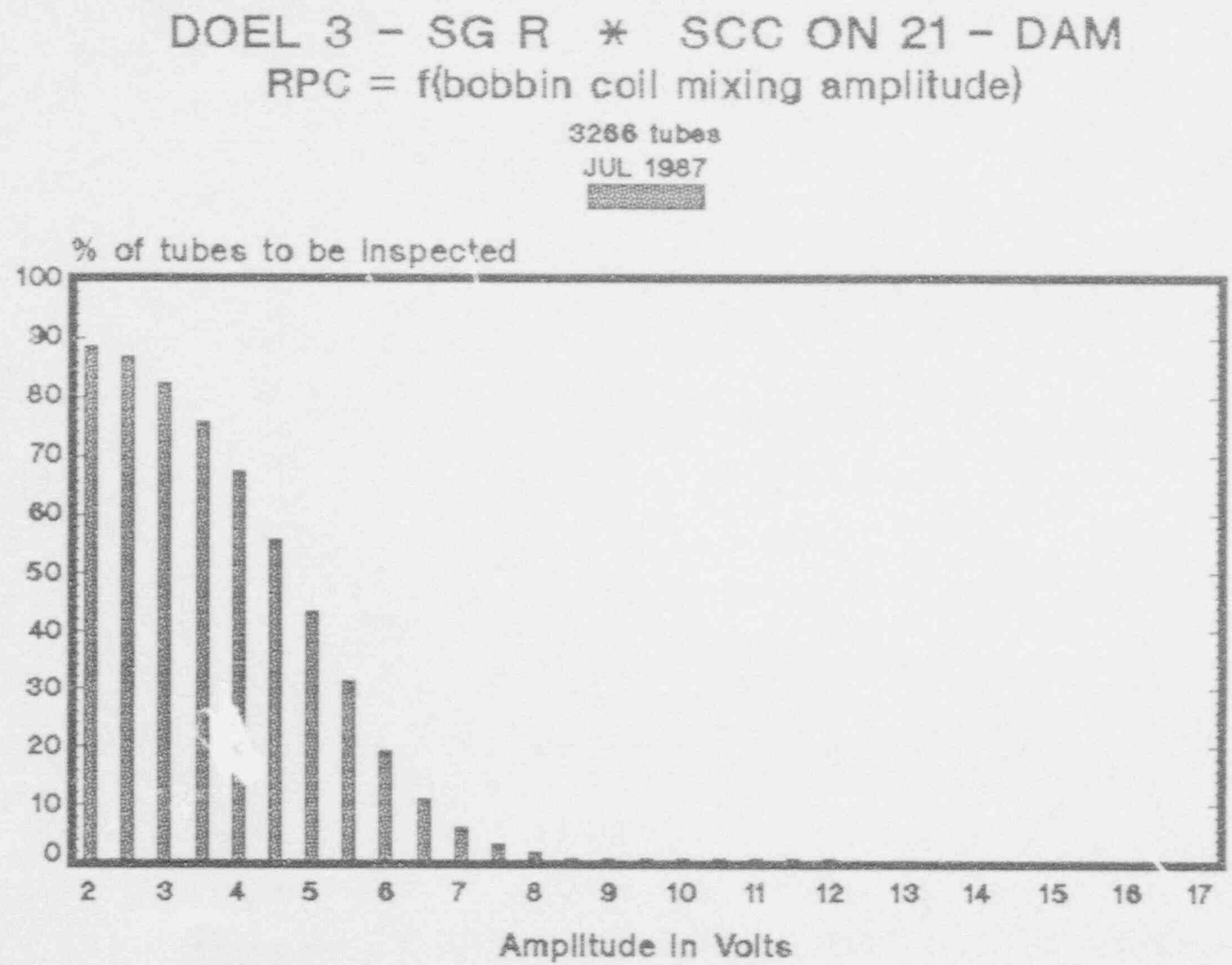
DOEL 3 - SG R * SCC ON 21 - DAM
RPC = f(bobbin coil mixing amplitude)
3266 tubes
JUL 1987
% of tubes to be inspected
100
90
80
70
60
50
40
30
20
10
0
2
3
4
5
6
7
8
9
10
11
12
13
14
15
16
17
Amplitude in Volts

Figure 7-31

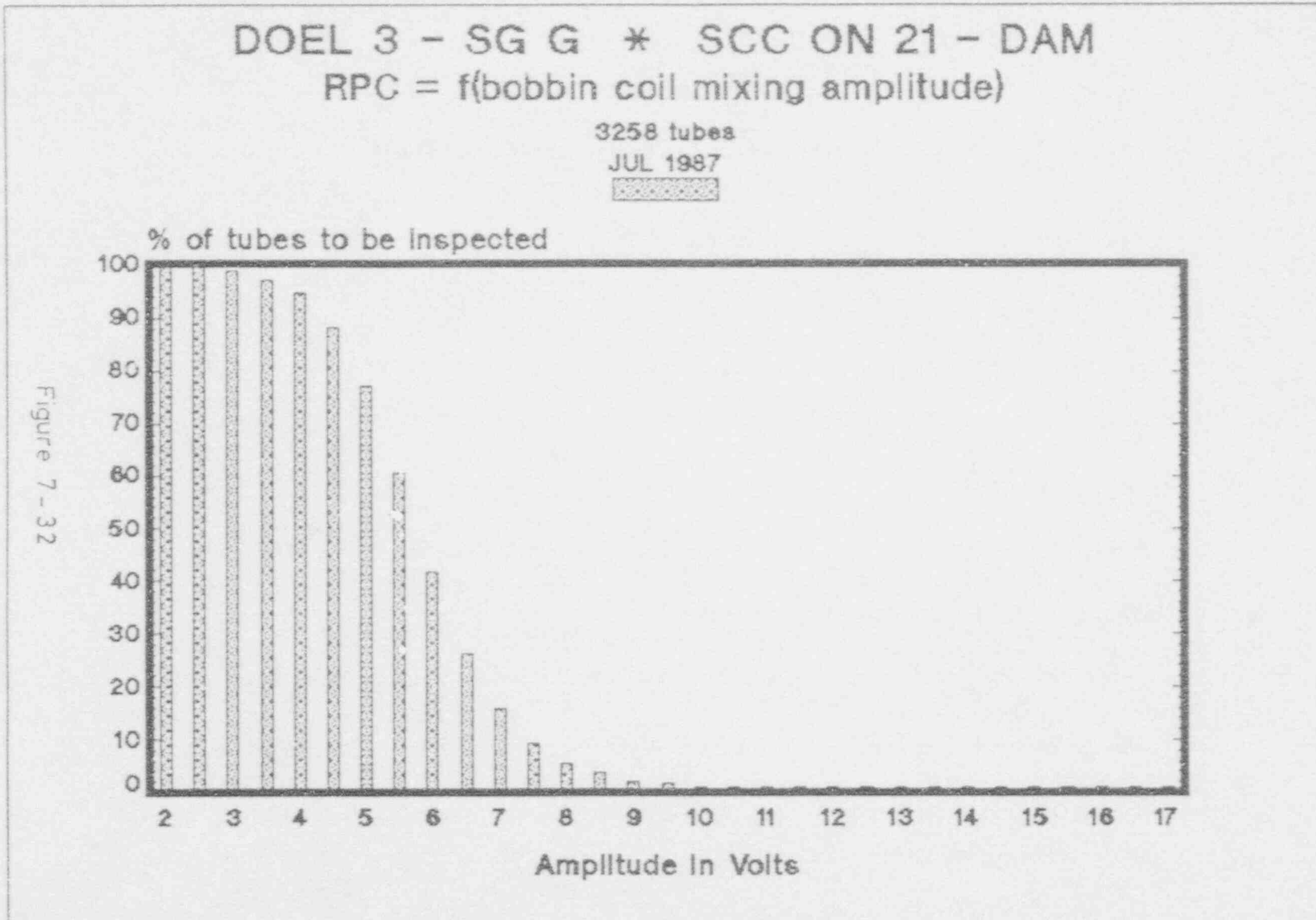
DOEL 3 - SG G * SCC ON 21 - DAM
RPC = f(bobbin coil mixing amplitude)
3258 tubes
JUL 1987
% of tubes to be inspected
100
90
80
70
60
50
40
30
20
10
0
2
3
4
5
6
7
8
9
10
11
12
13
14
15
16
17
Amplitude in Volts

Figure 7-32

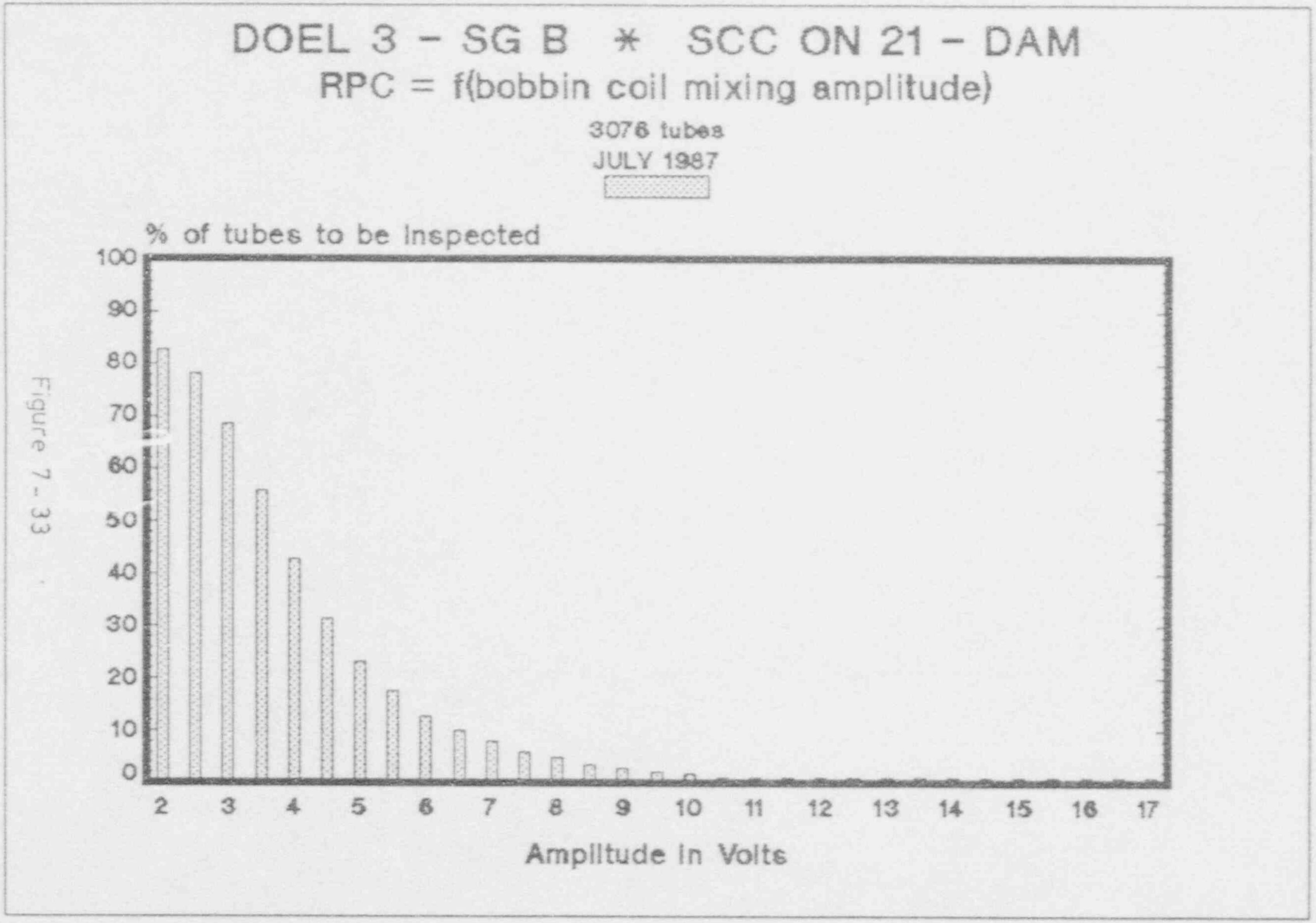
DOEL 3 - SG B * SCC ON 21 - DAM
RPC = f(bobbin coil mixing amplitude)
3076 tubes
JULY 1987
% of tubes to be inspected
100
90
80
70
60
50
40
30
20
10
0
2
3
4
5
6
7
8
9
10
11
12
13
14
15
16
17
Amplitude in Volts

Figure 7- 33

DOEL 3 - JULY 87 E C T INSPECTION

(100 % bobbin coil + R P C on amplitude > treshold)

CORRELATION BETWEEN BOBBIN COIL SIGNAL AMPLITUDE AND R P C MAXIMUM CRACK LENGTH IN ROLL TRANSITION (limited to L > 10 mm)

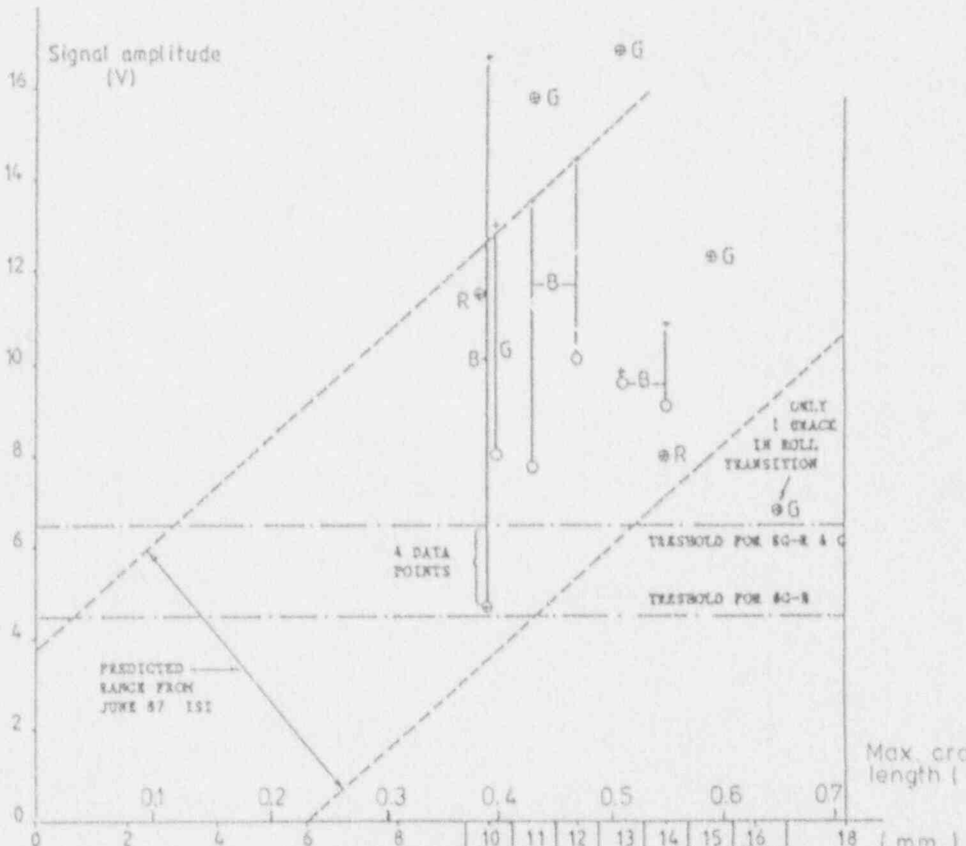

	10	11	12	13	14	15	16
B	27	2	5	2	1	1	-
G	5	1	-	1	-	-	1
R	1	-	-	-	1	-	-
SG	NUMBER OF CRACKED TUBES						

Figure 7-34

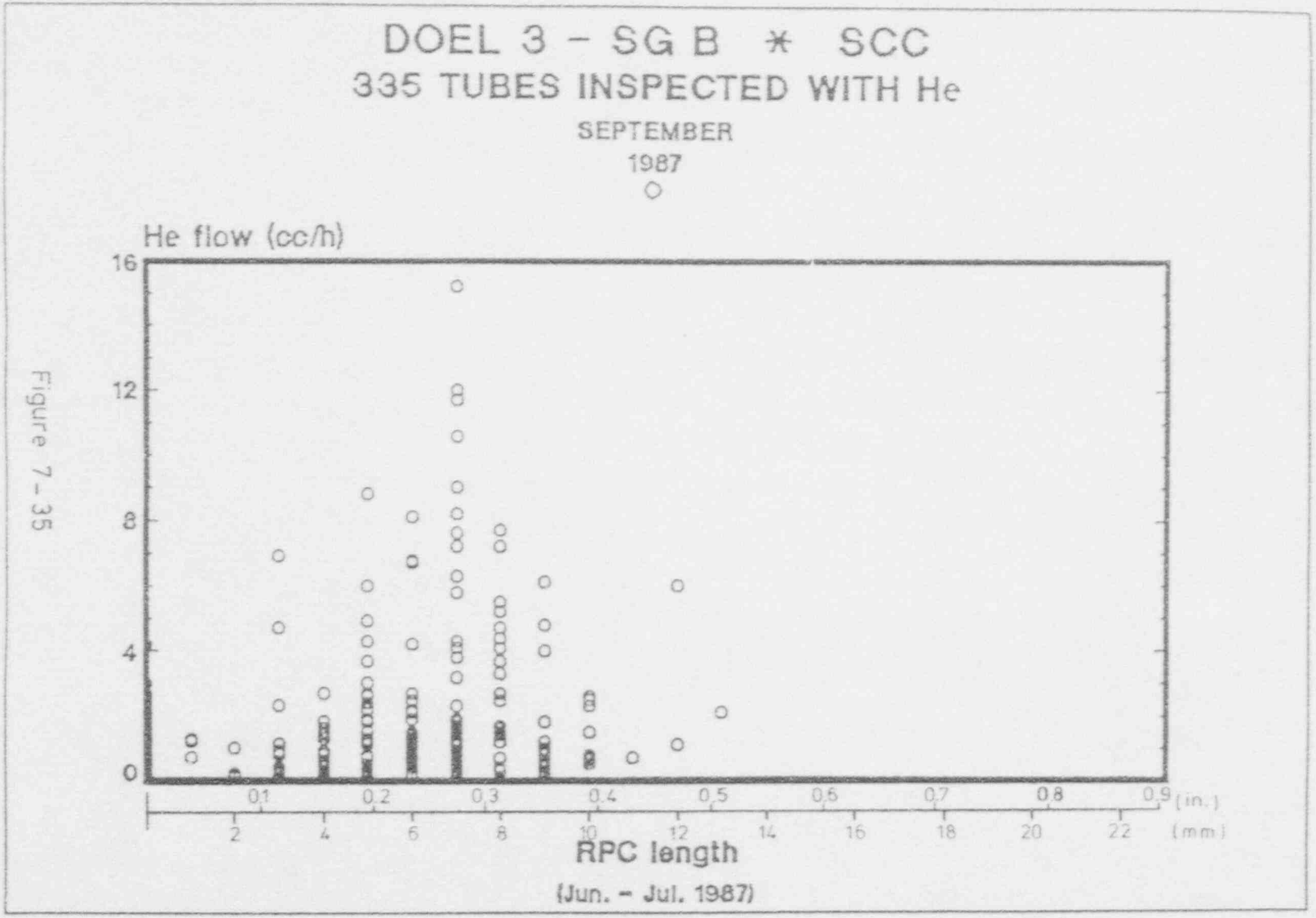
DOEL 3 - SG B * SCC
335 TUBES INSPECTED WITH He
SEPTEMBER
1987
He flow (cc/h)
16
12
8
4
0
0.1
0.2
0.3
0.4
0.5
0.6
0.7
0.8
0.9
(in.)
2
4
6
8
10
12
14
16
18
20
22
(mm)
RPC length
(Jun. - Jul. 1987)

Figure 7-35

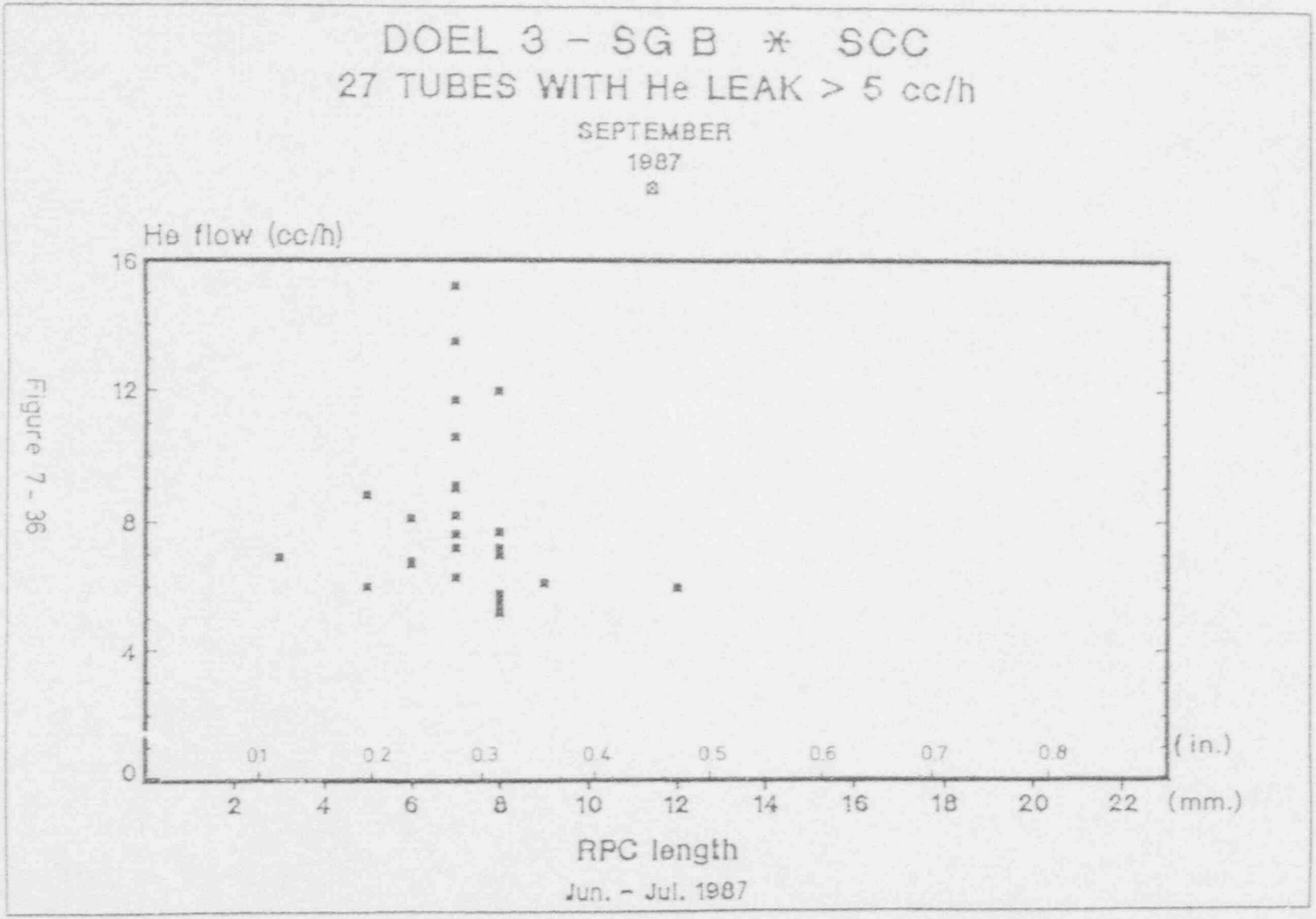
DOEL 3 - SG B * SCC
27 TUBES WITH He LEAK > 5 cc/h
SEPTEMBER
1987
He flow (cc/h)
16
12
8
4
0
01
0.2
0.3
0.4
0.5
0.6
0.7
0.8
(in.)
2
4
6
8
10
12
14
16
18
20
22
(mm.)
RPC length
Jun. - Jul. 1987

Figure 7 - 36

Belgian Approach to Steam Generator Tube Plugging for Primary Water Stress Corrosion Cracking

Appendix A: Experimental Work

Prepared by

BELGATOM
rue de la Loi, 75
B-1040 Brussels, Belgium

Principal Investigators
J. Mathonet
TRACTEBEL

P. Hernalsteen
LABORELEC

Prepared for

Electric Power Research Institute
3412 Hillview Avenue
Palo Alto, California 94304

EPRI Project Manager
A. R. McIlree

Steam Generator Reliability Program
Nuclear Power Division

CONTENTS

ILLUSTRATIONS

Figure		Page

TABLES

Section 1
INTRODUCTION

The purpose of the present addendum to EPRI report NP-6626 is to document the large experimental program conducted by BELGATOM, since the early 80's, to establish the critical dimensions of defects in rteam generator tubes.

This program addressed mainly through-wall cracks, in either the axial or circumferential direction, and established their critical length under a variety of configurations.

Several Inconel heats of 7/8" or 3/4" OD tubing as well as other materials in the same size range were used to verify the applicability of the theoretical plastic analyses (bulging factor, net section stress, ...) and to correlate their characteristic parameters to measured material properties.

Particular emphasis was put on quantifying the reinforcing effects provided by structures such as tubesheet (for axial cracks), tube support plate, and flow disbribution baffle (for circumferential cracks).

This provided a reliable data base for calculation of critical crack sizes under actual steam generator conditions and was used to support the establishment of new plugging limits for the Belgian plants.

Section 2

DESCRIPTION OF TESTS

The BELGATOM experimental program involved several sub-programs (further detailed under Sections 3 and 4) which are designated hereafter as

- programs A1 through A4, for axial cracks
- programs C1 through C3, for circumferential cracks.

The general structure of the program is detailed in Table 2-0.

The test samples used for these (sub)programs are defined in this Section.

2.1. MATERIALS

Materials included in the test program are :

- Inconel 600 (2 sizes x 9 heats)
- Austenitic stainless steel SA 376 TP 304 (2 sizes)
- Austenitic alloy AL-6X-HT (25 % Ni/20 % Cr/6 % Mo)
- Ferritic alloy SEA CURE (2.5 % Ni/26 % Cr/3 % Mo/.5 % Ti).

Dimensions and mechanical properties are given in Table 2-1.

In order to cover a wide range of mechanical properties and provide a broad theoretical basis for extrapolation to cases of practical interest, the materials in the test program were not limited to Inconel.

For the first programs (A1, A2), which were oriented towards a basic understanding of the behaviour of axial cracks and of the correlation of the "flow stress" with the conventional yield strength (YS) and ultimate tensile strength (UTS), it was considered appropriate to measure these properties in the direction of hoop stresses responsible for axial crack opening and extension; thus YS and UTS were measured from flattened transverse tensile specimens. However, it soon became clear that the unconventional transverse tensile test was inappropriate for general use; thus in order to derive data specific to the Inconel material, the usual longitudinal properties (available from mill certificates), were systematically used for correlation with the flow stress (programs A3 and A4).

2.2. GEOMETRY

The 8 sketches in Fig. 2-2 illustrate the various types and locations of defects machined on the test specimens, namely :

- Through wall axial electrodischarge machined (EDM) slits or natural (fatigue) cracks
- Through wall circumferential EDM or laser cut slits.

Tables 2-2 (a) through 2-2 (k) list all the test pieces according to defect type, number and length of defects, and the various sealing systems used (as described in Section 2-3).

The slits (produced by EDM or laser cutting) are about 0.2 mm wide, the corner radius at tip being 0.1 mm. In a few cases (program C2 and 4 specimens from program A4), the slits were machined with an increase in width from 0.55 mm (circumferential flaws) to 0.8 mm (axial flaws).

For circumferential flaws the tip fronts were initially aligned; this resulted in some variation of the crack length across the wall thickness in programs C1 and C2. Later on (program C3), a more elaborate EDM process allowed the flaw tips to be radial (with a constant flaw length).

As a general rule, for test specimens representative of the "free span" of a SG tube, any defect was at least 60 mm distant from a discontinuity such as another defect or the SWAGELOCK end fitting.

When two slits are machined in one specimen, they are sometimes identical and situated in orthogonal planes (sketch 4).

This geometry makes it possible to observe the deformation of one defect (at pre-critical conditions) after the unstable propagation of the other (at critical pressure). The bursted portion of the tube is then removed and the shortened test piece is further pressure tested until the burst of the second defect occurs.

While in the latter case, the two defects were located in different planes to minimize any possible interference, a different topology of aligned defects was used to compare the behaviour "next to" and "away from" the tubesheet discontinuity (see sketch 6). In this case, the collar around the test specimen eliminates any mutual influence while the flaw alignment minimizes the influence of other factors (such as wall thickness which might not be uniform along the tube circumference).

As to the test-specimens used to correlate mechanical properties (program A2), the lengths of flaws were calculated to be "equivalent" to 20 mm for a 7/8" O.D. (th. 1.27 mm) tube, from :

$$2\,C = 20\text{ mm} \,.\, \left(\frac{R.t}{R_o\,.\,t_o}\right)^{1/2} = 5.47\,\sqrt{(Rt)}$$

where : R = mean radius
t = wall thickness

For specimens used to evaluate the sharpness of flaw tips (programs A2 and A3), E.D.M. slits were lenghtened on both sides through cracks initiated by a fatigue test bench (pressure cycling).

The fatigue crack propagation proved difficult to control and, in some cases, the extended defect opened up sufficiently to permit the sealing system to extrude at a pressure well below the critical value. When the plastic deformation was excessive, the specimens could not be resealed and were lost for further testing.

2.3. SEALING SYSTEM

Several sealing systems were used to restore the leak tightness of specimens with through wall flaws. The main dimensions and characteristics of the flaws are listed in Table 2-3 (a).

Seal 1 - a brass patch, 0.2 or 0.3 mm thick and 10 mm wide, glued with a silicone compound; (Fig. 2-3; sketch 1)

Seal 2 - a copper patch, 0.3 mm thick and 25 mm wide, backed by a non reinforced plastic hose sealed at both ends of the test specimen with a silicone compound; (Fig. 2-3; sketch 2)

Seal 3 - similar to mode 2, but patch width reduced to 15 mm;

Seal 4 - no copper patch; the plastic tube sealed as for modes 2 and 3.

Seals 5 and 6 - the opportunity to get plastic tubes with an external diameter equal to the inner diameter of the specimen made it possible to seal tightly without the use of silicone.

Seals 5 to 10 - the burst pressure of the specimens was reached without installing a metallic patch to prevent the premature rupture of the plastic hose.

Seals 11 to 14 - the same system as for Seal 2 but the brass patches lead different thicknesses and widths.

Seals 15 to 17 used a different, simpler and more efficient way to insure leak tightness between plastic hose and Inconel tube; conical metal inserts were used at both ends to expand the plastic hose in tight contact with the metal tube. For seals 15 and 16, a thinner but stronger steel patch was used; in some cases (mentioned in the test result tables), it was necessary to use two such shims (total thickness about 0.25 mm). Seal 17 could only be used for relatively low critical pressures; the fiber-reinforced plastic hose proved more resistant than the combination of two standard hoses (seal 10) but was only available to fit the 7/8" OD tubes.

Seal 1 was aimed to minimize interference with the specimen behaviour; it did not reach the tube burst pressure because of premature rupture.

Seal 2 was satisfactory but was modified into systems 3 and 4 (for short cracks only) to reduce interference effects.

For sealing systems 1 to 14, the leak tightness of each test piece was systematically checked at a 6 bar pressure. Leaks resulting from a lack of adherence between silicone and the tube wall frequently occured. Some rare failures of seals were also observed at the beginning and during the course of testing. This required removal of the specimen from the test rig and building a new seal. For sealing system 15 and beyond, leak tightness problems were usually not observed.

The swelling of a plastic hose exposed to gradually increased internal pressure is recorded in Table 2-3 (b).

The mechanical characteristics of the metal patch were checked in two cases

copper plate : YS = 241 MPa
UTS = 302 MPa
A = 11 %
steel strip : UTS = 1200 MPa.

2.4. TEST RIG

Different types of test rigs were used in pressure tests, all were based on quasi-static, cold-water pressurization.

The first program (A1) used a volumetric pump (17 l/min; manually adjustable head up to 400 bar) with direct pressure reading from a large scale manometer.

The next programs (A2 + C1) used a sophisticated system consisting of a power operated air-water pressure amplifier (as shown in Fig. 2-4 (a)). The pressure was measured using a piezoelectric gauge connected to a multi-channel analogic recorder.

For programs A3, A4, C2, and C3, a simpler, manual high pressure (≤ 660 bar) pump was used, with either analog reading (C2 only) or digital reading + analog recording.

In all cases the test specimens were connected to the test rig by means of standard SWAGELOCK end fittings

In order to evaluate the effect on critical burst pressure of restraining geometries such as tubesheet or flow distribution baffle (FDB), special tools were designed to constrain the test-specimen, the description of which is given below.

Tubesheet constraint was simulated by either

1 : two half collars bolted together around the test specimen so as to leave practically zero clearance.
2 : a full collar, slipped around the test specimen, with minimum clearance and maintained in the desired position by a SWAGELOCK fitting.
3 : a full collar, slipped around the test specimen, with minimum clearance and maintained in the desired position by mechanical roll expansion of the tube.
4 : a full collar slipped around the test specimen, with diametral clearance within the tolerance range applicable to S.G. manufacturing (0.2 mm to 0.6 mm), and fixed by mechanical roll expansion (either by "underrolling" or "overrolling").

Modes 1 to 3 depicted in sketch 1 of Fig. 2-4 (b) have been used on test specimens with the intended flaw(s). For mode 4, shown in sketch 2 of Fig. 2-4 (b), the flaw(s) can only be machined (EDM) after roll expansion (to avoid non-representative opening of the flaw and, especially, stretching of the crack tip adjacent to the collar).

Axial flaws were located at various distances from the simulated tubesheet (including partial length engagement within the collar). Circumferential flaws were systematically located at 6 mm (1/4") from the face of the simulated tubesheet.

Lateral restraint (from Flow Distribution Baffle - FDB - and/or Tube Support Plate - TSP), was simulated by a special test rig, adjustable to the various geometries under consideration (7/8" or 3/4" OD, SG model 51 or D4).

Fig. 2-4 (c) shows a general assembly of this test rig with an installed 7/8" OD specimen. The test rig consists of a main frame (as detailed in Fig. 2-4 (d)) and four relocatable lateral restraint subassemblies (as detailed in Fig. 2-4 (e)).

Two restraint subassemblies were used to assemble and fix the two half collars simulating the tubesheet. The two other subassemblies were used to simulate the FDB and the TSP; These was consisted of plates with machined holes at the appropriate tube to TSP or FDB clearance (usually larger for FDB than for TSP). A different set of collars and plates was used to fit the tube diameter (7/8" or 3/4"); the plates location was adjusted in accordance with the geometry specific for each type of steam generator; an offset can be imposed to the plates (as illustrated on Fig. 2-4 (c)) prior to testing. A specially designed load cell (using strain gages) can be adapted to the TSP/FDB subassemblies in order to perform restraining force measurements.

Thus, this flexible mock-up allows full scale simulation of any actual field configuration.

2.5. TEST PROCEDURE

The pressure was slowly raised until burst; in case of seal failure, a retest was performed with a stronger sealing system.

For instance, specimens exhibiting sealing system 1 failure were refurbished with sealing system 2 which consisted of a wide patch that bridged the deformed slit area (widened slit, bulging).

In some cases, the crack extension under burst pressure was sufficiently small to permit the specimen to be resealed and retested (with the initial slit length increased by natural cracks at both ends).

For program A1, the pressurization was halted at a few intermediate pressure levels (scheduled at about 70, 80, and 90 % of the expected burst pressure) to allow for visual examination and the following geometrical measurements :

- flaw width, at mid span on the O.D. surface

- Crack Opening Displacement (COD) at both ends of initial slit (Fig. 2-5 sketch 2)

- for axial flaws, diametral extension (bulging) of the tube in the center of the slit (Fig. 2-5 sketch 1).

For safety reasons, measurements requiring close visual examination were taken only after releasing the pressure to less than 50 % (and frequently to 0). This approach did not affect the accuracy of results because the elastic restitution remained very small with regard to the large plastic opening stretch of the flaw.

Specimens equipped with two defects were retested after the removal of the ruptured portion and the earlier measurements were made again.

After dismantling the tested specimen from the rig, the following measurements were performed :

- COD at both ends of initial slit, by summation of the ruptured ligament widths on both sides of the tearing crack; only the mean value of these two measurements was recorded

- overall crack length

- crack central opening (width measured at the inner and outer surface b_{int} and b_{ext} in Fig. 2-5 sketch 1).

- overall tube deformation : bulging at the center of the defect, ovality at defect tips, and deflection (see sketches in Fig. 3-2 (a)), (the bulging is taken as the larger of diameters ø 1 and ø 2 as shown in Fig. 2-5 sketch 1).

- in some cases the leakage area, available through close-up photography of the cracked section.

While the two first measurements were performed almost systematically for all program phases, the others were essentially limited to program A1 which was more of a phenomenological nature.

However, some other measurements were also performed as a function of the increasing pressure, depending on the particular program objectives.

- Program C2 involved measurement (manual recording of gauge reading) of

  . lateral displacement of unrestrained specimens
  . axial elongation of restrained specimens

- Program A4 (first subset) involved measurement (manual recording of gauge reading) of the tube bulging

- Program C3 involved measurement (analog recording) of either

  . the maximum lateral deformation (subset 1)
  . the lateral load on the restraining plate (subset 2)

Additionally, the deformed profile of the test specimen was sometimes measured in the "post mortem" condition.

It should be noted that the simple pressurization (manual pump) used for all later phases of the program involved significant pressure fluctuations. Although these may slightly affect the ultimate value of critical pressure (thus contributing to some data scatter), they were not considered an undesirable feature as similar fluctuations could also be expected to occur also under actual steam generator accidental conditions.

Table 2-0

BELGATOM EXPERIMENTAL PROGRAM
GENERAL STRUCTURE

PROGRAM	SUBSET	CRACKS		MATERIAL		DIAMETER			PERIOD	MAIN OBJECTIVE
		AX.	CIRC.	Inconel	Other	7/8"	3/4"	Other		
A1	-	X		X	-	X	-	-	1980-81	phenomenology model validation
A2	-	X		X	X	X	X	X	1982-83	phenomenology flow stress characterization
A3	-	X		X	-	X	-	-	1987-88	LBB of Ni plated tube
A4	1	X		X	-	X	-	-	1987	preliminary (study of tubesheet influence)
	2	X		X	-	X	-	-	1988	statistical (study of tubesheet influence)
	3	X		X	-	X	-	-	1988-89	direct verification (study of tubesheet influence)
	4	X		X	-	-	X	-	1989	direct verification (study of tubesheet influence)
C1	-		X	X	-	-	X	-	1982-83	phenomenology
C2	-		X	X	-	-	X	-	1987	preliminary (study of lateral restraint)
C3	1		X	X	-	X	-	-	1988-89	representative mock-up (study of lateral restraint)
	2		X	X	-	-	X	-	1989	representative mock-up (study of lateral restraint)

Table 2-1

DIMENSIONS AND MECHANICAL PROPERTIES OF MATERIAL SELECTED FOR THE TEST PROGRAM

MATERIAL (INDEX)	LOT N°.	TEST REPORT	DIMENSIONS (mm)		YIELD STRENGTH (1) YS (MPa)		TENSILE STRENGTH (1) UTS (MPa)		A (2) %
			outside diameter	wall thickness	recorded	mean	recorded	mean	
(M1) Inconel 600 7/8" O.D. Program n°A1			22.3	1.27	376 398	387	696 706	701	33 33.7
(M2) Inconel 600 7/8" O.D. Program n°A2	20 185	G40/01099 G40/01099 34,539 35,667-1 -2	22.15	1.35	364 350 358 322 292	337	635 618 631 569 590	609	40.7 41.3 40.0 44.4 46.7
(M3) Inconel 600 3/4" O.D. Programs n° A2 and C1	9 866 (3)	G40/01099 G40/01099 34,539 35,667-1 -2	19.05	1.15	332 409 433 401 335	382	[illegible]94 689 695 647 656	676	35.3 35.3 36.3 35.3 37.5
(M4) Inconel 600 3/4" O.D. Program n°A2	9,787	34,539 35,667-1 -2	19.05	1.05	437 362 378	392	704 606 644	651	30.0 35.0 37.5

(1) Mechanical properties measured on transverse test-specimens machined from rings cut from tubes.
(2) Elongation in 5.65 √S
(3) Longitudinal properties (from W Blairsville mill certificate) : YS = 425 MPa; UTS = 730 MPa

Table 2-1 (cont'd)

DIMENSIONS AND MECHANICAL PROPERTIES OF MATERIAL SELECTED
FOR THE TEST PROGRAM

MATERIAL (INDEX)	LOT N°.	TEST REPORT	DIMENSIONS (mm)		YIELD STRENGTH (1) YS (MPa)		TENSILE STRENGTH (1) UTS (MPa)		A (2) %
			outside diameter	wall thickness	recorded	mean	recorded	mean	
(M5)									
AISI 304		G40/01099	19.1	1.2	289		607		49.3
3/4" O.D.		G40/01099			342		619		51.3
	-	32,192			408	334	669	633	50
Program n°A2		34,539			334		707		55.6
		35,667-1			299		565		50.0
(M6)									
AISI 304		32,192	20.9	2.65	369		720		50.0
1/2" Sch 40	-					402		723	
		34,539			434		727		61.7
Program n°A2									
(M7)									
AL-6X-HT		G40/01099	20.1	0.77	554		739		13.3
25 Ni/20 Cr/	-	"			585	603	696	758	14.7
6 Mo		32,192			639		805		14.6
Program n°A2		34,539			632		792		18.5
(M8)		G40/01099	20.0	0.71	569		654		15.3
SEA CURE		"			557	590	666	686	16.7
2.5 Ni/26 Cr		32,192			638		717		13.1
3 Mo/.5 Ti		34,539			596		707		20.8
Program n°A2									

(1) Mechanical properties measured on transverse test-specimens machined from rings cut from tubes.
(2) Elongation in 5.65 √S

Table 2-1 (cont'd)

DIMENSIONS AND MECHANICAL PROPERTIES OF MATERIAL SELECTED FOR THE TEST PROGRAM

MATERIAL (INDEX)	LOT N°.	TEST REPORT	DIMENSIONS (mm)		YIELD STRENGTH (1) YS (MPa)	TENSILE STRENGTH (1) UTS (MPa)	A (2) %
			outside diameter	wall thickness			
(M9) Inconel 600 7/8" OD Programs A3, A4 and C3	71 692	mill certificate VALLOUREC	22.22	1.27	292	701	42
(M10) Inconel 600 7/8" OD Program A3	74 749 (3)	LABORELEC (division C)	22.22	1.27	184	596	38
(M11) Inconel 600 7/8" OD Program C3	71 383	mill certificate FINETUBES	22.22	1.27	276	655	50
(M12) Inconel 600 3/4" OD Program A4 and C3	70 699	mill certificate VALLOUREC	19.05	1.09	346	740	44
(M13) Inconel 600 3/4" OD Program C2	UNDOCUMENTED STOCK MATERIAL						

(1) Mechanical properties measured in the longitudinal direction.
(2) Elongation in 5.65 $\sqrt{S}$
(3) Material (M11) + thermal heat treatment.

Table 2-2 (a)

GEOMETRY OF TEST SPECIMENS
PROGRAM A1 (THROUGH WALL AXIAL FLAWS)

MATERIAL (cf. Table 2-1)	DEFECT GEOMETRY		SKETCH N°. (cf. Fig. 2-2)	SEALING SYSTEM (INDEX)	TEST-PIECE N°.
	TYPE	LENGTH (mm)			
M1	7 specimens with 1 flaw	15 20 25 35 50 70 70	1	1; 2 1; 2 1; 2 1; 2 1+b; 2 1+b;2 2	1 2 3 4 5 6 12
	5 specimens with 2 flaws	12;12 15;15 20;20 35;20 50;20	4	2; 4 2; 4 2; 3 2; 4 2	7 8 9 10 11
	1 ovalized specimen (11 %) with 2 flaws	20;20	5	2	13

Table 2-2 (b)

GEOMETRY OF TEST SPECIMENS
PROGRAMS A2 AND C1 (THROUGH WALL FLAWS)

MATERIAL (cf. Table 2-1)	DEFECT GEOMETRY		SKETCH N°. (cf. Fig. 2-2)	SEALING SYSTEM (INDEX)	TEST-PIECE N°.
	TYPE	LENGTH (mm)			
M2	2 specimens with 2 axial flaws	18;18* 20;20	4 4	5-10 9-10	0 1
	1 specimen with 2 parallel axial flaws + 1 isolated flaw	20;20 20	3	8-8 10	23
M3	2 specimens with 2 axial flaws	16.5; 16.5 16.5; 16.5	4 4	12 12	7 8
	4 specimens with 2 circumferential flaws	15;15 30;31 20; 21.5 23;23	7 7 7 7	- 12 11 12	9 10 11 12
M4	1 specimen with 2 axial flaws	16.5; 16.5**	4	6	24

* slits increased in lenght to 19.7 and 20.3 mm, respectively, by fatigue crack propagation :
1.162.000 cycles at frequencies ranging from 3.75 to 7.5 Hz
partitioned as : 432,500 at 5 to 10 < p < 55 to 60 bar
592,000 at 15 < p < 50 bar
137,000 at 20 < p < 65 bar
Crack initiation was observed after 72.000 pressure cycles at one tip and after 89,500 cycles at the other.

** excessive fatigue propagation resulted in useless, deformed specimen.

Table 2-2 (b) (cont'd)

GEOMETRY OF TEST SPECIMENS
PROGRAMS A2 AND C1 (THROUGH WALL FLAWS)

MATERIAL (cf. Table 2-1)	DEFECT GEOMETRY		SKETCH N°. (cf. Fig. 2-2)	SEALING SYSTEM (INDEX)	TEST-PIECE N°.
	TYPE	LENGTH (mm)			
M5	2 specimens with 2 axial flaws	16.5 16.5	4	12	13
		16.5 16.5	4	12	14
M6	2 specimens with 2 axial flaws	27.5 27.5	2	14	15
		27.5 27.5	2	14	16
M7	2 specimens with 2 axial flaws	14.5 14.5	4	7	17
		14.5 14.5	4	7	18
	1 specimen with 2 x 2 parallel axial flaws	14.5 14.5	3	7	22
		14.5 14.5	3	7	
M8	2 specimens with 2 axial flaws	14.5 14.5	4	7	19
		14.5 14.5	4	7	20
	1 specimen with 2 parallel axial flaws	14.5 14.5	3	7	21

Table 2-2 (c)

GEOMETRY OF TEST SPECIMENS
PROGRAM C2 (THROUGH WALL CIRCUMFERENTIAL FLAWS)

MATERIAL (cf. Table 2-1)	DEFECT GEOMETRY		SKETCH N°. (cf. Fig. 2-2)	SEALING SYSTEM (INDEX)	TEST-PIECE N°.
	TYPE	LENGTH (deg. of arc)			
M13	1 specimen without flaw	0	-	-	1
	7 flawed specimens	180 180 180 180	8-1	16	2 3 4 8
		105 105 105	8-1	16	5 6 7

Table 2-2 (d)

GEOMETRY OF TEST SPECIMENS
PROGRAM A3 (THROUGH WALL AXIAL FLAWS)

MATERIAL (cf. Table 2-1)	DEFECT GEOMETRY			SKETCH N°. (cf. Fig. 2-2)	SEALING SYSTEM (INDEX)	TEST-PIECE N°.
	TYPE	LENGTH (mm)				
		EDM	Fatigue			
M9	unplated	16	-	1	15	2
		15.9	-			7
		16	18	1	15	33
		16	19.5			36
		16	19			37
	Ni plated	16	-	1	15	1
		16.3	-			6
		15.9	-			8
		16.1	-			9
		16	-			10
		16	-			11
		16.4	18	1	15	5
		12	12 +			18
		12	12 +			20
		12	12 +			23
		12	23			24
		12	12.5			25
		12	14			26
		12	12.5			27
		12	15.5			28
		16	18			35
		16	17			40
		16	17			43
M10	Ni plated	16	-	1	15	3
		16	-			4
		16	-			5
		16	-			6
		16	-			7
		16	-			10

Notes

1) For easy reference, the specimens are noted
   [Ni for M9
   [Ni* for M10
   where i is the test piece number
2) For all specimens, the initial EDM flaw was machined only part through wall (remaining ligament in the range from 0.2 to 0.3 mm); through wall penetration was obtained by fatigue cycling to minimize the crack width and allow representative nickel plating. In a number of cases, this fatigue cycling also initiated cracking

in the axial direction (the extended length is quoted as the "fatigue length"). A typical cycling sequence is given hereafter (from test specimen N°. 33)

initial [EDM flaw length : 16 mm
[remaining ligament thickness : 195 µm

[10.500 cycles between 0 and 70 bar (resulting in first leakage)
[14.000 cycles between 0 and 70 bar
[13.400 cycles between 0 and 65 bar

final [fatigue crack length (measured after tube bursting) : 18 mm
[fatigue crack width (max) : 7 µm

Table 2-2 (e)

GEOMETRY OF TEST SPECIMENS
PROGRAM A4 - SUBSET 1 (THROUGH WALL AXIAL CRACKS)

MATERIAL (cf. Table 2-1)	DEFECT GEOMETRY				SKETCH N°. (cf. Fig. 2-2)	SEAL-LING SYSTEM INDEX	TEST-PIECE N°.
	TYPE	DISTANCE FROM TS (mm)	LENGTH (mm)				
			Total	Outside TS			
M9	INFLUENCE OF TUBE-SHEET (TS)	0	12	12	1 + mode 1	15	1
		0	12	12			2
		0	12	12			3
		0	16	16			5
		0	16	16			6
		8	16	16			7
		16	16	16			8
		0	16	16			9
		0	16	16			11
		8	16	16			12
		- 4	20	16			14
		0	20	20			15
		0	20	20			16
		0	24	24			17
		- 8	24	16			18
		- 8	24	16			19
		0	24	24			20
	REFERENCE	-	16	-	1	15	4
		-	16	-			10
		-	16	-			13

Notes :
1) For easy reference, the specimens are noted Pi where i is the test-piece N°.
2) Specimen dimensions are given in Table 2-2 (k)
3) Indicated "mode" refers to tubesheet constraint, as defined by Section 2.4.

Table 2-2 (f)

GEOMETRY OF TEST SPECIMENS
PROGRAM A4 - SUBSET 2 (THROUGH WALL AXIAL CRACKS)

MATERIAL (cf. Table 2-1)	DEFECT GEOMETRY				SKETCH N°. (cf. Fig. 2-2)	SEALING SYSTEM INDEX	TEST-PIECE N°.
	TYPE	DISTANCE FROM TS (mm)	LENGTH (mm)				
			Total	Outside TS			
M9	INFLUENCE OF TUBE-SHEET (TS)	8	19	19	1 + mode 4 (gap = 0.4mm)	15	1
		8	19	19			2
		8	19	19			3
		0	19	19			4
		0	19	19			5
		0	19	19			6
		0	19	19	1 + mode 3	15	7
		0	19	19			8
		0	19	19			9
		- 19	38	19			10
		- 19	38	19			11
		- 19	38	19			12
		0	19	19	1 + mode 1	15	13
		0	19	19			14
		0	19	19	1 + mode 2		60(2)
		0	18	18			Y18G1
		0	18	18			Y18G2
		0	18	18			Y18G3
		- 6	24	18			Y24C1
		- 6	24	18			Y24C2
		- 5	24	19			Y24D1
		- 5	24	19			Y24D2
		- 5	24	19			Y24D3
		- 5	24	19	1 + mode 3	15	Y24F1
		- 5	24	19			Y24F2

1) Indicated "mode" refers to tubesheet constraint, as defined by Section 2.4.

Table 2-2 (f) (cont'd)

GEOMETRY OF TEST SPECIMENS
PROGRAM A4 - SUBSET 2 (THROUGH WALL AXIAL CRACKS)

MATERIAL (cf. Table 2-1)	DEFECT GEOMETRY				SKETCH N°. (cf. Fig. 2-2)	SEALING SYSTEM INDEX	TEST-PIECE N°.
	TYPE	DISTANCE FROM TS (mm)	LENGTH (mm)				
			Total	Outside TS			
M9	REFERENCE	NA	16	NA	1	15	50
			16				52
			16				54
			16				61
			16				Y16B1
			16				Y16B2
			16				Y16B3
			18				Y18G4
			18				Y18G5
			18				F7 ⎤
			18				F8 ⎥ 3
			18				F9 ⎥
			18				F10⎦
			19				15
			19				30
			19				51
			19				53

Notes :
1) For easy reference, the specimens are noted Pi*, where i is the test-piece N°. (N°. already beginning with a letter are left unchanged)
2) Specimen N°. 60 had no backing device (the collar was forced onto the tube with a small negative clearance)
3) The flaws of test specimens F7 to F9 were machined to 0.8 mm in width, with a prior hydrostatic expansion of 0.2 % (residual plastic deformation) for F7 and F8.

Table 2-2 (g)

GEOMETRY OF TEST SPECIMENS
PROGRAM A4 - SUBSET 3 (THROUGH WALL AXIAL CRACKS)

MATERIAL (cf. Table 2-1)	DEFECT GEOMETRY			SKETCH N°. (cf. Fig. 2-2)	SEALING SYSTEM (INDEX)	TEST-PIECE N°.
	TYPE	LENGTH (mm)				
		outside TS	next to TS			
M9	INFLUENCE OF TUBE-SHEET (TS)	15	17	6 + mode 4 (gap = 0.6 mm)	15	1
		15	17			8
		15	18			3
		15	18			6
		17	19			4
		17	19			7
		17	20			2
		17	20			5
		15	17	6 + mode 4 (gap = 0.2 mm)	15	1*
		15	17			2*
		15	17			3*
		15	17			4*
		17	19			5*
		17	19			6*
		17	19			7*
		17	19			8*

Notes :
1) For easy reference, the specimens are noted Di, where i is the test-piece number.
2) The number engraved on the test specimens is 75315/i for the first set of 8 and 75316/i for the second set of 8.
3) Indicated "mode" refers to tubesheet constraint, as defined by Section 2.4.

Table 2-2 (h)

GEOMETRY OF TEST SPECIMENS
PROGRAM A4 - SUBSET 4 (THROUGH WALL AXIAL CRACKS)

MATERIAL (cf. Table 2-1)	DEFECT GEOMETRY			SKETCH N°. (cf. Fig. 2-2)	SEALING SYSTEM (INDEX)	TEST-PIECE N°.
	TYPE	LENGTH (mm)				
		outside TS	next to TS			
M12	INFLUENCE OF TUBE-SHEET (TS)	12	14	6 + mode 4 (gap = 0.2 mm)	16	1
		12	14			2
		12	15			3
		12	15			4
		14	16			5
		14	16			6
		14	17			7
		14	17			8

MATERIAL (cf. Table 2-1)	TYPE	outside TS	next to TS	SKETCH N°. (cf. Fig. 2-2)	SEALING SYSTEM (INDEX)	TEST-PIECE N°.
M12	INFLUENCE OF TUBE-SHEET (TS)	12	14	6 + mode 4 (gap = 0.6 mm)	16	9
		12	14			10
		12	15			15
		12	15			16
		14	16			11
		14	16			12
		14	17			13
		14	17			14

Notes :

1) For reference in summary tables, the specimens are noted Ki, where i is the test-piece number.
2) Indicated "mode" refers to tubesheet constraint, as defined by Section 2.4.

Table 2-2 (i)

GEOMETRY OF TEST SPECIMENS
PROGRAM C3 - SUBSET 1 (THROUGH WALL CIRCUMFERENTIAL CRACKS)

MATERIAL (cf. Table 2-1)	DEFECT GEOMETRY		SKETCH N°. (cf.Fig. 2-2)	SEALING SYSTEM (INDEX)	TEST-PIECE N°.
	TYPE	LENGTH (deg.)			
M9	NO LATERAL RESTRAINT (flaw at 6 mm from TS)	120	8-3	15 and/or 17	29
		120			62
		150			26
		150			31
		180			22
		180			25
		210			27
		210			28
		240			23
		240			24
M11	LATERAL RESTRAINT AT TSP (1100 mm)	210			8
		270			11
		300			1
		300			2
	LATERAL RESTRAINT AT FDB (500 mm) TSP (1100 mm)	180	8-4	15 and/or 17	4
		180			12
		210			5
		210			6
		210			(15) *
		240			7
		240			9
		270			3
		270			10
		300			13
		300			14

* Machined flaw (width = 0.55 mm) / used for testing methodology.

Table 2-2 (j)

GEOMETRY OF TEST SPECIMENS
PROGRAM C3 - SUBSET 2 (THROUGH WALL CIRCUMFERENTIAL CRACKS)

MATERIAL (INDEX) (cf. Table 2-1)	DEFECT GEOMETRY		SKETCH N°. (cf.Fig. 2-2)	SEALING SYSTEM (INDEX)	TEST-PIECE N°.
	TYPE	LENGTH (deg. of arc)			
M12	NO LATERAL RESTRAINT (flaw at 6 mm from TS)	165 165 165	8-1	16	4 5 11
	LATERAL RESTRAINT AT FDB (150 mm)	270 270 270 270 300 300 300 300	8-1 + offset 10 mm + offset 20 mm 7-1 + offset 10 mm + offset 20 mm	16	7 8 9 6 1 10 3 2
	LATERAL RESTRAINT AT TSP (900 mm)	270 270 300 300	8-2	16	18 20 19 22
	LATERAL RESTRAINT AT FDB AND TSP	270 300	8-2	16	17 21

Table 2-2 (k)

PROGRAM A4- SUBSET 1
DIMENSIONAL CONTROL

TUBESHEET INFLUENCE - PROGRAM A4-1 - SAMPLE DEFINITION

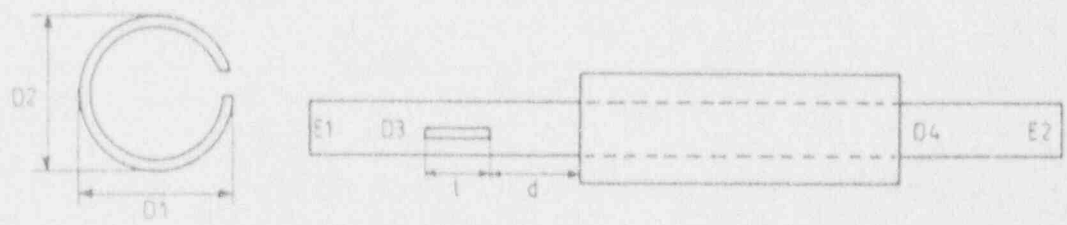

Specimen	l	d	D1	D2	D3	D4	E1	E2
1	12	0	22,24	22,25	22,50	22,25	1,34	1,31
2	12	0	22,26	22,23	22,42	22,25	1,25	1,25
3	12	0	22,24	22,21	22,34	22,24	1,24	1,28
4	16	∞	22,25	22,30	22,22	22,21	1,26	1,30
5	16	0	22,24	22,28	22,20	22,24	1,32	1,32
6	16	0	22,24	22,27	22,23	22,25	1,28	1,31
7	16	8	22,23	22,27	22,16	22,20	1,32	1,28
8	16	16	22,26	22,24	22,23	22,23	1,26	1,29
9	16	0	22,26	22,24	22,23	22,24	1,20	1,28
10	16	∞	22,28	22,23	22,21	22,26	1,28	1,28
11	16	0	22,24	22,26	22,21	22,22	1,28	1,28
12	16	8	22,25	22,22	22,21	22,26	1,32	1,31
13	16	∞	22,22	22,23	22,23	22,23	1,30	1,28
14	20	-4	22,28	22,24	22,28	22,28	1,29	1,26
15	20	0	22,26	22,26	22,21	22,20	1,27	1,25
16	20	0	22,22	22,21	22,19	22,23	1,35	1,32
17	24	0	22,26	22,23	22,23	22,24	1,32	1,32
18	24	-8	22,23	22,27	22,19	22,24	1,26	1,28
19	24	-8	22,24	22,22	22,21	22,24	1,26	1,28
20	24	0	22.23	22.23	22,16	22,24	1,28	1,32

Table 2-3 (a)

DIMENSIONS AND CHARACTERISTICS OF SEALING SYSTEMS

Sealing system Index	Plastic tube Dimensions	Patch Characteristics			Sealing Material
		Material	Thickness (mm)	Width (mm)	
1	No	Brass	02. to 0.3	10	Silicone
2	?	Copper	0.3	35	Silicone
3	?	Copper	0.3	15	Silicone
4	?	No	No	No	Silicone
5	20 x 16 (th. 2)	No	No	No	No
6	17 x 12 (th. 2.5)	No	No	No	No
7	16 x 12 (th. 2)	No.	No	No	Silicone
8	18 x 14 (th. 2)	No	No	No	Silicone
9	18.5 x 12.5 (th. 3)	No	No	No	Silicone
10	18 x 14 + 14 x 10 (th. 4)	No	No	No	Silicone
11	14 x 10 (th. 2)	Brass	0.2	20	Silicone
12	16 x 12 (th. 2)	Brass	0.2	20	Silicone
13	14 x 10 (th. 2)	Brass	0.3	20	Silicone
14	14 x 8 (th. 3)	Brass	0.3	20	Silicone

Table 2-3 (a) (cont'd)

DIMENSIONS AND CHARACTERISTICS OF SEALING SYSTEMS

Sealing system Index	Plastic tube Dimensions	Patch Characteristics			Sealing Material
		Material	Thickness (mm)	Width (mm)	
15	18 x 14 (th. 2)	Steel	0.13 to 0.15	15	Pressure insert
16	16 x 12 (th. 2)	Steel	0.13 to 0.15	15	Pressure insert
17	18 x 14 (reinforced)	No	No	No	Pressure insert

Table 2-3 (b)

SWELLING VERSUS INTERNAL PRESSURE
OF A PLASTIC HOSE (16 x 12; th 2 mm)

The diameter was measured in 3 sections

Pressure bar	1st Φ (mm)	2nd Φ (mm)	3rd Φ (mm)
0	16	15.5	16.0
0.5	16.2	15.8	15.8
1.0	15.8	16.0	15.7
1.5	16.0	16.0	16.4
2.0	16.8	16.8	16.8
2.5	17.0	17.0	17.0
3.0	17.2	17.2	17.3
3.5	17.9	18.0	18.0
4.0	18.0	18.0	18.0
4.5	18.5	18.5	18.8
5.0	19.5	19.3	19.0
5.5	20.2	20.2	20.0
6.0	20.8	20.4	21.1
6.5	21.2	20.9	22.0
7.0	22.0	22.5	22.5
7.5	23.5	24.0	24.0
8.0	25.2	25.0	24.8
8.5	28.0	27.0	28.0

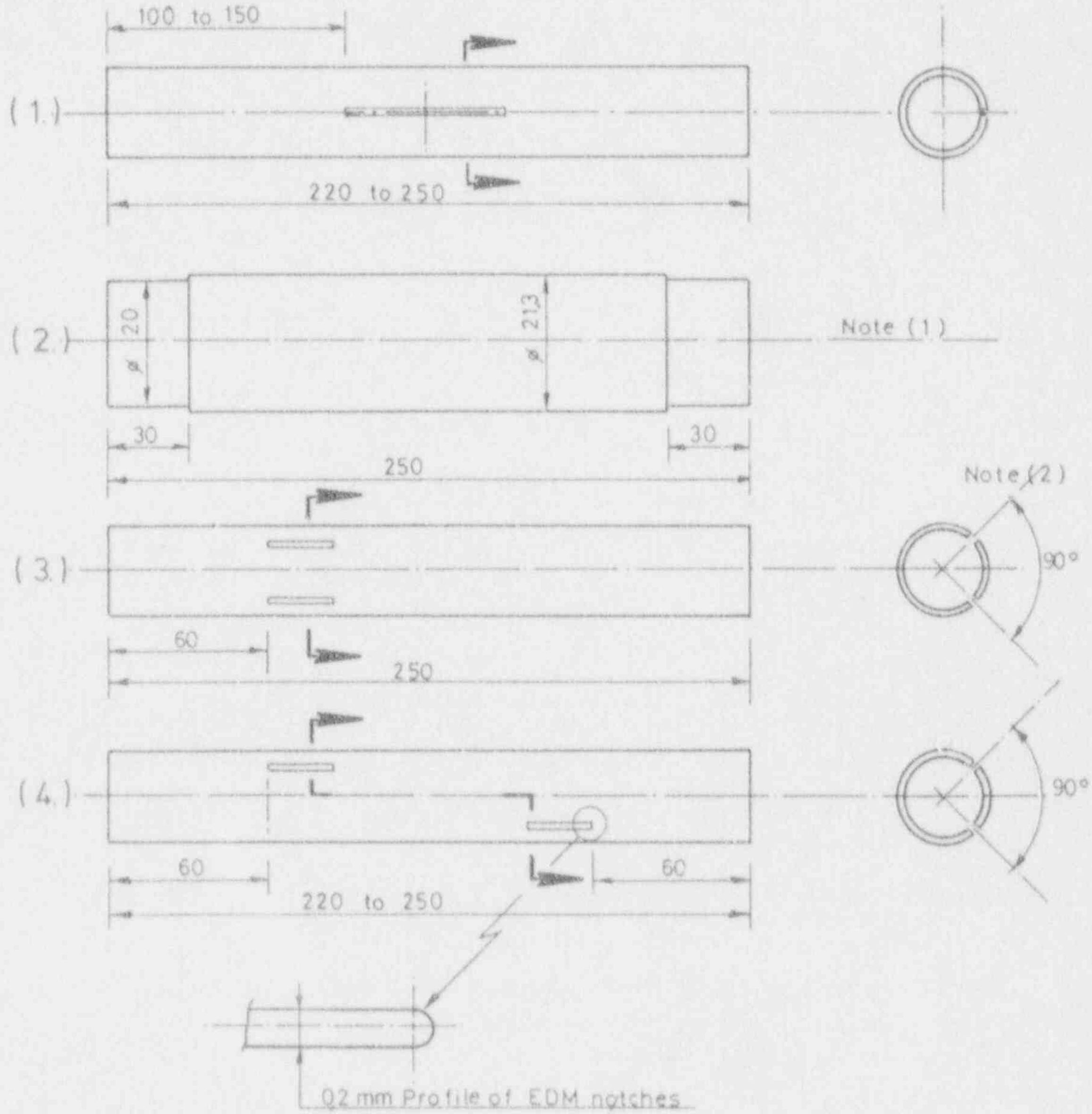

Notes (1) : The specimen is notched like sketch 1

(2) : The other side of the specimen is either smooth (No. 21) or has only one slit (No. 23) or two parallel slits 5 mm apart (No 22)

Figure 2-2 Types of Test Specimens

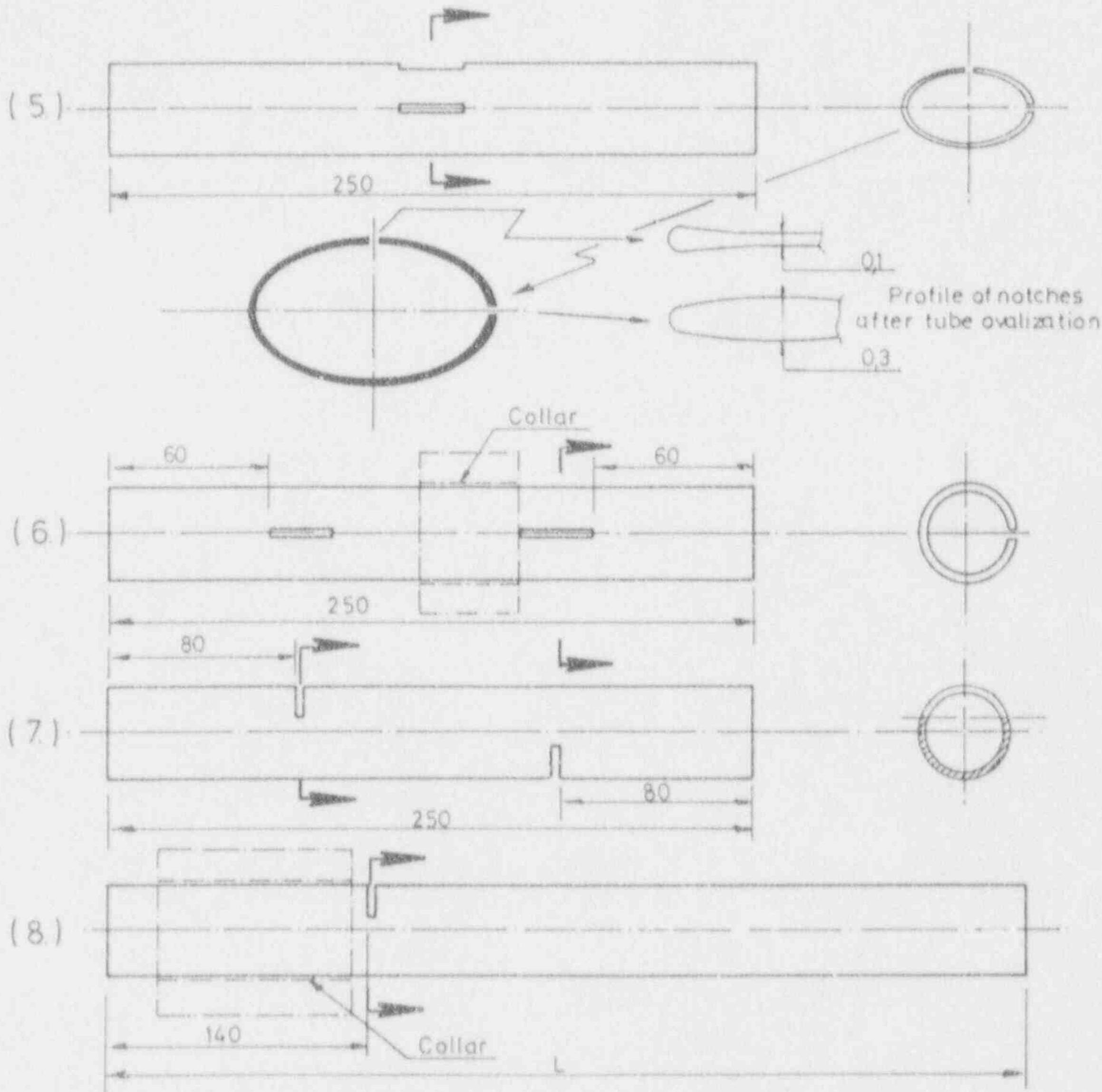

	OD.	L (mm)
8.1	3/4"	370 to 400
8.2		1120
8.3	7/8"	250
8.4		1300

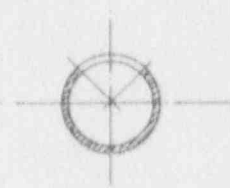

Figure 2-2 (cont'd)

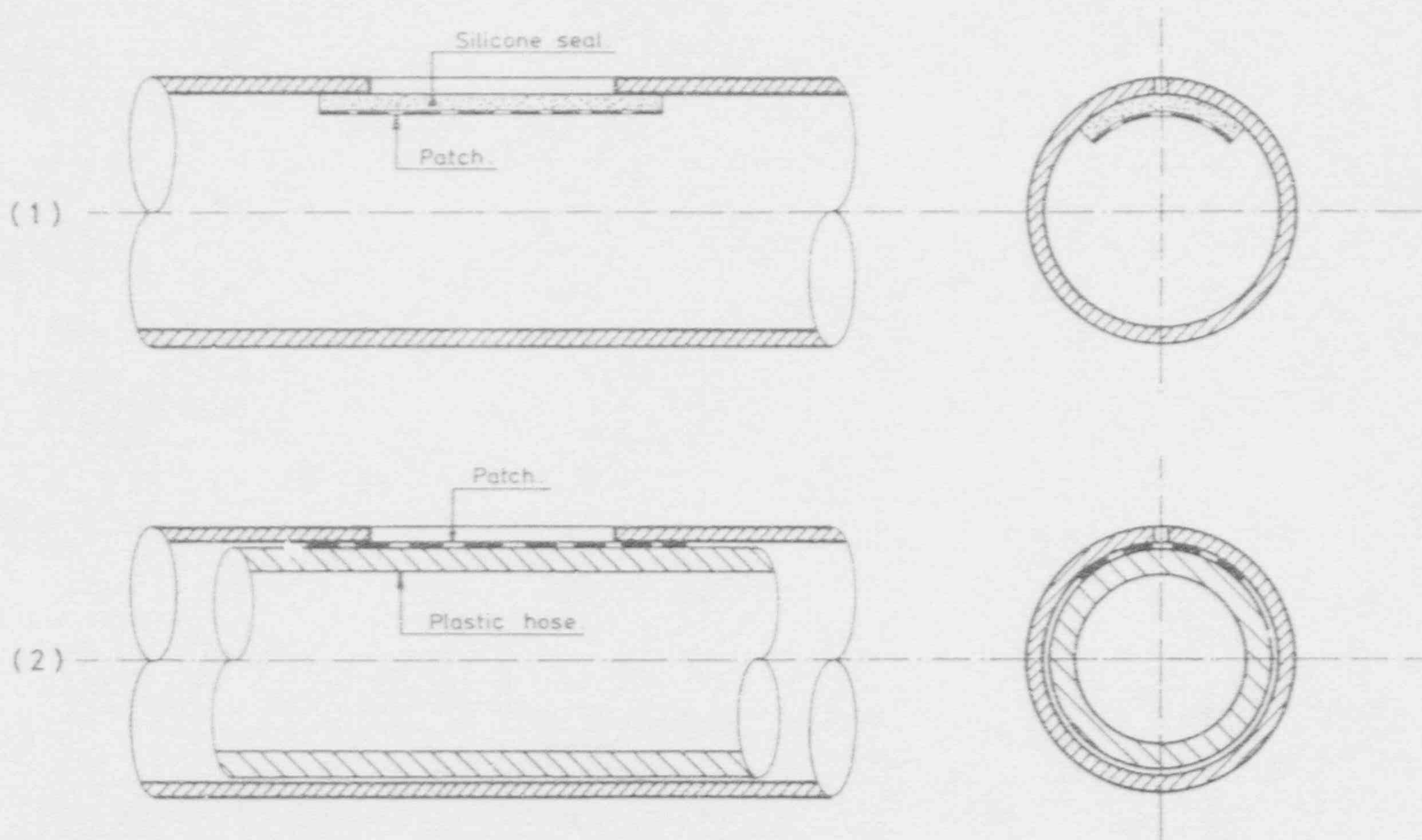

Figure 2-3 Sketches of systems used to keep leak tight specimens with through wall flaws

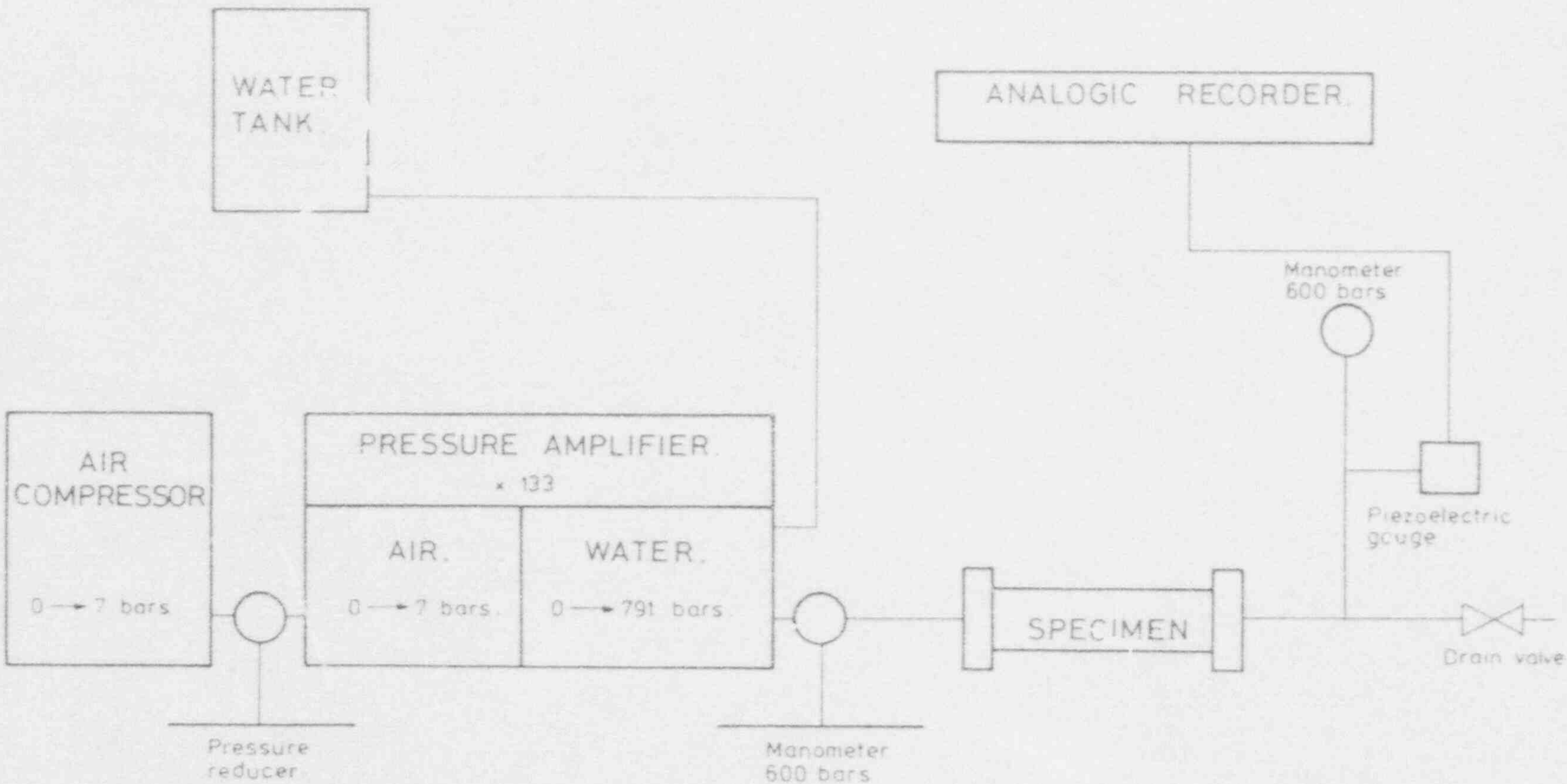

Figure 2-4(a) Test rig

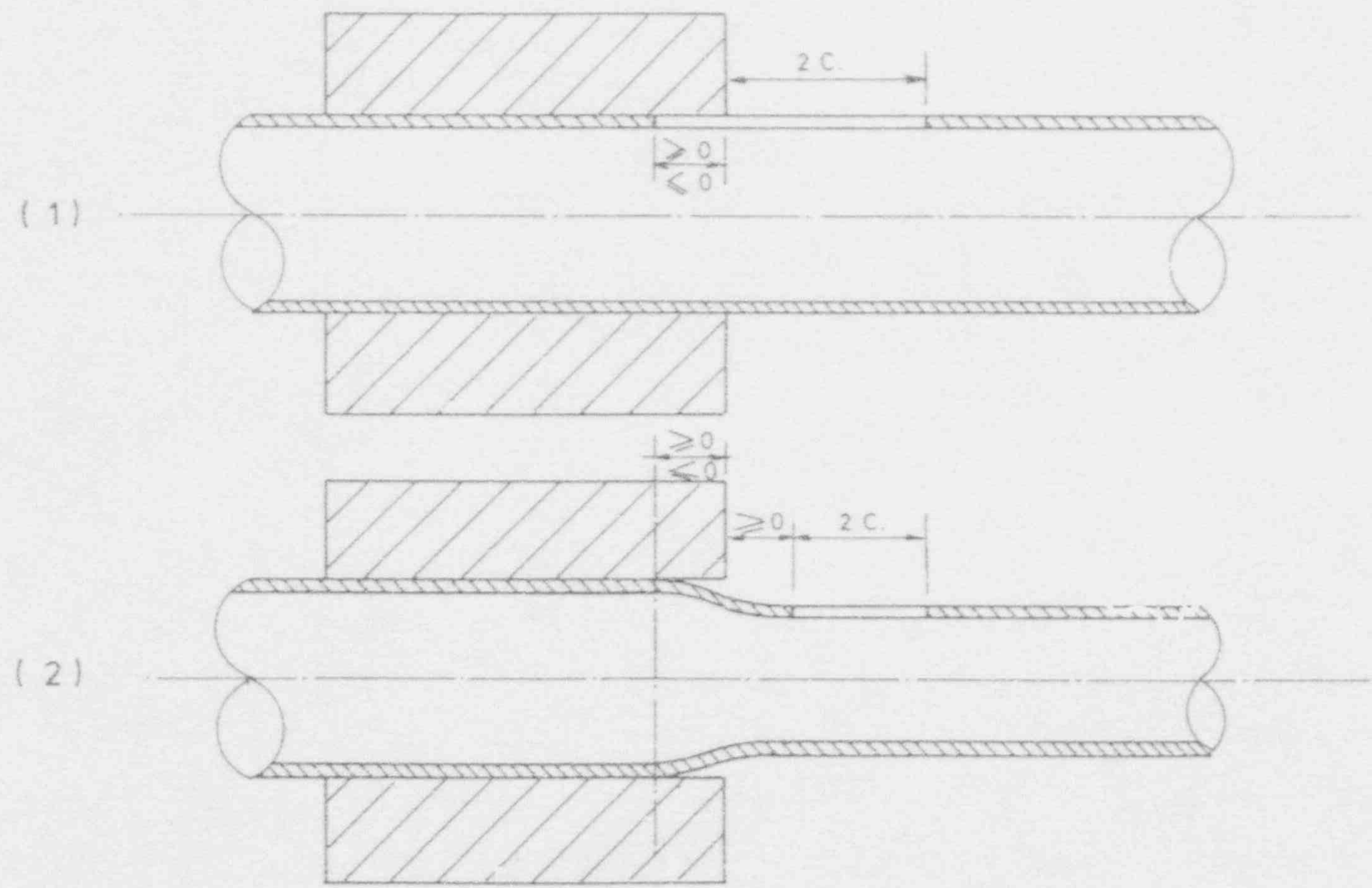

Figure 2-4(b) Sketches of tubesheet simulation

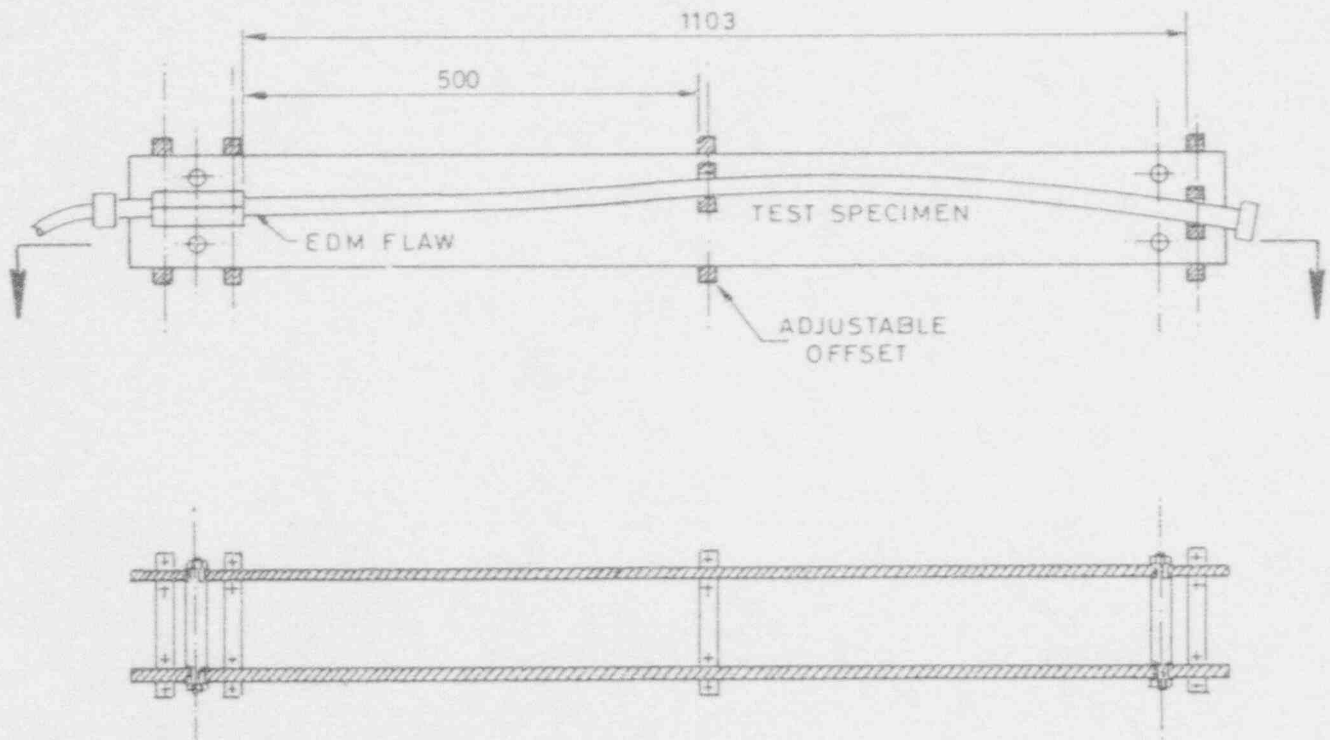

Figure 2-4(c) Lateral restraint test rig
General Assembly with test specimen
illustrated for 7/8" OD tubing (Model 51 S.G)

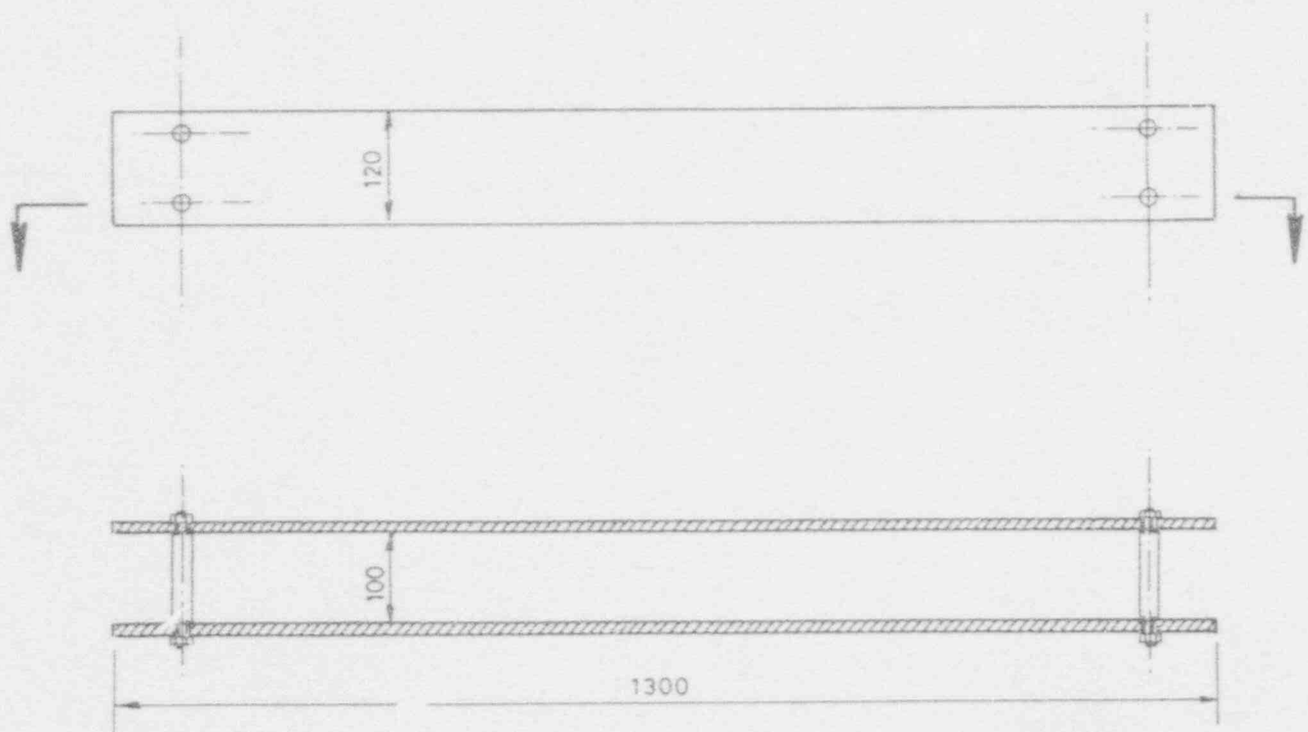

Figure 2-4(d) Lateral restraint test rig
Main frame

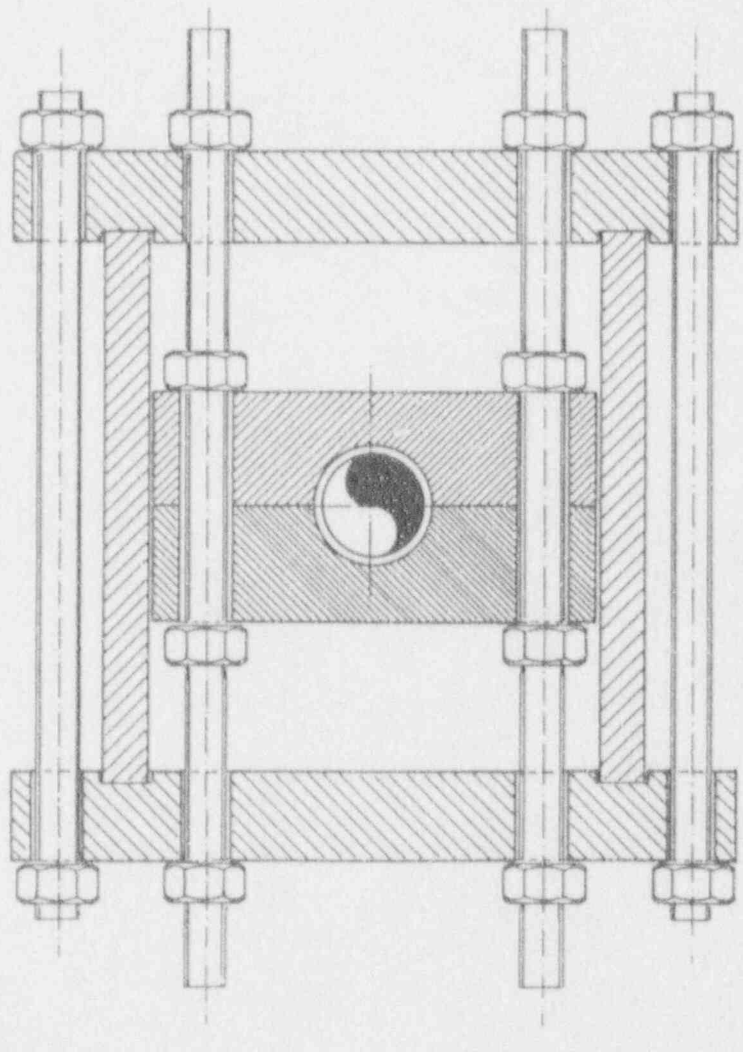

Figure 2-4(e) Lateral restraint test rig restraining plate (typical)

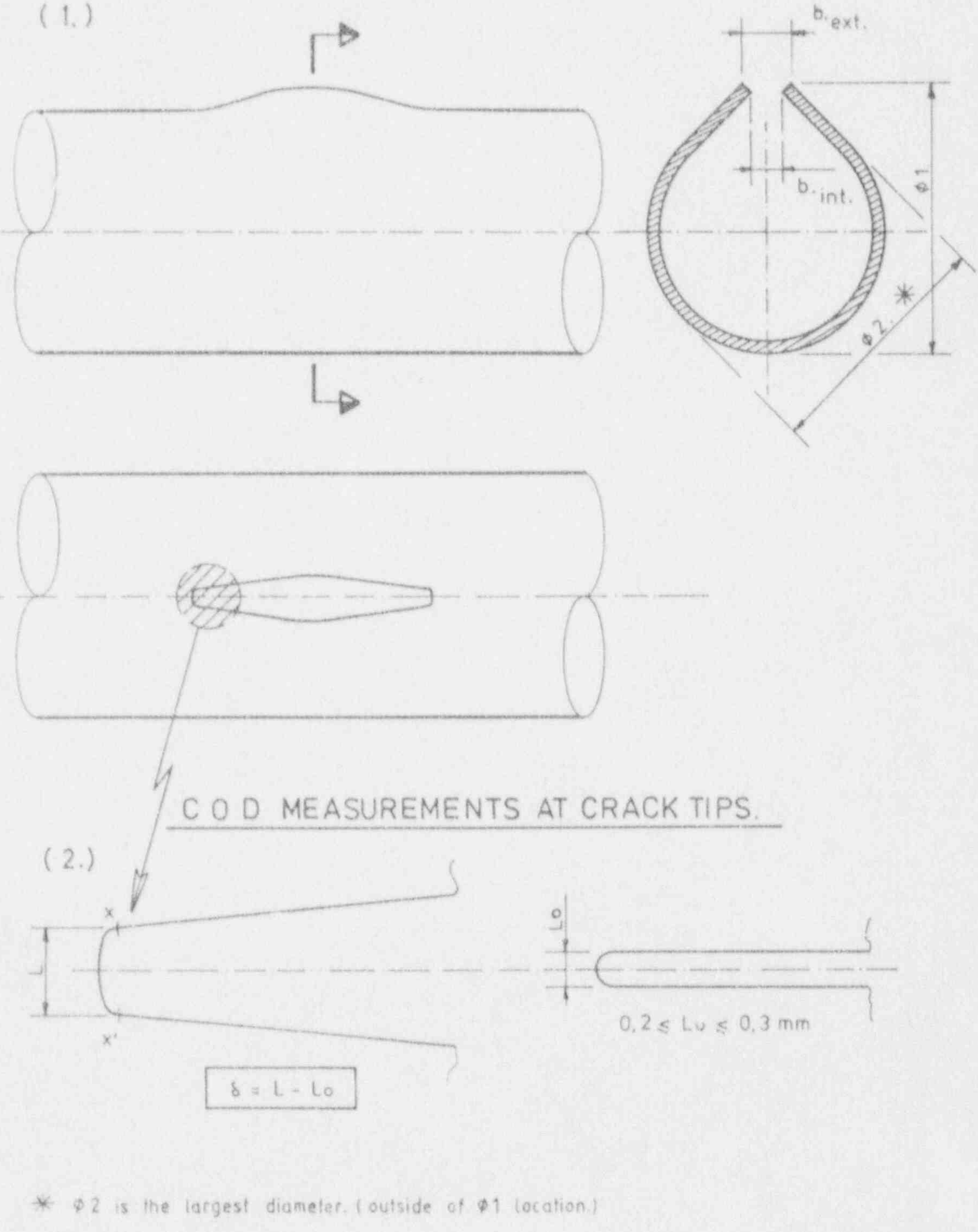

Figure 2-5 Measurements of tube deformation

Section 3

THROUGH WALL AXIAL CRACKS

3.1. THEORETICAL MODEL

3.1.1. Plate theory

If we consider a through wall crack of length 2c in an infinite plate subjected to a uniform tensile stress σ,

- a brittle fracture will be predicted by LEFM* when the stress intensity factor $K_I = \sigma \sqrt{(\pi c)}$ reaches a critical value K_{Ic} ("fracture toughness");

- a plastic collapse will be predicted by limit analysis when the net section stress in the plane of the crack reaches an ultimate flow stress value.

Assuming an elastic - perfectly plastic material and the so-called "Dugdale strip yield model" - Goodier and Field (1), Burdekin and Stone (2) established the following formulation of the crack tip opening displacement COD :

$$\delta = (8\sigma_y/\pi E)\ c\ \ln \sec\ (\pi\sigma/2\sigma_y) \qquad (3\text{-}1)$$

In this formula σ_y denotes the yield strenght and E is the Modulus of elasticity.

According to the COD theory, failure will occur when δ reaches a critical value δ_c.

Hence,

$$\delta_c = (8\sigma_y/\pi E)\ c\ \ln \sec\ (\pi\ \sigma_c/2\sigma_y) \qquad (3\text{-}2)$$

---

* LEFM : Linear Elastic Fracture Mechanics

or, conversely

$$\sigma_c = (2\sigma_y/\pi) \text{ arc cos exp } (\pi E\delta_c/2\sigma_y) \quad (3\text{-}3)$$

- For small values of σ/σ_y or of $\delta E/c\sigma_y$ Eq. 3-1 reduces to :

$$\delta = \sigma^2 \pi c/E\sigma_y = K^2{}_I/E\sigma_y \quad (3\text{-}4)$$

and, as $\delta_c = K^2{}_{Ic}/E\sigma_y$ the critical condition reduces to the classical LEFM formulation $K_I = K_{Ic}$. That is the reason why

Eq. (3-1) is often written as :

$$K^2{}_I = (8\sigma_y{}^2/\pi)c \ln \sec (\pi\sigma/2\sigma_y) \quad (3\text{-}5)$$

- Under plane stress conditions and limited amount of yielding at the crack tips, failures will still be predicted by Eqs. (3-3) or (3-4). However, unstable fracture might be preceded by stable crack growth under monotonically increasing load. Under such conditions, only the initiation COD value (denoted δ_i) is considered to be fully reliable. Eq. (3-1) has also been shown experimentally to be valid only up to about $\delta = 0.25$ mm.

- When gross yielding occurs, the COD formulation is no longer valid but the collapse load is predicted as $\sigma = \sigma_y$. The shape of Eq. (3-2) can nevertheless be retained as a transition fitting curve between the fracture mechanics and collapse load extremes, by making changes as follows :

$$\delta_c E\sigma_y/\sigma^2 \pi c = 8/\pi^2 \ (\sigma_y/\sigma)^2 \ln \sec (\pi\sigma/2\sigma_y)$$

or

$$K_r = \pi S_r/\sqrt{8}.(\ln \sec (\pi S_r/2))^{0.5} \quad (3\text{-}6)$$

with

$$K_r = \sigma \ (\pi c/E\sigma_y \delta_c)^{0.5} = K_I/K_{Ic}$$

and

$$S_r = \sigma/\sigma_y$$

- For low plastic strain, rupture is predicted by fracture mechanics at $K_r = 1$.
- For large plastic strain, rupture is predicted by limit analysis at $S_r = 1$.
- For intermediate conditions, rupture is expected according to Eq. (3-6).

It can be shown that Eq. (3-6) can be replaced (to a 5 % accuracy on the σ value) by :

$K_r = 1$ for $E\delta/\sigma_y c \leq 0.75$

$S_r = 1$ for $E\delta/\sigma_y c \geq 6.5$

3.1.2 Pipe theory

Retaining the elastic, perfectly plastic material model, the critical length of an axial crack in a pipe can be directly derived from the plate theory by considering the stress magnification factor induced by the "bulging effect", which is often expressed as a function of the non dimensional parameter

$$\lambda = (12\ (1 - \nu^2))^{0.25}\ .\ c/\sqrt{(Rt)} \approx 1.8\ c/\sqrt{(Rt)}$$

where ν is the Poisson's ratio, R the mean radius of the pipe and t its thickness

3.1.2.1. Through wall crack

In the elastic range, the stress intensity factor K_I is multiplied by a factor m, first calculated by Folias (3) and often referred to by his name, for which refined numerical values have been further calculated by Krenk (4) up to a value of λ equal to 10.

Figure 3-1(a) illustrates the various analytical expressions that can be used.

The initial Folias law

$$m = (1 + 1.62\ c^2/Rt)^{0.5} = (1 + 0.5\ \lambda^2)^{0.5} \qquad (3\text{-}7)$$

used by Kiefner and al (5), although still often used, has been recognized to be overconservative. Valid numerical data have been further approximated by the following expressions :

$$m = [1 + 1.255\ c^2/Rt - 0.0135\ (c^2/Rt)^2]^{0.5} \qquad (3\text{-}8)$$

which on simplifying gives

$$m = [1 + 0.387\ \lambda^2 - 0.00129\ \lambda^4]^{0.5}$$

used by Schulze et al (6)

or :

$$m = 0.614 + 0.386\ \exp\ (-\ 2.25\ c/\sqrt{(Rt)}) + 0.866\ c/\sqrt{(Rt)}$$

which on simplifying gives (3-9)

$$m = 0.614 + 0.386\ \exp\ (-\ 1.25\ \lambda) + 0.481\ \lambda$$

proposed by Erdogan (7).

As can be seen from Fig. 3-1(a), Eq.(3-8) cannot be used for $\lambda > 8$; Eq. (3-9), while not validated for $\lambda > 10$ (no data available), exhibits a consistent linear trend and will thus be further used in this paper.

In the plastic range, Erdogan (7) used the yield strip model to calculate COD as a function of σ and used the asymptotic behaviour of the calculated curve to define the collapse stress, which appears to match σ_y/m closely.

In conclusion, the plate theory can be directly extrapolated to the cylindrical geometry (vessel or pipe) by replacing σ by $m\ \sigma$.

The applicable formulas are thus :

$$\delta = (8\sigma_y/\pi E)\ c\ \ln \sec\ (\pi m\sigma/2\sigma_y) \qquad (3\text{-}10)$$

and, at failure,

$$\delta_c = (8\,\sigma_y/\pi E)\ c\ \ln \sec (\pi m \sigma_c/2\sigma_y) \qquad (3\text{-}11)$$

Eq. (3-6) remains valid as a general transition curve.

Remark : the factor m considered above is applicable to the membrane stress. A different factor applies to bending stresses but is generally neglected; this appears fully justified when failure is preceded by extensive plastic deformation at the crack tip.

3.1.2.2. Surface cracks

A semi-empirical expression has been proposed by Kiefner et al (5) for a surface crack of depth a. This amounts to replacing m in Eq. (3-11) by :

$$m_p = \frac{1 - a/tm}{1 - a/t} \qquad (3\text{-}12)$$

Again, the yield strip model used by Erdogan (7) can be used to support Eq. (3-12).

3.1.3. Strain hardening materials

The assumption of elastic-perfectly plastic behavior of course does not apply to most real materials.

Real materials may exhibit considerable strain hardening and a correspondingly high ratio σ_u/σ_y of ultimate tensile strength to yield strength.

Most authors have circumvented this difficulty by substituting, in Eq. (3-5), σ_y with a "flow stress" σ_f.

Thus,

$$K^2_{Ic} = (8\sigma^2_f/\pi)\ c\ \ln \sec (\pi m \sigma_c/2\sigma_f) \qquad (3\text{-}13)$$

$$\delta c = (8\,\sigma^2_f/\pi E \sigma_y)\ c\ \ln \sec (\pi m \sigma_c/2\sigma_f)$$

or, conversely,

$$\sigma_c = (2\sigma_f / m\pi) \text{ arc cos exp } (-\pi E \sigma_y \delta_c / 8 \sigma^2_f c) \qquad (3\text{-}14)$$

where m is defined by Eq. (3-9) for a through wall crack or is replaced by m_p as defined by Eq. (3-12) for a partial penetration crack.

σ_f may take any value between σ_y and σ_u in order to best fit the experimental data. The most frequently used correlations are :

$$\sigma_f = \sigma_y + 70 \text{ MPa (10 ksi)}$$

for carbon steels (see (5) and (8)), and

$$\sigma_f = \sigma_y + k (\sigma_u - \sigma_y) \text{ with } 0.3 \le k \le 0.4$$

for austenitic stainless steels (see (9) and (10)).

It should be noted that Eqs. (3-13) and (3-14) can no longer be transposed to a subcritical loading condition.

Eq. (3-6) still remains unchanged as :

$$K_r = (\pi/\sqrt{8}) S_r [\ln \sec (\pi S_r / 2)]^{-0.5}$$

but with

$$K_r = K_I / K_{Ic} = m\sigma\sqrt{(\pi c / E \sigma_y \delta_c}$$

$$S_r = m\sigma/\sigma_f$$

In fact, this is a special application of a general approach originally developed by Downling and Townley and often used by the British CEGB as a "two parameter design curve" (11).

Fig. 3-1(b) illustrates this curve, which is a failure locus dividing the plane into a "safe area" and an "unsafe area".

For a particular material and geometry, the ratio K_r/S_r is a constant

$$k = (\pi\sigma^2_f c/E\sigma_y \delta_c)^{0.5}$$

and defines the slope of a "load line"; increasing σ will move the representative point (K_r ; S_r) along this line, from the safe towards the unsafe area.

To allow easy drawing of the appropriate load line, Fig. 3-1(b) is provided with 2 scales :

- general graduation (constant k)
- graduation in c/δ_c, applicable to any material with $\sigma^2_f/E\sigma_y = 0.05$;

  this value is typical for Inconel and very ductile steels.

3.1.4. Inconel S.G. tubing

In the early 80's, when BELGATOM first adressed the problem of critical crack size in steam generator tubing (PWSCC detected in Doel 2 roll transitions), there was no literature available regarding the applicability of the above theories to this particular case. For instance, there was practically no informatio about

- small diameter pipes (< 3" dia.)
- Inconel material (flow stress) of any size.

Based upon a reasonable estimation of $\delta_c \approx 0.5$ mm for the critical COD value and the crack length range of practical interest ($2c \leq 20$ mm), the index used in Fig. 3-1 (b) ($c/\delta_c \leq 20$) shows that only the collapse failure mode need be considered, i.e. $\sigma_c = \sigma_f/m$
The remaining uncertainties were essentially related to

- confirmation of the bulging factor m to be used and, more precisely, its dependance on the $c/\sqrt{(Rt)}$ parameter
- establishment of the flow stress σ_f applicable to Inconel and, more precisely its dependance on the conventional mechanical properties (YS and UTS).

3.1.5. Influence of tubesheet confinement

All of the above considerations are applicable to defects located in the free span of a tube; more precisely, they apply to straight runs but can be extrapolated to large radius bends without much loss of accuracy. However a significant conservatism would result if the tube geometrical environment was not taken into consideration.

If the tube is surrounded with zero clearance by a resistant structure (such as in the case of the expanded area in the tubesheet), there is no more a critical crack size as unstable propagation is prevented because the load is taken over by the surrounding structure. This is also true if the clearance is less than the precritical bulging deformation of the crack. This is the case for through wall cracks, the length of which is entirely within the thickness of the tubesheet (when tubes are only partially rolled at the lower end), the flow distribution baffle, or another tube support plate.

When the crack extends outside the confinement, there is still a reinforcement effect, raising the critical pressure (or increasing the critical length) beyond the "free span" value; the actual critical pressure of a crack partially extended into a confining collar will fall between that of the full crack length and the protruding length of the crack as a function of gap value.

Only the extreme cases (infinite and zero gap) can be evaluated on a theoretical basis.

For an axial crack located entirely outside but adjacent to a zero gap confinement (such as a roll transition crack at the top of a full depth expansion tubesheet), there is also a reinforcement effect.

As the tubesheet's constraining effect on the crack tip (farthest away from the TS) is the controlling factor, a semi-quantitative knowledge can be derived from the radial deformation of a locally pressure loaded tube.

According to Roark (12) (Table 30, case 12) the order of magnitude of the radial deformation at a distance x from the built-in section is

$$\delta_r = (p/4D\gamma^4)\ \exp\ (-\ \gamma x)$$

where

$$\begin{cases} \gamma = [3\ (1 - \nu^2)/R^2 t^2]^{1/4} \\ D = E\ t^3\ /\ 12\ (1 - \nu^2) \end{cases}$$ with ν = Poisson's ratio

reducing to

$$\varepsilon = \delta_r/R = (pR/Et)\ \exp\ (-\ 1.28x/\sqrt{(Rt)})$$

or

$$\varepsilon = \varepsilon_0\ \exp\ (-\ 1.28x/\sqrt{Rt})$$

where

ε is the residual constraining effect at distance x

ε_0 is the maximum constraining effect at confinement outlet (x = 0)

Rt is the product of the mean radius by the tube thickness.

The following tentative conclusions can be drawn

- similar reinforcing effects (relative increase of critical pressure) are expected for distances (and crack lengths) normalized to $\sqrt{(Rt)}$
- the reinforcing effect is expected to "die out" exponentially with distance (or crack length). For a crack adjacent to the tubesheet, it is not clear, however, what fraction of the crack length should be considered in the exponent; if half length is assumed, the reinforcing effect should decrease as

  $\exp\ (-1.28c/\sqrt{(Rt)})$
- the reinforcing effect should be significant for $\varepsilon/\varepsilon_0 > 5.10^{-2}$, leading to $c < 2.3\ \sqrt{(Rt)}$. This should be observable for crack lengths up to an order of magnitude of $2\ c \approx 4.5\ \sqrt{(Rt)}$, i.e., a range of about 17 mm for SG 3/4" to 7/8" OD tubing.

3.2. EXPERIMENTAL PROGRAMS AND TEST RESULTS

3.2.1. Objectives

The experimental program conducted by BELGATOM involved four consecutive phases with the following specific objectives :

- Program A1 : validation of general theory for small diameter Inconel tubing.

  . limited to through wall flaws in a single heat of 7/8" OD Inconel tube
  . main results presented at the 6th SMIRT Conference (Paris, 1981) (13)

- Program A2 : extension of program A1

  . other materials and diameters in order to investigate flow stress dependance on conventional mechanical properties
  . parametric investigations (effect of notch sharpness, multiple flaws, residual stresses, partial penetration cracks)
  . main results presented at the 7th SMIRT Conference (Chicago, 1983) (14)

- Program A3 : leak before break (LBB) behaviour of Nickel-plated cracked tubes

  . within the frame of a general R & D program for SG tube repair by Nickel plating, conducted jointly by BELGATOM and FRAMATOME
  . completed in 1988

- Program A4 : effect of geometric confinement (tubesheet or tube support plate)

  . completed in 1989.

3.2.2. Program A1

The first program involved Material M1 with test-pieces N°. 1 through 15 (see Table 2-2 (a)).

The test results are listed in Tables 3-2(a) and (b) and further detailed in Figs. 3-2(a) and (b).

3.2.3. Program A2

The second program intended to define the tube plugging limits for the SG's at Doel 3 and 4 and Tihange 2 and 3 in agreement with the requirements of R.G. 1.121. As a consequence, that program focused on the definition of critical dimensions of axial through wall flaws, as a function of the specific SG characteristics.

Special attention was given to the dependance of critical defect sizes on :

- geometrical characteristics (diameter and thickness)
- mechanical properties (namely yield strength YS and ultimate tensile strengh UTS)

in order to allow reliable extrapolation to other sizes (in the same range) and mechanical properties.

This was made possible by selecting other materials which experience large plastic deformation prior to rupture (austenitic stainless steel type AISI 304, ...).

That program was conducted on Materials M2 to M8 (see Tables 2-2 (b) and 2-2 (c)). The test-results are listed in Tables 3-2 (c) and (d) and further detailed in Figs. 3-2 (c) to (i).

3.2.4. Program A3

According to the Leak Before Break (LBB) principle, a crack that would have a critical length (leading to unstable propagation) under the most unfavourable accidental conditions (main steam or feedwater line break) should be detectable by a large leak (in excess of the "technical specification" allowable limit) under normal service conditions.

As the nickel electroplating process, which was jointly developed by BELGATOM and FRAMATOME as a repair method for PWSCC in SG tube roll transitions, involves deposition of a thin leak tight layer of ductile material on preexisting tube cracks, there was a potential concern that nickel electroplating might unfavourably affect the desirable LBB feature. In order to eliminate this concern, BELGATOM conducted an experimental program from 1986 to 1988, to establish that the LBB behaviour still was in force on the repaired tubes. Detailed results of this program are the common property of BELGATOM and FRAMATOME and cannot be disclosed within this report. However, all of the burst data obtained on either the nickel plated or reference unplated samples are reported below. These program results are of special interest because a significant proportion of the test samples contained fatigue crack extension of the initial EDM flaw.

28 samples, from 2 different 7/8" OD Inconel heats and 14 samples from one 3/4" OD Inconel heat, were selected from this program and considered relevant to this report. Table 3-2 (e) lists the sample characteristics and the corresponding test results.

3.2.5. <u>Program A4</u>

When it became evident that PWSCC continued to propagate in the roll transitions of the full-depth rolled tubes at Doel 3 and Tihange 2, the reinforcing effect of the tubesheet was investigated in order to increase the applicable plugging limit.

A preliminary program (subset 1)conducted in 1987 on a set of 20 samples yielded conclusive results. However, the large scatter of data points did not allow an accurate quantitative assessment (Fig. 3.2 (j)). The tube bulging was recorded as a function of pressure; the comparison of curves recorded in Fig. 3.2 (k) and 3.2 (l) clearly illustrates the constraining effect of the tubesheet.

Later, when the longest site defects were approaching the contemplated plugging limit, the program was resumed (in 1988) as follows :

- increase of the number of test samples with single defects, in order to provide a better statistical representation (subset 2).

- Direct verification by use of test specimens provided with 2 flaws, the shorter one in the free span and the longer one adjacent to the tubesheet, the difference in length being in the range of the expected equivalent burst pressure (subsets 3 and 4).

In addition the half collar assemblies used initially were replaced by full collars to improve the representativity of tubesheet simulation,; the tube was either force fitted or actually rolled into the collar with either the minimum or maximum clearance allowed by the manufacturer's specification.

Tables 3-2 (f) and (g) list the sample characteristics and test results for the 4 program subsets.

3.3. DISCUSSION OF RESULTS

3.3.1. Phenomenology

3.3.1.1. Failure Mode

For all burst tests (a total of 155 flaws), the reported critical pressure corresponds to unstable crack propagation; at this pressure, there is an instantaneous crack extension of several mm at both ends of the initial flaw (Fig. 3-3 (a) sketch 2). Crack propagation was arrested by the immediate pressure drop of the uncompressible cold water; the release of the elastic energy stored in the metal pressure boundary cannot sustain a larger propagation (as would be the case for hot water or gas pressurization).

The axial propagation sometimes ends up in some circumferential deviation (this behaviour seems to be material dependant and was seldom observed on Inconel).

However, for Inconel samples in tubesheet simulations, the flaw tip adjacent to the collar usually failed in the circumferential direction.

For EDM flaws, no stable growth took place before bursting; this was observed, depending on the test series, by

- visual observation and/or video recording of the flaw behaviour during pressure build-up.
- visual (optical) examination of samples at intermediate pressure levels close to the final burst value.
- final examination of the unfailed flaw for those samples containing two identical defects.

However, a small crack initiation (less than 0.1 mm long and not extending through the entire wall thickness) was observed in a few cases. For fatigue cracks, a more significant, but still small, amount of stable crack propagation was occasionally observed to precede the unstable bursting.

Fracture appearance was typically ductile, with 45° shear lips and significant wall thinning (similar to the cracking in a conventional tensile test); Fig. 3-3 (a) sketch 3 illustrates a cross section at the tip of an arrested crack.

3.3.1.2. Plastic Deformations

In all cases, large plastic deformations were observed prior to criticality (Fig. 3-3 (a) sketch 1); deformations were initiated at values as low as half the critical pressure; they include

- local blunting of the flaw tips, or Crack Opening Displacement COD, increasing up to a fairly constant failure value of about 1 mm for EDM flaws and 0.8 mm for fatigue cracks.
- flaw opening (with a maximum central width of a few mm) and increasing leak area.
- tube "bulging", with a large increase of the diameter measured at the center of the flaw (Fig. 3-2 (h)); this may lead to contact with a surrounding structure (such as tube support plate or tubesheet in an unexpanded area) and prevent any critical (unstable) condition when the pressure is increased further.

Ultimate tube failure (flaw unstable propagation) was further characterized by

- "fishmouth" shaped deformation of the crack area (Fig. 3-3 (a) sketch 2 and Figs. 3-2 (b); 3-2 (c); 3-2 (i))
- general bending deformation of the tube (the center of curvature being on the crack side) (Fig. 3-2 (a))
- tube section ovalization at both tips of the (extended) crack (Figs. 3-2 (a); 3-2 (d)); surprisingly, the minor axis of the deformed section lies in the crack plane. This also means that the observation of ovalization in a steam generator tube rupture (in a tube bend, for instance) should differentiate between that present in the component before rupture and that caused by the rupture.

3.3.1.3. Sealing Patch Behaviour

The sealing system exhibited a variety of behaviours at the time of failure.

Occasionally the sealing system did not fail (while the crack propagated to some extent in an unstable manner); the plastic membrane remained leaktight and the plastically deformed metal patch remained in the tube.

More often than not, leaktightness was lost through perforation of the plastic membrane; the metal patch might either

- be extruded (without any tearing) through the opening crack; this is the usual behaviour for the longest cracks
- tear along the crack (in the longitudinal direction); this was often observed with the softer (brass) but thicker shims used initially (programs A1 and A2)
- tear across the crack (in the circumfential direction); this was usually observed with the stronger (steel) but thinner shims used later in programs A3 and A4
- show a combined pattern of axial and circumferential tearing components (a less often occurring but not exceptional behaviour)

It was not possible to correlate the sealing patch behaviour with any significant variation in the burst pressure value.

While the friction action of the metal patch introduced tangential loads that interfered with the tube failure process, this influence was mainly observed in the (sometimes large) scatter of precritical deformations but does not seem to significantly affect the actual value of ultimate failure. For instance, the various sealing systems (including the few cases with no metal shim at all) cannot be differentiated within the usual (relatively small) scatter band of burst data points. This might be due to the fact that the dominant contribution to burst strength is in the longitudinal direction (as the result of the bulging process) while the friction load developed by the sealing patch is mainly in the transverse direction (as it follows the direction of major displacement associated with flaw opening). While some residual effect on burst pressure still must exist, it is not expected to exceed a 5 to 10 % range.

3.3.1.4. Effect of Loading path

In most cases where a pressure test was interrupted (by full unloading from a level close to the expected failure value), and further resumed, the resulting failure appeared to be premature (usually not exceeding or being even lower than the initial pressure level).

This is possibly related to an oligocyclic plastic fatigue process. It may have significantly reduced the reported burst pressure values of some tests and contributes some conservatism to the experimental program.

This is likely to be more applicable to programs A1 and A2, as

- pressure loading interruptions were scheduled to better observe precritical deformations
- dual slit specimens were used with repressurization of the second flaw after cutting off the first failed section.

Some (probably smaller) effects of the same type might also occasionaly have been present in the later phases as the pressurizing process being used did not result in monotonic loading but involved successive (small) unloading and reloading steps associated with the strokes of manual pump actuation.

3.3.1.5. Effect of Residual Stresses

The effect of residual stresses was simulated by plastic deformation of the cracked area prior to pressurizing the flawed tube.
This resulted in a calculated high residual stress field either enhancing or opposing the tensile loading of the crack tips.
As expected on theoretical grounds, this did not differentiate the burst pressure.

3.3.1.6. Effect of Parallel Flaws

A few tests were conducted with 2 parallel flaws of equal length and variable spacing in the circumferential direction.
This did not result in a significant modification of burst pressure within the usual scatter band of failure data points.

3.3.1.7. Effect of Notch Sharpness

Various degrees of notch sharpness were used

- "large" width machined flaws (0.8 mm)
- EDM flaws (typical width 0.2 to 0.3 mm)
- ductile tear crack (from repressurization of a former burst test with small crack extension)
- fatigue crack extension of EDM flaws.

The resulting effect on burst pressure was shown to be very low, if present at all.

A possible reduction factor of 2 % for fatigue cracks has been assumed and is further discussed under Section 3.3.2.

3.3.2. Model validation

The model validation was performed in three steps :

- verification of the collapse load theory for a large range of crack lengths
- establishment of the flow stress value dependance on the conventional mechanical properties
- measurement of the actual flow stress value applicable to Inconel material.

The first step was achieved in program A1; it confirmed that the failure (unstable extension of the length of a through wall flaw) can accurately be predicted by the "collapse load" model $\sigma_c = \sigma_f/m$ as illustrated by Fig. 3-3 (b) for a range of cracks from 10 to 70 mm in length (single heat of 7/8" OD Inconel tubes).
Similar curves have later been produced by other research teams, as illustrated by Fig. 3-3 (c), from the French R & D program.

The second step was achieved in program A2 due to the availability of a large range of conventional mechanical properties (ratio in excess of 1.5 between maximum and minimum values).
As the properties YS and UTS governing the behaviour of an axially flawed tube are clearly those in the circumferential direction, a correlation was established between the flow stress, derived from the burst pressure, and a direct measurement of the tensile properties in

the transverse direction; the latter involved somewhat unconventional techniques

- flattened tensile test specimens (YS and UTS measurements)
- "ring" tensile test (only applicable to UTS measurement).

Several correlations were attempted, as summarized in Table 3-3 (a).

The best experimental fit was with a relation of the type

$$\sigma_f = k\,(YS + UTS)$$

as illustrated by Fig. 3-3 (d) from results calculated in Table 3-3 (a).

Some care must be exercised when using this figure

- For practical reasons, the ordinate is labelled as $mp_c R/t$, which is a close approximation but not equal to σ_f (the actual flow stress value would be about 6 % lower)
- The abscissa refers to transverse properties measured by unconventional means (requiring multiple test samples because of a significant data scatter) which are not usually available for commercial batches of tube material.

This means that only the concept that flow stress is proportional to (YS + UTS) and not the parameter value (proportionnal constant = 0.57) can be considered for Inconel tubing in the field.

The third step, dedicated to the Inconel material, was achieved by integrating the results from the larger set of data produced by programs A3 and A4, where the calculated value of the flow stress (from m R_i/t x burst pressure) was systematically correlated to the conventional properties (YS + UTS) as measured in the longitudinal direction by the tube supplier.

All of these data are summarized in Table 3-2 (e); they refer to 81 axial flaws burst tested without tubesheet simulation (or sufficiently far away from it). A further set of 8 data points from Table 3-2 (g) (relative to tubesheet influence) was also used because it was demonstrated (see Section 3.3.3.) that they were not significantly affected by TS proximity.

From the resulting 89 data points, 3 extreme values were disregarded because they fell either below (1 case) or above (2 cases) 15 % of the average. The remaining set of 86 "qualified" data points were further analysed as indicated in Table 3-3 (b).

In order to avoid any bias from the particular testing conditions, the data were first grouped into 9 consistent data sets for which

- the number of samples
- the average value of $K = \sigma_f / (UTS + YS)$
- the standard deviation

are systematically reported.

Examination of these data indicated that the following sets can be grouped together

- sets 1, 2 and 3 (46 data)
- sets 5 and 6 (14 data)
- sets 7 and 8 (16 data)

A comparison of the average values for the remaining 5 sets of data, covering a range from 0.547 to 0.603, tended to suggest that they belong to a single family.
Because, the observed differences were consistent with theoretical expectations, they are and taken into account as further discussed below.

The ratio of set 4 to set (1 + 2 + 3) amounts to 0.547/0.557 = 0.98 and can be considered to reflect a slight effect of notch sharpness (fatigue crack versus EDM notch). A similar difference is not observed between sets 5 (EDM notch) and 6 (fatigue crack) of the 7/8" OD nickel-plated specimens; however this might result from a compensating effect of the nickel coating thickness (average of 90 µm for set 5 and 125 µm for set 6).

The effect of a 125 µm coating can be approximated by the ratio of set 4 (unplated) to 6 (plated), i.e. 0.547/0.576 ≈ 0.95; this appears reasonable as the mechanical properties (YS, UTS, and ductility) are lower for Nickel than for Inconel. The compensating effect between notch sharpness and the difference in coating thickness can thus be checked by noting that

$$1 - 0.05\ ((125 - 90)/125) = 0.985 \approx 0.98$$

Both adjustment factors (0.98 for notch sharpness and 0.95 for coating) have thus been applied to the last set (N°. 9) of data.

This allowed for recombining the adjusted data sets.

First, all 64 data points of 7/8" OD - heat 1 were combined with an average value of 0.547.

This value was consistent with the average of 0.532 (16 data points) of 3/4" OD, so that the resulting combination yielded an average of 0.544 (80 data points).

Finally, this was compared with the last set of 6 data points, with an average of 0.562. The difference was quite small but might be significant because the material of set N°. 9 had been heat treated in order to reduce the ratio of YS/UTS to a value of 0.31 well below the range of commercial heat values or of the materials considered in the BELGATOM program A2. Nevertheless, the combination was made with an overall average adjusted value of

$$K = 0.545$$

for all 86 "qualified" data points, with a standard deviation of 0.030.

The corresponding distribution is shown in Fig. 3-3 (e) together with its "normal" (Gaussian) approximation.

Thus, the value selected to perform all critical length calculations of axial cracks was conservatively taken at one standard deviation below the average, i.e.

$$K_{calc} = K_{av} - \Sigma = 0.545 - 0.030 = 0.515$$

Notes :

1. It can be checked that the "adjusted" values of the only three cases excluded from the "qualified" set of data (0.652; 0.638 and > 0.442) are all outside a ± 3 Σ range and are thus confirmed "outliers".

2. If no adjustment had been made, the average of all 86 "raw" data points would have been 0.561 with Σ = 0.034.

3. Since lower bound values (from 13 nonburst specimens) were included in the distribution of qualified data, the resulting analysis is clearly conservative.

4. It is interesting to review the only values of K falling below that retained for further calculations (K = 0.515). The 4 lowest ones are in fact lower bounds (> 0.470; > 0.487; > 0.496 and > 0.499) which do not conflict with the retained value. Among the 9 others (0.514; 0.513; 0.512; 0.510; 0.509; 0.509; 0.508; 0.501; 0.501), only two (at 0.501) are significantly lower (by about 2.5 %) than the retained value, which can thus be considered as a lower bound value for all experimental data.

3.3.3. Influence of Tubesheet

The influence of the tubesheet was established in two different ways :

- Statistical evaluation of the "Reinforcing Factor" RF defined as the ratio of K values (as calculated under 3.3.2. above) for any particular configuration and for the free span. RF thus represents the expected relative increase of burst pressure due to the proximity of the tubesheet.

- Direct verification using "dual defects" test specimens.

3.3.3.1. Statistical Evaluation

All results from program A4 have been regrouped in Tables 3-2 (f) (7/8" OD) and 3-2 (g) (3/4" OD)

- by general configuration

  . flaw tangent to the tubesheet
  . flaw partially engaged within the tubesheet
  . flaw at some distance from the tubesheet (with reference to the closest effective contact point, which may be inside the tubesheet hole)

- by crack length (for flaws partially engaged in TS, the length outside TS is considered).

Lower bound values from the nonburst flaw of dual specimens were also included. One invalid result P60* and 6 abnormal values (differing by more than 10 % from the average of their particular category) were disregarded. The remaining 66 "qualified" data points were divided into 15 categories with an average of 4 data points per category. the normal scatter of values made the analysis particularly delicate.
For each of the 66 data points, a "K" value was calculated by

$$R_i r_{p} / (t\ (YS + UTS))\ \text{or}\ 7.75\ mp_c / (YS + UTS)$$

The average of K was calculated for each category and "adjusted" by a .98 coefficient (assumed effect between EDM and fatigue crack) before performing the ratio RF to the known average figure in the free span of a tube (0.545).

The following conclusions can be drawn

- the RF becomes negligible when the crack tip farthest away from the TS is at a distance of ≥ 24 mm (for 7/8" OD) from the TS contact point.
  This includes

  . 24 mm long flaws tangent to TS
  . 19 mm long flaws, 5 to 8 mm away from TS
  . 16 mm long flaws, 8 mm away from TS

  The average of these 8 data points leads to an insignificantly lower RF value of 0.976, well within the scatter band (30/545 = 5.5 %) of free span data (no TS effect).

- the RF of flaws engaged within the TS is systematically lower than that of flaws of the same length tangent to the tubesheet.
  This effect is considered to be specific to the EDM nature of the flaws. In fact, the finite width (0.2 to 0.3 mm) of the flaw allows for an easier angular deflection of the flaw lips at the TS contact point than would be possible for an actual (fatigue or corrosion) crack with negligible width. Thus, the corresponding tests (13 data points) yield only lower bound values that are too low to be of actual use.

- For flaws tangent to the tubesheet, the calculated RF yields a relatively consistent inverse relationship to crack length, with a maximum of about 20 % for the length range under investigation. There are, however, two notable exceptions

  . for 3/4" OD where RF is apparently lower for 14 mm than for 15 and 16 mm.

. for 7/8" OD where RF is apparently lower for 12 mm than for 16 mm.

These result most probably from a data scatter effect which can be expected when only a few data points, each particular category contains.

To get a better synthetic picture, by integrating the 7/8" OD and 3/4" OD test results, all RF values were evaluated as a function of the reduced crack length $c/\sqrt{(Rt)}$, as suggested theoretically (Section 3.1.5.). Fig. 3-3 (f) is taken from Table 3-3 (c); a further reference data point has been added from results published by EDF (25 % pressure increase for a 15 mm long crack tangent to TS in a 7/8" OD tube - (17))

Referring to the theoretical calculations, a shape dependance factor of exp $(-1.28\ x\ \sqrt{(Rt)})$ should be expected, with x being some fraction of the crack length 2 c.

There was good agreement when x was taken to be equal to $\sqrt{2}$ times half of the crack length c (or $1/\sqrt{2}$ times the full crack length).

An overall description of all qualified data tests can be summarized by the following relationship with $1.28\ \sqrt{2} = 1.8$.

$$RF = 1 + 10\ \exp\ (-\ 1.8\ c/\sqrt{(Rt)}) = 1 + 10\ \exp\ (-\ \lambda)$$

This again can be translated into equivalent length margin (see Table 3.3 (d) and Fig. 3-3 (g))

3.3.3.2. Direct verification

For 7/8" OD tubes, the previous statistical analysis predicts a length margin in excess of 2 mm for crack lengths (in free span) in the range of 15 to 17 mm.
Out of 16 tests performed with dual flaws :

For 15 mm long cracks in free span

. 5 failed outside the TS for a 2 mm difference (the inverse behaviour of the 6th case was clearly related to the flaw being 1 mm away from the TS)

- 1 failed outside and 1 failed next to the TS, for a 3 mm difference.

For 17 mm long cracks in free span

- 5 failed outside the TS for a 2 mm difference (the inverse behaviour of the 6th case was associated with unexplained low burst pressure, and was discarded for the statistical analysis).

- 2 failed next to the TS for a 3 mm difference.

This can be considered in excellent agreement with the statistical conclusion.

Similarly, for 3/4" OD tubes, the statistical analysis predicts a length margin in excess of 1.9 mm for crack lengths in free span in the range of 12 to 14 mm.

Out of 16 tests performed with dual flaws :
For 12 mm long cracks in free span

- 1 failed outside the TS and 3 failed next to the TS (with one case of crack initiation outside the TS) for a 2 mm difference.

- 1 failed outside the TS (with crack initiation next to the TS) and 3 failed next to the TS for a 3 mm difference.

For 14 mm long cracks in free span

- 4 failed outside the TS for a 2 mm difference

- 1 failed outside the TS and 3 failed next to the TS for a 3 mm difference.

This is consistent with the statistical conclusions, with the exception of 3 tests (with 12 mm outside TS and 14 mm next to TS) which were considered an abnormal data set within the statistical analysis.

3.3.3.3. Conclusions

Considering the usual data scatter typical of this type of tests (as evidenced by the larger data basis relative to the free span), it is not surprising to observe some local inconsistencies. When all the data are considered, in view of the supporting theory, a reliable (average) quantitative assessment of the reinforcement factor for a crack adjacent to the tubesheet is given by the semi-empirical formulation

$$RF = 1 + 10 \exp(-\lambda)$$

where

$$= [12\,(1 - \nu^2)]^{0.25}\, c/\sqrt{(Rt)} \approx 1.8\, c/\sqrt{(Rt)}$$

Unless further validation becomes available, the domain of application should be restricted to

$$1.5 \le c/\sqrt{(Rt)} \le 2.5$$

i.e. 15 mm $\le$ 2 c $\le$ 20 mm for 7/8" OD tubing
13 mm $\le$ 2 c $\le$ 17 mm for 3/4" OD tubing

which is the useful range when establishing tube plugging limits for axial cracks in the roll transition area.

Table 3-2 (a)

SUMMARY OF RESULTS (program A1)

Material Index	Test-piece number and type	Slit length (mm)	Sealing system	Press-ure (bar)	Flaw width (mm) tip	Flaw width (mm) mid-length outer	Flaw width (mm) mid-length inner	Flaw length (mm)	⌀ max. (mm)	Oval. (%)	Def. (mm)	Leak-age area (mm^2)	Notes
M1	1	15	1	230 ?	1.05	2.4	2	-	23.6		-		1
			2	>250	1.40	18.4	16	49	28		0.4	370	3
	2	20	1	170	0.8	3.3	2.5	-	24.3	-	-	-	1
			2	(234)	1.35	21	18.5	54	27.5	4.5	0.6	450	-
	3 repeated burst	25	1	125	0.45	1.9	1.65	-	23.5	-	-	37	6
			2	150	0.6	2.1	-	-	-	-	-	-	
				(226)	1.35	11	9.2	35	26	-	-	200	
		35 (crack)	2	(138)	0	25.5	23	61	29.5	4.9	0.9	815	4-5
	4	35	1	75	0.4	3.4	2.7	-	24.1	-	-	-	1
			2	(143)	1.35	20.5	18	60	29	5.8	0.8	580	
	5	50	2	(104)	1.35	28.5	26	77	32	6.3	1.9	1150	
			1 + r	150	0.40	0.6	-	-	22.6		-	-	1-6-7
	6	70	2	(89)	1.35	21	18.5	82	29	6.3	> 1.9	920	
			1 + r	180 ?	0.40	1.15	0.95	-	22.8	-	-	-	1-6-7
	7	12	2	320	0.7	1.1	1	-	23	-	-	-	9
			4	(328)	1.3	14.6	12.5	41	27	3.6	0.3	260	
	dual slit	12	2	320	0.65	1	1	-	23	-	-	-	9
			4	328	1.2	2.4	1.7	-	23.7	1	-	-	2

(...) denotes burst pressure

Table 3-2 (a)

SUMMARY OF RESULTS (program A1) (cont'd)

Material Index	Test-piece number and type	Slit length (mm)	Sealing system	Pressure (bar)	Flaw width (mm)			Flaw length (mm)	φ max. (mm)	Oval. (%)	Def. (mm)	Leakage area (mm²)	Notes
					tip	mid-length outer	mid-length inner						
M1	8	15	2	165	0.2	0.35	-	-	-	-	-	-	
				230	0.4	0.7	-	-	-	-	-	-	
				(314)	1.3	9.5	8	31	26	3.1	-	150	13
	dual slit		2	314	0.7	1.5	-	-	23.3	-	-	-	
		15	4	252	0.9	-	-	-	-	-	-	-	10-11
				(252)	1.4	10	8	32	26.2	2.7	-	170	
	9	20	2	120	0.2	0.3	-	-	-	-	-	-	
				160	0.3	0.4	-	-	-	-	-	-	
	dual			200	0.5	1	-	-	-	-	-	-	
	slit			(261)	1.2	22.5	20	59	29	5.4	-	490	13
		20	2	(261)	0.7	1.8	-	-	23.5	-	-	-	
			3	289	1.4	12.4	10.5	38	26.5	3.1/4.4	-	235	10
	10 dual slit repeated burst	35	2	?	1.2	8.1	7.6	38	26	-	-	190	12
		38	2	140	0	9.5	-	-	-	-		-	4
		(crack)		(148)	0	14.5	12.4	46	27	5.5	-	350	13
		20	4	148	0.35	0.6	-	22.6		-	-	-	

(...) denotes burst pressure

Table 3-2 (a)

SUMMARY OF RESULTS (program A1) (cont'd)

Material Index	Test-piece number and type	Slit length (mm)	Sealing system	Pressure (bar)	Flaw width (mm) tip	Flaw width (mm) mid-length outer	Flaw width (mm) mid-length inner	Flaw length (mm)	ø max. (mm)	Oval. (%)	Def. (mm)	Leakage area (mm²)	Notes
M1	11	50	2	65	0.3	0.8	-	-	-	-	-	-	
				80	0.4	1.4	-	-	-	-	-	-	
	dual slit			(99)	1.25	18	15.6	58	28	5.7	1.3	575	
		20	2	99	0.2	0.3	-	-	22.3	-	-	-	
	12	70	2	65	0.5	3	-	-	-	-	-	-	
				75	0.6	5	-	-	-	-	-	-	
				(89)	1.2	22.5	20	79	30	6.3	1.5	925	
	13	20 (minor axis)	2	(243)	1.25	16	13.5	46	27	-	-	330	13-14-15
	dual slit ovalized	20 (major axis)	2	243	0.5	1.2	0.9	-	23.5	-	-		14-16
	15	25	-	50									
				105	0.25	0.3	-						

(...) denotes burst pressure

NOTES FOR TABLES 3-2 (a)

(1) Test arrested after the extrusion of the patch (without rupture)

(2) Crack initiation visible at one flaw tip, from ID surface to mid wall thickness

(3) Burst pressure beyond manometer range

(4) The slit lengthened in the first test is resealed for the second test

(5) Extrusion of the patch

(6) Test conducted with a ring centered over the slit (with a 0.4 mm diametral clearance)

(7) The ring becomes tight for p = 55 bar and becomes loose again when depressurized after p = 150 bar

(8) Manometer valve left closed by omission: inaccurate reading on pump manometer

(9) Maximum pump pressure

(10) Tube recut to perform the test on the second slit

(11) Rupture occuring (after ≈ 30 s) at constant pressure during the visual measurement of the COD

(12) Uncontrolled fast pressure rise, inaccurate reading of the pump manometer, low crack extension (2 and 1.3 mm on both sides, respectively) as a result of the high circumferential excentricity of the patch which is responsible for fast depressurization

(13) Tear of the patch

(14) Ovalized tube

(15) Slit situated on the small diameter (initial width narrowed)

(16) Slit situated on the large diameter (initial width stretched)

TABLE 3-2 (b)

CRACK OPENING DISPLACEMENTS (COD)
VERSUS INTERNAL PRESSURE
(from table 3-2 (a))

2 c (mm)	p_c (bar)	p (bar)	δ (mm)	$\frac{\delta}{c}$ (10^{-3})	$\frac{\delta}{\delta_m}$ *** %	$\frac{p}{p_c}$ * %	Sealing system
12	363	320	0.45	75	68	88	2
		320	0.5	83	75	88	2
		328**	1	167	91	99 (100)	4
15	303	165	0	0	0	54	2
		230	0.2	27	18	76	2
		314**	0.5	67	45	103 (100)	2
		252**	0.8	93	64	83 (100)	4
20	243	170	0.6	60	55	70	1
		120	0	0	0	49	2
		160	0.1	10	9	66	2
		200	0.3	30	27	82	2
		261**	0.5	50	45	107 (100)	2
		148	0.15	15	14	61	4
		99	0	0	0	41	2
25	203	125	0.25	20	23	61	1
		150	0.4	32	36	74	2
35	153	75	0.2	23	18	49	1
50	111	65	0.1	4	9	59	2
		80	0.2	8	18	72	2
70	82	65	0.3	9	27	79	2
		75	0.4	11	36	91	2

* calculated critical pressure
** experimental burst pressure
*** δ_m = 1.1 mm

TABLE 3-2 (c)

SUMMARY OF RESULTS (program A2)

Material Index	Test-piece number and type	Slit length (mm)	Sealing system	Pressure (bar)	Flaw width (mm) tip	Flaw width (mm) mid-length outer	Flaw width (mm) mid-length inner	Flaw length (mm)	φmax (mm) central	φmax (mm) extr.	Oval. (%)	Codes	Notes
M2	16	18	5	161	0.7	3.3	3.2	0.4	24.45	22.15	0.9	0	1-2
		18	10	(182)	0.9	18.7	16.2	43	27	-	4.1	0	
	17	20	9	175	1.15	12.3	10.	33	26.35	22.15	1.8	0	3
		20	10	(219)	1.2	11.8	9.8	32	26.3	-	-	0	
	39	20	8	175	1.05	4.6	3.4	-	24.7	-	1.0	1	2-1
		20	8	175	0.75	4.6	-	-	-	-	-	1	7
		20	10	(252)	1.25	12.6	10.3	32	26.7	-	3.5	?	
M3	23	16.5	12	(256)	0.8	17	15	41	23.2	19.05	4.7	2	
		16.5	12	(279)	1.0	14.6	12.6	33	23.1	-	4.7	2	
	24	16.5	12	(266)	1.0	10.0	8.2	29	22.7	19.05	1.8	4	
		16.5	12	(272)	1.0	9.6	7.8	27	22.5	-	2.6	2	
M4	40	16.5	6	105	0.0	5.5	4.3	35.5	21.2	19.05	1.5	0	9
		16.5	6	105	0.0	1.1		30.0	19.7			0	9

(...) denotes burst pressure

TABLE 3-2 (c)

SUMMARY OF RESULTS (program A2) (cont'd)

Material Index	Test-piece number and type	Slit length (mm)	Sealing system	Pressure (bar)	Flaw width (mm) tip	Flaw width (mm) mid-length outer	Flaw width (mm) mid-length inner	Flaw length (mm)	Φmax (mm) central	Φmax (mm) extr.	Oval. (%)	Codes	Notes
M5	29	16.5	12	(274)	2.0	13.5	11.4	28	23.0	19.1	3.7	4	
		16.5	12	(255)	2.0	13.7	11.5	28	23.0	-	3.7	2	4
	30	16.5	12	(280)	2.0	15.4	14	35	23.3	19.15	4.7	2	5
		16.5	12	(266)	2.1	10.7	9.5	25	22.9	-	2.6	4	5
M6	31	27.5	14	440	1.2	7.0	5.0	-	23.4	20.9	1.0	5	2
		27.5	14	480	1.2	6.6	4.5	-	23.3	20.9	1.0	6	6
	32	27.5	13	414	1.0	5.5	3.9	-	23.2	21.0	1.5	5	2
		27.5	13	414	1.0	5.5	3.9	-	22.7	-	1.5	-	6
M7	33	14.5	7	(208)	0.5	12.0	12.0	40	24.0	20.1	2.8	0	5
		14.5	7	(215)	0.5	12.2	10.9	47	24.2	-	5.0	0	
	34	14.5	7	(214)	0.5	8.9	7.8	36	23.7	20.1	3.5	0	
		14.5	7	(215)	0.5	10.10	-	36	23.6	-	3.5	0	5
	38	14.5	7	(186)	0.4	14.0	-	50.5	26	-	5.0	0	5
		14.5	7	186	0.35	0.8	-	-	-	-	-	0	7
		14.5	7	(220)	0.6	13.0	-	45	23.9	-	5.0	0	5
		14.5	7	220	0.35	1.0	-	-	-	-	-	0	7

(...) denotes burst pressure

TABLE 3-2 (c)

SUMMARY OF RESULTS (program A2) (cont'd)

Material Index	Test-piece number and type	Slit length (mm)	Sealing system	Pressure (bar)	Flaw width (mm) tip	Flaw width mid-length outer	Flaw width mid-length inner	Flaw length (mm)	ϕ_{max} (mm) central	ϕ_{max} (mm) extr.	Oval. (%)	Codes	Notes
M8	35	14.5	7	(171)	0.7	100	-	33	23.7	20.0	3.0	0	5
		14.5	7	(164)	0.7	3.45	-	+ 2	21.8	-	0.5	0	4-6
	36	14.5	7	(190)	0.7	12.9	-	41.5	23.6	-	4.5	0	5
		14.5	7	(170)	0.7	17.0	-	38	24.2	-	3.0	0	4
	37	14.5	7	(150)	0.5	13.0	-	39	25.0	20.0	2.5	0	5
		14.5	7	150	0.3	0.8	-	-	-	-	-	0	7

(...) denotes burst pressure

NOTES FOR TABLES 3-2 (c)

(1) A stable crack growth is observable prior to the instability of precracked slit.
Slit N°. : 1: (161 bar) both sides (+ 0.1 and + 0.3 mm)
Slit N°. : 2 : (167 bar) at one side (+ 0.1 mm)

(2) Test arrested after patch leak and not reconducted

(3) Burst pressure abnormaly low, for the same pressure a slight initiation of crack is observed on the second slit

(4) The critical pressure of the second defect is lower than that already sustained by bursting of the first defect (both defects were the same)

(5) Both defects propagated in a non-axial maner.
The length was measured as shown below.

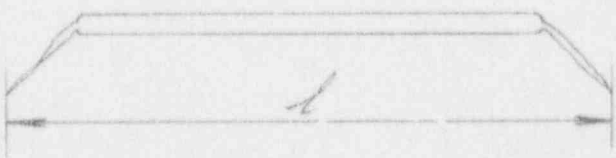

(6) The burst pressure could never be reached because the flaw opening was large enough to permit every patch to be extruded

(7) Slit parallel to the previous one

(8) Slight crack initiation detectable at one tip

(9) Fatigue crack propagation (f = 4 Hz), faster than expected (long crack propagation). Test arrested after patch bursting at about 17,100 cycles.
Test parameters :
11,600 cycles at p = 85 to 90 bar (higher than 80 specified)
800 cycles at p = 105 to 55 bar
1,800 cycles at p linearly decreasing from 105 to 55 bar
1,500 cycles at p = 50 to 55 bar
1,400 cycles at p decreasing from 50 to 0 bar.

Code	Description of patch after tube burst
0	no patch
1	stay in place
2	extruded without break
4	break orthogonal to the slit
5	orthogonal twin breaks (at both flaw tips)
6	orthogonal breaks in the center.

TABLE 3-2 (d)

PROGRAM A2
MEASUREMENTS OF : COD (δ); SLIT OPENING (b)
AND BULGING (ϕ_{max}) VERSUS INTERNAL PRESSURE

Material Index	Test-piece Number and type	Slit length (mm)	Sealing System	p bar	δ mm	b mm	ϕ_{max} mm	p/p_{max}
M2	16	18	5	80	.03	.03		0.44
			5	120	.10	.15		0.66
			5	161	.70	3.3	24.45	0.89
	dual slit	18	5	80	.05			0.44
			5	120	.08			0.66
			5	161	.70		23.6	0.89
			5	167	.90	3.6	24.3	0.92
			10	(182)	(.9)	16.2	27.0	1.00
	17 dual slit	20	9	125		0.65		
			9	175	.40	2.8	23.9	0.80
			10	(219)	(1.2)	11.8	26.3	1.00
	39	20	8	127	.20	.75	22.5	0.50
			8	141	.35	1.4	23.0	0.56
			8	155	.85	2.5	23.5	0.62
			8	175	1.05	4.6	24.6	0.69
	2 // slit + 1 alone	20	8	127	.20	.75	22.5	0.50
			8	141	.35	1.4	23.0	0.56
			8	155	.60	2.3	23.5	0.63
			9	175	1.05	4.3	24.5	0.69
		20	8	127	.10	.60	22.4	0.50
			8	141	.25	1.0	22.7	0.56
			8	155	.45	1.6	23.2	0.62
			8	175	.75	2.8	23.8	0.69
			10	(252)	(1.25)	12.6	26.7	1.00
M3	23 dual slit	16.5	7	200	.75	2.7	20.6	0.78
			12	250	.80		20.7	0.98
			12	(256)	(.80)	17	23.2	1.00
		16.5	7	200	.15	.7	19.5	0.72
			12	250	.55	1.7	20.0	0.90
			12	256	.60	1.9	20.2	0 92
			12	(279)	(1.0)	12.6	23.1	1.00

(...) denotes burst pressure

TABLE 3-2 (d) (cont'd)

PROGRAM A2
MEASUREMENTS OF : COD (δ); SLIT OPENING (b)
AND BULGING (ϕ_{max}) VERSUS INTERNAL PRESSURE

Material Index	Test-piece Number and type	Slit length (mm)	Sealing System	p	δ	b	ϕ_{max}	p/p_{max}
				bar	mm	mm	mm	
M3	24	16.5	7	170	.15	.45	19.4	0.64
			7	192	.30	1.0	19.8	0.72
	dual		12	246	.70	2.5	20.6	0.92
	slit		12	(266)	(1.0)	10.0	22.7	1.00
		16.5	7	170	.15	.45	19.4	0.62
			7	192	.30	1.0	19.8	0.71
			12	246	.70	2.5	20.6	0.91
			12	266	.90	3.9	20.9	0.98
			12	(272)	(1.0)	9.6	22.5	1.00
M5	29	16.5	7	147	.15	.7	19.4	0.54
			7	166	.30	1.5	19.9	0.61
	dual		7	190	.55	2.0	20.5	0.69
	slit		12	218	.75	2.8	20.7	0.80
			12	241	1.25	3.7	21.1	0.88
			12	260	2.0	5.1	22.2	0.95
			12	(274)	(2.0)	13.5	23.0	1.00
	29	16.5	7	147	.15	-	19.4	0.54
			7	166	.30	1.25	19.9	0.61
	dual		7	190	.55	2.0	20.5	0.69
	slit		12	218	.75	2.8	20.7	0.80
			12	241	1.25	3.7	21.1	0.88
			12	260	2.0	5.1	22.0	0.95
			12	(255)	(2.0)	13.7	23.0	-
	30	16.5	12	140	.05	.35	19.2	0.50
			12	172	.20	.70	19.5	0.61
	dual		12	195	.50	1.4	20.0	0.70
	slit		12	220	1.70	2.5	20.4	0.79
			12	265	2.0	5.7	21.6	0.95
			12	(280)	(2.0)	15.4	23.3	1.00
		16.5	12	140	.05	.35	19.2	0.50
			12	172	.20	.70	19.4	0.61
			12	195	.40	1.25	19.8	0.70
			12	220	.65	2.15	20.3	0.79
			12	265	1.55	4.8	21.4	0.95
			12	280	1.9	5.4	21.6	1.00
			12	(266)	(2.1)	10.7	22.9	-
M6	31	27.5	13	320	.05	.55	21.0	(0.52)
			13	372	.30	1.6	21.5	(0.61)
	dual		14	415	.90	5.4	22.8	(0.68)
	slit		14	440	1.20	7.0	23.4	(0.72)

(...) denotes burst pressure

TABLE 3-2 (d) (cont'd)

PROGRAM A2
MEASUREMENTS OF : COD (δ); SLIT OPENING (b)
AND BULGING (ϕ_{max}) VERSUS INTERNAL PRESSURE

Material Index	Test-piece number and type	Slit length (mm)	Sealing System	p	δ	b	ϕ_{max}	p/p_{max}
				bar	mm	mm	mm	
M6	31	27.5	[illegible]	320	.05	.55	21.0	(0.52)
			13	[illegible]	.15	.95	21.2	(0.61)
	dual		14	415	.50	3.2	22.0	(0.68)
	slit		14	440	1.10	6.5	23.2	(0.72)
			14	480	1.20	6.6	23.3	(0.79)
	32	27.5	13	260	.05	.30	21.0	(0.43)
			13	320	.15	1.0	21.3	(0.53)
	dual		13	370	.50	3.0	22.1	(0.61)
	slit		13	414	1.0	5.5	23.2	(0.68)
		27.5	13	260	.05	.30	21.0	(0.43)
			13	320	.15	1.0	21.2	(0.53)
			13	370	.50	2.7	22.0	(0.61)
			13	414	1.0	5.5	22.7	(0.68)
M7	33	14.5	7	147	.05	.45	20.4	0.71
			7	168	.15	.65	20.5	0.81
	dual		7	190	.25	1.05	20.9	0.91
	slit		7	(208)	(.5)	12.0	24.0	1.00
		14.5	7	162	.05	.45	20.4	0.68
			7	168	.15	.65	20.5	0.78
			7	190	.25	1.05	20.9	0.88
			7	208	.30	1.10	20.9	0.97
			7	(215)	(.5)	12.2	24.2	1.00
	34	14.5	7	162	.10	.35	20.3	0.76
			7	192	.25	.75	20.7	0.90
	dual		7	210	.40	1.2	21.0	0.98
	slit		7	(214)	(.5)	8.9	23.7	1.00
		14.5	7	162	.10	.35	20.3	0.76
			7	192	.25	.70	20.7	0.90
			7	210	.40	1.1	21.0	0.98
			7	214	.45	1.25	21.0	1.00
			7	(215)	(.5)	10.0	23.6	1.00
	38	14.5	7	150	.10	.55	20.6	0.81
			7	170	.20	.85	21.0	0.91
			7	180	.35	1.1	21.3	0.97
			7	(186)	(.4)	1.4	-	1.00
	2 // slit							
		14.5	7	150	.10	.55	20.6	0.81
			7	170	.20	.85	21.0	0.91
			7	180	.35	1.1	21.3	0.97
			7	186	.35	14	-	1.00

(...) denotes burst pressure

TABLE 3-2 (d) (cont'd)

PROGRAM A2
MEASUREMENTS OF : COD (δ); SLIT OPENING (b)
AND BULGING (ϕ_{max}) VERSUS INTERNAL PRESSURE

Material Index	Test-piece Number and type	Slit length (mm)	Sealing System	p	δ	b	ϕ_{max}	p/p_{max}
				bar	mm	mm	mm	
M7	38	14.5	7	150	.10	.45	20.3	0.68
			7	170	.20	.65	20.4	0.77
			7	186	.30	.9	20.8	0.85
			7	(220)	(.6)	13	23.9	1.00
	2 // slit	14.5	7	150	.10	.45	20.3	0.68
			7	170	.20	.65	20.4	0.77
			7	186	.30	.9	20.8	0.85
			7	220	.35	1.0	-	1.00
M8	35	14.5	7	119	.05	.35	20.1	0.70
			7	136	.15	.70	20.5	0.80
			7	153	.30	1.20	20.9	0.90
			7	(171)	(.7)	10.0	23.7	1.00
	dual slit	14.5	7	119	.05	.35	20.1	0.70
			7	136	.15	.70	20.5	0.80
			7	153	.30	1.20	20.9	0.90
			7	171	.60	1.85	21.4	1.00
			7	(164)	(.7)	3.45	21.8	-
	36	14.5	7	120	.05	.35	20.1	0.63
			7	143	.15	.60	20.3	0.75
			7	160	.30	1.05	20.8	0.84
			7	(190)	(.7)	17	23.6	1.00
	dual slit	14.5	7	120	.05	.35	20.1	0.63
			7	143	.15	.60	20.3	0.75
			7	160	.30	1.05	20.8	0.84
			7	190	.70	2.0	21.6	1.00
			7	(170)	(.7)	13	24.2	-
	37	14.5	7	116	.05	.5	20.3	0.77
			7	140	.45	1.0	20.8	0.93
			7	(150)	(.5)	13	25	1.00
	2 // slit	14.5	7	116	.05	.5	20.3	0.77
			7	140	.30	.8	20.6	0.93
			7	150	.30	.8	-	1.00

(...) denotes burst pressure

TABLE 3-2 (e)

PROGRAMS A3 AND A4 - CORRELATION OF FLOW STRESS WITH (YS + UTS)
FOR ALL AXIAL CRACKS IN FREE SPAN

DATA SET	REF N°.	2 c mm	m	p_c bar	K =7.75 mp_c/(YS + UTS) RAW	ADJUSTED	COMMENT
7/8" - 71692	D1	15	2.40	335	0.627	0.614	
EDM flaw	D3			>310	>0.581	>0.569	failed at +3 next to TS
√(RT) = 3.65 mm	D6			308	0.577	0.565	
YS+UTS = 993 MPa	D8			280	0.524	0.514	
	D1*			300	0.562	0.551	
	D2*			312	0.584	0.572	
	D3*			317	0.594	0.582	
	D4*			>309	>0.579	>0.567	failed at +2 next to TS
	P4	16	2.51	297	0.582	0.570	
	P8			303	0.594	0.582	
	P10			297	0.582	0.570	
	P13			268	0.525	0.515	
	P50*			274	0.537	0.526	
	P52*			265	0.519	0.509	
	P54*			292	0.572	0.561	
	P61*			265	0.519	0.509	
	Y16-1			286	0.560	0.549	
	Y16-2			282	0.552	0.541	
	Y16-3			297	0.582	0.570	
	N2			285	0.558	0.547	
	N7			275	0.539	0.528	
	D2	17	2.63	>278	>0.571	>0.560	failed at +3 next to TS
	D4			305	0.626	0.613	

TABLE 3-2 (e) (cont'd)

PROGRAMS A3 AND A4 - CORRELATION OF FLOW STRESS WITH (YS + UTS)
FOR ALL AXIAL CRACKS IN FREE SPAN

DATA SET	REF N°.	2 c mm	m	p_c bar	K = 7.75 mp_c / (YS + UTS) RAW	ADJUSTED	COMMENT
	D5			>242	>0.497	>0.487	failed at +3 next to TS
	D7			(>220)	(>0.451)		abnormally low
	D5*			281	0.577	0.565	
	D6*			286	0.587	0.575	
	D7*			290	0.595	0.583	
	D8*			286	0.587	0.575	
	Y18-4	18	2.75	250	0.537	0.526	
	Y18-5			238	0.511	0.501	
	F7			270	0.579	0.567	machined at 0.8 mm width
	F8			260	0.558	0.547	
	F9			245	0.526	0.515	prior 0.2 % expansion
	F10			282	0.605	0.593	for # 7 and 8
	P15*	19	2.87	245	0.549	0.538	
	P30*			235	0.526	0.515	
	P51*			228	0.511	0.501	
	P53*			232	0.520	0.510	
7/8" - 71692	N34	15.5	2.46	278	0.534	0.534	
fatigue crack	N33	18	2.75	268	0.575	0.575	
√(RT) = 3.65 mm	N37	19	2.87	244	0.547	0.547	
YS+UTS = 993 MPa	N36	19.5	2.93	233	0.533	0.533	

TABLE 3-2 (e) (cont'd)

PROGRAMS A3 AND A4 - CORRELATION OF FLOW STRESS WITH (YS + UTS)
FOR ALL AXIAL CRACKS IN FREE SPAN

DATA SET	REF N°.	2 c mm	m	p_c bar	K =7.75 mp_c/(YS + UTS) RAW	ADJUSTED	COMMENT
7/8" - 71692	N1	16	2.51	310	0.607	0.577	(65) µm nickel
EDM flaw	N6			310	0.607	0.577	120
nickel plated	N8			273	0.535	0.508	105
√(RT) = 3.65 mm	N9			285	0.558	0.530	120
YS+UTS = 993 MPa	N10			285	0.558	0.530	55
	N11			287	0.562	0.534	75
7/8" - 71692	N23	12	2.05	371	0.594	0.564	85 µm nickel
fatigue crack	N25	12.5	2.11	328	0.540	0.513	125
nickel plated	N27			368	0.606	0.576	170
√(RT) = 3.65 mm	N26	14	2.28	360	0.641	0.609	
YS+UTS = 993 MPa	N28	15.5	2.46	298	0.572	0.543	120
	N40	17	2.63	272	0.558	0.530	130
	N43			289	0.593	0.563	155
	N5	18	2.75	(320)	(0.687)		120] abnormally
	N35			(313)	(0.672)		120] high
	N24	23	3.34	217	0.566	0.538	(105)
7/8" - 74749 (TT)	N3*	16	2.51	237	0.591	0.550	160 µm nickel
EDM flaw	N4*			248	0.618	0.575	115
nickel plated	N5*			238	0.594	0.553	120
√(RT) = 3.65 mm	N6*			243	0.606	0.564	115
YS+UTS = 780 MPa	N7*			249	0.621	0.578	115
	N10*			236	0.589	0.548	120

TABLE 3-2 (e) (cont'd)

PROGRAMS A3 AND A4 - CORRELATION OF FLOW STRESS WITH (YS + UTS)
FOR ALL AXIAL CRACKS IN FREE SPAN

DATA SET	REF	2 c	m	p_c	$K = 7.75\, m p_c/(YS + UTS)$		COMMENT
	N°.	mm		bar	RAW	ADJUSTED	
3/4" - 70699	K1	12	2.27	331	0.536	0.525	
EDM flaw	K2			≥314	≥0.509	≥0.499	crack initiated but tube
√(RT) = 3.13 mm							failed at +2 next to TS
YS+UTS = 1086 MPa	K3			330	0.535	0.524	
	K4			>350	>0.570	>0.559	failed at +3 next to TS
	K9			>325	>0.526	>0.515	failed at +2 next to TS
	K10			>340	>0.551	>0.540	id.
	K15			>296	>0.480	>0.470	failed at +3 next to TS
	K16			>366	>0.593	>0.581	id.
	K5	14	2.55	313	0.570	0.559	
	K6			298	0.542	0.531	
	K7			>312	>0.568	>0.557	failed at +3 next to TS
	K8			>336	>0.611	>0.599	id.
	K11			297	0.540	0.529	
	K12			287	0.522	0.512	
	K13			297	0.540	0.529	
	K14			>278	>0.506	>0.496	failed at +3 next to TS

* Adjusted values of K, differing by more than 15 % from the average (0.545) have been disregarded ($K < 0.46$ or $K > 0.63$).

TABLE 3-2 (f)

PROGRAMS A3 AND A4 - CORRELATION OF FLOW STRESS WITH (YS + UTS)
FOR ALL AXIAL CRACKS ADJACENT TO TUBESHEET IN 7/8" OD TUBING
(batch 71692; YS + UTS = 993 MPa; $\sqrt{(Rt)}$ = 3.65 mm)

DATA SET	REF N°.	2 c mm	m	p_c bar	$K = \frac{7.75\ m p_c}{YS + UTS}$	RF*	COMMENT
Flaw tip tangent to tubesheet	P1	12	2.05	418	0.669		
	P2			415	0.664		
	P3			394	0.630	1.177	
	P5	16	2.51	348	0.682		
	P6			320	0.627		
	P9			334	0.654	1.184	
	P11			342	0.670		
	D1	17	2.63	> 335	> 0.688		failed at -2 in free span
	D8			> 280	> 0.575		failed at -2 in free span
	D1*			> 300	> 0.616		failed at -2 in free span
	D2*			> 312	> 0.640	>1.140	failed at -2 in free span
	D3*			> 317	> 0.651		failed at -2 in free span
	D4*			> 309	> 0.634		crack tip 1 mm from TS
	Y18G1	18	2.75	286	0.614		
	Y18G2			295	0.633		
	Y18G3			272	0.584		
	D3	18	2.75	310	0.665		
	D6			> 308	> 0.661	1.135	failed at -3 in free span

TABLE 3-2 (f) (cont'd)

PROGRAMS A3 AND A4 - CORRELATION OF FLOW STRESS WITH (YS + UTS)
FOR ALL AXIAL CRACKS ADJACENT TO TUBESHEET IN 7/8" OD TUBING
(batch 71692; YS + UTS = 993 MPa; √(Rt) = 3.65 mm)

DATA SET	REF N°.	2 c mm	m	p_c bar	$K = \frac{7.75\ m p_c}{YS + UTS}$	RF*	COMMENT
Flaw tip	P13*	19	2.87	257	0.576		
tangent to	P14*			252	0.564		
tubesheet	D4			(>305)	(>0.683)		abnormally high
	D7			?(220)	(0.493?)		abnormally low
	P60*			(>235)	(>0.526)		slipping ring (unvalid)
	P7*			245	0.549	>1.077	┐ underrolled
	P8*			252	0.564		│ in minimum
	P9*			257	0.576		┘ clearance
	D5*			> 281	> 0.629		┐
	D6*			> 286	> 0.641		│
	D7*			> 290	> 0.650		│ failed at ~2 in free span
	D8*			> 286	> 0.641		┘
	P15	20	2.99	254	0.569		
	P16			263	0.589		
	D2			278	0.623	1.044	
	D5			242	0.542		
	P17	24	3.46	217	0.586		
	P20			203	0.548	1.020	

TABLE 3-2 (f) (cont'd)

PROGRAMS A3 AND A4 - CORRELATION OF FLOW STRESS WITH (YS + UTS)
FOR ALL AXIAL CRACKS ADJACENT TO TUBESHEET IN 7/8" OD TUBING
(batch 71692; YS + UTS = 993 MPa; $\sqrt{(Rt)}$ = 3.65 mm)

DATA SET	REF N°.	2 c mm	m	p_c bar	$K = \frac{7.75\ m p_c}{YS + UTS}$	RF*	COMMENT
Flaw tip within tubesheet	P14	16	2.51	322	0.631	1.084	20 mm total length
	P18			292	0.572		24 mm total length
	P19			309	0.605		24 mm total length
	Y24C1	18	2.75	270	0.579	1.046	
	Y24C2			272	0.584		
	Y24D1	19	2.87	232	0.520		24 mm total length
	Y24D2			250	0.560		24 mm total length
	Y24D3			250	0.560		24 mm total length
	Y24F1			260	0.582		24 mm total length
	Y24F2			245	0.549	1.005	24 mm total length
	P10*			247	0.553		38 mm total length
	P11*			256	0.573		underrolled in
	P12*			256	0.573		minimum clearance

TABLE 3-2 (f) (cont'd)

PROGRAMS A3 AND A4 - CORRELATION OF FLOW STRESS WITH (YS + UTS)
FOR ALL AXIAL CRACKS ADJACENT TO TUBESHEET IN 7/8" OD TUBING
(batch 71692; YS + UTS = 993 MPa; $\sqrt{(Rt)}$ = 3.65 mm)

DATA SET	REF N°.	2 c mm	m	p_c bar	$K = \frac{7.75\ m p_c}{YS + UTS}$	RF*	COMMENT
Flaw tip away from tubesheet	P7	16	2.51	(342)	(0.670)		8 mm from TS
	P12			278	0.545		one value abnormally high
	P4*	19	2.87	242	0.542		tangent to TS but
	P5*			242	0.542		underrolled (5 mm)
	P6*			237	0.531	0.961	in large clearance
	P1*			233	0.522		8 mm from TS underrolled
	P2*			(215)	(0.482)		in minimum clearance
	P3*			235	0.526		one value abnormally low

* The reinforcement factor (RF) is calculated by 0.98 (average of K)/0.545.
Individual values of K differing by more than 10 % from the average have been diregarded.

TABLE 3-2 (g)

PROGRAMS A3 AND A4 - CORRELATION OF FLOW STRESS WITH (YS + UTS)
FOR ALL AXIAL CRACKS ADJACENT TO TUBESHEET IN 3/4" OD TUBING
(batch 75317; YS + UTS = 1086 MPa; $\sqrt{(Rt)}$ = 3.13 mm)

DATA SET	REF N°.	2 c mm	m	p_c bar	$K = \frac{7.75\ m p_c}{YS + UTS}$	RF*	COMMENT
Flaw tip tangent to tubesheet	K1	14	2.55	> 331	> 0.602		failed at -2 in free span
	K2			314	0.571		
	K9			325	0.591		
	K10			340	0.619	1.071	
	K3	15	2.69	≥ 330	≥ 0.633		crack initiation but tube
	K4			350	0.672		failed at -3 in free span
	K15			(296)	(0.568)	1.204	abnormally low
	K16			366	0.703		
	K5	16	2.83	> 313	> 0.632		failed at -2 in free span
	K6			> 298	> 0.602		failed at -2 in free span
	K11			> 297	> 0.600	>1.085	failed at -2 in free span
	K12			> 287	> 0.580		failed at -2 in free span
	K7	17	2.97	312	0.661		
	K8			(336)	(0.712)		abnormally high
	K13			> 297	> 0.629	1.126	failed at -3 in free span
	K14			278	0.589		

* The reinforcement factor RF is calculated by 0.98 (average of K)/0.545.
Individual values of K differing by more than 10 % from the average have been diregarded.

TABLE 3-3 (a)
CORRELATION BETWEEN σ_f, UTS AND YS (from test results on axial through Wall Flaws

Metallurgical Data			Geometrical Data					Experimental Data					Correlation Criteria				Note
MATERIAL INDEX	YS*	UTS*	R	t	2c	$\frac{C}{\sqrt{RT}}$	m	COD	p_c (MPa)		σ_c	σ_f	UTS-σ_f	$\frac{\sigma_f}{UTS}$	$\frac{\sigma_f - YS}{UTS-YS}$	$\frac{\sigma_f}{UTS+YS}$	(1)
	MPa	MPa	mm	mm	mm	-	-	mm	ind.	mean	MPa	MPa	MPa				
M1	385	700	10.5	1.27	VARIOUS			1.0	VARIOUS			605	95	.86	.70	.56	(2)
M2	335	619	10.4	1.35	20	2.67	2.94	1.2	21.9 25.2	23.5	181	530	70	.88	.66	.56	(3)
M3	380	675	8.95	1.05	16.5	2.57	2.89	1.0	25.6 26.6 27.2 27.9	26.8	209	605	60	.91	.78	.57	
M5	335	635	8.95	1:20	16.5	2.52	2.87	2.0	27.4 27.4 28.0 28.0	27.7	207	595	55	.91	.82	.61	(4)
M7	605	760	9.7	0.77	14.5	2.66	2.93	.5	20.8 21.4 21.5 21.5	21.3	267	780	20	.98	.88	.57	
M8	590	685	9.6	0.71	14.5	2.77	2.98	.7	17.1 17.1 19.0 19.0	18.0	245	730	-20	1.03	1.21	.57	(4)

Formulas used in the calculation

$R = (\phi - t)/2$

$m = 0.614 + 0.386\, e^{-2.25\, C/\sqrt{(RT)}} + 0.866 \frac{C}{\sqrt{(RT)}}$

$\sigma_c = p_c \frac{R}{t}$

$\sigma_f = m\sigma_c$ (not true flow stress)

Notes

(1) Tests on parallel slits and on fatigue precracked specimen are not included
(2) Values from the program A1
(3) An abnormal low burst pressure (p_c = 17.5 MPa) was disregarded
(4) The second slit of each specimen bursted at a lower pressure than the first one; the first (higher) value was retained

* from table 2-1 (values rounded off to the next 5 MPa)

TABLE 3-3 (b)

PROGRAMS A3 AND A4 - STATISTICAL ANALYSIS OF σ_f/(YS+UTS)

	COMBINATION OF 86 "QUALIFIED" DATA POINTS								
	7/8" - heat 1						3/4"		7/8" heat 2
	UNPLATED				PLATED		UNPLATED		PLATED
	EDM			CRACK	EDM	CRACK	EDM		EDM
	BURST		UNBURST	BURST	BURST	BURST	BURST	UNBURST	BURST
DATA SET	1*	2**	3	4	5	6	7	8	9
nr	34	8	4	4	6	8	7	9	6
AVG	0.561	0.543	>0.555	0.547	0.571	0.584	0.541	>0.545	0.603
Σ	0.033	0.020	0.045	0.020	0.029	0.032	0.015	0.046	0.014
nr	46				14		16		
AVG	0.557				0.578		0.543		
Σ	0.032				0.030		0.035		
ADJUSTMENT	0.98			1	0.95		0.98		0.98 x0.95
AVG	0.546			0.547	0.549		0.532		0.562
Σ	0.031			0.020	0.029		0.034		0.013
nr	64								
AVG	0.547								
Σ	0.030								
nr	80								
AVG	0.544								
Σ	0.030								
nr	86								
AVG	0.545								
Σ	0.030								

* without tubesheet simulation

** with negligible effect from tubesheet

TABLE 3-3(c)

PROGRAM A4 - TUBESHEET REINFORCING FACTOR (66 cases)

ø	CONDITION	NUMBER OF CASES	2 c (mm)	$\frac{2c}{\sqrt{(RT)}}$	RF
7/8" OD	a. flaw tip tangent to tube-sheet	3	12	3.29	1.177
		4	16	4.38	1.184
		6	17	4.66	>1.140
		5	18	4.93	1.135
		9	19	5.21	>1.077
		4	20	5.48	1.044
	b. flaw tip within tubesheet	3	16	4.38	1.084
		2	18	4.93	1.046
		8	19	5.21	1.005
	c. flaw tip away from tubesheet (distance of farthest point)	8	≥24	≥6.58	0.976
3/4" OD	d. flaw tip tangent to tube-sheet	4	14	4.47	1.071
		3	15	4.79	1.204
		4	16	5.11	>1.085
		3	17	5.43	1.126

TABLE 3-3 (d)

PROGRAM A4 - TUBESHEET REINFORCING FACTOR
EXPRESSED AS CRITICAL CRACK
LENGTH MARGIN

ø	2C* mm	C*/√(Rt)	m*	RF	m = m*xRF	C/√(Rt)	2 C mm	(2C) mm
7/8" OD	15	2.055	2.397	1.247	1.922	1.495	10.9	4.1
	16	2.192	2.515	1.193	2.108	1.715	12.5	3.5
	17	2.329	2.633	1.151	2.288	1.928	14.1	2.9
	18	2.466	2.751	1.118	2.461	2.130	15.5	2.5
	19	2.603	2.869	1.092	2.627	2.322	17.0	2.0
	20	2.740	2.988	1.072	2.787	2.508	18.3	1.7
3/4" OD	12	1.917	2.279	1.317	1.730	1.263	7.9	4.1
	13	2.077	2.416	1.238	1.952	1.532	9.6	3.4
	14	2.236	2.552	1.179	2.165	1.783	11.2	2.8
	15	2.396	2.691	1.134	2.373	2.027	12.7	2.3
	16	2.556	2.829	1.100	2.572	2.258	14.1	1.9
	17	2.716	2.967	1.075	2.760	2.477	15.5	1.5

C and m refer to crack in free span
C* and m* refer to crack adjacent to tubesheet TS
$m = 0.614 + 0.386 \exp(-2.25\, c/\sqrt{Rt}) + 0.866\, c/\sqrt{Rt}$
$RF = 1 + 10 \exp(-1.8\, c^*/\sqrt{Rt})$

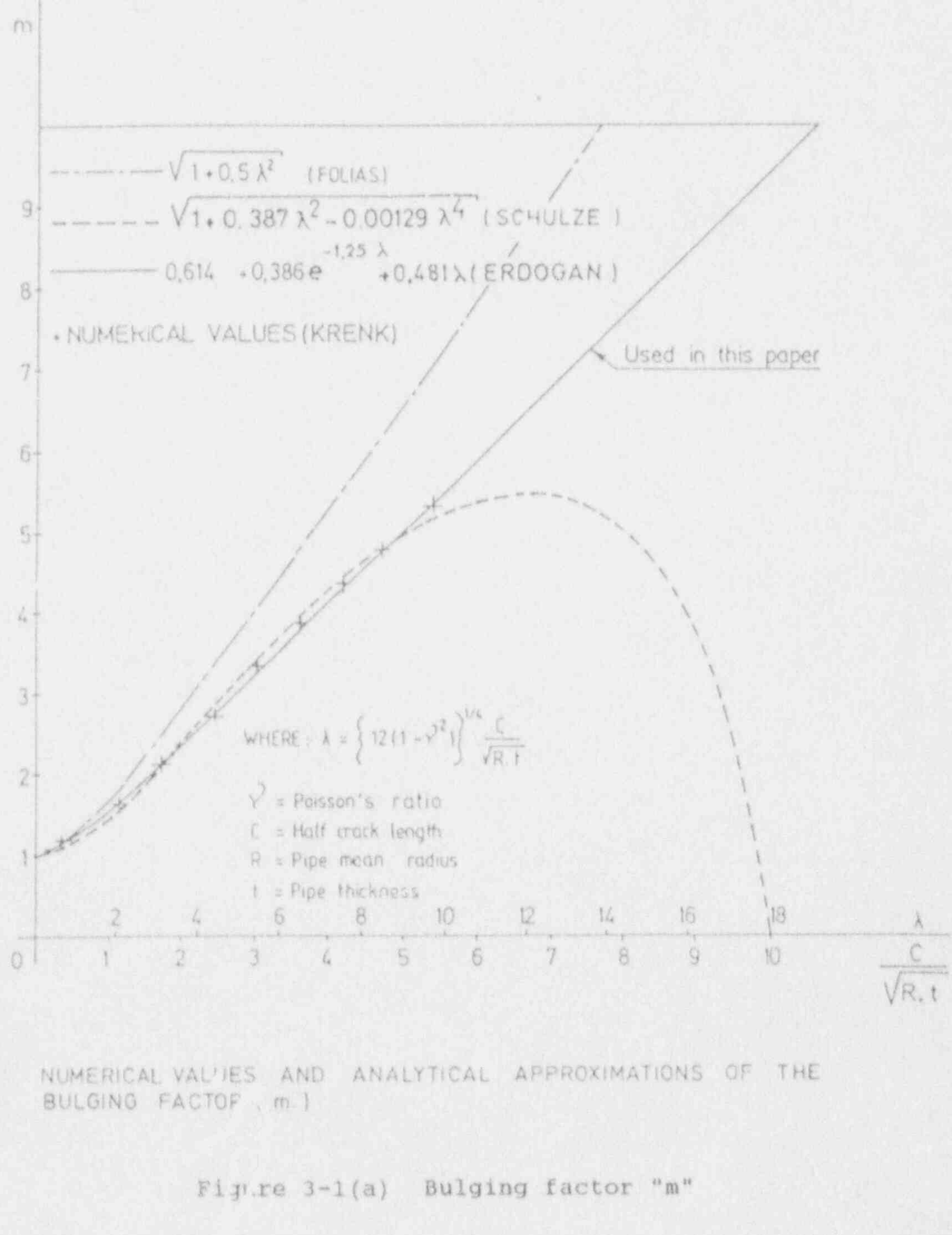

NUMERICAL VALUES AND ANALYTICAL APPROXIMATIONS OF THE BULGING FACTOR (m)

Figure 3-1(a) Bulging factor "m"

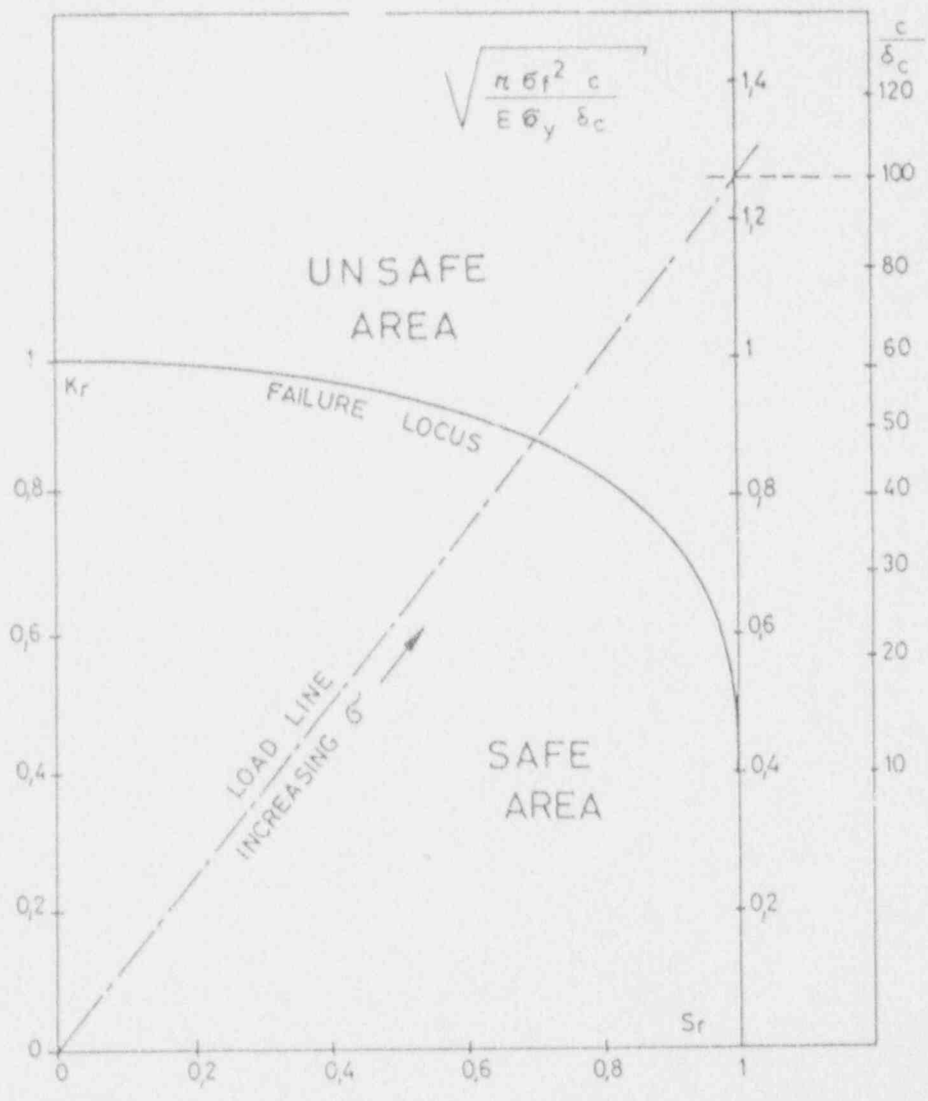

Figure 3-1(b) Universal "two parameter design curve"

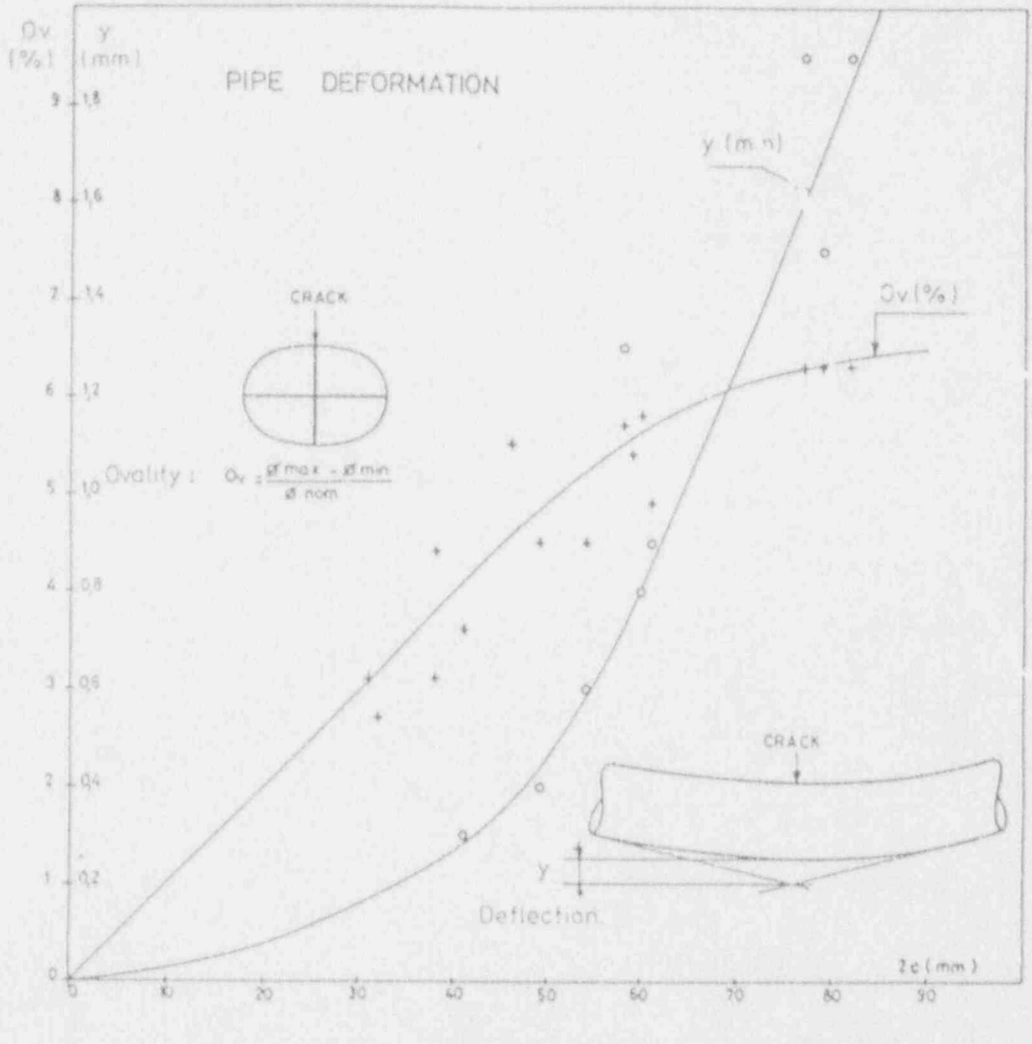

Figure 3-2(a) General tube deformation (deflection, ovality at the crack tips) as a function of the final crack length (from tables 3-2(a); (b))

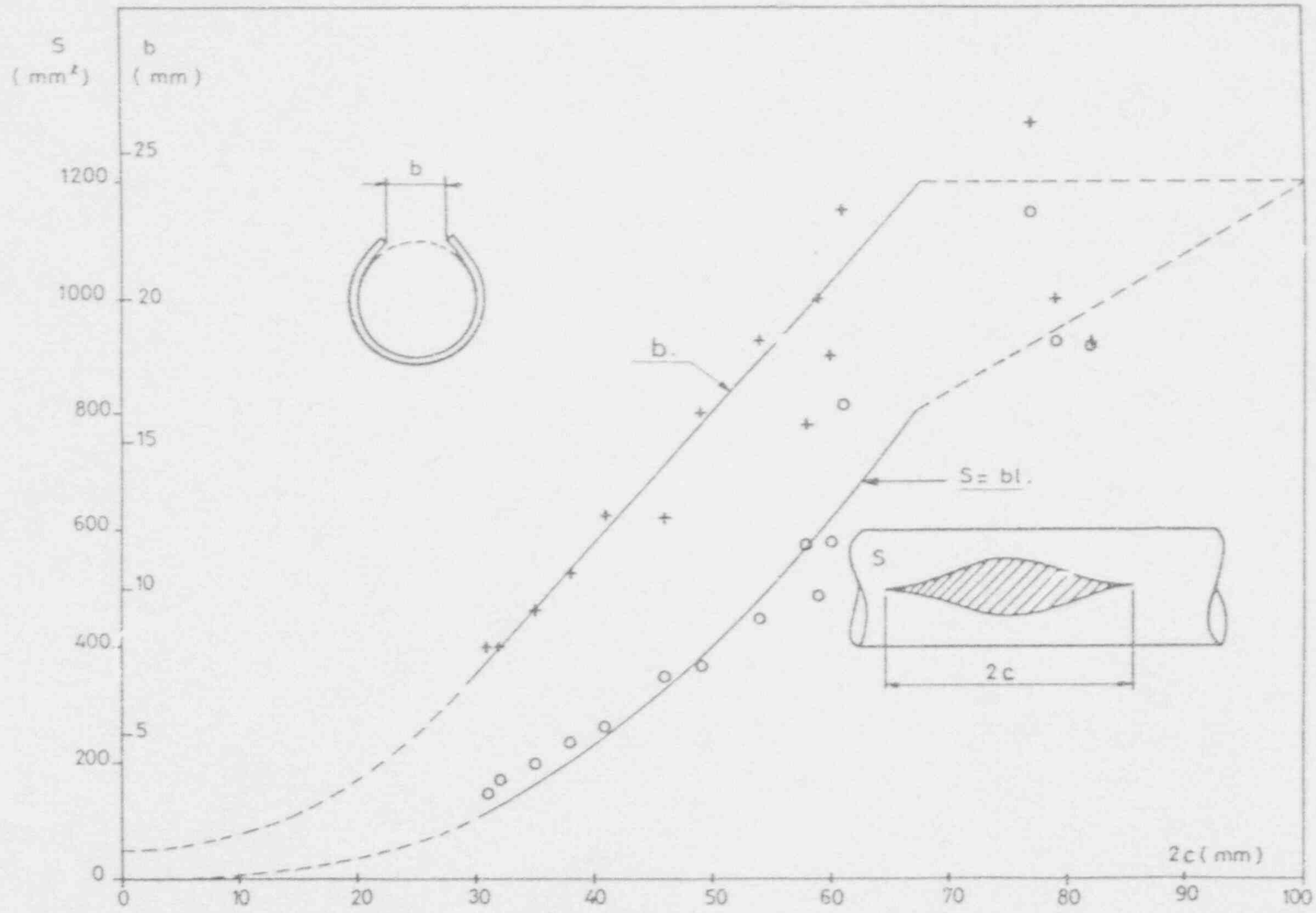

Figure 3-2(b) Flaw width and leakage area, as a function of the final crack length (from tables 3-2(a); (b))

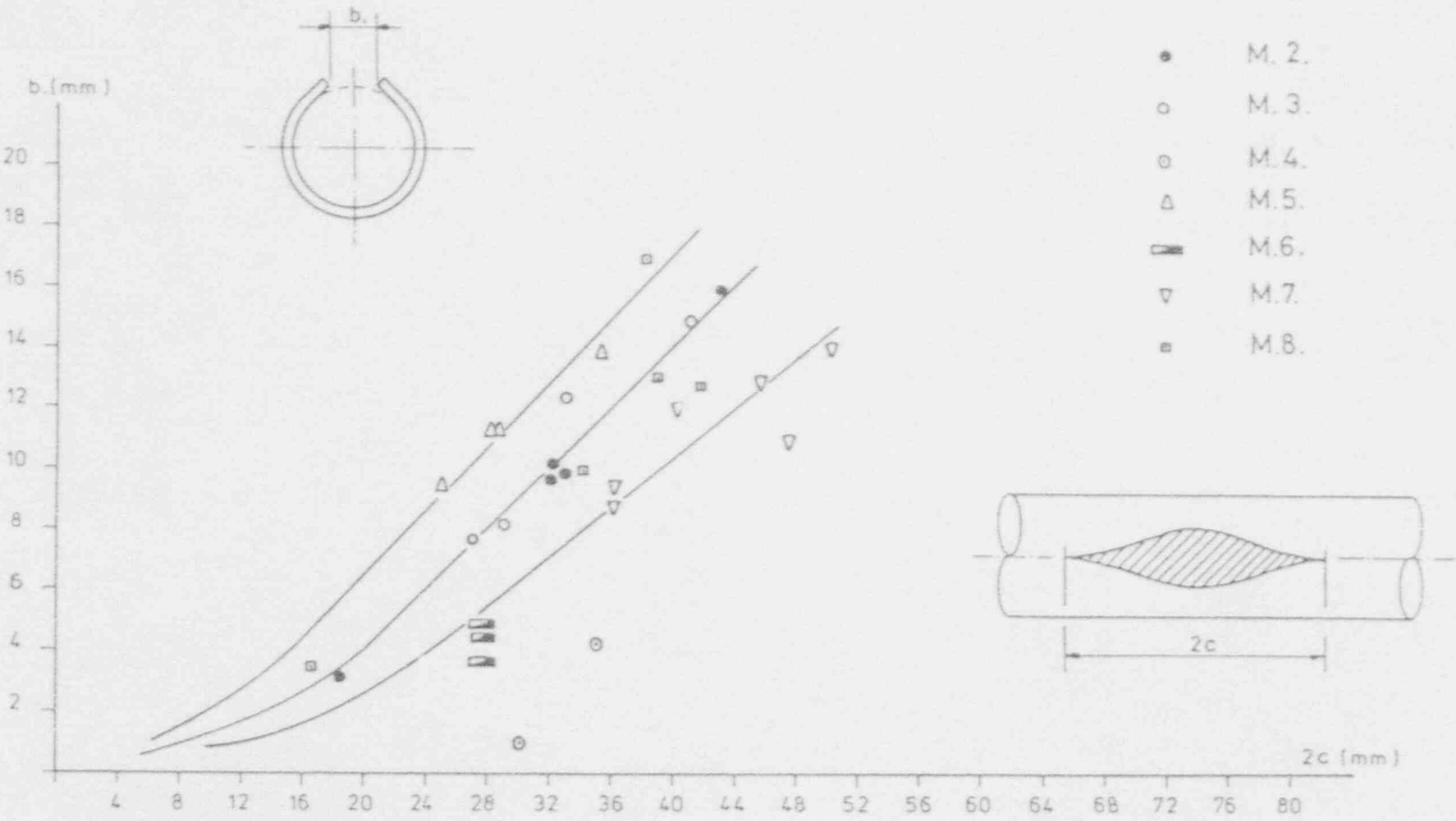

Figure 3-2(c) Flaw width (b) as a function of the final crack length (2c) (from tables 3-2(c); (d))

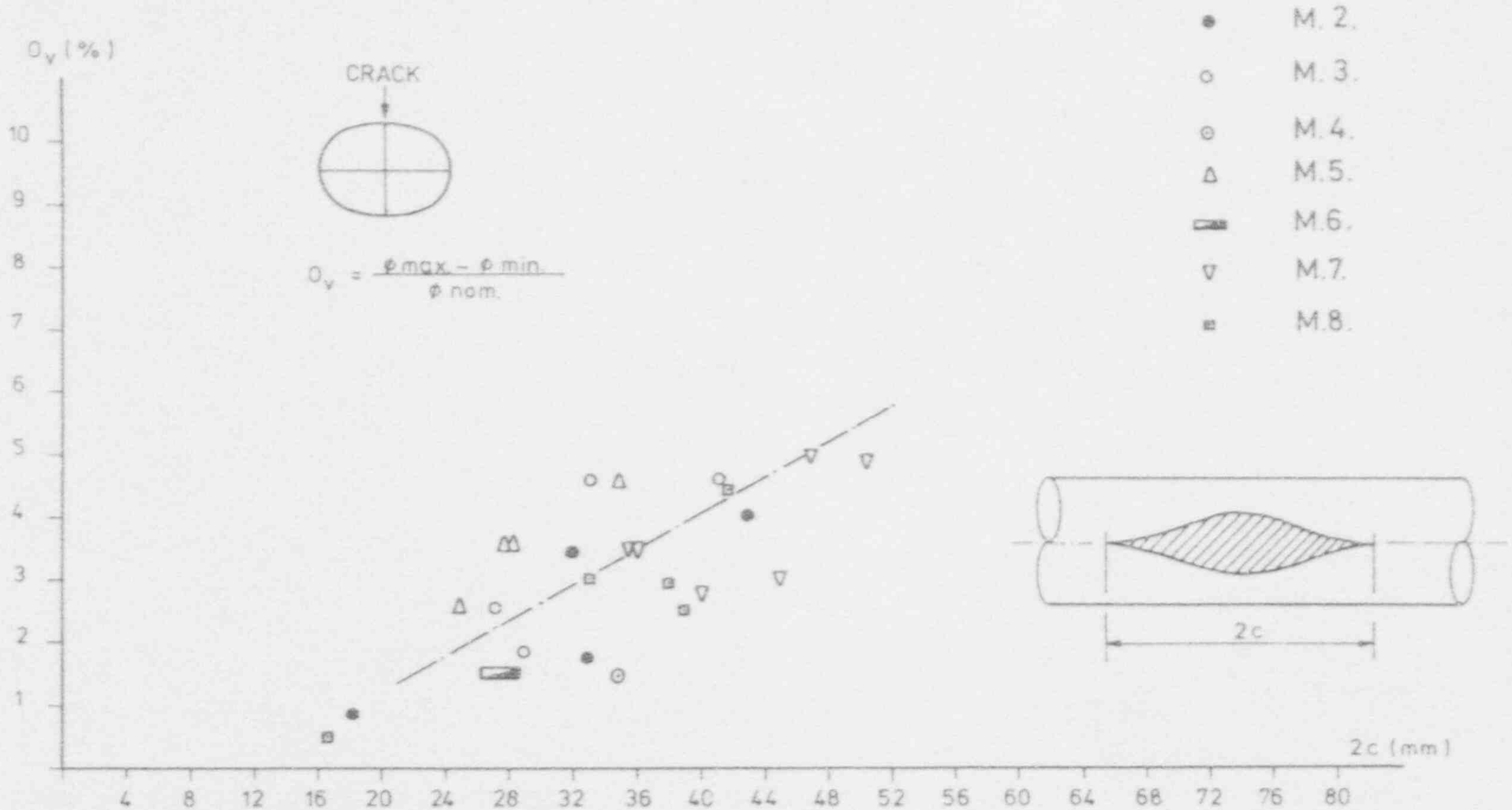

Figure 3-2(d) Ovalization as a function of the final crack length (2c) (from tables 3-2(c); (d))

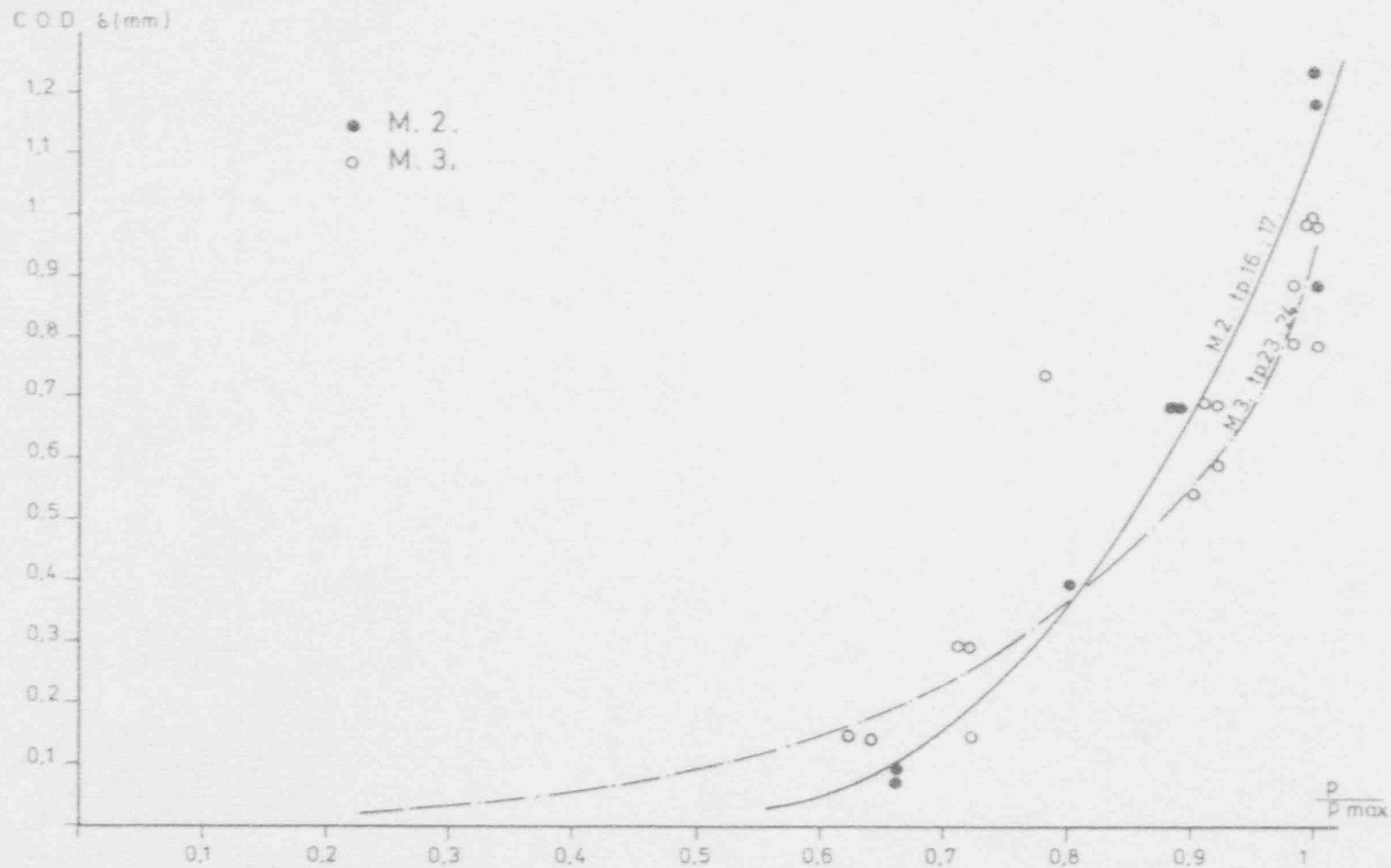

Figure 3-2(e) COD versus p/p max (from table 3-2(d))

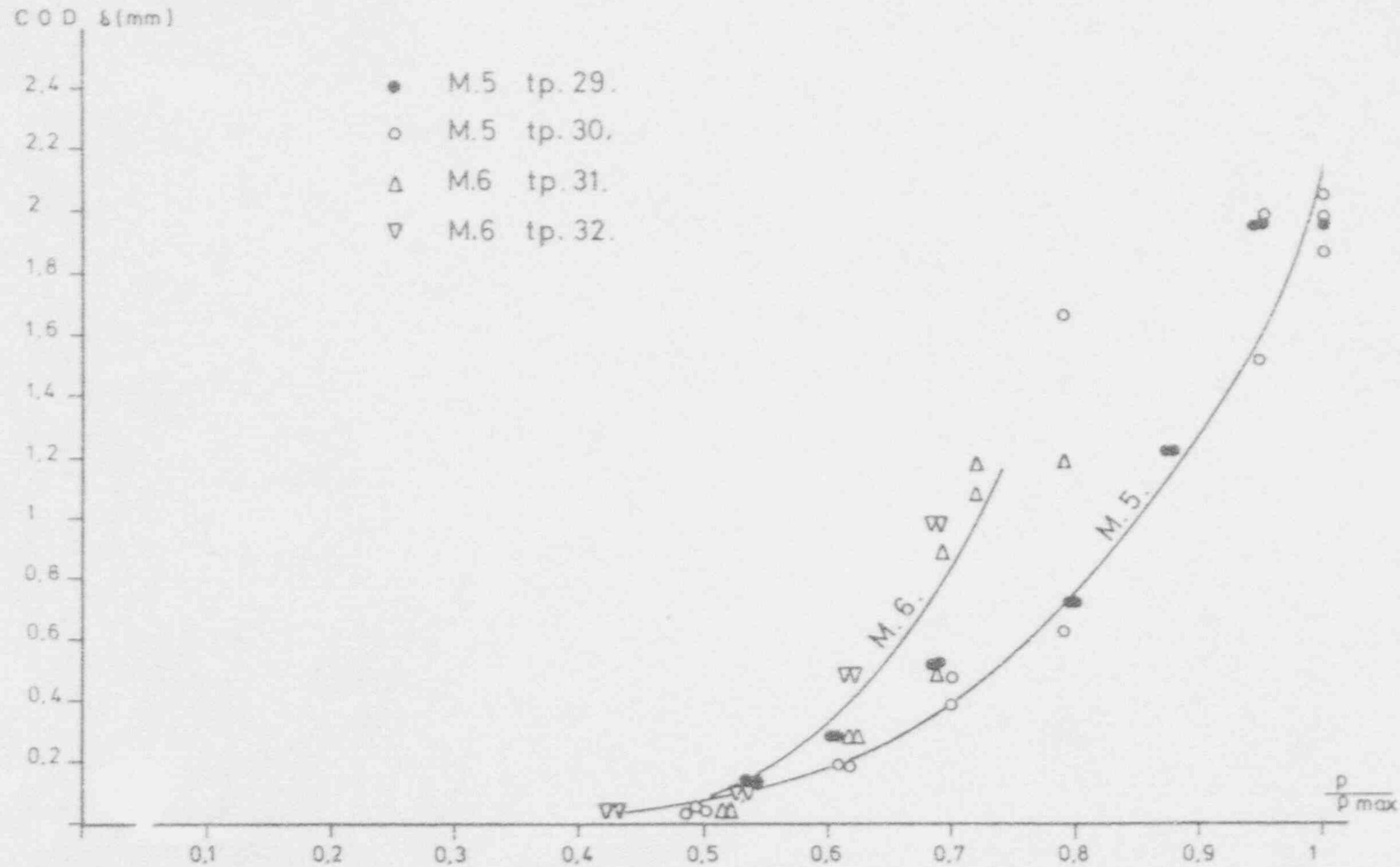

Figure 3-2(f) COD versus p/p max (from table 3-2(d))

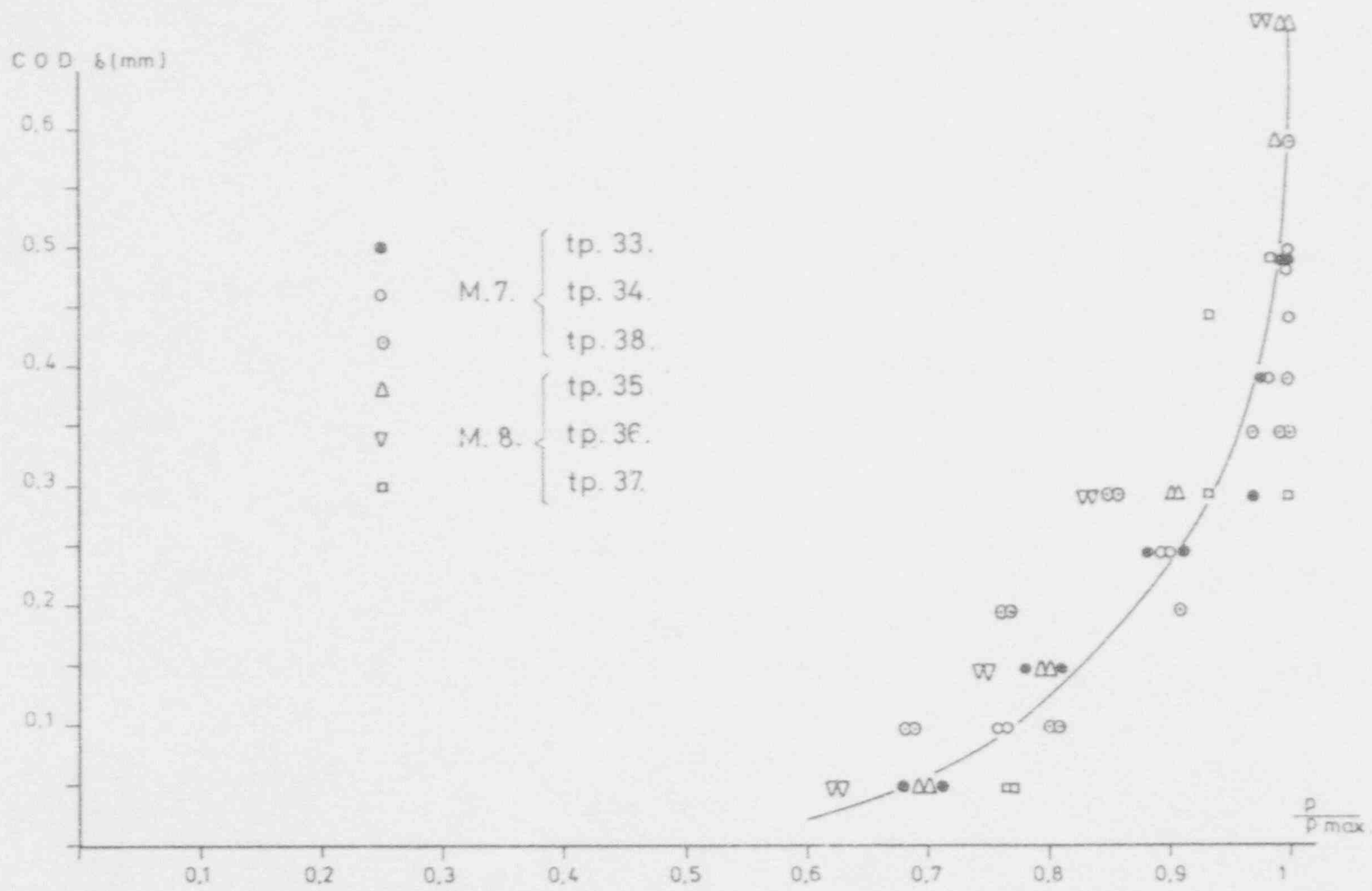

Figure 3-2(g) COD versus p/p max (from table 3-2(d))

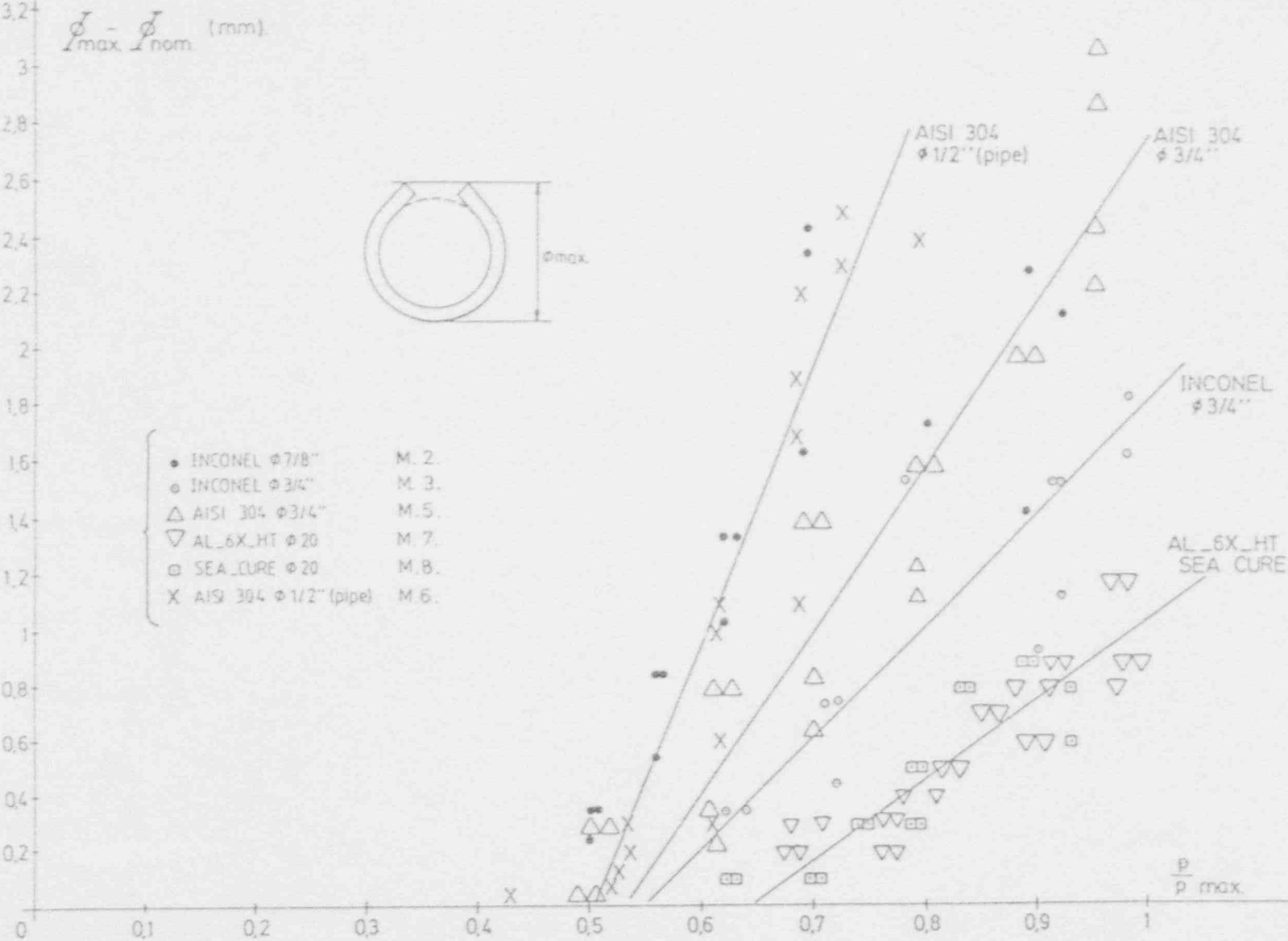

Figure 3-2(h) Through wall axial flaws Bulging as a function of pressure

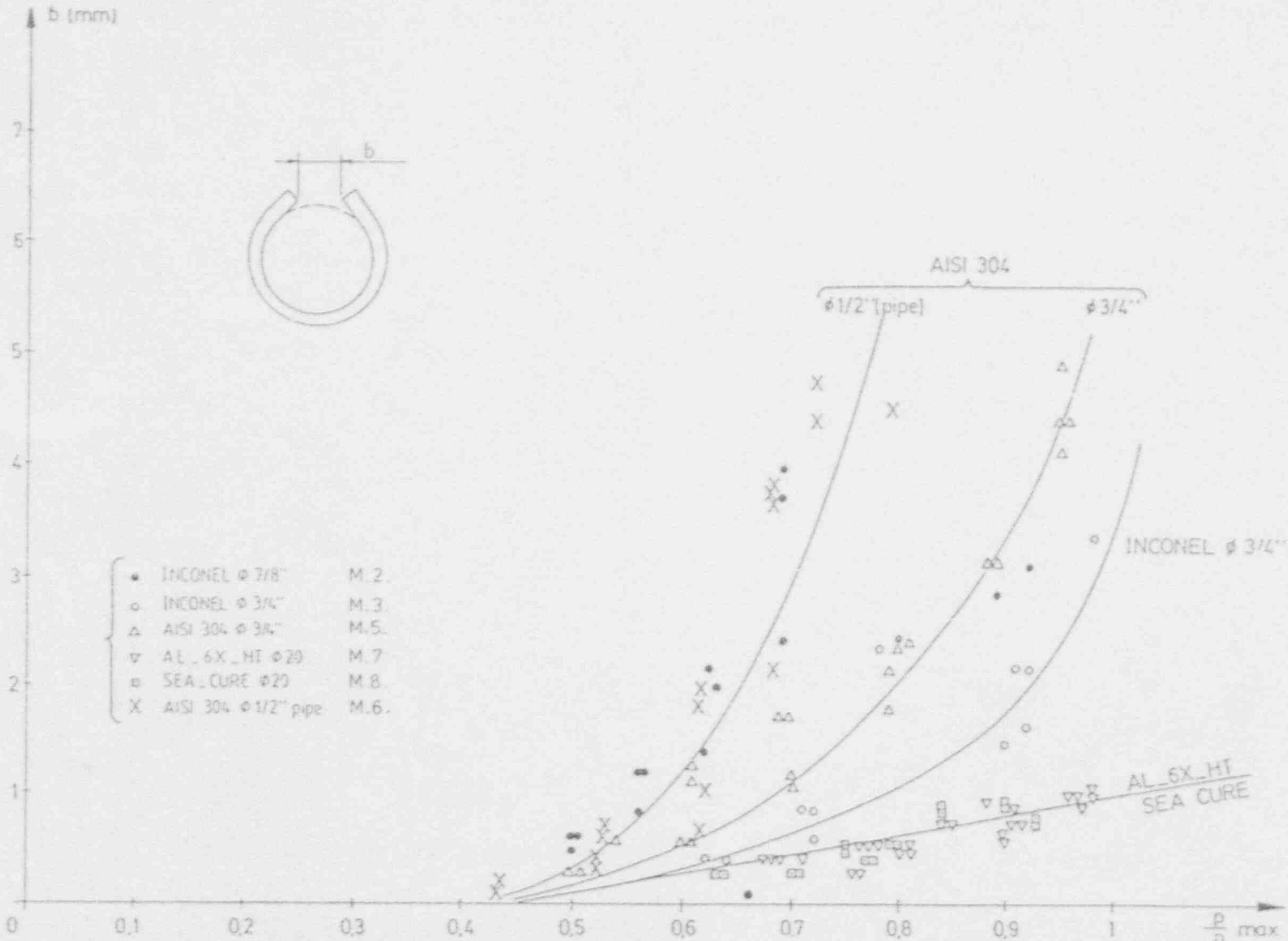

Figure 3-2(i) Through wall axial flaws

Flaw (central) opening as a function of pressure

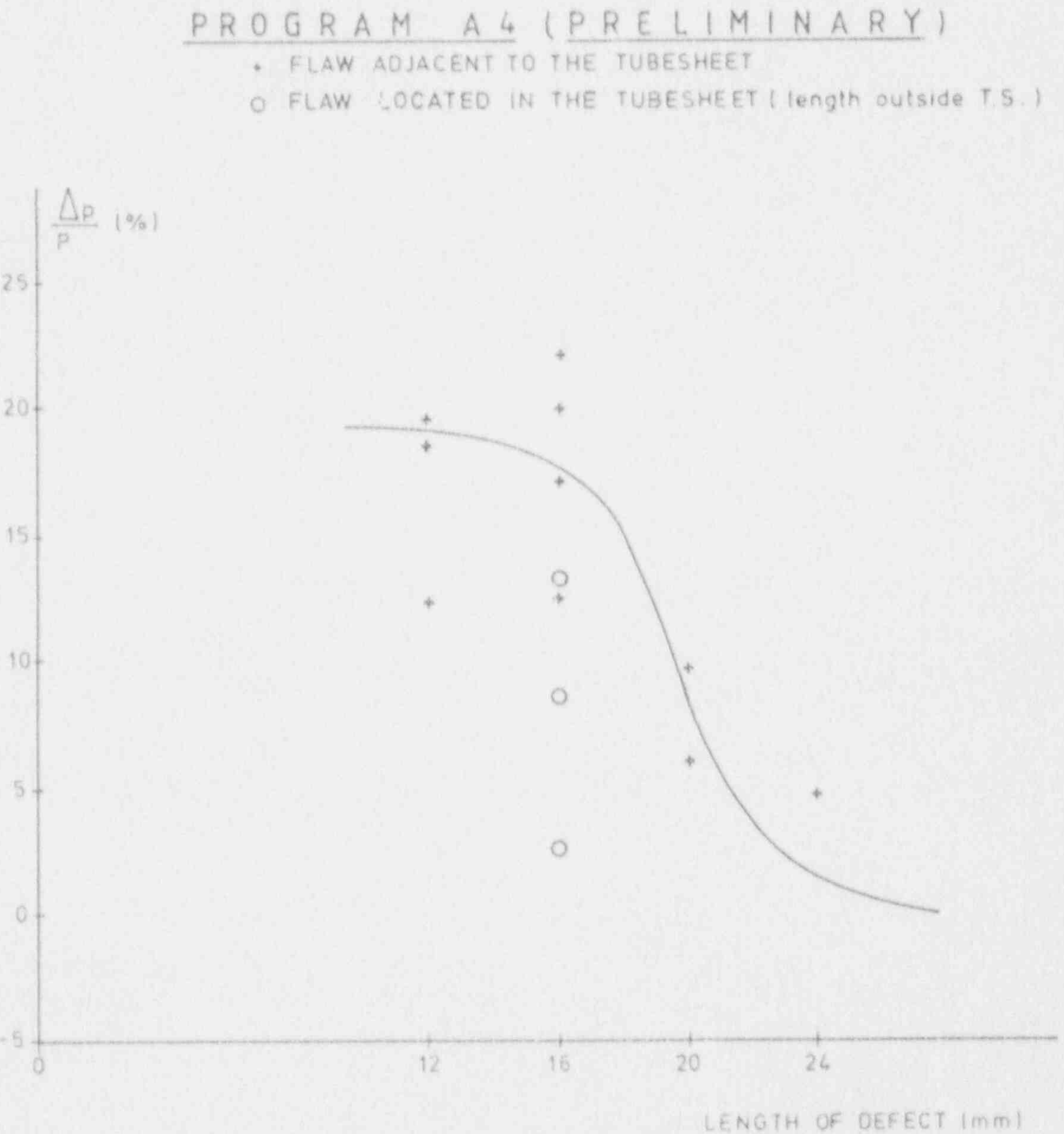

Figure 3-2(j) Influence of the proximity of tubesheet - Increase in burst pressure

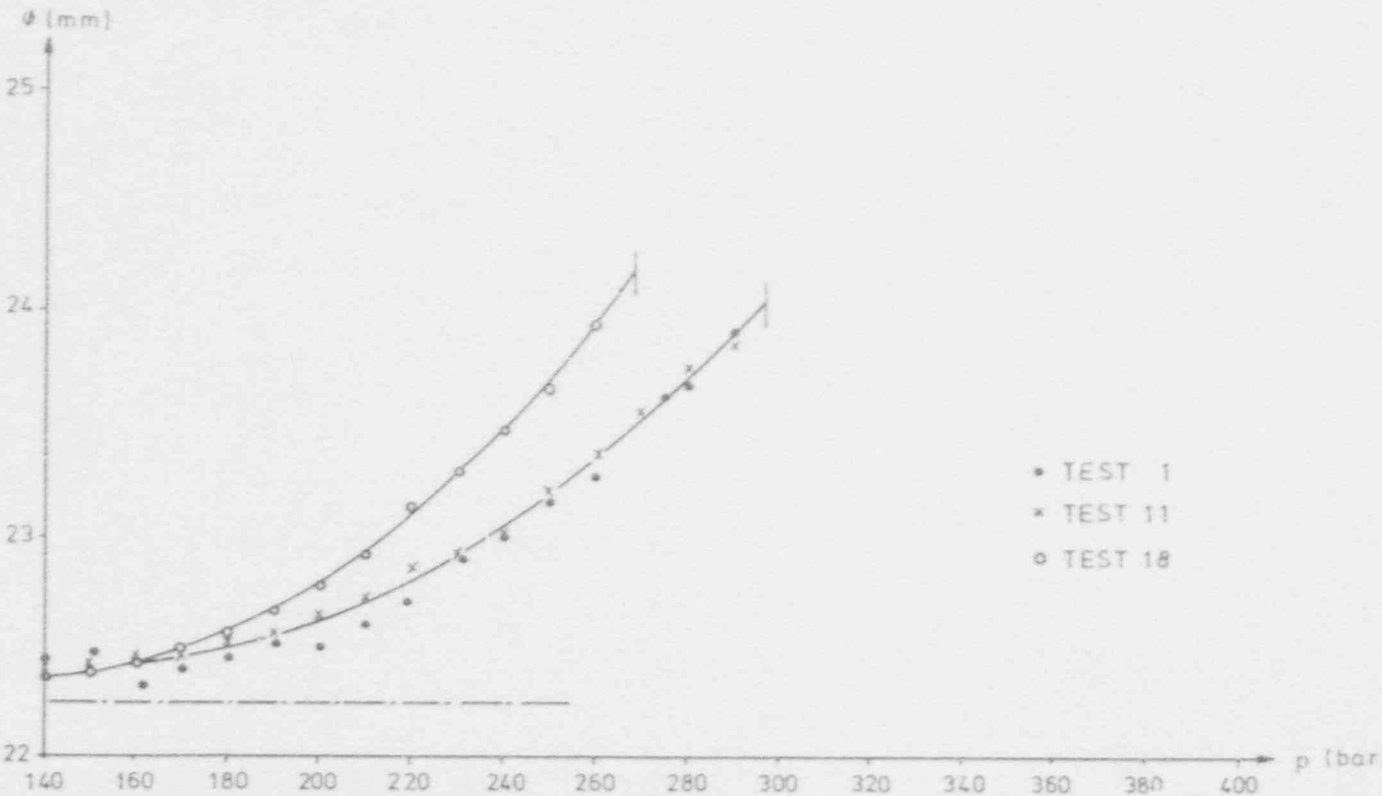

Figure 3-2(k) Bulging measurement

Axial defect in free span - Length : 16 mm

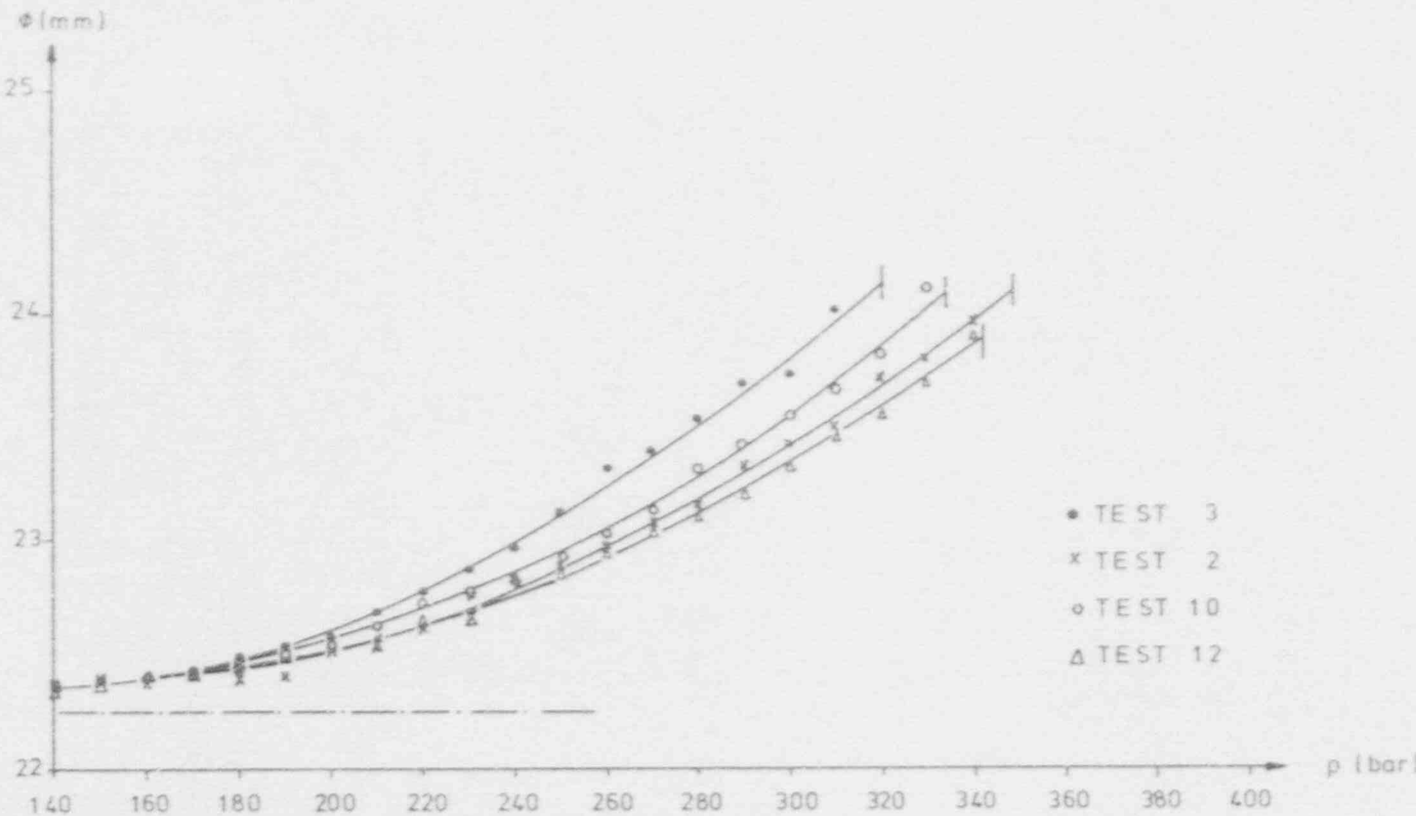

Figure 3-2(1) Bulging measurement
Axial defect tangent to tubesheet - Length : 16 mm

(1.)

(2.)

(3.)

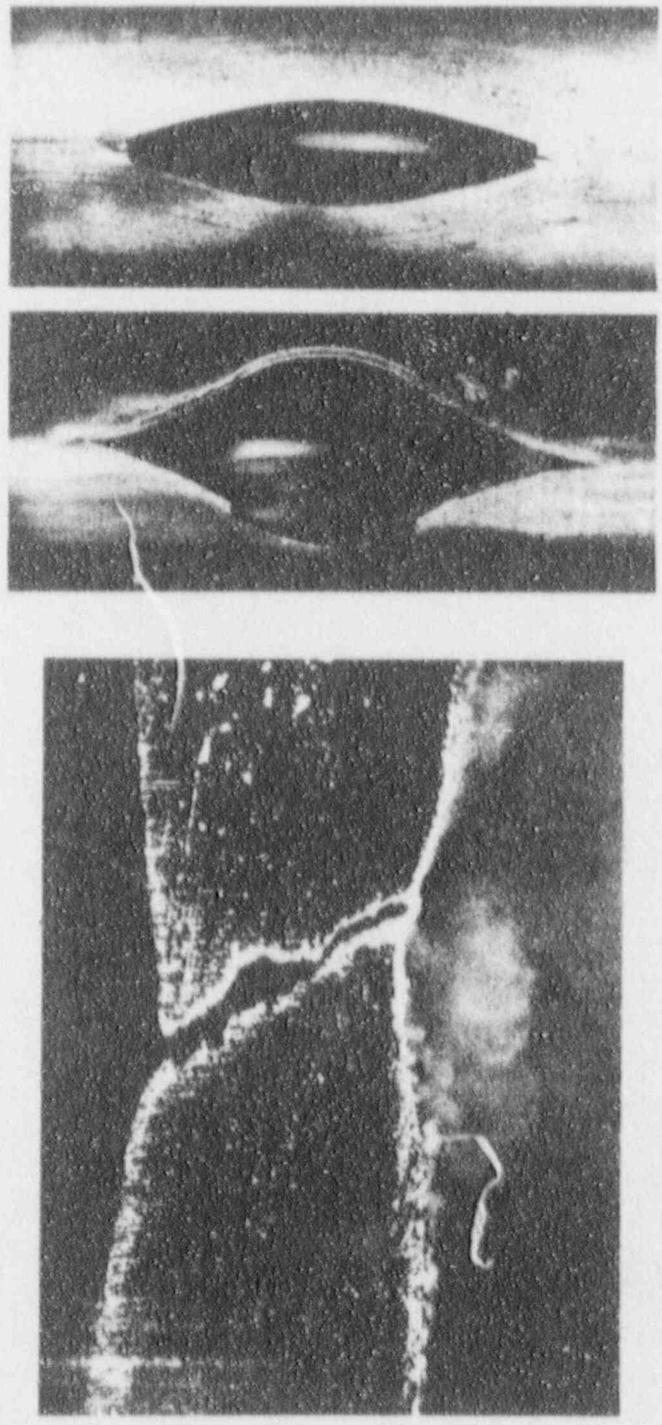

Figure 3-3(a) Test specimens after bursting

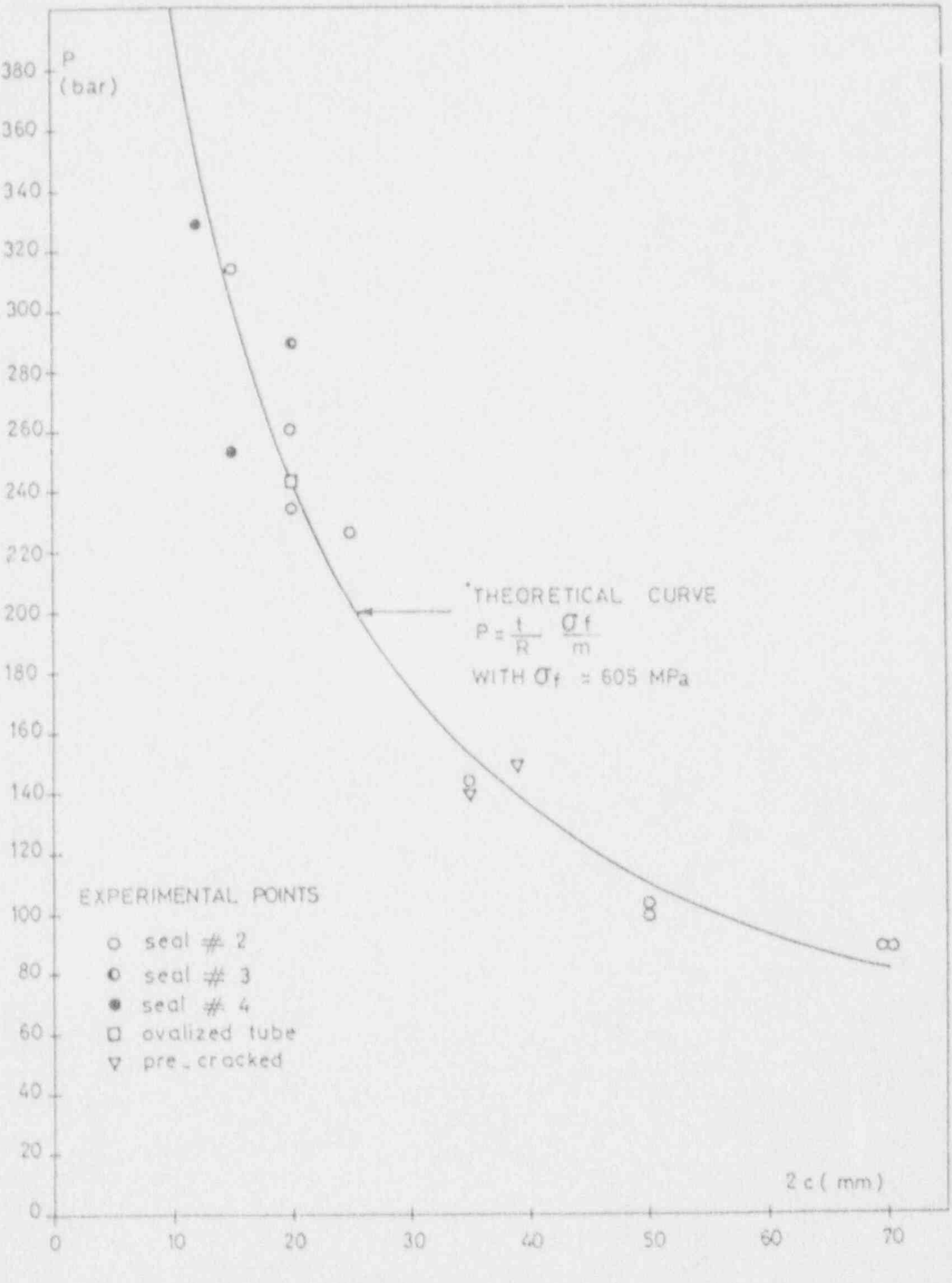

EXPERIMENTAL FAILURE PRESSURE AS A FUNCTION OF THE FLAW LENGTH

Figure 3-3(b) Burst pressure for axial crack through wall

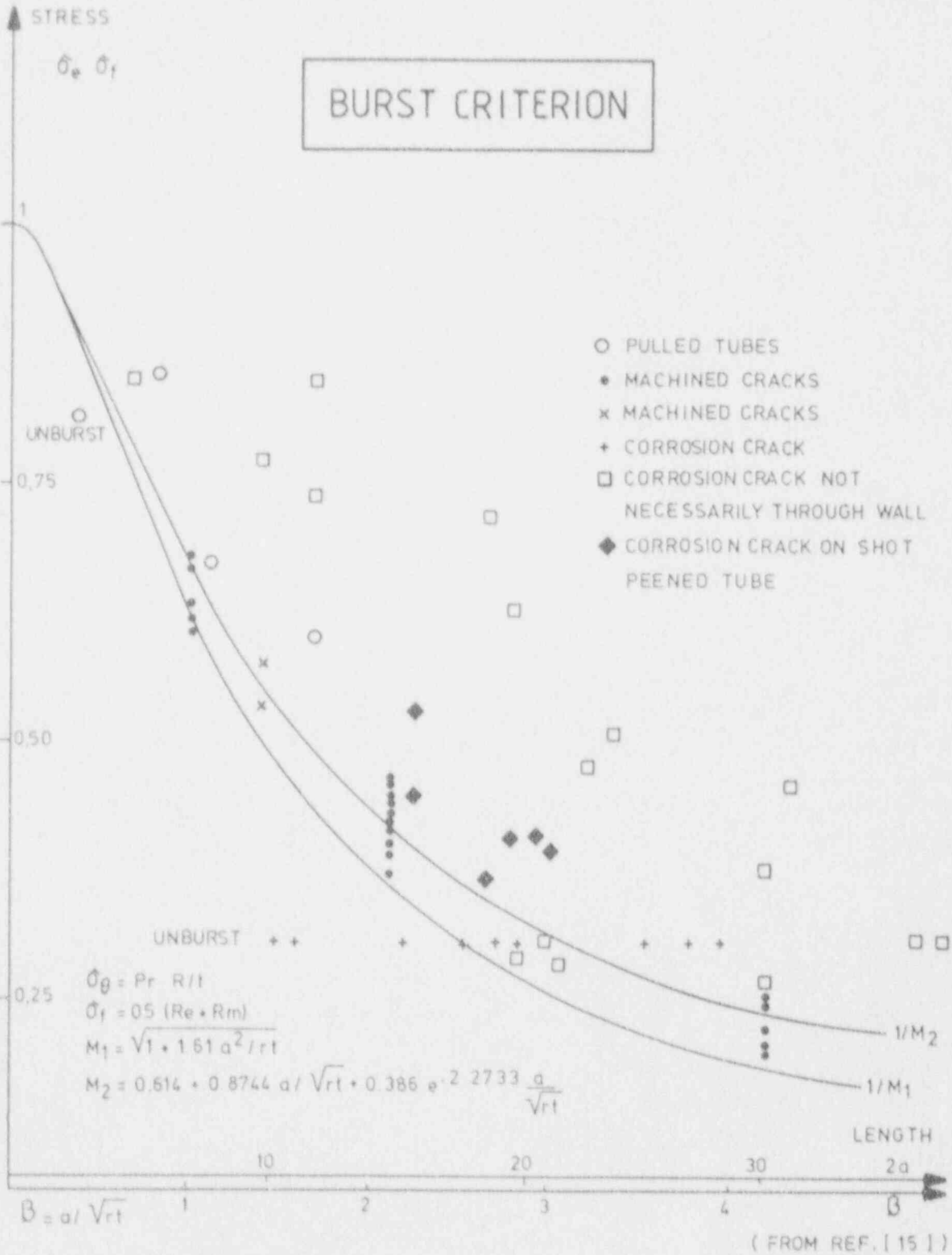

Figure 3-3(c) 7/8" tubes perforating axial cracks in typical areas "Burst Criterion"

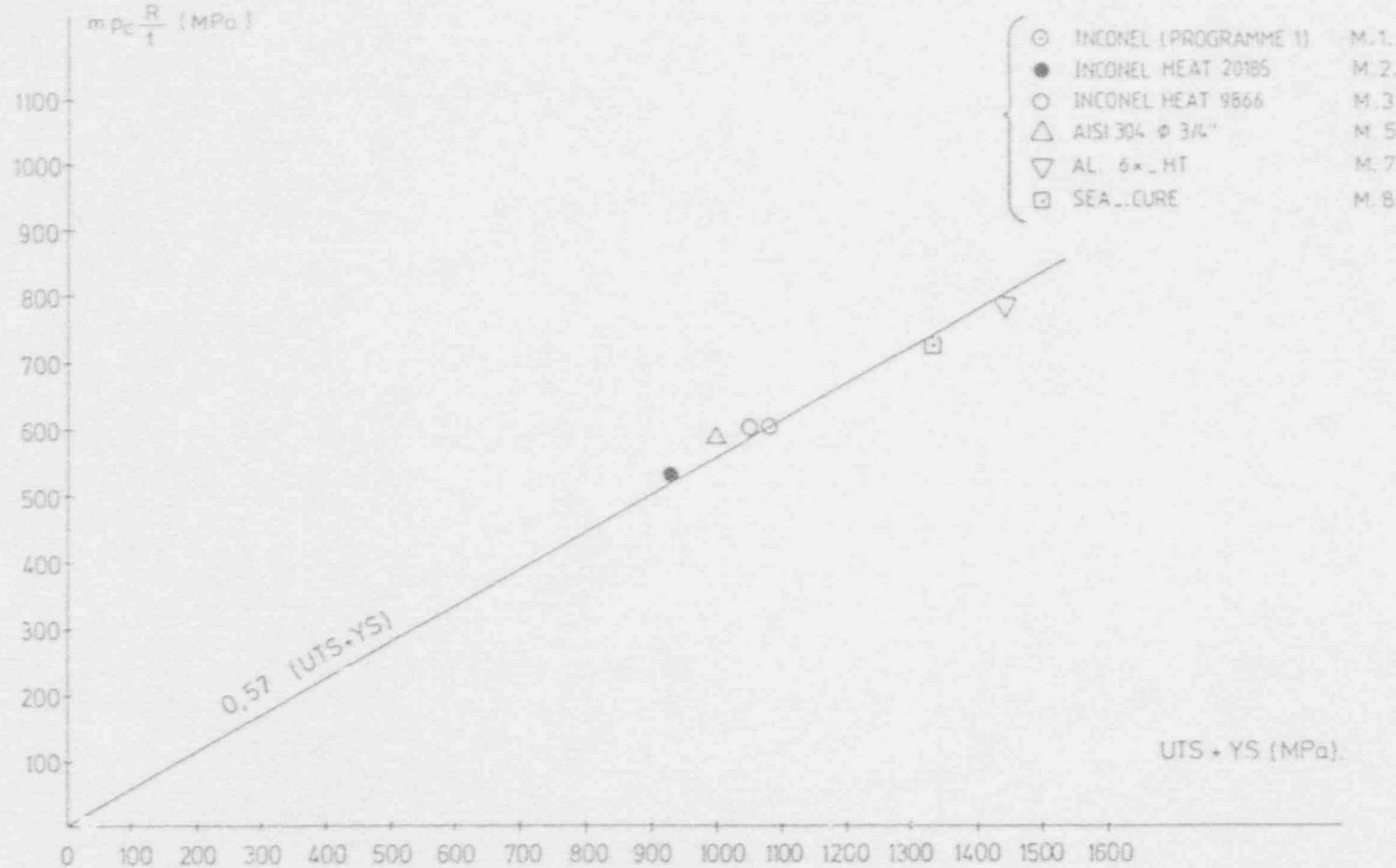

Figure 3-3(d) Correlation between "flow stress" and the transverse mechanical properties YS and UTS

Figure 3-3(e) Frequency histogram

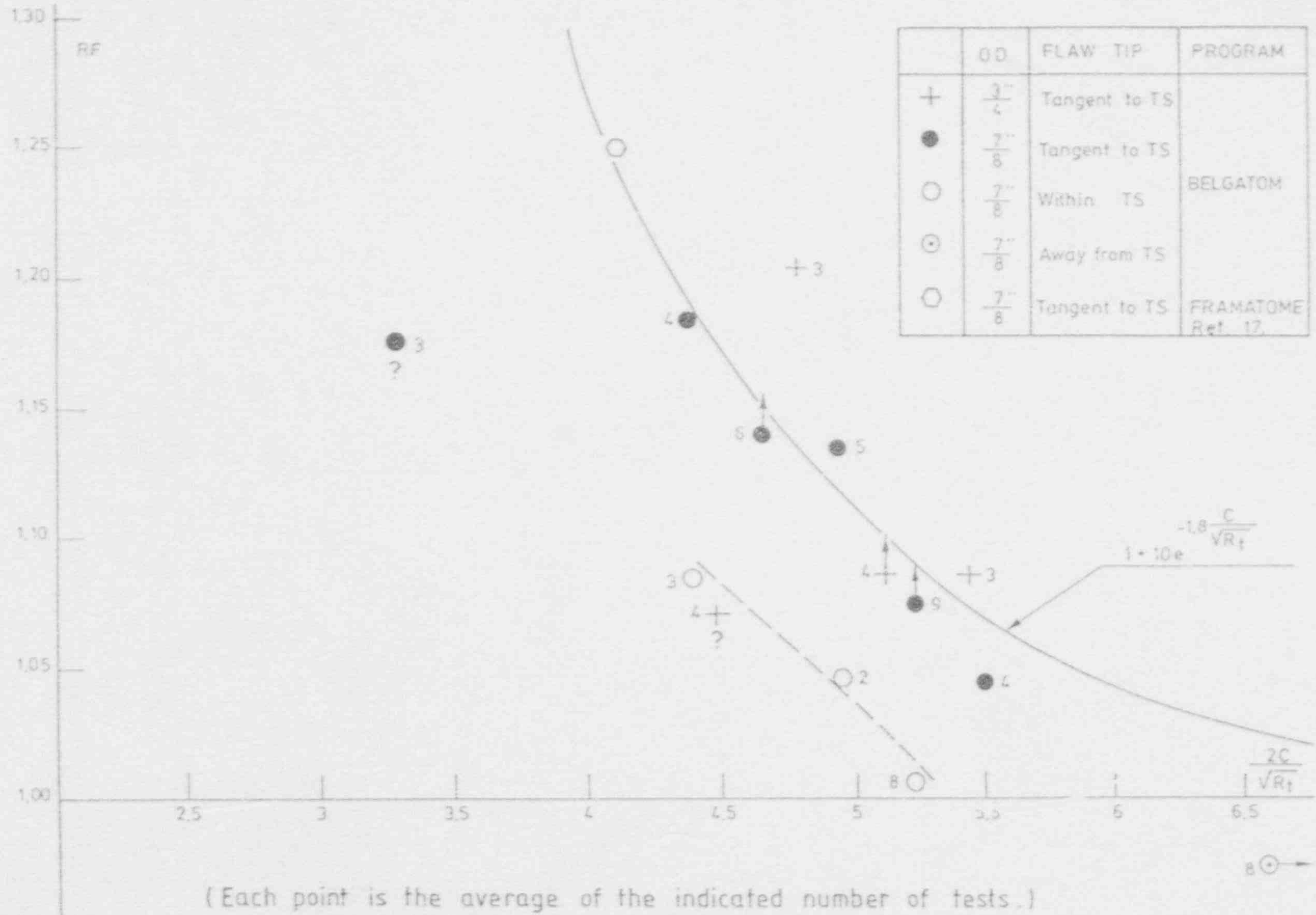

Figure 3-3(f) Tubesheet reinforcing factor

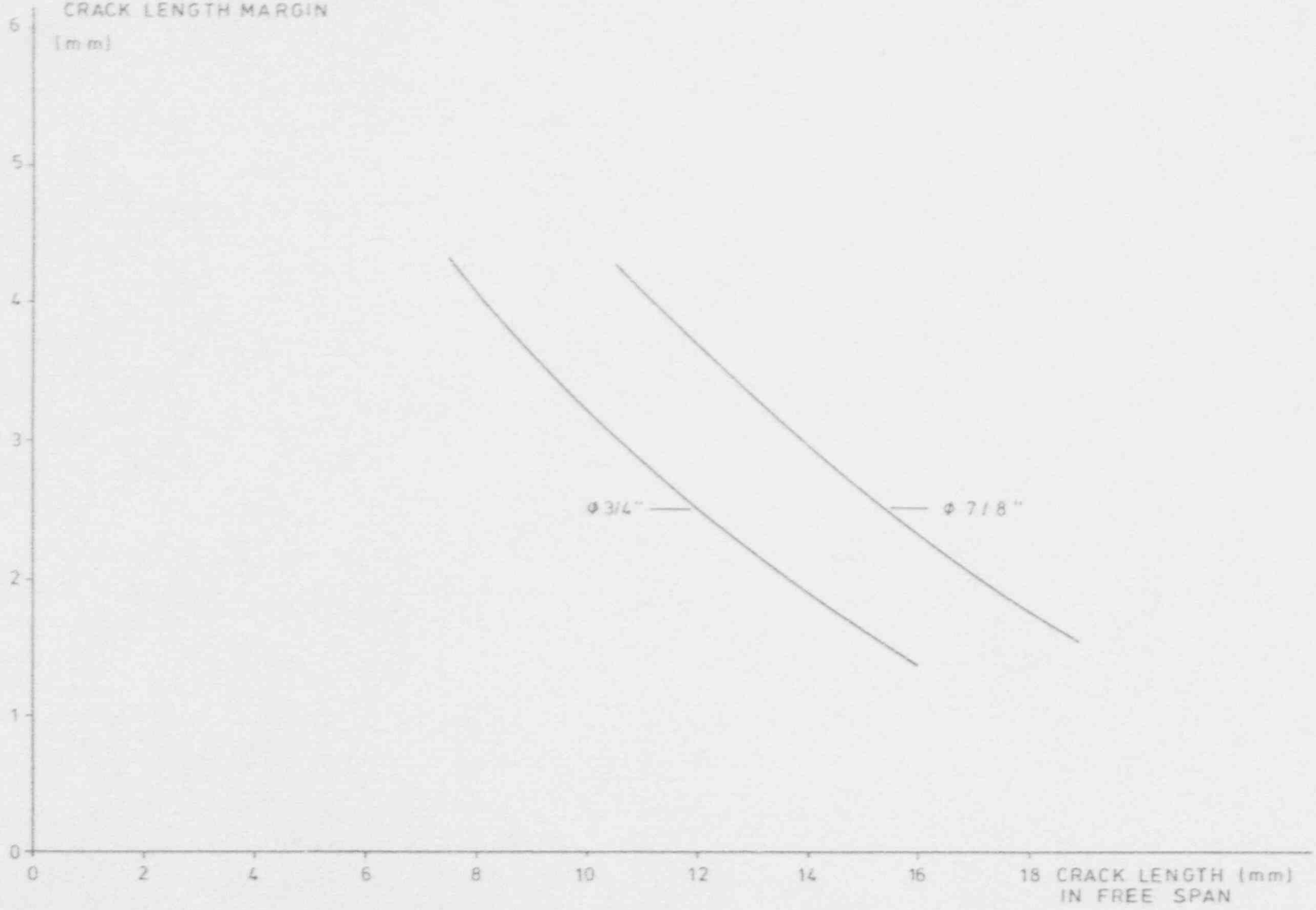

Figure 3-3(g) Reinforcement effect of tubesheet

Section 4

THROUGH WALL CIRCUMFERENTIAL CRACKS

4.1. THEORETICAL MODEL

The critical size of a circumferential through-wall flaw can be calculated by the "collapse load" or "net section stress" theory (as documented by various authors, e.g. (18), assuming a perfectly plastic material.

This can be formalized in a way similar to the axial case, by defining a "shape factor" n.

Tube rupture (unstable circumferential crack propagation) occurs when the local longitudinal stress nσ reaches a critical value σ_f (flow stress) typical of the material.

The nominal circumferential stress σ is calculated by

$$\sigma = p \frac{\pi R_i^2}{2 \pi R t} = \frac{p}{2} \frac{(R - t/2)^2}{Rt} = \frac{p}{2} (R/t - 1)$$

where p, R_i, R and t are as defined for the axial case.

The flow stress is also defined by the same expression as for the axial case

$$\sigma_f = 0.515 \, (YS + UTS)$$

The "shape factor" n will be derived hereafter in the case of pressure loading for various configurations and assumptions

- with or without lateral support (from FDB or TSP)
- with or without friction effects (from the sealing patch used in test specimens)
- with or without consideration of second order effect from the tube thickness to diameter ratio.

4.1.1. Base model

It is common practice to consider the simple model as defined by Fig. 4-1 (a).

According to the "perfectly plastic" assumption, the stress distribution in the cracked section has a birectangular shape.

No restraint nor friction are assumed and the tube radius is only considered at its mean value (this neglects second order thickness effect and will be referred to as the "thin wall" assumption).

With the signs convention defined in Figure 4-1 (a), the loads to be considered are (moments being taken with respect to x axis).

Pressure :
$$\begin{cases} F_p = -2\pi Rt\sigma \\ M_p = 0 \end{cases}$$

Reaction load :
$$\begin{cases} F_r = 2[(\beta - \alpha)\sigma_f - (\pi - \beta)\sigma_f]Rt \\ \quad = 2\sigma_f(2\beta - \alpha - \pi)Rt \\ M_r = 2[\sigma_f \int_\alpha^\beta r\cos\theta d\theta - \sigma_f \int_\beta^\pi r\cos\theta d\theta]Rt \\ \quad = 2\sigma_f(2\sin\beta - \sin\alpha)R^2t \end{cases}$$

Solving the equilibrium equations

$$\begin{cases} F_p + F_r = 0 \\ M_p + M_r = 0 \end{cases}$$

yields σ and β, hence

- the shape factor

$$n = \sigma_f / \sigma = \pi/2/(\text{arc cos } (\sin \alpha/2) - \alpha/2)$$

- the neutral axis position

$$h = R \cos \beta = R \sqrt{[1 - (\frac{\sin \alpha}{2})^2]}$$

4.1.2. General "thin wall" model

This model upgrades the base model by considering both the friction load induced by the sealing patch and the restraining effect of FDB or TSP.

The model and sign convention are defined by Fig. 4-1 (b).

Experimental evidence indicates that a large, well defined COD value must be reached before unstable propagation can be initiated. This requires a large angular deflection at the cracked section which is prevented by the lateral restraint until plasticity is reached in the tube; thus to allow large deflections, the bending moment resulting from the restraint must reach the plastic threshold value

$$M_o = \frac{I}{v} \sigma_y = \pi \, t \, R^2 \, \sigma_y$$

However the "true" yield strength should be considered, rather than the conventionnal YS, which corresponds already to a 0.2 % plastic strain.

Thus

$$M_o = k \, t \, R^2 \, \sigma_y \text{ where } k \leq \pi$$

For practical reasons, another parameter will be used

$$K = k\,\sigma_y / 2\,\sigma_f$$

Thus

$$M_e = 2\,K\,t\,R^2\,\sigma_f$$

with

$$K \leq \pi\sigma_y / 2\,\sigma_f$$

The loads to be considered are now

Pressure $\begin{cases} F_p = -\,2\,\pi\,Rt\,\sigma \\ M_p = 0 \end{cases}$

Friction $\begin{cases} F_f = 2\,f\,\alpha\,R\,lp \\ M_f = 2\,f\,\sin\alpha\,R^2\,lp \end{cases}$

Bending $\begin{cases} F_b = 0 \\ M_b = 2\,K\,\sigma_f\,R^2\,t \end{cases}$

Reaction $\begin{cases} F_r = 2\,\sigma_f\,(2\,\beta - \alpha - \pi)\,Rt \\ M_r = 2\,\sigma_f\,(2\sin\beta - \sin\alpha)\,R^2 t \end{cases}$

Solving the equilibrium equations

$$\begin{cases} F_p + F_f + F_b + F_r = 0 \\ M_p + M_f + M_b + M_r = 0 \end{cases}$$

yields.

$$\begin{cases} \beta = \dfrac{\pi}{2} \,/\, \left(\arccos \dfrac{X \sin\alpha - K}{2} - \dfrac{X\,\alpha}{2}\right) \\ h = R\,\sqrt{\left[1 - \left(\dfrac{X \sin\alpha - K}{2}\right)^2\right]} \end{cases}$$

where

$$X = 1 - \frac{2\, f\, R\, l}{\pi\, (R - t/2)^2}$$

As X is a function of the unknown π, this allows an analytical solution only for $f = 0$ ($X = 1$).

The general case can be solved numerically.

Care must be taken to remain within the limits of applicability of this approach. Indeed, for large crack lengths, when α approaches π, the tube may rupture under pure tension, without any significant general deformation.

This corresponds to a tangent location of the neutral axis ($\beta = \pi$), so that only the force equilibrium needs to be solved, leading to

$$n^* = \frac{\pi}{\pi - \alpha} \left(1 - \frac{\alpha}{\pi} \frac{2\, f\, R\, l}{(R - t/2)^2}\right)$$

and

$$\boxed{n \geq n^*}$$

It should be noted that, for the purely tensile failure mode, the "thin wall" approximation is not useful.

Taking correct dimensions into consideration yields the following equations

$$\begin{cases} -\pi\, (R_2^2 - R_1^2)\, \sigma + (R_2^2 - R_1^2)\, \sigma_f\, (\pi - \alpha) + 2\, \alpha f l R_1 p = 0 \\ \pi\, R_1^2\, p = \pi\, (R_2^2 - R_1^2)\, \sigma \end{cases}$$

which are solved into

$$n^* = \sigma_f / \sigma = \frac{\pi}{\pi - \alpha} \left(1 - 2 \frac{\alpha}{\pi} \frac{f1}{R_1}\right)$$

4.1.3. <u>General "thick wall" model</u>

For "thick walled" pipes (R/t << 10), the above approximation would lead to significant inaccuracy. For the relatively thin-walled SG tubes, no significant difference is expected, except maybe when α is very large (and K = 0) because the residual bending inertia of the remaining ligament is neglected by the "thin-wall" model.

Only the principles of the "thick wall" approach will be outlined hereafter.

The "perfectly plastic" assumption is kept for the material behaviour. The friction and restraint effect are taken into account similarly as for the "thin wall" model

Three different geometries must be considered in the derivation of the reaction load of the cracked section.

The geometries are defined by Fig. 4-1 (c) as a function of the neutral axis location.

The corresponding reaction loads are established as follows

<u>Case 1</u>

$$F_r = 2 \sigma_f \int_\alpha^\pi \left[\int_{R_1}^{h/\cos\Theta} \rho d\rho - \int_{h/\cos\Theta}^{R_2} \rho d\rho \right] d\Theta$$

$$= \sigma_f \int_\alpha^\pi \left[\frac{2 h^2}{\cos^2 \Theta} - (R_2{}^2 + R_1{}^2) \right] d\Theta$$

$$= \sigma_f \left[- (R_2{}^2 + R_1{}^2) (\pi - \alpha) - 2 h^2 \text{ tg } \alpha \right]$$

$$M_r = 2\,\sigma_f \int_{\alpha}^{\pi} \left[\int_{R_1}^{h/\cos\Theta} p^2 \cos\Theta dp - \int_{h/\cos\Theta}^{R_2} p^2 \cos\Theta dp \right] d\Theta$$

$$= \frac{2\,\sigma_f}{3} \int_{\alpha}^{\pi} \left[\frac{2\,h^3}{\cos^2\,\Theta} - (R_2{}^3 + R_1{}^3)\cos\Theta \right] d\Theta$$

$$= \frac{2\,\sigma_f}{3} \left[(R_1{}^3 + R_2{}^3)\ \sin\,\alpha - 2\,h^3\ tg\ \alpha \right]$$

<u>Case 2</u>

$$F_r = 2\,\sigma_f \left[\int_{\alpha}^{\beta} \int_{R_1}^{R_2} p dp d\Theta + \int_{\beta}^{\pi} \left[\int_{R_1}^{h/\cos\Theta} p dp - \int_{h/\cos\Theta}^{R_2} p dp \right] d\Theta \right]$$

$$= \sigma_f \left[(R_2{}^2 - R_1{}^2)\ (\beta - \alpha) + \int_{\beta}^{\pi} \left(\frac{2\,h^2}{\cos^2\,\Theta} - R_1{}^2 - R_2{}^2 \right) d\Theta \right]$$

$$= \sigma_f \left[2\,R_2{}^2\ \beta - (R_2{}^2 - R_1{}^2)\ \alpha - (R_2{}^2 + R_1{}^2)\ \pi - 2\,h^2\ tg\ \beta \right]$$

$$M_r = 2\,\sigma_f \left[\int_{\alpha}^{\beta} \int_{R_1}^{R_2} p^2 \cos\Theta dp d\Theta + \int_{\beta}^{\pi} \left[\int_{R_1}^{h/\cos\Theta} p^2 \cos\Theta dp \quad \int_{h/\cos\Theta}^{R_2} p^2 \cos\Theta dp \right] d\Theta \right]$$

$$= 2\,\sigma_f \left[\frac{R_2{}^3 - R_1{}^3}{3} \int_{\alpha}^{\beta} \cos\Theta d\Theta + \frac{1}{3} \int_{\beta}^{\pi} \left(\frac{2\,h^3}{\cos^3\,\Theta} - R_2{}^3 - R_1{}^3 \right) \cos\Theta\ d\Theta \right]$$

$$= \frac{2\,\sigma_f}{3} \left[2\,R_2{}^3\ \sin\,\beta - (R_2{}^3 - R_1{}^3)\ \sin\,\alpha - 2\,h^3\ tg\ \beta \right]$$

Case 3

$$F_r = 2\sigma_f \left[\int_{\alpha}^{\beta_2} \int_{R_1}^{R_2} p\,dp\,d\Theta + \int_{\beta_2}^{\beta_1} \left[\int_{R_1}^{h/\cos\Theta} p\,dp - \int_{h/\cos\Theta}^{R_2} p\,dp \right] d\Theta - \int_{\beta_1}^{\pi} \int_{R_1}^{R_2} p\,dp\,d\Theta \right]$$

$$= \sigma_f \left[(R_2^2 - R_1^2)(\beta_1 + \beta_2 - \alpha - \pi) + \int_{\beta_2}^{\beta_1} \left(\frac{2h^2}{\cos^2\Theta} - R_1^2 - R_2^2 \right) d\Theta \right]$$

$$= \sigma_f \left[2(R_2^2\beta_2 - R_1^2\beta_1) - (R_2^2 - R_1^2)(\alpha + \pi) + 2h^2(\mathrm{tg}\,\beta_1 - \mathrm{tg}\,\beta_2) \right]$$

$$M_r = 2\sigma_f \left[\int_{\alpha}^{\beta_2} \int_{R_1}^{R_2} p^2\cos\Theta\,dp\,d\Theta + \int_{\beta_2}^{\beta_1} \left[\int_{R_1}^{h/\cos\Theta} p^2\cos\Theta\,dp - \int_{h/\cos\Theta}^{R_2} p^2\cos\Theta\,dp \right] d\Theta \right.$$

$$\left. - \int_{\beta_1}^{\pi} \int_{R_1}^{R_2} p^2\cos\Theta\,dp\,d\Theta \right]$$

$$= 2\sigma_f \left[\frac{R_2^3 - R_1^3}{3} \left(\int_{\alpha}^{\beta_2} \cos\Theta\,d\Theta - \int_{\beta_1}^{\pi} \cos\Theta\,d\Theta \right) + \right.$$

$$\left. \frac{1}{3} \int_{\beta_2}^{\beta_1} \left(\frac{2h^3}{\cos^3\Theta} - R_2^3 - R_1^3 \right) \cos\Theta\,d\Theta \right]$$

$$= \frac{2\sigma_f}{3} \left[2(R_2^3 \sin\beta_2 - R_1^3 \sin\beta_1) - (R_2^3 - R_1^3)\sin\alpha \right.$$

$$\left. + 2h^3(\mathrm{tg}\,\beta_1 - \mathrm{tg}\,\beta_2) \right]$$

From here on the equilibrium equations can be established as before and solved numerically to yield n and h.

Again, n is only valid if

$$n \geq n^* = \frac{\pi}{\pi - \alpha}\left(1 - 2\,\frac{\alpha}{\pi}\,\frac{f_1}{R_i}\right)$$

Numerical results are given in Tables 4-1 (a) to 4-1 (g) for 7/8" OD tubes and in Tables 4-1 (h) to 4-1 (n) for 3/4" OD tubes. Table 4-1 (p) also compares selected results by the "thin wall" and "thick wall" models. It can be verified that the difference is negligible except for the largest α values.

4.2. EXPERIMENTAL PROGRAMS AND TEST RESULTS

4.2.1. Objectives

The experimental program, relative to circumferential through wall cracks, was conducted by BELGATOM in 3 phases with the following specific objectives

- program C1 : validation of general theory (base model) for unsupported tubes. This phase was simultaneous to phase 2 of the axial crack program completed in 1983.
- program C2 : preliminary investigation of the effect of lateral support completed in 1987.
- program C3 : validation of the general analytical model for both supported and unsupported tubes completed in 1989.

4.2.2. Program C1 and test results

This program involved only a preliminary investigation on 4 3/4" OD test specimens, each being provided with 2 EDM through wall circumferential flaws (test-pieces N°. 9; 10; 11; 12 in Table 2-2(b)).

The external OD length of defects covered the range from 15 to 31 mm, corresponding to an angle opening 2 α of 90 through 186 deg. However, the lower value (2 flaws) did not allow circumferential failure (the hoop stress prevailing over the cracked section axial stress); test results from the remaining 6 flaws are listed in Tables 4-2 (a) and 4-2 (b) and illustrated by Fig. 4-2 (a).

4.2.3. Program C2 and test results

This program was limited to a preliminary investigation of the beneficial effect (increase of critical pressure or critical length) provided by lateral restraint.

More specifically, the program was aimed at cross-checking some experimental results presented by WESTINGHOUSE on the effect of an offset of the flow distribution baffle FDB (see Fig. 4-2 (b)); these results were showing a steep decrease of burst pressure as the result of a lateral offset of the FDB, which BELGATOM considered to be inconsistent with the "secondary" loading type (imposed displacement).

Eight test specimens of 3/4" OD tubing were pressure bursted under the following conditions

- 1 without flaw
- 2 without lateral restraint (2 α = 105 and 180 deg. of arc)
- 1 with centered lateral restraint (105 deg. of arc)
- 4 with offset lateral restraint (10 and 20 mm, 105 and 180 deg. of arc).

The test specimens and testing conditions are further defined in Table 4-2 (c) which also reports the corresponding test results.

The results are also summarized in Fig. 4-2 (c) for comparison to the initial data reported by WESTINGHOUSE. This confirms that an FDB offset does not significantly reduce the beneficial effect of lateral restraint, especially for the larger crack sizes. The large discrepancy with the W results was explained later on when the associated testing conditions were learned : no reinforcing patch was used by W and the reported pressures referred to extrusion of the plastic bladder (without any crack propagation). When a lateral FDB offset is imposed, the flaw mouth is opened even before pressure is applied, so that the "extrusion pressure" is very much lowered while the effective "burst pressure" is not significantly affected; thus,the W results were so overly conservative as to become useless and even misleading.

For some tests of the phase 2 BELGATOM program, the tube deformations and displacements were also documented as illustrated by Figures 4-2 (c) to 4-2 (h).

The latter Figure shows that unstable propagation occurs when the axial extension reaches about 1.0 mm in length; most of this measured extension corresponds to the plastic deformation of the ligament in the cracked section. This explains why the observed constant value is close to the critical COD measured at both ends of the crack.

4.2.4. Program C3 and test results

Program C3 was initiated by BELGATOM in 1988 as a consequence of some reported occurences of circumferential cracking in the tube roll transition area of plants outside Belgium.

This was an incentive to provide less conservative and well documented plugging limits that could be applied to the Belgian plants in case of similar occurences.

Program C3 consists of two subsets of test specimens

- the first subset, aimed at the Belgian steam generators of more immediate concern, used 7/8" OD tubing and investigated a range of crack lengths
  - . from 120 to 240 degrees of arc, in the unsupported condition
  - . from 180 to 300 degrees of arc, in the supported condition.
- the second subset, aimed at extrapolating the first results to the case of 3/4" OD tubing, investigated thoroughly a smaller range of crack lengths of direct interest for the establishment of tube plugging limits, i.e.,
  - . 165 degrees of arc, in the unsupported condition
  - . 270 and 300 degrees of arc, in the supported condition.

The first subset included 25 specimens. Simulation of lateral support was generally aimed at the combination of Flow Distribution Baffle FDB and first Tube Support Plate TSP. A few cases of support by TSP only were also considered. All tests were conducted with no imposed offset from the restraining plates. Even the unrestrained specimens were tested within a simulated tubesheet, the circumferential flaw being located 6 mm outside the constraining collar.

The test specimens and testing conditions are further defined in Table 4-2 (d), which reports the corresponding test results as well.

These include

- The burst pressure p_c, in the 150 to 600 bar range.
- The maximum value of tube lateral deflection, which was continuously recorded during pressurization.
- The Crack Opening Displacement COD, measured by the flaw width increase (average of both ends) on the failed specimens.
- A short description of the failure mode (extent of circumferential propagation).

The experimentally derived "shape factor" $n = \sigma_c/\sigma$ is also listed for further comparison to the theoretical approach.

In some cases, the full profile (lateral deflection) of the deformed test specimens has also been documented; an example is illustrated by Fig. 4-2 (i). Fig. 4-2 (j) illustrates the burst behaviour based on video recording.

The second subset includes 17 specimens of 3/4" OD, of which only 3 were tested in the unsupported condition (single value of 165 degrees of arc, selected close to the critical crack size under accidental conditions).

The remaining 14 specimens were tested under a variety of lateral restraint configurations, fully representative of model D4 steam generator geometry.

- Flow Distribution Baffle only (FDB located at 150 mm from tubesheet)
- Tube Support Plate only (TSP located at 900 mm from tubesheet)
- Combined FDB and TSP.

The effect of a plate offset, in the 10 to 20 mm range, was also investigated for the FDB configuration.

All of these conditions were tested for 2 crack lengths (270 and 300 degrees of arc, selected in the range of the critical sizes under accidental conditions.

As for the first subset, all specimens were tested within a simulated tubesheet, the circumferential flaw being located 6 mm away from the constraining collar.

The test specimens and testing conditions are further defined in Table 4-2 (e), which also reports the corresponding test results as well

These include

- the burst pressure p_c, in the 300 to 600 bar range.
- the maximum value of the lateral load on the restraining plate which was continuously recorded during pressurization; the corresponding moment, at the cracked section, is also reported for comparison with the theoretical approach.
- the crack opening displacement COD, measured by the flaw width increase (average of both ends) on the failed specimens.
- a short description of the failure mechanism with the total amount of circumferential propagation.

The experimentally derived "shape factor" $n = \sigma_f / \sigma$ is also listed for further comparison to the theoretical approach.

Fig. 4-2 (k) illustrates a typical record of pressure and load time history for the specimen N°. 20.

In a few cases, the full profile (lateral deflection) of the deformed test specimens has also been documented.

4.3. DISCUSSION OF RESULTS

4.3.1. Phenomenology

4.3.1.1. Failure mode

For all burst tests (a total of 51 flaws), the reported critical pressure corresponds to unstable propagation; at this pressure, there is an instantaneous crack extension at both ends of the initial flaw (ranging from crack initiation, a fraction of mm long, to full circumferential severance). Crack arrest, when present, results from the quick pressure drop of the uncompressible pressurizing medium; this would never be expected from hot water or gas pressurization.

In cases of small flaws, typically 105 degrees of arc, the general swelling of the tube under the very high burst pressure may lead to a prevailing axial crack failure initiated at one of the circumferential flaw ends (resulting in a "flap behaviour").

Stable crack growth was generally not observed, as evidenced by

- visual examination and/or video recording of the flaw behaviour during pressure build-up.
- final examination of either
  - . the non failed flaw for those samples containing two identical defects
  - . the non failed flaw when the test was arrested through leakage (usually with extrusion of the reinforcing patch) at a pressure close to the expected burst value.

However a small amount of stable crack initiation was occasionally reported.

Fracture appearance was typically ductile, with 45° shear lips and significant wall thinning, as for the axial case.

4.3.1.2. Plastic deformations

Local plastic deformations are observed before unstability is reached, but to a lesser extent than for the axial case.

The most typical feature is the blunting of the flaw tips, or Crack Opening Displacement COD, increasing up to a fairly constant failure value of about 1 mm for EDM flaws (no testing was performed with sharper corrosion or fatigue cracks).

4.3.1.3. Sealing patch behaviour

At the burst pressure, leaktightness is lost through perforation of the plastic bladder and the metal patch (1 or 2 shims) may either

- stay intact in place or
- be extruded, without any tearing, through the opening flaw
- tear along the crack in the circumferential direction
- tear in a mixed mode of axial and circumferential components with occasional ejection of a small detached part.

The first behaviour is usually associated with the lower burst pressures (typically less than 300 bar).

The sealing patch behaviour clearly influences the burst pressure value, especially for the case of the longest flaws. The influence of the corresponding friction load can be taken into account in the analytical model and is further discussed in Section 4.3.2. hereafter.

4.3.1.4. Effect of loading path

In cases where a test was interrupted by full unloading at a pressure level close to the expected failure value, additional failure appeared to be premature (bursting at a pressure equal to or lower than the initial one).

This oligocyclic plastic fatigue process may have reduced somewhat the reported burst pressures and contributes some conservatism to the experimental program, as already commented for the axial case.

4.3.1.5. Load on lateral restraint

Loads measured on the restraining plates FDB or TSP are a quasi linear function of pressure until plastic deformation is reached in the full (uncracked) tube section (see Fig. 4-3 (a)).

4.3.2. Model validation with and without lateral restraint

All experimentally derived values of the "shape factor" $n = \sigma_f/\sigma$ were plotted as a function of the angular crack length (Fig. 4-3 (b)) and compared with the predicted model values as discussed under Section 4.1.

The friction factor f was assumed to lie in the 0.1 to 0.2 range.

For the supported configurations (lateral restraint from simulated FDB and/or TSP), an appropriate value of the K parameter was selected according to the following procedure.

For a 3/4" tube OD, the section modulus is

$$\frac{I}{v} = \frac{R_2^4 - R_1^4}{4\ R_2} = 83.2\ 10^{-9}\ m^3$$

where R_2 and R_1 denote respectively outside and inside radius of the tube.

For subset 2 of program C3, the only part where the restraining load was measured and documented, the yield strength is 346 MPa, leading to

$$\left(\frac{I}{v}\right) \sigma_y = 29\ Nm$$

and a K value may be defined by

$$K = \frac{\sigma_y}{2\ \sigma_f} \frac{M_o}{29} = 0.01065\ M_o$$

where M_o is the measured value of the restraining bending moment.

Average measurements yield

M_o = 73 Nm for FDB support

54 Nm for TSP support

with corresponding K values of 0.78 and 0.58, respectively.

This led to the selection of K = 0.6 which is shown by Fig. 4-3 (b) to compare fairly well with the full set of experimental data.

Thus K = 0.6 can be considered as a practically lower bound value which can be used (with f = 0) in theoretical analyses.

Table 4-1 (a)

NET SECTION STRESS - THICK WALL MODEL FOR 7/8" OD

CIRCUMFERENTIAL CRACK - NEUTRAL AXIS and SHAPE FACTOR FOR K = 0

ALPHA	F=0		F=.1		F=.2	
degree	H	SF	H	SF	H	SF
175	-0.660	999.99	-0.660	999.99	-0.660	652.65
170	-0.620	592.55	-0.620	508.54	-0.620	424.54
165	-0.553	386.00	-0.553	331.39	-0.553	276.76
160	-0.458	272.32	-0.458	233.85	-0.458	195.37
155	-0.337	192.95	-0.338	165.75	-0.339	138.55
150	-0.221	134.49	-0.222	115.58	-0.223	96.67
145	-0.115	93.76	-0.116	80.61	-0.118	67.46
140	-0.018	66.15	-0.020	56.91	-0.023	47.66
135	0.083	47.53	0.079	40.99	0.074	34.39
130	0.196	35.09	0.189	30.24	0.179	25.39
125	0.290	24.51	0.298	22.84	0.284	19.21
120	0.419	20.39	0.389	16.96	0.381	14.85
115	0.520	16.00	0.497	13.86	0.467	11.71
110	0.590	12.39	0.578	11.09	0.537	9.40
105	0.681	10.36	0.641	9.02	0.588	7.67
100	0.735	8.52	0.685	7.44	0.619	6.36
95	0.769	7.09	0.690	6.13	0.627	5.34
90	0.780	5.98	0.690	5.20	0.613	4.54
85	0.769	5.09	0.683	4.50	0.577	3.91
80	0.735	4.38	0.639	3.89	0.523	3.41
75	0.681	3.80	0.577	3.40	0.453	3.00
70	0.590	3.30	0.498	2.99	0.369	2.66
65	0.520	2.94	0.390	2.64	0.278	2.39
60	0.419	2.62	0.289	2.37	0.181	2.16
55	0.290	2.33	0.189	2.14	0.084	1.96
50	0.196	2.11	0.095	1.96	0.011	1.81
45	0.083	1.92	0.011	1.80	AXIAL FAILURE	
40	-0.018	1.75	AXIAL FAILURE			
35	AXIAL FAILURE					

Table 4-1 (b)

NET SECTION STRESS - THICK WALL MODEL FOR 7/8" OD

CIRCUMFERENTIAL CRACK - NEUTRAL AXIS and SHAPE FACTOR FOR K = .5

ALPHA	F=0		F=.1		F=.2	
degree	H	SF	H	SF	H	SF
175	-1.270	36.00	-1.270	31.02	-1.270	26.04
170	-1.270	18.00	-1.270	15.58	-1.270	13.16
165	-1.270	12.00	-1.270	10.43	-1.270	8.87
160	-1.270	9.00	-1.270	7.86	-1.270	6.72
155	-1.270	7.20	-1.270	6.32	-1.270	5.44
150	-1.270	6.00	-1.270	5.29	-1.270	4.58
145	-0.986	5.82	-1.027	5.02	-1.090	4.21
140	-0.827	5.62	-0.865	4.84	-0.920	4.07
135	-0.699	5.39	-0.738	4.65	-0.793	3.92
130	-0.592	5.14	-0.633	4.44	-0.691	3.75
125	-0.489	4.93	-0.545	4.22	-0.590	3.61
120	-0.425	4.59	-0.472	3.98	-0.538	3.38
115	-0.362	4.30	-0.413	3.74	-0.483	3.18
110	-0.310	4.01	-0.366	3.50	-0.442	2.98
105	-0.271	3.72	-0.331	3.26	-0.413	2.79
100	-0.243	3.45	-0.290	3.07	-0.397	2.60
95	-0.226	3.18	-0.297	2.81	-0.393	2.43
90	-0.220	2.94	-0.297	2.60	-0.400	2.26
85	-0.226	2.71	-0.290	2.43	-0.419	2.11
80	-0.243	2.49	-0.332	2.23	-0.450	1.96
75	-0.271	2.30	-0.366	2.06	-0.492	1.83
70	-0.310	2.12	-0.412	1.92	-0.545	1.71
65	-0.362	1.96	-0.470	1.78	AXIAL FAILURE	
60	-0.425	1.81	AXIAL FAILURE			
55	-0.489	1.69	AXIAL FAILURE			
50	AXIAL FAILURE					

Table 4-1 (c)

NET SECTION STRESS - THICK WALL MODEL FOR 7/8" OD

CIRCUMFERENTIAL CRACK - NEUTRAL AXIS and SHAPE FACTOR FOR K = .6

ALPHA	F=0		F=.1		F=.2	
degree	H	SF	H	SF	H	SF
175	-1.270	36.00	-1.270	31.02	-1.270	26.04
170	-1.270	18.00	-1.270	15.58	-1.270	13.16
165	-1.270	12.00	-1.270	10.43	-1.270	8.87
160	-1.270	9.00	-1.270	7.86	-1.270	6.72
155	-1.270	7.20	-1.270	6.32	-1.270	5.44
150	-1.270	6.00	-1.270	5.29	-1.270	4.58
145	-1.270	5.14	-1.270	4.55	-1.270	3.96
140	-1.072	4.78	-1.142	4.13	-1.270	3.50
135	-0.889	4.65	-0.961	3.98	-1.048	3.36
130	-0.778	4.42	-0.834	3.82	-0.915	3.23
125	-0.676	4.21	-0.733	3.65	-0.815	3.09
120	-0.592	4.00	-0.651	3.47	-0.736	2.95
115	-0.523	3.77	-0.586	3.28	-0.675	2.80
110	-0.468	3.55	-0.535	3.09	-0.629	2.64
105	-0.425	3.32	-0.497	2.91	-0.598	2.49
100	-0.395	3.10	-0.473	2.72	-0.580	2.34
95	-0.377	2.88	-0.461	2.54	-0.576	2.20
90	-0.371	2.68	-0.461	2.37	-0.584	2.07
85	-0.377	2.48	-0.474	2.21	-0.589	1.95
80	-0.395	2.30	-0.498	2.06	-0.638	1.82
75	-0.425	2.14	-0.536	1.92	-0.684	1.71
70	-0.468	1.98	-0.585	1.79	AXIAL FAILURE	
65	-0.523	1.84	-0.649	1.68	AXIAL FAILURE	
60	-0.592	1.71	AXIAL FAILURE			
55	AXIAL FAILURE					

Table 4-1 (d)

NET SECTION STRESS - THICK WALL MODEL FOR 7/8" OD

CIRCUMFERENTIAL CRACK - NEUTRAL AXIS and SHAPE FACTOR FOR K = .7

ALPHA	F=0		F=.1		F=.2	
degree	H	SF	H	SF	H	SF
175	-1.270	36.00	-1.270	31.02	-1.270	26.04
170	-1.270	18.00	-1.270	15.58	-1.270	13.16
165	-1.270	12.00	-1.270	10.43	-1.270	8.87
160	-1.270	9.00	-1.270	7.86	-1.270	6.72
155	-1.270	7.20	-1.270	6.32	-1.270	5.44
150	-1.270	6.00	-1.270	5.29	-1.270	4.58
145	-1.270	5.14	-1.270	4.55	-1.270	3.96
140	-1.270	4.50	-1.270	4.00	-1.270	3.50
135	-1.270	4.00	-1.270	3.57	-1.270	3.15
130	-0.989	3.91	-1.094	3.36	-1.270	2.86
125	-0.877	3.72	-0.956	3.23	-1.083	2.73
120	-0.778	[illegible].55	-0.856	3.08	-0.975	2.62
115	-0.700	[illegible].37	-0.780	2.93	-0.899	2.50
110	-0.638	[illegible].18	-0.722	2.78	-0.844	2.38
105	-0.592	3.00	-0.680	2.63	-0.790	2.27
100	-0.559	2.82	-0.653	2.47	-0.787	2.14
95	-0.540	2.64	-0.640	2.33	-0.782	2.02
90	-0.533	2.46	-0.640	2.18	-0.791	1.90
85	-0.540	2.30	-0.654	2.05	-0.815	1.80
80	-0.559	2.14	-0.681	1.92	-0.854	1.69
75	-0.592	2.00	-0.723	1.80	AXIAL FAILURE	
70	-0.638	1.86	-0.780	1.69	AXIAL FAILURE	
65	-0.700	1.74	AXIAL FAILURE			
60	AXIAL FAILURE					

Table 4-1 (e)

NET SECTION STRESS - THICK WALL MODEL FOR 7/8" OD

CIRCUMFERENTIAL CRACK - NEUTRAL AXIS and SHAPE FACTOR FOR K = .8

ALPHA	F=0		F=.1		F=.2	
degree	H	SF	H	SF	H	SF
175	-1.270	36.00	-1.270	31.02	-1.270	26.04
170	-1.270	18.00	-1.270	15.58	-1.270	13.16
165	-1.270	12.00	-1.270	10.43	-1.270	8.87
160	-1.270	9.00	-1.270	7.86	-1.270	6.72
155	-1.270	7.20	-1.270	6.32	-1.270	5.44
150	-1.270	6.00	-1.270	5.29	-1.270	4.58
145	-1.270	5.14	-1.270	4.55	-1.270	3.96
140	-1.270	4.50	-1.270	4.00	-1.270	3.50
135	-1.270	4.00	-1.270	3.57	-1.270	3.15
130	-1.270	3.60	-1.270	3.23	-1.270	2.86
125	-1.152	3.34	-1.270	2.95	-1.270	2.63
120	-0.989	3.21	-1.132	2.78	-1.270	2.43
115	-0.890	3.07	-1.019	2.66	-1.270	2.27
110	-0.832	2.89	-0.944	2.53	-1.134	2.17
105	-0.778	2.74	-0.892	2.40	-1.077	2.06
100	-0.741	2.58	-0.860	2.27	-1.047	1.96
95	-0.719	2.43	-0.844	2.15	-1.039	1.87
90	-0.712	2.28	-0.844	2.03	-1.052	1.77
85	-0.719	2.14	-0.861	1.91	-1.087	1.68
80	-0.741	2.01	-0.894	1.80	AXIAL FAILURE	
75	-0.778	1.88	-0.945	1.69	AXIAL FAILURE	
70	-0.832	1.76	AXIAL FAILURE			
65	AXIAL FAILURE					

Table 4-1 (f)

NET SECTION STRESS - THICK WALL MODEL FOR 7/8" OD

CIRCUMFERENTIAL CRACK - NEUTRAL AXIS and SHAPE FACTOR FOR K = .9

ALPHA	F=0		F=.1		F=.2	
degree	H	SF	H	SF	H	SF
175	-1.270	36.00	-1.270	31.02	-1.270	26.04
170	-1.270	18.00	-1.270	15.58	-1.270	13.16
165	-1.270	12.00	-1.270	10.43	-1.270	8.87
160	-1.270	9.00	-1.270	7.86	-1.270	6.72
155	-1.270	7.20	-1.270	6.32	-1.270	5.44
150	-1.270	6.00	-1.270	5.29	-1.270	4.58
145	-1.270	5.14	-1.270	4.55	-1.270	3.96
140	-1.270	4.50	-1.270	4.00	-1.270	3.50
135	-1.270	4.00	-1.270	3.57	-1.270	3.15
130	-1.270	3.60	-1.270	3.23	-1.270	2.86
125	-1.270	3.27	-1.270	2.95	-1.270	2.63
120	-1.270	3.00	-1.270	2.72	-1.270	2.43
115	-1.270	2.77	-1.270	2.52	-1.270	2.27
110	-1.080	2.66	-1.270	2.35	-1.270	2.12
105	-0.989	2.54	-1.270	2.20	-1.270	2.00
100	-0.957	2.39	-1.139	2.11	-1.270	1.89
95	-0.929	2.26	-1.113	2.00	-1.270	1.80
90	-0.920	2.13	-1.114	1.89	-1.270	1.72
85	-0.929	2.01	-1.141	1.79	AXIAL FAILURE	
80	-0.957	1.89	-1.270	1.69	AXIAL FAILURE	
75	-0.989	1.78	AXIAL FAILURE			
70	-1.080	1.67	AXIAL FAILURE			
65	AXIAL FAILURE					

Table 4-1 (g)

NET SECTION STRESS - THICK WALL MODEL FOR 7/8" OD

CIRCUMFERENTIAL CRACK - NEUTRAL AXIS and SHAPE FACTOR FOR k = 1

ALPHA	F=0		F=.1		F=.2	
degree	H	SF	H	SF	H	SF
175	-1.270	36.00	-1.270	31.02	-1.270	26.04
170	-1.270	18.00	-1.270	15.58	-1.270	13.16
165	-1.270	12.00	-1.270	10.43	-1.270	8.87
160	-1.270	9.00	-1.270	7.86	-1.270	6.72
155	-1.270	7.20	-1.270	6.32	-1.270	5.44
150	-1.270	6.00	-1.270	5.29	-1.270	4.58
145	-1.270	5.14	-1.270	4.55	-1.270	3.96
140	-1.270	4.50	-1.270	4.00	-1.270	3.50
135	-1.270	4.00	-1.270	3.57	-1.270	3.15
130	-1.270	3.60	-1.270	3.23	-1.270	2.86
125	-1.270	3.27	-1.270	2.95	-1.270	2.63
120	-1.270	3.00	-1.270	2.72	-1.270	2.43
115	-1.270	2.77	-1.270	2.52	-1.270	2.27
110	-1.270	2.57	-1.270	2.35	-1.270	2.12
105	-1.270	2.40	-1.270	2.20	-1.270	2.00
100	-1.270	2.25	-1.270	2.07	-1.270	1.89
95	-1.270	2.12	-1.270	1.96	-1.270	1.80
90	-1.270	2.00	-1.270	1.86	-1.270	1.72
85	-1.270	1.89	-1.270	1.77	AXIAL FAILURE	
80	-1.270	1.80	-1.270	1.69	AXIAL FAILURE	
75	-1.270	1.71	AXIAL FAILURE			
70	AXIAL FAILURE					

Table 4-1 (h)

NET SECTION STRESS - THICK WALL MODEL FOR 3/4" OD

CIRCUMFERENTIAL CRACK - NEUTRAL AXIS and SHAPE FACTOR FOR K = 0

ALPHA	F=0		F=.1		F=.2	
degree	H	SF	H	SF	H	SF
175	-0.567	999.99	-0.567	993.83	-0.567	796.46
170	-0.532	592.09	-0.532	494.17	-0.533	396.25
165	-0.474	385.66	-0.475	322.00	-0.475	258.33
160	-0.393	272.11	-0.393	227.27	-0.394	182.43
155	-0.290	192.86	-0.291	160.88	-0.291	129.23
150	-0.190	134.38	-0.191	112.34	-0.192	90.30
145	-0.099	93.75	-0.089	109.14	-0.089	91.56
140	-0.016	66.13	-0.018	55.36	-0.021	44.57
135	0.071	47.64	0.067	39.89	0.061	32.19
130	0.167	35.09	0.160	29.44	0.150	23.78
125	0.264	26.46	0.253	22.23	0.238	18.00
120	0.358	20.38	0.342	17.16	0.319	13.93
115	0.445	16.00	0.422	13.50	0.389	11.00
110	0.521	12.78	0.490	10.81	0.446	8.84
105	0.583	10.36	0.542	8.79	0.485	7.23
100	0.630	8.52	0.578	7.26	0.490	5.86
95	0.658	7.09	0.595	6.07	0.490	4.96
90	0.668	5.98	0.593	5.14	0.493	4.31
85	0.658	5.09	0.571	4.40	0.459	3.72
80	0.630	4.38	0.532	3.81	0.390	3.21
75	0.583	3.80	0.477	3.33	0.348	2.86
70	0.521	3.33	0.390	2.91	0.276	2.55
65	0.445	2.94	0.330	2.62	0.198	2.29
60	0.358	2.62	0.244	2.35	0.117	2.08
55	0.264	2.34	0.155	2.12	0.038	1.90
50	0.167	2.11	0.067	1.93	-0.032	1.75
45	0.071	1.92	-0.013	1.77	AXIAL FAILURE	
40	-0.016	1.75	AXIAL FAILURE			
35	AXIAL FAILURE					

Table 4-1 (i)

NET SECTION STRESS - THICK WALL MODEL FOR 3/4" OD

CIRCUMFERENTIAL CRACK - NEUTRAL AXIS and SHAPE FACTOR FOR K = .5

ALPHA	F=0		F=.1		F=.2	
degree	H	SF	H	SF	H	SF
175	-1.090	36.00	-1.090	30.19	-1.090	24.38
170	-1.090	18.00	-1.090	15.18	-1.090	12.36
165	-1.090	12.00	-1.090	10.17	-1.090	8.35
160	-1.090	9.00	-1.090	7.67	-1.090	6.34
155	-1.090	7.20	-1.090	6.17	-1.090	5.14
150	-1.090	6.00	-1.090	5.17	-1.090	4.34
145	-0.847	5.82	-0.889	4.88	-0.961	3.94
140	-0.690	5.72	-0.749	4.72	-0.811	3.82
135	-0.589	5.45	-0.640	4.53	-0.689	3.71
130	-0.490	5.24	-0.550	4.33	-0.615	3.52
125	-0.431	4.87	-0.476	4.11	-0.544	3.35
120	-0.365	4.59	-0.414	3.88	-0.486	3.17
115	-0.311	4.30	-0.363	3.65	-0.441	2.99
110	-0.267	4.01	-0.324	3.41	-0.390	2.85
105	-0.233	3.72	-0.294	3.18	-0.385	2.64
100	-0.190	3.51	-0.276	2.96	-0.373	2.47
95	-0.194	3.18	-0.267	2.74	-0.372	2.30
90	-0.189	2.94	-0.268	2.54	-0.380	2.15
85	-0.194	2.71	-0.279	2.36	-0.399	2.01
80	-0.190	2.52	-0.300	2.18	-0.428	1.87
75	-0.233	2.30	-0.330	2.03	-0.466	1.75
70	-0.267	2.12	-0.371	1.88	AXIAL FAILURE	
65	-0.311	1.96	-0.421	1.75	AXIAL FAILURE	
60	-0.365	1.81	AXIAL FAILURE			
55	-0.431	1.68	AXIAL FAILURE			
50	AXIAL FAILURE					

Table 4-1 (j)

NET SECTION STRESS - THICK WALL MODEL FOR 3/4" OD

CIRCUMFERENTIAL CRACK - NEUTRAL AXIS and SHAPE FACTOR FOR K = .6

ALPHA	F=0		F=.1		F=.2	
degree	H	SF	H	SF	H	SF
175	-1.090	36.00	-1.090	30.19	-1.090	24.38
170	-1.090	18.00	-1.090	15.18	-1.090	12.36
165	-1.090	12.00	-1.090	10.17	-1.090	8.35
160	-1.090	9.00	-1.090	7.67	-1.090	6.34
155	-1.090	7.20	-1.090	6.17	-1.090	5.14
150	-1.090	6.00	-1.090	5.17	-1.090	4.34
145	-1.090	5.14	-1.090	4.46	-1.090	3.77
140	-0.920	4.78	-0.994	4.02	-1.090	3.34
135	-0.777	4.61	-0.835	3.88	-0.935	3.15
130	-0.668	4.42	-0.725	3.72	-0.817	3.03
125	-0.581	4.21	-0.639	3.56	-0.730	2.90
120	-0.490	4.06	-0.569	3.38	-0.664	2.77
115	-0.449	3.77	-0.514	3.20	-0.613	2.63
110	-0.389	3.58	-0.471	3.02	-0.576	2.49
105	-0.365	3.32	-0.440	2.84	-0.551	2.36
100	-0.340	3.10	-0.419	2.66	-0.538	2.22
95	-0.324	2.88	-0.390	2.52	-0.536	2.09
90	-0.319	2.68	-0.411	2.32	-0.546	1.96
85	-0.324	2.48	-0.423	2.16	-0.566	1.85
80	-0.340	2.30	-0.445	2.02	-0.598	1.74
75	-0.365	2.14	-0.478	1.89	AXIAL FAILURE	
70	-0.389	1.99	-0.522	1.76	AXIAL FAILURE	
65	-0.449	1.84	AXIAL FAILURE			
60	-0.490	1.73	AXIAL FAILURE			
55	AXIAL FAILURE					

Table 4-1 (k)

NET SECTION STRESS - THICK WALL MODEL FOR 3/4" OD

CIRCUMFERENTIAL CRACK - NEUTRAL AXIS and SHAPE FACTOR FOR K = .7

ALPHA	F=0		F=.1		F=.2	
degree	H	SF	H	SF	H	SF
175	-1.090	36.00	-1.090	30.19	-1.090	24.38
170	-1.090	18.00	-1.090	15.18	-1.090	12.36
165	-1.090	12.00	-1.090	10.17	-1.090	8.35
160	-1.090	9.00	-1.090	7.67	-1.090	6.34
155	-1.090	7.20	-1.090	6.17	-1.090	5.14
150	-1.090	6.00	-1.090	5.17	-1.090	4.34
145	-1.090	5.14	-1.090	4.46	-1.090	3.77
140	-1.090	4.50	-1.090	3.92	-1.090	3.34
135	-1.090	4.00	-1.090	3.50	-1.090	3.00
130	-0.863	3.89	-0.956	3.28	-1.090	2.74
125	-0.753	3.72	-0.835	3.15	-0.987	2.57
120	-0.668	3.55	-0.749	3.01	-0.885	2.47
115	-0.589	3.39	-0.684	2.86	-0.818	2.36
110	-0.548	3.18	-0.635	2.71	-0.772	2.24
105	-0.490	3.03	-0.599	2.56	-0.742	2.13
100	-0.480	2.82	-0.577	2.42	-0.727	2.02
95	-0.464	2.64	-0.566	2.27	-0.725	1.92
90	-0.458	2.46	-0.568	2.14	-0.736	1.81
85	-0.464	2.30	-0.581	2.01	-0.761	1.71
80	-0.480	2.14	-0.590	1.89	AXIAL FAILURE	
75	-0.490	2.02	-0.643	1.77	AXIAL FAILURE	
70	-0.548	1.86	AXIAL FAILURE			
65	-0.589	1.75	AXIAL FAILURE			
60	AXIAL FAILURE					

Table 4-1 (1)

NET SECTION STRESS - THICK WALL MODEL FOR 3/4" OD

CIRCUMFERENTIAL CRACK - NEUTRAL AXIS and SHAPE FACTOR FOR K = .8

ALPHA	F=0		F=.1		F=.2	
degree	H	SF	H	SF	H	SF
175	-1.090	36.00	-1.090	30.19	-1.090	24.38
170	-1.090	18.00	-1.090	15.18	-1.090	12.36
165	-1.090	12.00	-1.090	10.17	-1.090	8.35
160	-1.090	9.00	-1.090	7.67	-1.090	6.34
155	-1.090	7.20	-1.090	6.17	-1.090	5.14
150	-1.090	6.00	-1.090	5.17	-1.090	4.34
145	-1.090	5.14	-1.090	4.46	-1.090	3.77
140	-1.090	4.50	-1.090	3.92	-1.090	3.34
135	-1.090	4.00	-1.090	3.50	-1.090	3.00
130	-1.090	3.60	-1.090	3.17	-1.090	2.74
125	-0.989	3.34	-1.090	2.90	-1.090	2.52
120	-0.863	3.20	-0.999	2.71	-1.090	2.34
115	-0.778	3.05	-0.896	2.59	-1.090	2.18
110	-0.714	2.89	-0.831	2.47	-1.090	2.05
105	-0.668	2.74	-0.787	2.34	-1.090	1.94
100	-0.636	2.58	-0.759	2.22	-0.986	1.86
95	-0.617	2.43	-0.747	2.10	-0.982	1.77
90	-0.611	2.28	-0.748	1.98	-1.090	1.67
85	-0.617	2.14	-0.764	1.87	AXIAL FAILURE	
80	-0.636	2.01	-0.795	1.76	AXIAL FAILURE	
75	-0.668	1.88	AXIAL FAILURE			
70	-0.714	1.76	AXIAL FAILURE			
65	AXIAL FAILURE					

Table 4-1 (m)

NET SECTION STRESS - THICK WALL MODEL FOR 3/4" OD

CIRCUMFERENTIAL CRACK - NEUTRAL AXIS and SHAPE FACTOR FOR K = .9

ALPHA	F=0		F=.1		F=.2	
degree	H	SF	H	SF	H	SF
175	-1.090	36.00	-1.090	30.19	-1.090	24.38
170	-1.090	18.00	-1.090	15.18	-1.090	12.36
165	-1.090	12.00	-1.090	10.17	-1.090	8.35
160	-1.090	9.00	-1.090	7.67	-1.090	6.34
155	-1.090	7.20	-1.090	6.17	-1.090	5.14
150	-1.090	6.00	-1.090	5.17	-1.090	4.34
145	-1.090	5.14	-1.090	4.46	-1.090	3.77
140	-1.090	4.50	-1.090	3.92	-1.090	3.34
135	-1.090	4.00	-1.090	3.50	-1.090	3.00
130	-1.090	3.60	-1.090	3.17	-1.090	2.74
125	-1.090	3.27	-1.090	2.90	-1.090	2.52
120	-1.090	3.00	-1.090	2.67	-1.090	2.34
115	-1.090	2.77	-1.090	2.48	-1.090	2.18
110	-0.927	2.66	-1.090	2.31	-1.090	2.05
105	-0.863	2.52	-1.090	2.17	-1.090	1.94
100	-0.821	2.39	-1.090	2.04	-1.090	1.84
95	-0.798	2.26	-0.996	1.95	-1.090	1.75
90	-0.790	2.13	-0.999	1.85	-1.090	1.67
85	-0.798	2.01	-1.090	1.75	AXIAL FAILURE	
80	-0.821	1.89	-1.090	1.67	AXIAL FAILURE	
75	-0.863	1.78	AXIAL FAILURE			
70	-0.927	1.67	AXIAL FAILURE			
65	AXIAL FAILURE					

1

IMAGE EVALUATION TEST TARGET (MT-3)

150mm

6"

1

IMAGE EVALUATION TEST TARGET (MT-3)

1.0 1.1 1.25 1.4 1.6 1.8 2.0 2.2 2.5 2.8 3.2 3.6 4.0

150mm

6"

1

IMAGE EVALUATION
TEST TARGET (MT-3)

1.0 1.1 1.25 1.4 1.6 1.8 2.0 2.2 2.5 2.8

150mm

6"

Table 4-1 (n)

NET SECTION STRESS - THICK WALL MODEL FOR 3/4" OD

CIRCUMFERENTIAL CRACK - NEUTRAL AXIS and SHAPE FACTOR FOR K = 1

ALPHA	F=0		F=.1		F=.2	
degree	H	SF	H	SF	H	SF
175	-1.090	36.00	-1.090	30.19	-1.090	24.38
170	-1.090	18.00	-1.090	15.18	-1.090	12.36
165	-1.090	12.00	-1.090	10.17	-1.090	8.35
160	-1.090	9.00	-1.090	7.67	-1.090	6.34
155	-1.090	7.20	-1.090	6.17	-1.090	5.14
150	-1.090	6.00	-1.090	5.17	-1.090	4.34
145	-1.090	5.14	-1.090	4.46	-1.090	3.77
140	-1.090	4.50	-1.090	3.92	-1.090	3.34
135	-1.090	4.00	-1.090	3.50	-1.090	3.00
130	-1.090	3.60	-1.090	3.17	-1.090	2.74
125	-1.090	3.27	-1.090	2.90	-1.090	2.52
120	-1.090	3.00	-1.090	2.67	-1.090	2.34
115	-1.090	2.77	-1.090	2.48	-1.090	2.18
110	-1.090	2.57	-1.090	2.31	-1.090	2.05
105	-1.090	2.40	-1.090	2.17	-1.090	1.94
100	-1.090	2.25	-1.090	2.04	-1.090	1.84
95	-1.090	2.12	-1.090	1.93	-1.090	1.75
90	-1.090	2.0[illegible]	-1.090	1.83	-1.090	.67
85	-1.090	1.8[illegible]	-1.090	1.75	AXIAL FAILURE	
80	-1.090	1.30	-1.090	1.67	AXIAL FAILURE	
75	-1.090	1.71	AXIAL FAILURE			
70	AXIAL FAILURE					

Table 4-1 (p)

CIRCUMFERENTIAL THROUGH WALL CRACKS IN 7/8" OD TUBE
CALCULATED VALUES OF $\sigma/\sigma_f = 1/n$

by THICK WALL / THIN WALL MODEL

2 α	f = 0	0	0	0	0	0.1	0.1	0.1	0.1	0.1	0.2	0.2	0.2	0.2	0.2
	K = 0	0.6	0.7	0.8	0.9	0	0.6	0.7	0.8	0.9	0	0.6	0.7	0.8	0.9
120	0.382 0.381	0.583 0.581	AXIAL FAILURE			0.422 0.422	AXIAL FAILURE				0.464 0.472	AXIAL FAILURE			
150	0.263 0.262	0.468 0.466	0.500 0.498	0.532 0.530	0.562 0.562	0.294 0.296	0.520 0.524	0.556 0.560	0.591 0.595		0.334 0.341	0.586 0.597			
180	0.167 0.166	0.373 0.371	0.405 0.404	0.437 0.436	0.469 0.468	0.192 0.191	0.421 0.424	0.458 0.461	0.493 0.498	0.528 0.534	0.220 0.225	0.484 0.495	0.525 0.537	0.565 0.580	0.582 0.582
210	0.096 0.095	0.301 0.299	0.333 0.331	0.365 0.363	0.394 0.395	0.111 0.111	0.344 0.346	0.381 0.383	0.417 0.420	0.454 0.457	0.130 0.133	0.401 0.410	0.440 0.454	0.484 0.498	0.500 0.500
240	0.049 0.048	0.250 0.248	0.281 0.280	0.311 0.312	0.333 0.333	0.059 0.056	0.288 0.289	0.324 0.327	0.359 0.364	0.368 0.378	0.067 0.068	0.339 0.347	0.381 0.391	0.411 0.417	0.411 0.411
270	0.021 0.019	0.215 0.215	0.250 0.247	0.250 0.250	0.250 0.250	0.024 0.023	0.251 0.253	0.280 0.282	0.280 0.280	0.280 0.280	0.029 0.028	0.298 0.306	0.318 0.318	0.318 0.318	0.318 0.318
300	0.007 0.005	0.166 0.166	0.166 0.166	0.166 0.166	0.166 0.166	0.009 0.006	0.189 0.189	0.189 0.189	0.189 0.189	0.189 0.189	0.010 0.008	0.218 0.218	0.218 0.218	0.218 0.218	0.218 0.218
330	0.002 0.000	0.083 0.083	0.083 0.083	0.083 0.083	0.083 0.083	0.003 0.000	0.096 0.096	0.096 0.096	0.096 0.096	0.096 0.096	0.003 0.001	0.113 0.113	0.113 0.113	0.113 0.113	0.113 0.113

Figures within boldlines correspond to tensile failure

Table 4-2 (a)

PROGRAM C1
TUBE DIAMETER : 3/4" (HEAT 9866) M3
UNSUPPORTED GEOMETRY

TEST PIECE N°.	CRACK LENGTH (2 α)		p_c	COD	n *	FAILURE MODE
	mm (OD)	deg (AVG)	bar	mm	-	
10a	31	186	> 385	1.0	< 4.27	crack initiation (≈ 0.5 mm)
10b	30	180	442	0.8	3.72	2.2 mm length extension
11a	21.5	128	565	0.8	2.91	7 mm length extension
11b	20	120	612	1.0	2.69	1 mm length extension
12a	23	137	> 548	0.75	< 3.0	leakage
12b	23	137	572	0.9	2.87	14 mm length extension

* The "shape factor" is calculated by $n = \sigma_f / \sigma$

with
$$\sigma = \frac{p}{2} (R/t - 1) = 3.62\,p$$
$$\sigma_f = 0.515\,(YS + UTS) = 0.515\,(425 + 730) = 595\ MPa$$

Table 4-2 (b)

PROGRAM C1
MEASUREMENTS OF : C.O.D. (δ); SLIT OPENING (b)
AND BULGING (ϕ_{max}) VERSUS INTERNAL PRESSURE
(circumferential through wall flaws)

Material Index	Test-piece Number and type	Slit length (mm)	Sealing System	p bar	δ mm	b mm	ϕ_{max} mm	p/p_{max}
M3	10	31	12	290	.05	.50		0.75
			12	330	.10	.75		0.86
			12	380	.30	1.2		0.99
			12	385	1.0	3.2	19.3	1
		30	12	290	.05	.45		0.65
			12	330	.10	.50		0.75
			12	380	.15	.80		0.86
			12	385	.30	1.10	19.15	0.87
			12	442	.8	2.10		1
	11	21.5	7	373	.05	.50	19.1	0.66
			7	425	.10	.65	19.2	0.75
			7	465	.15	.70	19.2	0.82
			11	475	.20	.75	19.2	0.84
			11	507	.25	.80	19.3	0.90
			11	550	.75	1.8	19.9	0.97
			11	565	.8	4.8	20.4	1
		20	7	373	.05	.45	19.1	0.61
			7	425	.05	.50	19.2	0.69
			7	465	.10	.55	19.2	0.76
			11	475	.10	.55	19.2	0.78
			11	507	.15	.55	19.2	0.83
			11	550	.20	.75	19.5	0.90
			11	565	.45	1.3	19.7	0.92
			11	612	1.0	2.5	20.6	1
	28	23	12	427	.05	.60		0.75
			12	500	.15	.80		0.87
			12	548	.75	1.8	19.7	0.96
		23	12	427	.05	.45		0.75
			12	500	.10	.55		0.87
			12	548	.25	.90		0.96
			12	572	.9	5.6		1

Table 4-2 (c)

PROGRAM C2

Tube diameter : 3/4" (*)

Test #	Crack length 2 α (deg.)	FDB support	offset (mm)	p_c bar	Failure mode
1	-	X	0	> 660	no failure (large bulging)
2	180	-	-	240	propagation (4 mm)
3	180	X	0	520	propagation (2 mm)
4	180	X	10	> 480	leakage (COD = 1.6 - 0.55 = 1.05 mm)
5	105	X	10	620	axial crack (17mm)
6	180	X	20	490	propagation (2 mm)
7	105	-	-	555	axial crack (19mm)
8	105	X	20	585	axial crack (18mm)

(*) undocumented origin

Table 4-2(d)
PROGRAM C3
TUBE DIAMETER 7/8"
(TEST PERFORMED WITH 1 SHIM OF 0.13 mm, EXCEPT AS NOTED)

TEST	CRACK LENGTH (2a)		SUPPORT		pc	COD	δ max	n *	FAILURE MODE	COMMENTS
	deg	mm (ID)	FDB	TSP	bar	mm	mm			
1	300	51	-	X	350	-	9.6	3.79	full circumference	
2	300	51	-	X	372	-	6.0	3.56	full circumference	
3	270	46	X	X	>410	-	4.6	<3.23	leakage	failure at lower pressure when repressurized with 2 shims
4	180	31	X	X	545	1.1	11.1	2.57	crack initi. (1.5 mm)	2 shims
5	210	36	X	X	>462	1.0	12.0	<2.87	leakage	small crack initiation (< 0.5 mm) at one end only
6	210	36	X	X	450	1.0	20.8	2.95	propagation (6 mm)	2 shims (2 prior tests resulted in leakage at 438 and 424 bar)
7	240	41	X	X	462	0.9	16.1	2.87	full circumference	2 shims (prior test resulted in leakage at 428 bar)
8	210	36	-	X	442	1.0	43.8	3.00	propagation (3 mm)	2 shims
9	240	41	X	X	450	-	12	2.95	propagation	id.
10	270	46	X	X	415	1.1	10.1	3.20	crack initi. (1.5 mm)	.
11	270	46	-	X	388	-	33.8	3.42	propagation	2 shims
12	180	31	X	X	543	-	13.8	2.44	propagation	id.
13	300	51	X	X	>301	1.0	2.4	<4.40	leakage	Without shim (full circ. failure at 301 bar when repressurized with 1 shim
14	300	51	X	X	352	-	2.2	3.77	full circumference	
(15)	210	36	X	X	478	1.0	2.1	2.77	crack initiation(1mm)	
22	180	31	-	-	323	0.9	-	4.10	propagation (18 mm)	
23	240	41	-	-	154	0.8	-	8.61	propagation (3 mm)	
24	240	41	-	-	146	0.8	-	9.08	propagation (10 mm)	
25	180	31	-	-	235	1.0	-	5.64	propagation (8 mm)	without shim
26	150	26	-	-	419	0.8	-	3.16	propagation (20 mm)	
27	210	36	-	-	-	0.8	-	-	propagation (14 mm)	lost pressure record
28	210	36	-	-	245	1.0	-	5.41	propagation (13 mm)	
29	120	21	-	-	519	1.0	-	2.55	propagation (6 mm)	
31	150	26	-	-	341	1.0	-	3.8[illegible]	crack initiation(1mm)	without shim
62	120	21	-	-	581	0.9	-	2.28	propagation (4mm)	

* The "shape factor" is calculated by $n = \sigma_f/\sigma$

with $\sigma_f = 0.515$ (YS+UTS) = 0.515 (276+655) = 480 MPa for nr. 1 to 15 (heat 71383)
= 0.515 (292+701) = 510 MPa for nr. 22 to 32 (heat 71692)

$\sigma = p/2\ (9/t - 1) = 3.62\ p$

Table 4-2(e)

PROGRAM C3
TUBE DIAMETER 3/4" (HEAT 70699)
(TEST PERFORMED WITH 1 SHIM OF 0.13 mm, EXCEPT AS NOTED)

TEST	CRACK LENGTH (2a)		SUPPORT		p_c	COD	F max	M max	n *	FAILURE MODE	COMMENTS
	deg	mm (ID)	FDB	TSP	bar	mm	N	Nm			
1	300	44.2	X	-	377	0.9	210	32	4.10	full circum.	
2	300	44.2	X	-	515	1.1	380	57	3.00	id..	FDB offset (20mm)/2 shims
3	300	44.2	X	-	> 320	0.9	375	56	< 4.83	id.	FDB offset (10mm)/interrupted test/failed at 308 bar after repressurization
4	165	24.3	-	-	428	1.0	-	-	3.61	propagation (8 mm)	
5	165	24.3	-	-	398	0.9	-	-	3.89	propagation (9 mm)	
6	270	39.7	X	-	> 622	1.1	430	65	< 2.49	full circum.	FDB offset (20mm)/2 shims/interrupted test/failed at 498 bar after repressurization
7	270	39.7	X	-	590	0.9	520	78	2.62	full circum.	2 shims
8	270	39.7	X	-	590	1.1	460	69	2.62	propag.(3mm)	2 shims
9	270	39.7	X	-	> 605	1.0	505	75	< 2.56	full circum.	FDB offset (10mm)/2 shims/interrupted test/failed at 545 bar after repressurization
10	300	44.2	X	-	436	0.9	210	32	3.55	id.	
11	165	24.3	-	-	442	1.0	-	-	3.50	crack initiation-.6mm	
17	270	39.7	X	X	610	1.1	595	89	2.54	propagation (1.5 mm)	
18	270	39.7	-	X	496	0.9	60	54	3.12	id. (3 mm)	
19	300	44.2	-	X	423	0.9	35	32	3.66	full circum.	
20	270	39.7	-	X	492	0.9	60	54	3.14	id.	2 shims
21	300	44.2	X	X	441	0.8	125	19	3.51	id.	
22	300	44.2	-	X	447	1.0	20	18	3.46	id.	

* The "shape factor" is calculated by $n = \sigma_f/\sigma$ with $\sigma = p/2\ (R/t - 1) = 3.62\ p$; $\sigma_f = 0.515\ (YS + UTS) = 0.515\ (346 + 740) = 560$ MPa

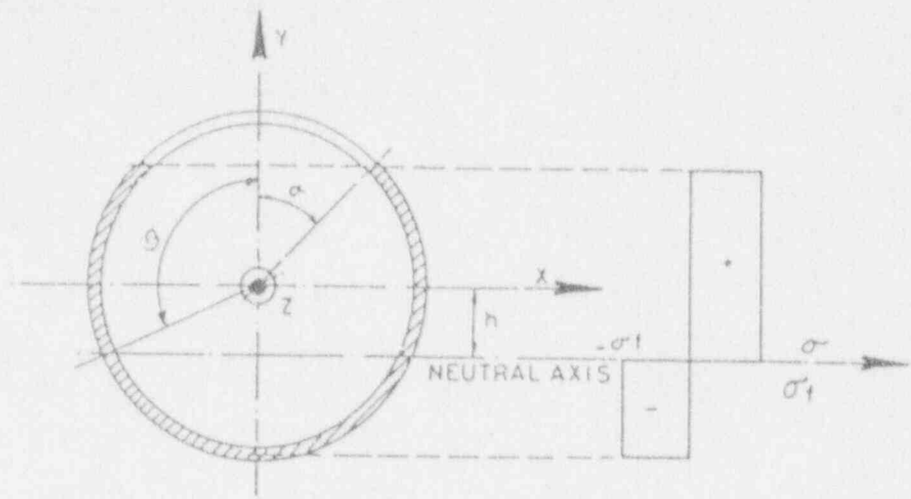

FIG 4.1 (a)

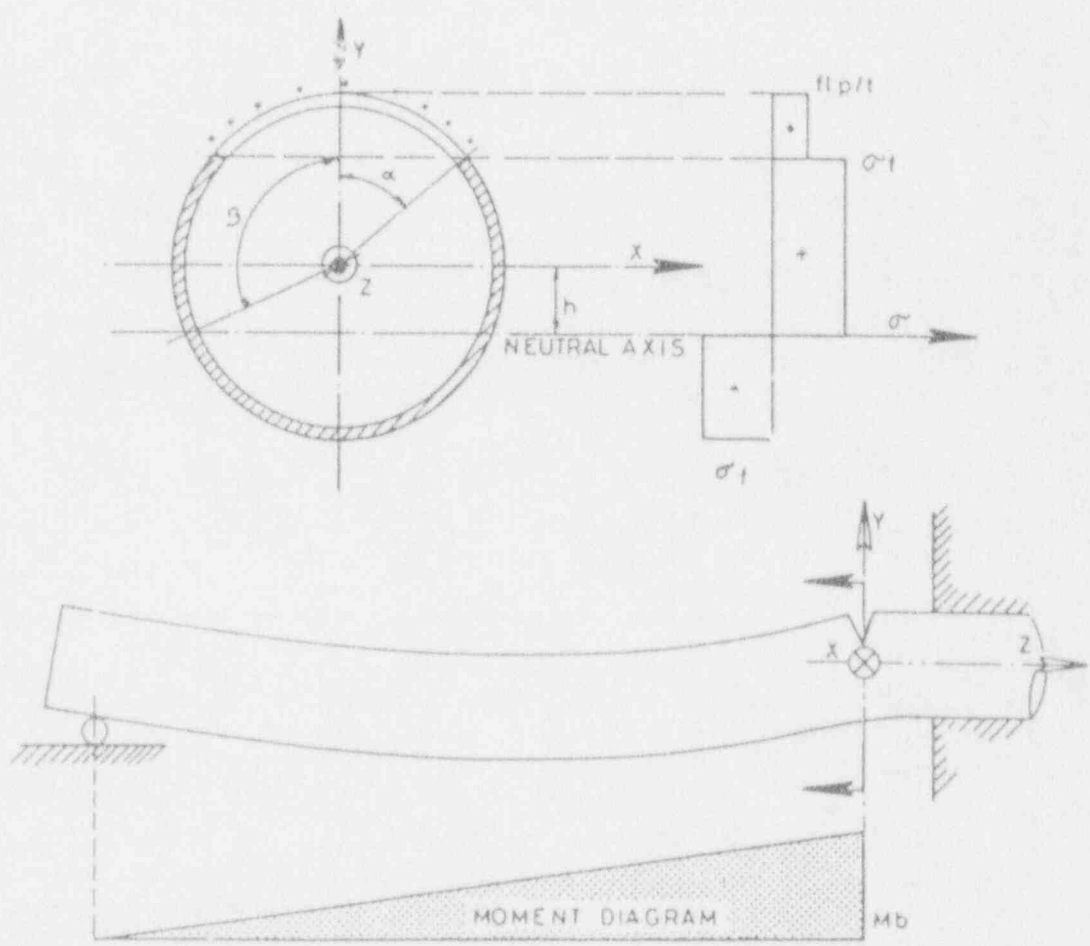

Figure 4-1(b) Net section stress - thin wall model

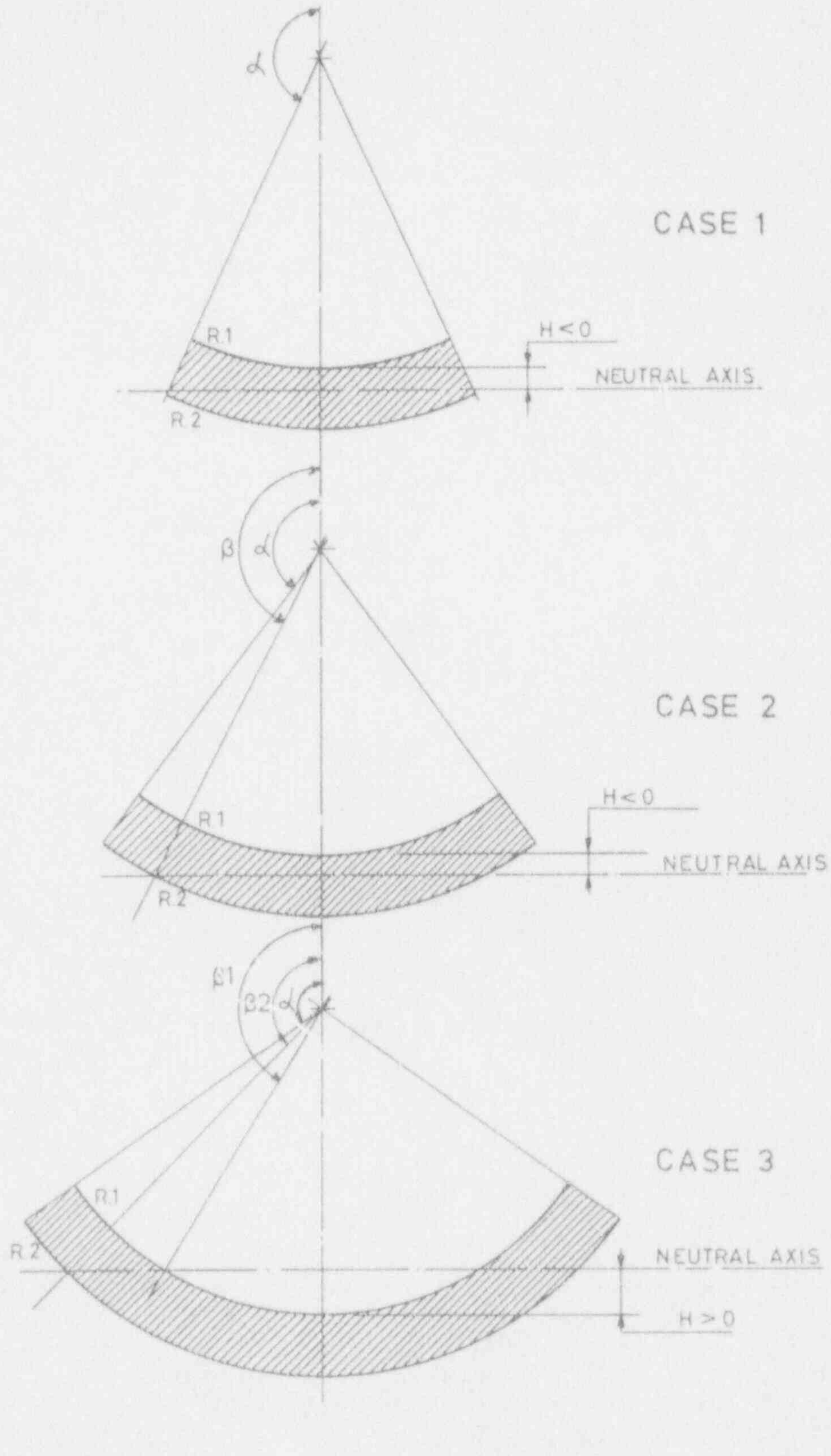

Figure 4-1(c) Net section stress - thick wall model

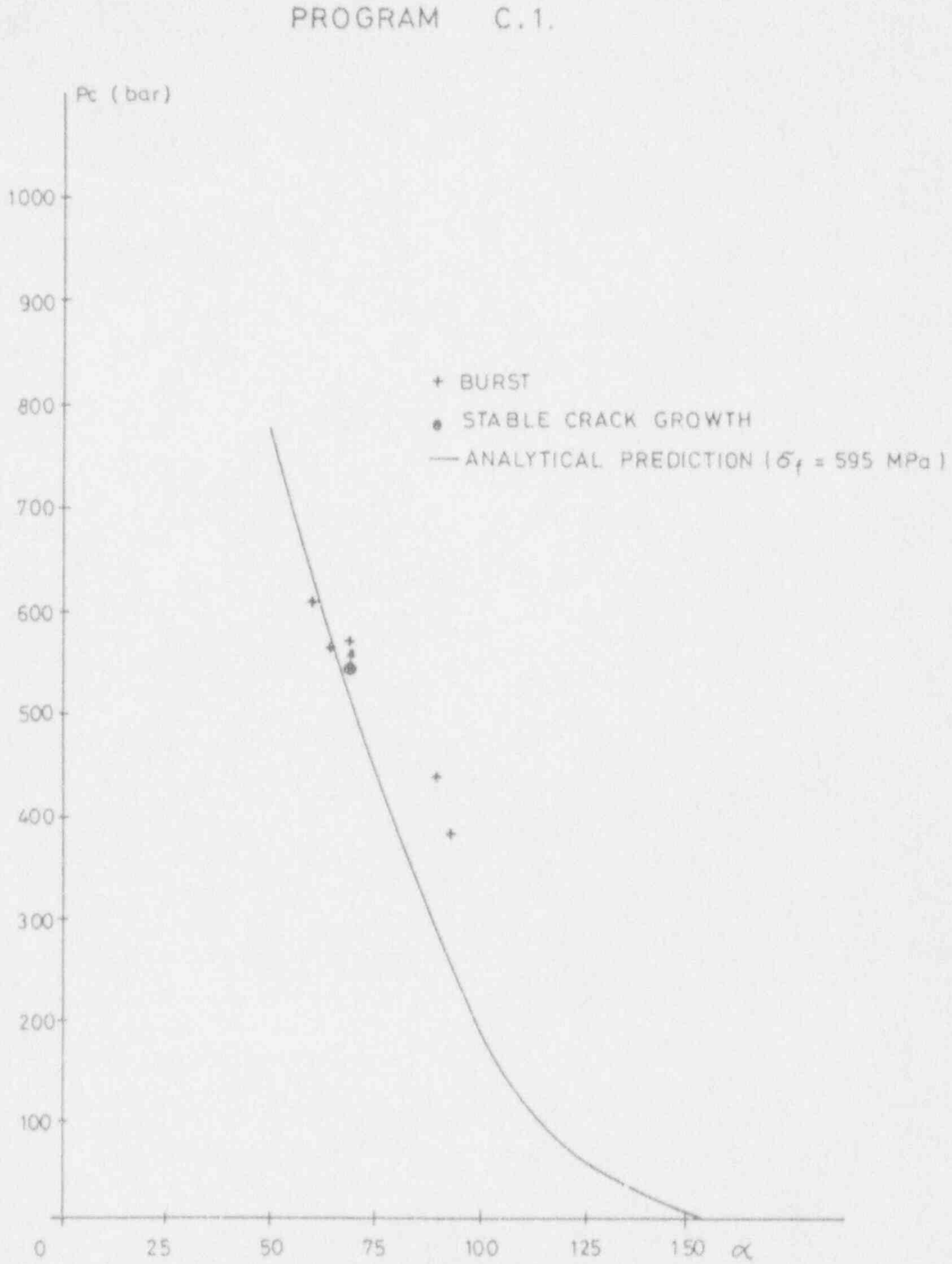

Figure 4-2(a) Circumferential through wall flaws
Inconel 3/4" OD

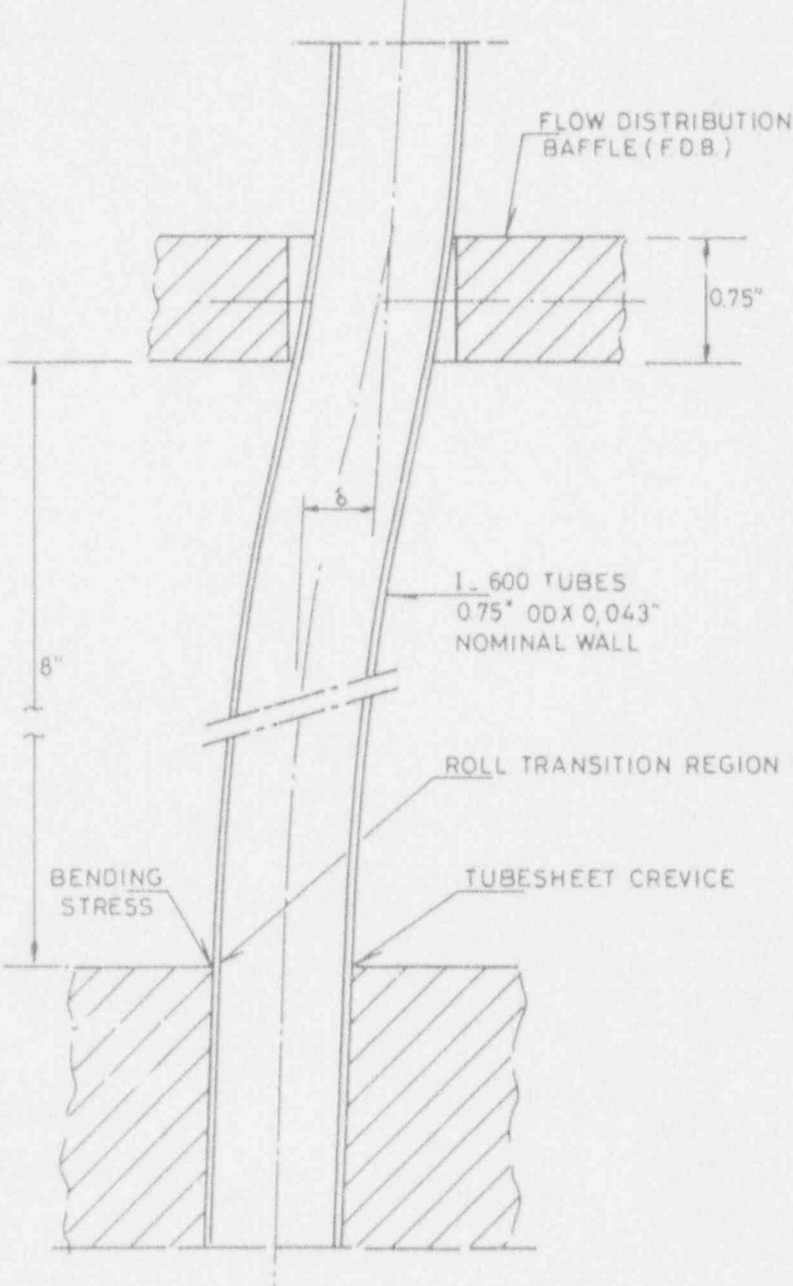

Figure 4-2(b) Bending stresses in tube roll transition region due to tubesheet - FDB alignment offset (δ)

(NOTE : DIMENSIONS EXAGGERATED FOR CLARITY OF ILLUSTRATION)

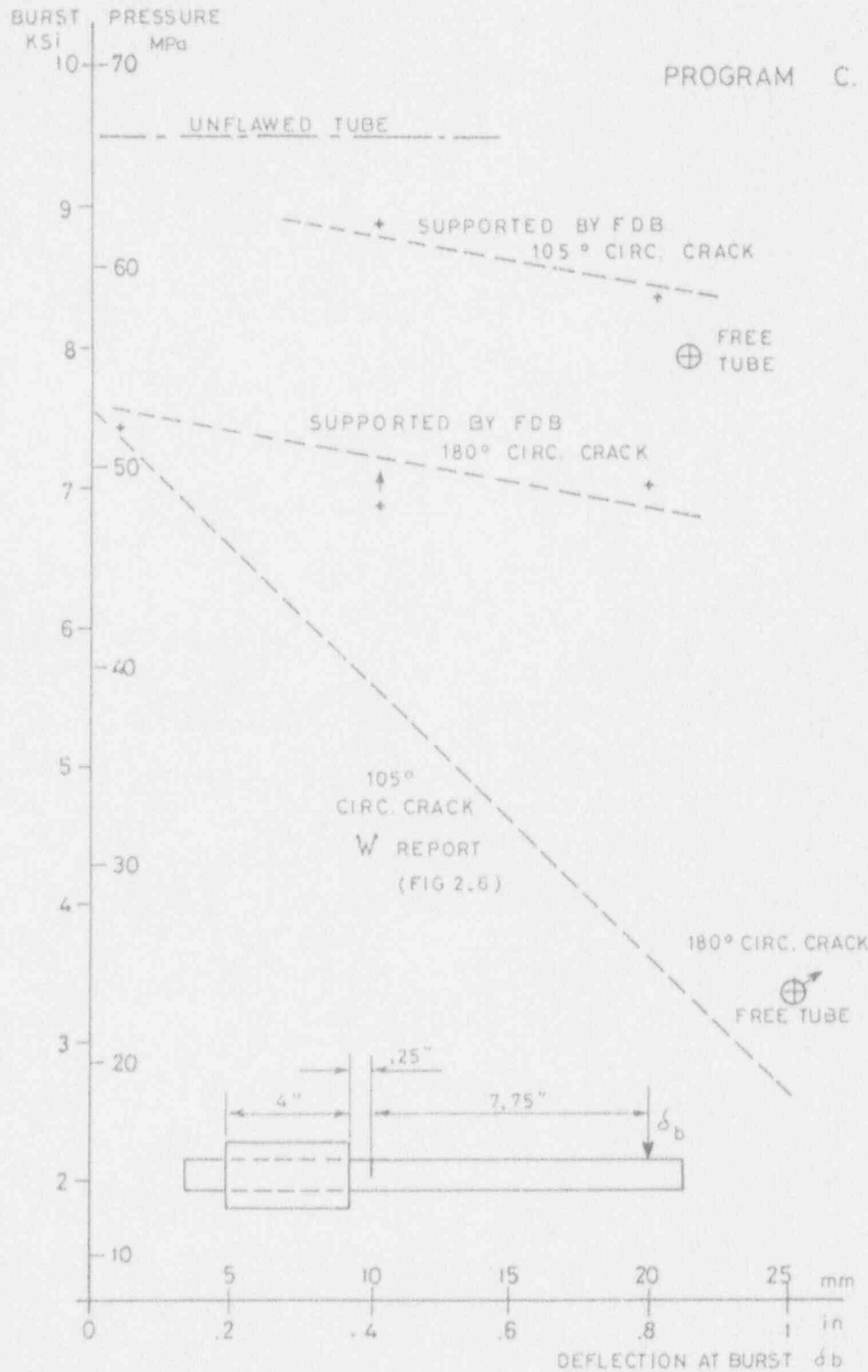

Figure 4-2(c) Circumferential through wall flaws
Inconel 3/4" OD

PROGRAM C.2.

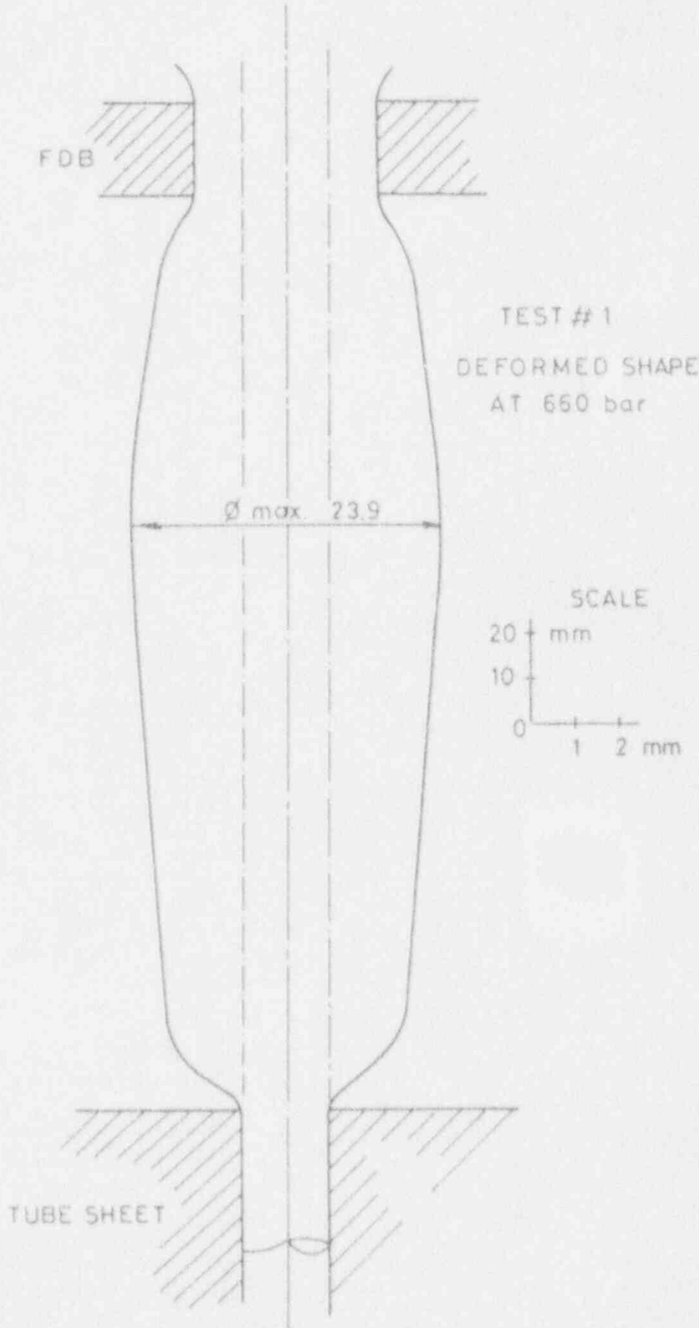

Figure 4-2(d) Unflawed test specimen Inconel 3/4" OD

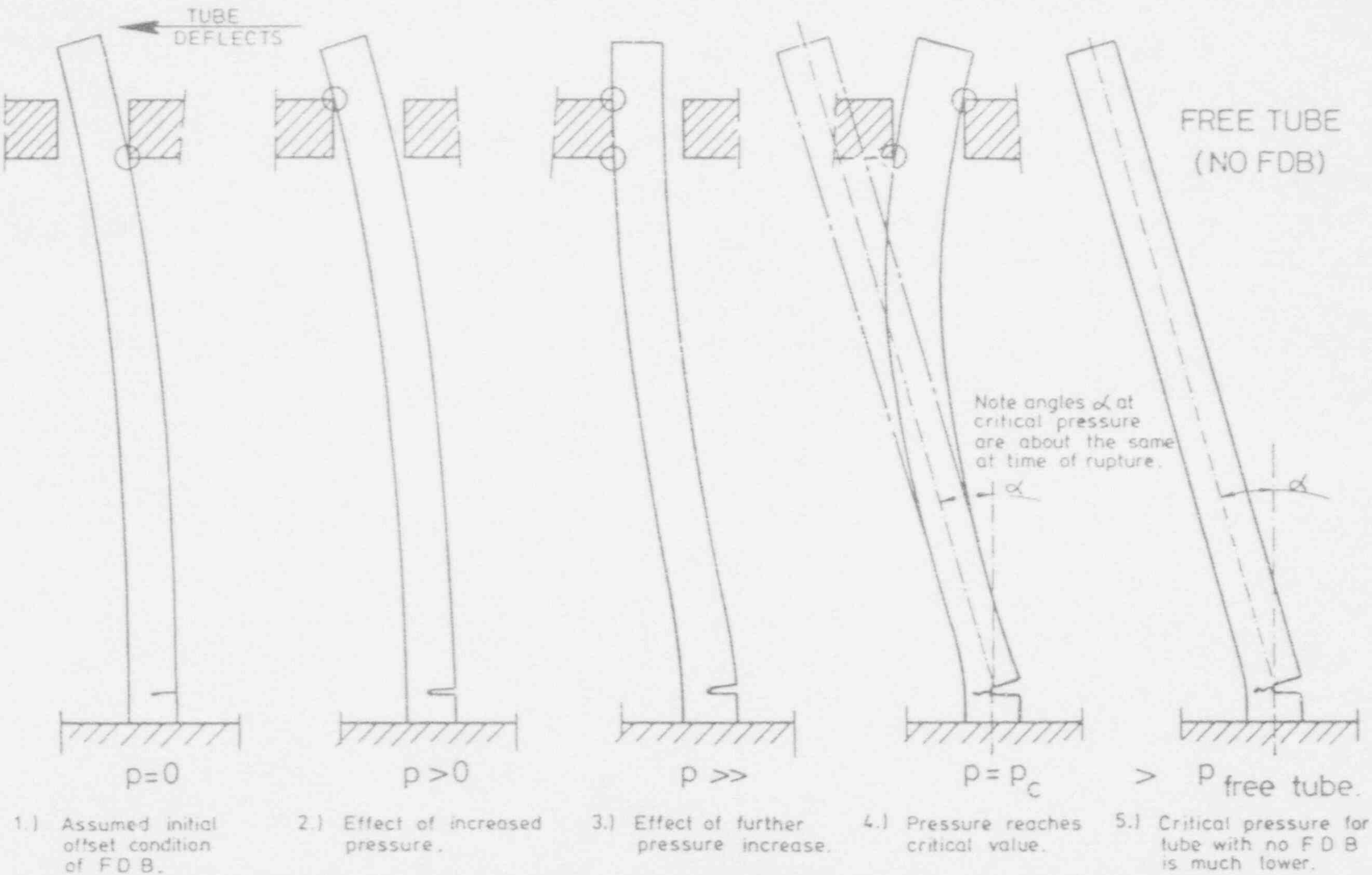

Figure 4-2(e) Schematic illustration of influence of a FDB offset on the burst of a tube with 180° circ. crack

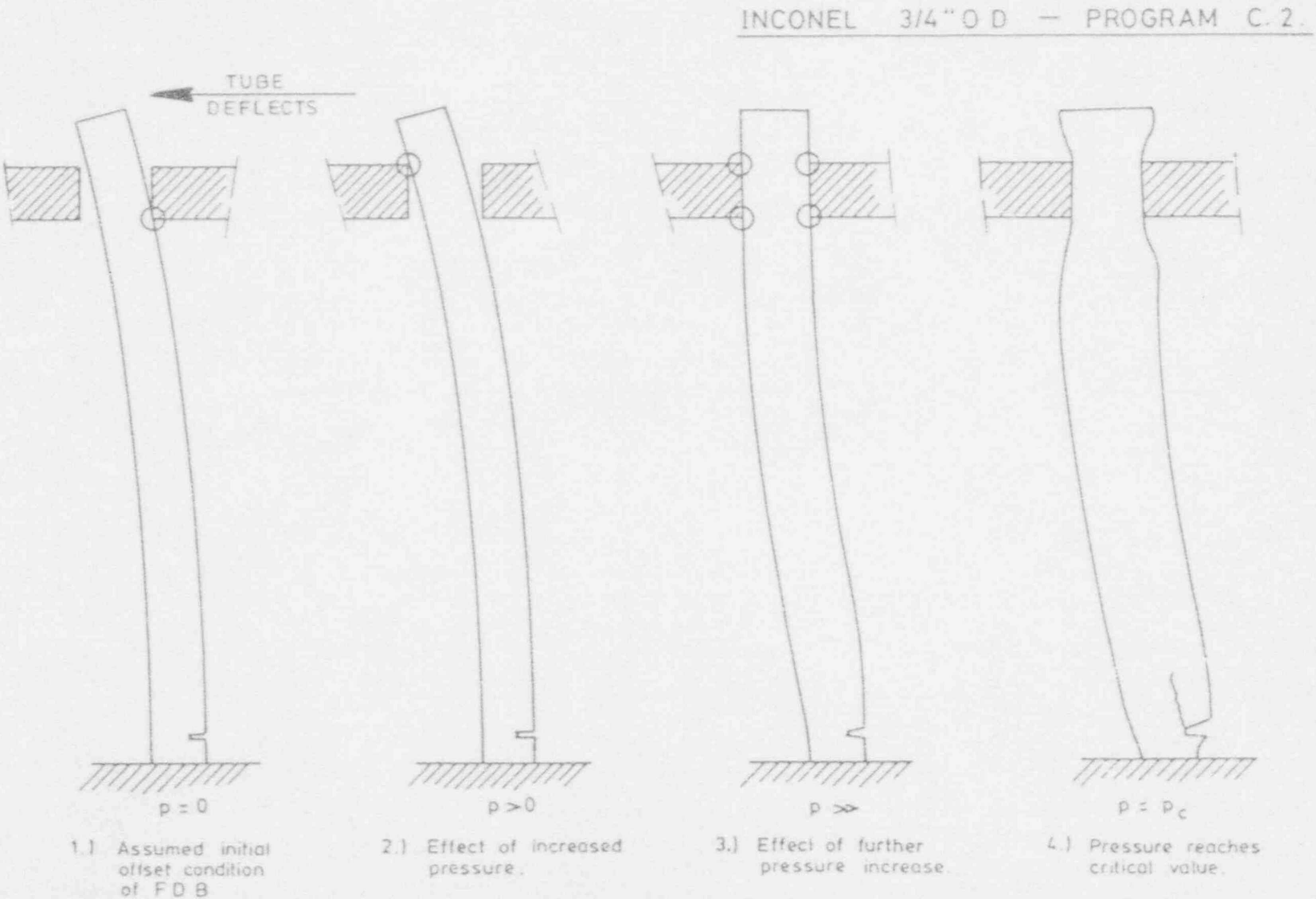

Figure 4-2(f) Schematic illustration of influence of a FDB offset on the burst of a tube with 105° circ. crack

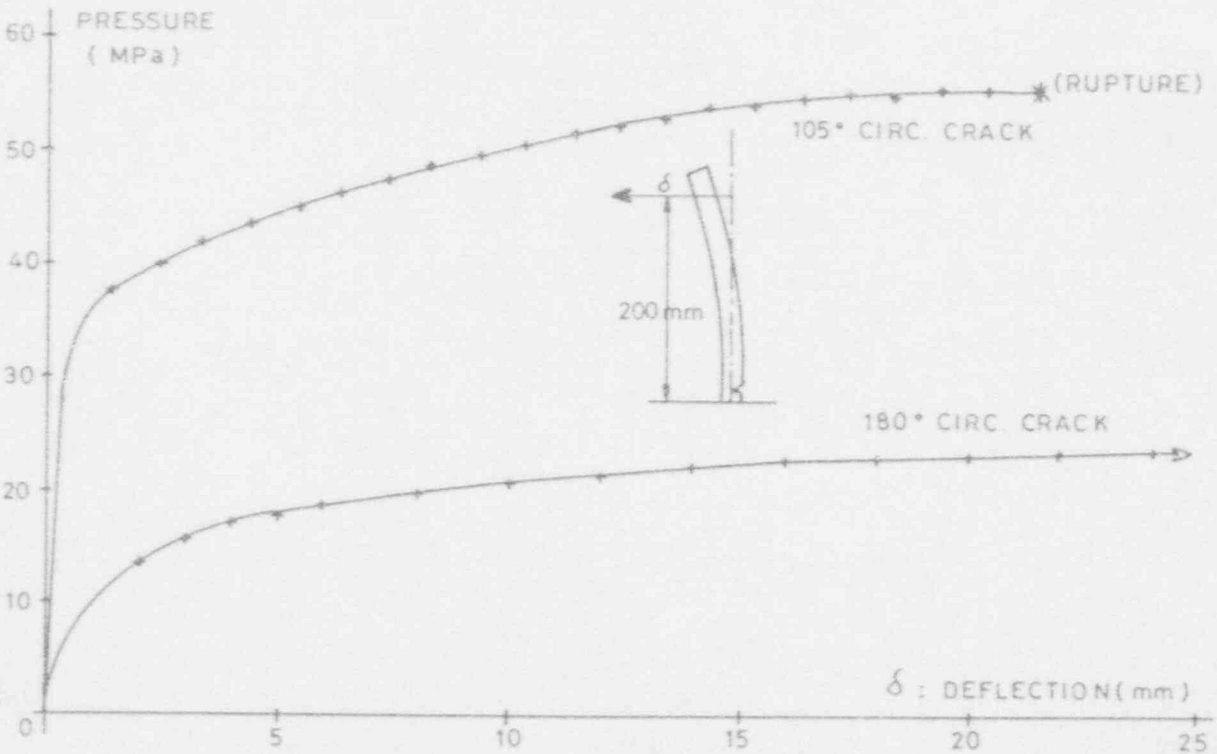

CIRCUMFERENTIAL THROUGH-WALL FLAWS. INCONEL 3/4" O D - PROGRAM C.2.

Figure 4-2(g) Burst testing without FDB

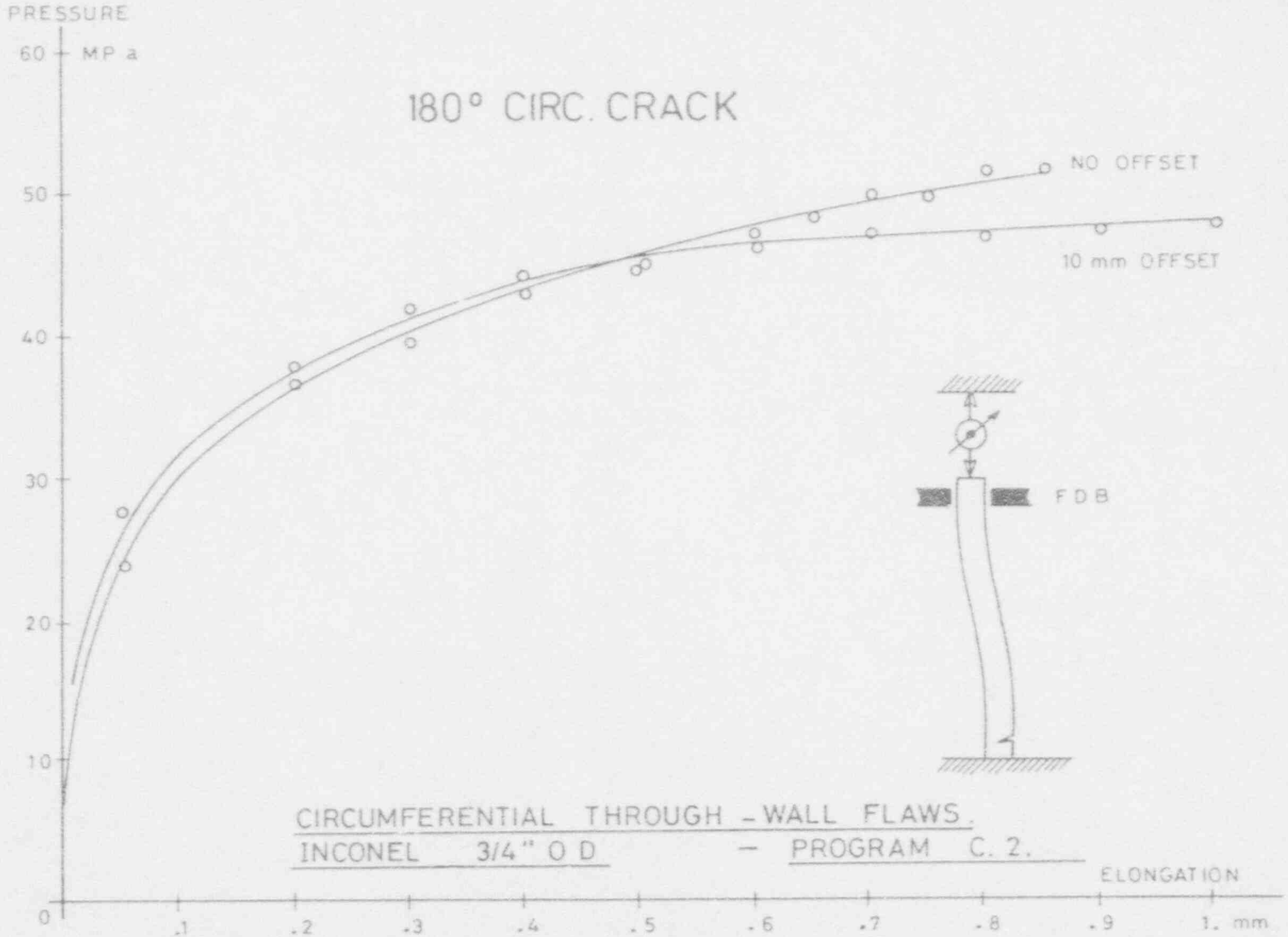

Figure 4-2(h) Burst testing with FDB

PROGRAM C. 3 (Subset 1.)

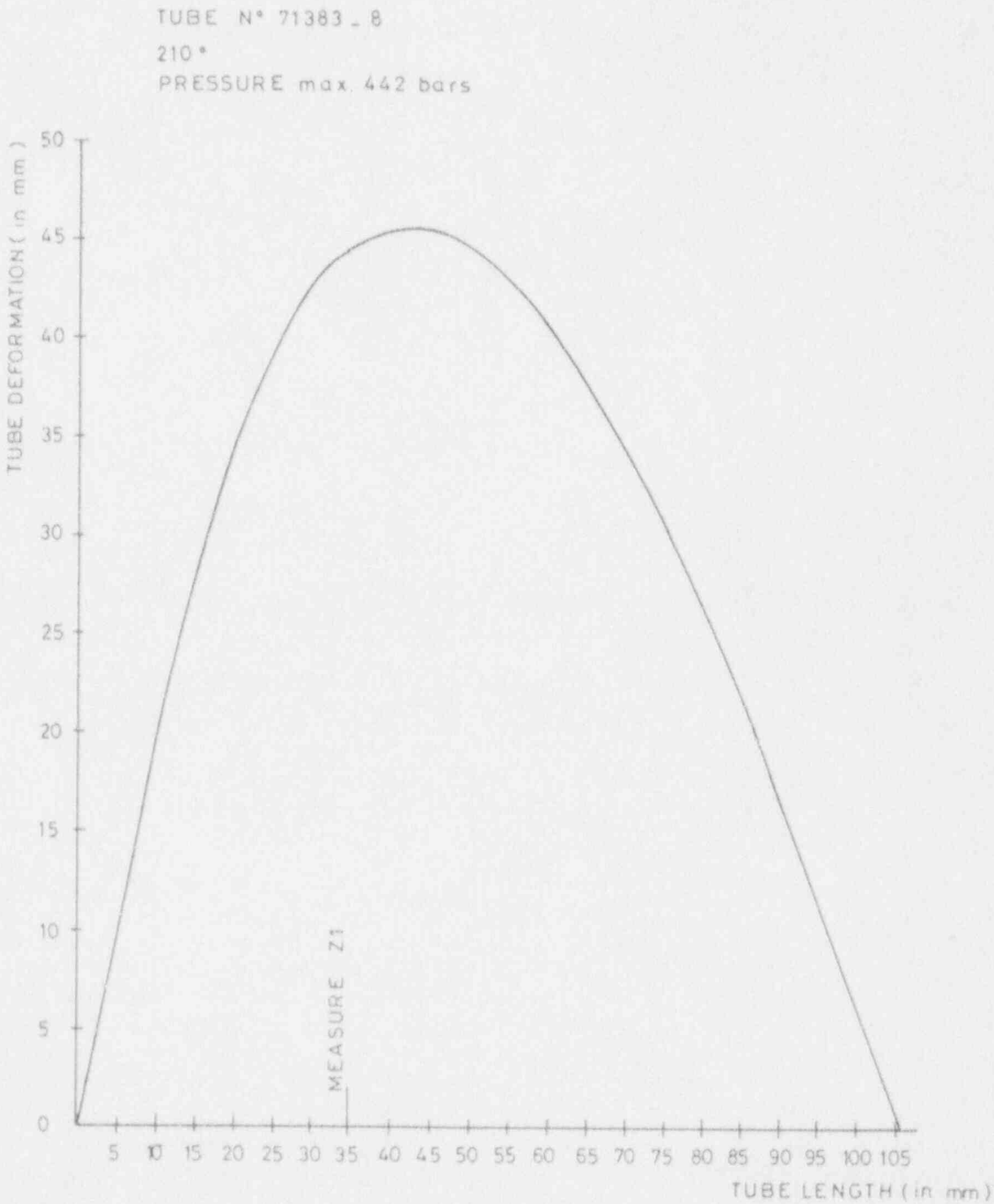

Figure 4-2(i) Circumferential through wall flaws

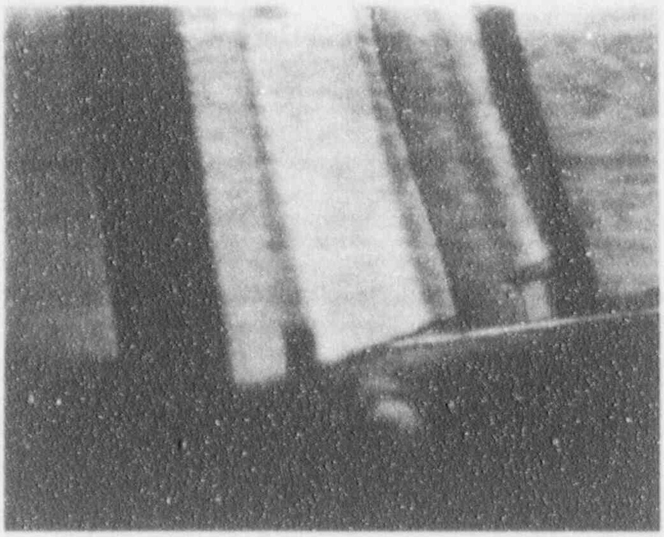

71383-6

JUST BEFORE BURST

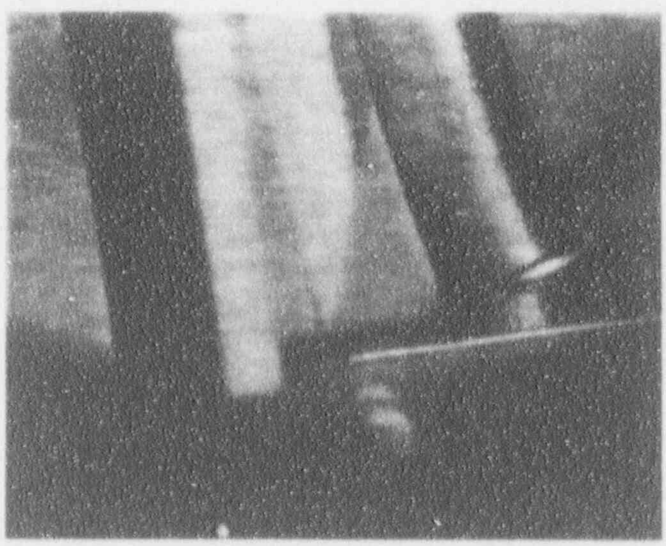

71383-6

JUST AFTER BURST

Figure 4-2 (j) Program C3 (subset 1) - Pictures from video recording

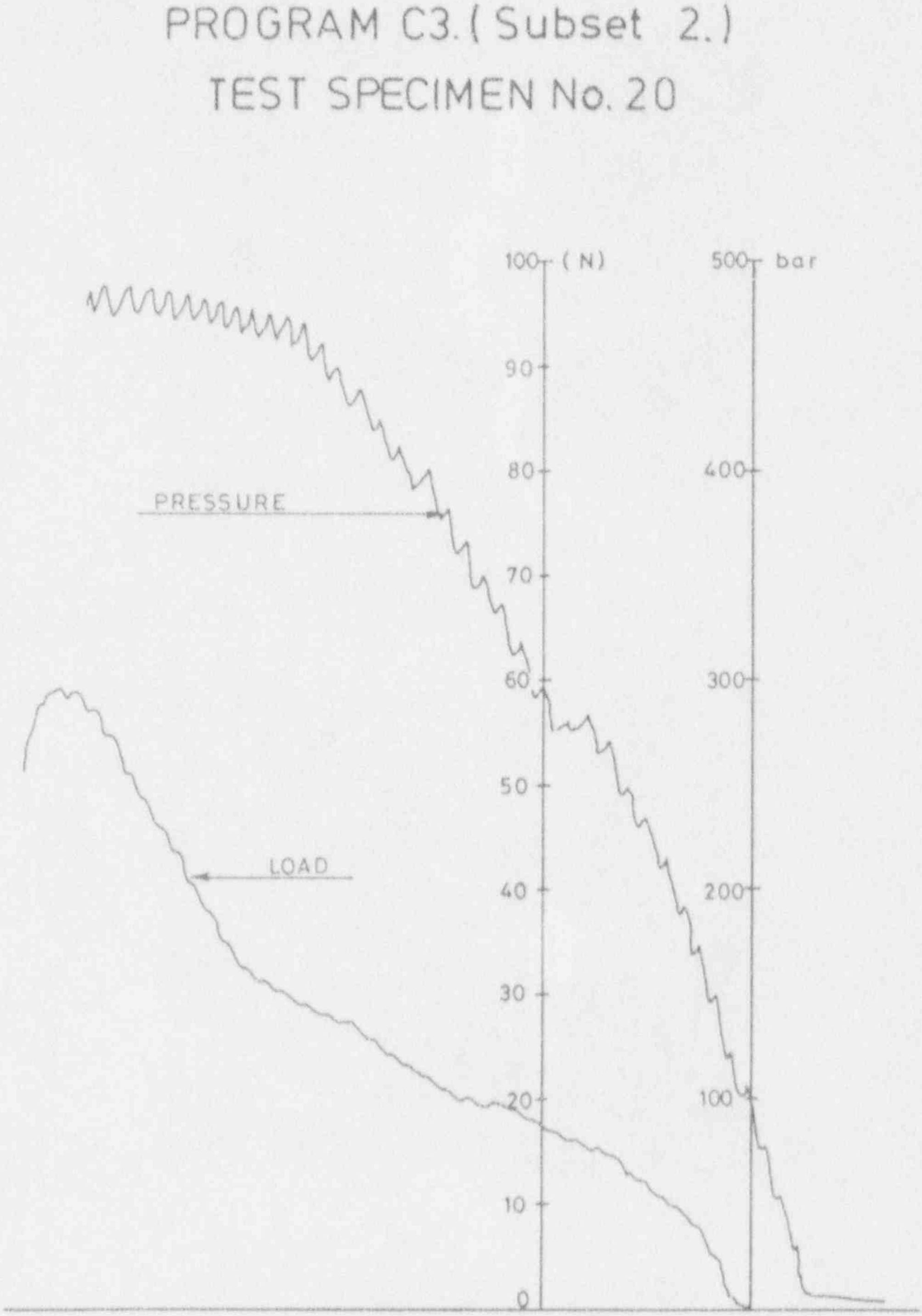

Figure 4-2(k) Circumferential through wall flaws. Typical record of pressure and load - Time history

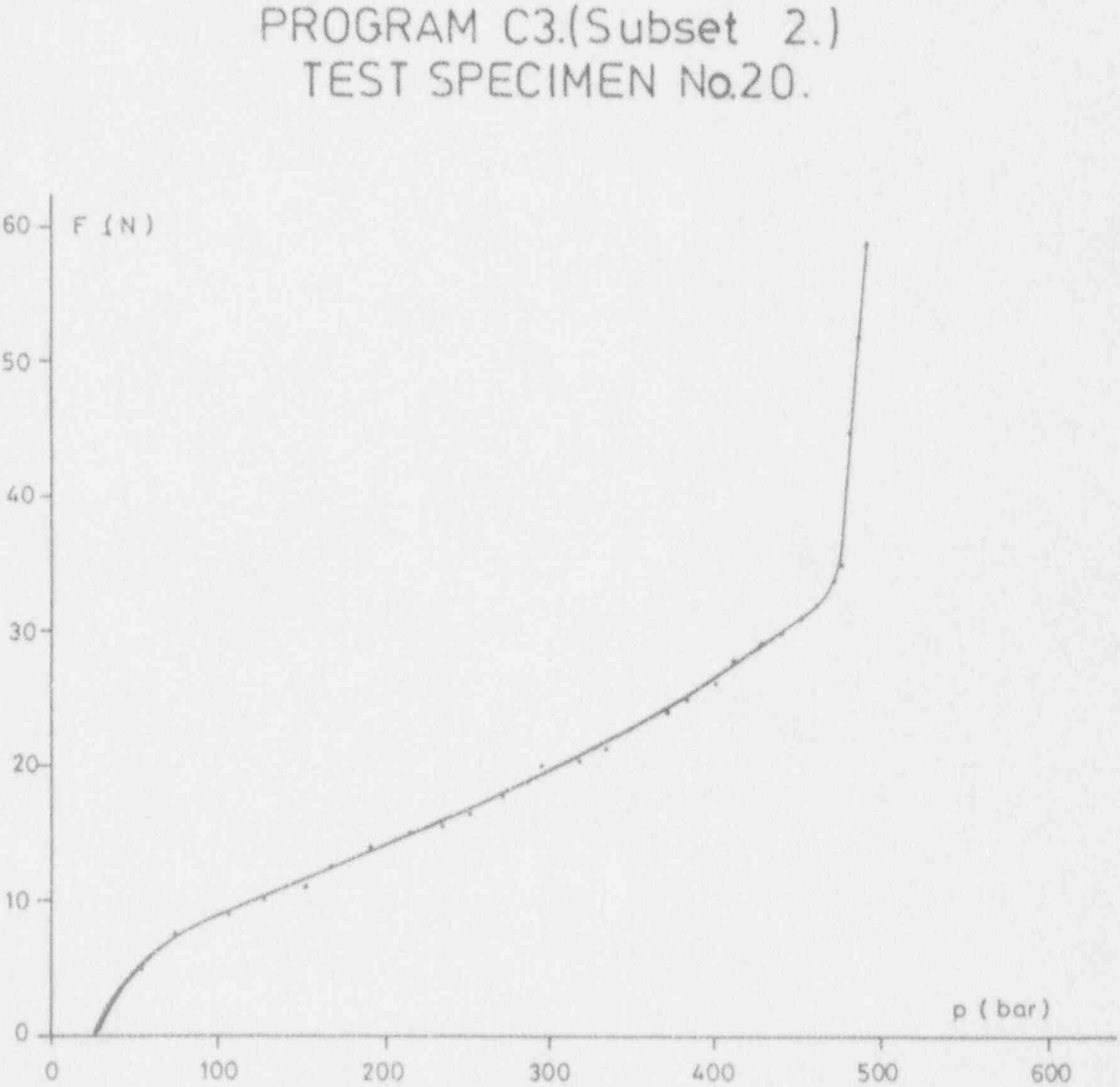

Figure 4-3(a) Circumferential through wall flaws. Lateral restraint load as a function of pressure

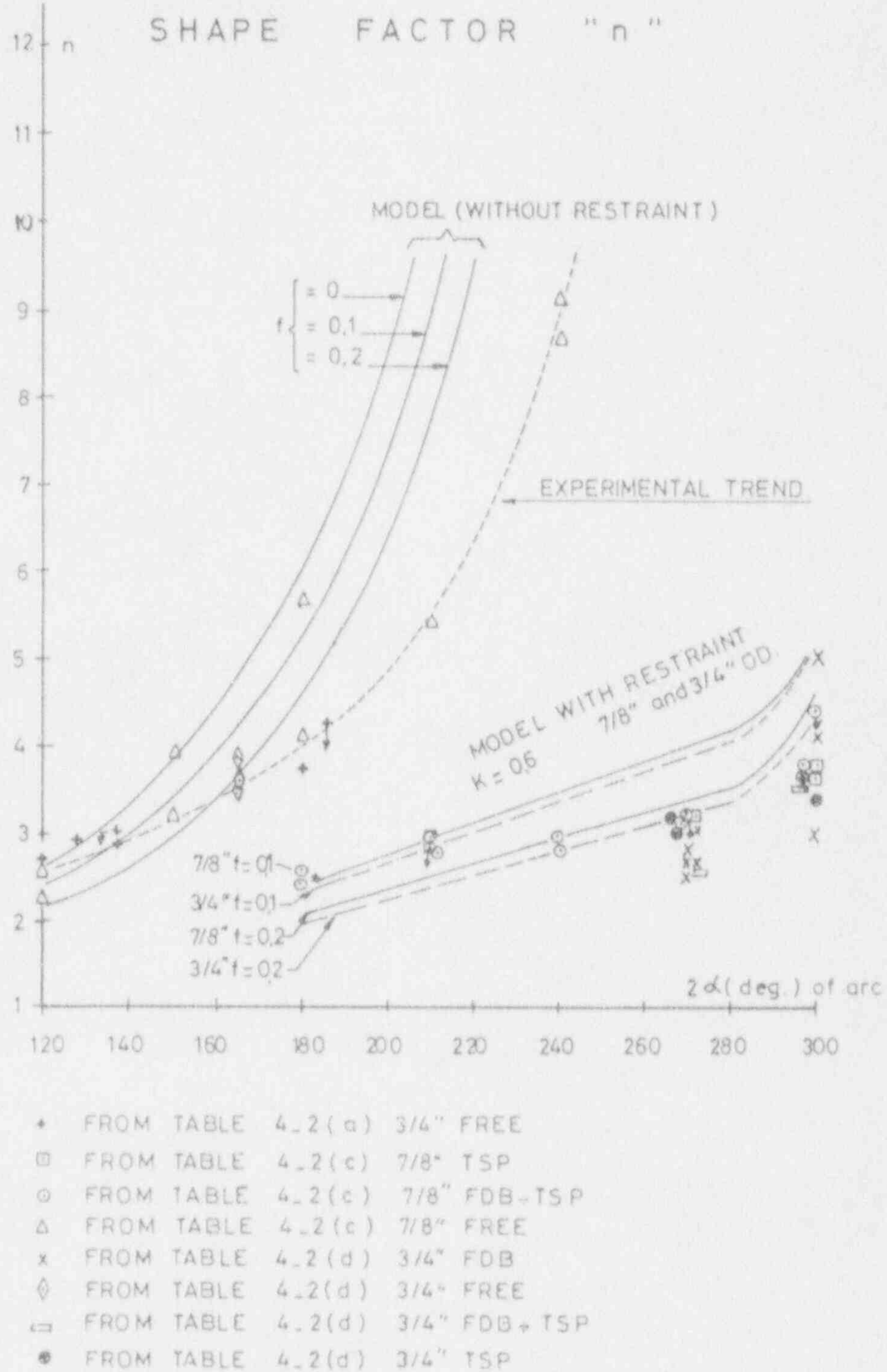

Figure 4-3(b) Circumferential through wall cracks with and without lateral restraint. Shape factor n

Section 5

REFERENCES

1. Goodier J.N. and Field, F.A.
   American Inst. Mining Met. and Petrol Eng. "Fracture of Solids"
   1963 Wiley, New York

2. Burdekin F.M. and Stone, D.E.W.
   J. Strain Anal. 1,145 (1966)

3. Fol_as E.S.
   "The Stresses in a Cylindrical Shell Containing an Axial Crack"
   ARL 64-174, Aerospace Research Laboratories (Oct. 1964)

4. Krenk S.
   "Influence of Transverse Shear on an Axial Crack in a Cylindrical Shell"
   Int. J. of Fracture 14, No 2 (1978)

5. Kiefner J.F., Maxey W.A., Eiber R.J. and Duffy A.R.
   "Failure Stress Levels of Flaws in Pressurized Cylinders"
   ASTM STP 536

6. Schulze H.D., Togler G. and Bodmann E.
   "Fracture Mechanics Analysis on the Initiation and Propagation of Circumferential and Longitudinal Cracks in Straight Pipes and Pipe Bends"
   Nucl. Eng. and Design 58 (1980)

7. Erdogan F.
   "Ductile Fracture Theories for Pressurized Pipes and Containers"
   Int. J. Pres. Ves. & Piping 4 (1976)

8. Eiber R.J., Maxey W.A., Duffy A.R. and Atterbury T.J.
   "Investigation of the Initiation and Extent of Ductile Pipe Rupture"
   Battelle Memorial Institute Report BMI - 1866 (1969)

9. Larsson H. and Bernard J.
   "Fracture of Longitudinally Cracked Ductile Tubes"
   Int. J. Pres. Ves. & Piping, 6 (1978)

10. Ziebig H. and Fortmann F.
    "Fracture Behaviour of Ferritic and Austenitic Steel Pipes"
    2nd Int. Conf. SMIRT, Berlin, 1973(paper F 4/8)

11. Connors D.C. and Darlaston B.J.L.
"Factors of the Fail Safe Approach to Pressure Vessel Assessment" in I. Mech. E. Conference Publications 1978-10 "Tolerance of Flaws in Pressurized Components" (paper C 101)

12. Roark R.J. and Young W.
"Formulas for Stress and Strain" (fifth ed.)

13. P. Hernalsteen
"Evaluation of Critical Lengths for Through Thickness Axial Cracks in Steam Generator Tubing"
6th Int. Conf. SMIRT, Paris, 1981 (paper F 7/6)

14. P. Hernalsteen
"Evaluation of Critical Sizes for Defects in Small Diameter Tubing"
7th Int. Conf. SMIRT, Chicago, 1983 (paper G/F 4/3)

15. J.P. Hutin
"EDF Steam Generator Surveillance and Maintenance"
EPRI Workshop on PWSCC remedial measures, Clearwater (February 1989)

16. Henry B., Bernard J. and Gieb Ph.
"Fatigue Crack Growth in Austenitic Stainless Steel Structures"
2nd Int. Conf. SMIRT, Berlin, 1973 (paper F 4/7)

17. Cochet
"Application of the Leak before Break Concept to Steam Generator Tubes"
NUCSAFE 88, Avignon (October 1988)

18. C. Ruiz and R.J.S. Corian
"Practical Application of Extremal Elastic. Ideally Plastic Solutions for the Assessment of the Severity of Cracks"
Int. J. Pres. Ves. & Piping 10 (1982)